

Elucidation of the molecular and cellular mechanisms of FKBP51-selective inhibitors

Haehle, Andreas

(2020)

DOI (TUprints): <https://doi.org/10.25534/tuprints-00013235>

Lizenz:



CC-BY-SA 4.0 International - Creative Commons, Attribution Share-alike

Publikationstyp: Ph.D. Thesis

Fachbereich: 07 Department of Chemistry

Quelle des Originals: <https://tuprints.ulb.tu-darmstadt.de/13235>

Elucidation of the molecular and cellular mechanisms of FKBP51-selective inhibitors

Aufklärung der molekularen und zellulären Mechanismen FKBP51-selektiver Inhibitoren

Vom Fachbereich Chemie
der Technischen Universität Darmstadt



TECHNISCHE
UNIVERSITÄT
DARMSTADT

zur Erlangung des Grades
Doctor rerum naturalium (Dr. rer. nat.)

Dissertation von
Andreas Hähle, M.Sc.

Erstgutachter:

Prof. Dr. Felix Hausch

Zweitgutachter:

Prof. Dr. Harald Kolmar

Darmstadt 2019



Überarbeitete Version vom 29.01.2020

Tag der Einreichung: 04.07.2019

Tag der mündlichen Prüfung: 14.10.2019

Hähle, Andreas: „Elucidation of the molecular and cellular mechanisms of FKBP51-selective inhibitors“,
Technische Universität Darmstadt, Jahr der Veröffentlichung der Dissertation auf TUprints: 2020

Tag der mündlichen Prüfung: 14.10.2019

Veröffentlicht unter CC BY-SA 4.0

International <https://creativecommons.org/licenses/>

Datum:

Erklärung

Ich erkläre hiermit, dass ich meine Dissertation selbstständig und nur mit den angegebenen Hilfsmitteln angefertigt und noch keinen Promotionsversuch unternommen habe.

Unterschrift



Erklärung der Übereinstimmung

Datum:

Ich erkläre hiermit, dass die elektronische Version der Doktorarbeit mit der schriftlichen Version übereinstimmt. Die elektronische Version liegt dem Prüfungssekretariat vor.

Unterschrift

Fiat iustitia et pereat mundus

**μείζονα ταύτης ἀγάπην οὐδεὶς ἔχει, ἵνα τις τὴν ψυχὴν
αὐτοῦ θῆ ὑπὲρ τῶν φίλων αὐτοῦ.**

Gewidmet den Menschen, die ich liebe



Table of content

Table of content	i
1.....Abstract	1
1.1. Zusammenfassung	1
1.2. Abstract	3
2.....Introduction	4
2.1. FK506 Binding Proteins	4
2.2. FKBP51 – a disease relevant protein	4
2.3. Structure of FKBP51 ligand development	5
2.4. PROTACs	8
2.5. Interactome of FKBP51	10
2.5.1. Hsp90	11
2.5.2. Steroid Hormone Receptors	12
2.5.3. Akt and NF κ B	13
2.5.4. Glomulin	15
2.5.5. Other pathways and interactors associated with FKBP51	16
2.6. Objectives of the work	17
3.....Materials	19
3.1. General Chemicals	19
3.2. General Plastics and Materials	20
3.3. Cell Culture Plastics	20
3.4. HTRF Material	20
3.5. Devices	20
3.6. Readers	21
3.7. Software	21
3.8. List of used group internal ligands	21
3.9. Primary Antibodies	21
3.10. Secondary Antibodies	21
3.11. Bacterial Strains	21
3.12. Expression Plasmids	22
3.12.1. Bacterial expression	22
3.12.2. Eukaryotic expression	23

3.13.	Mammalian Cell Lines	24
3.14.	Cell Culture Media and Additives	24
4.....	Methods	27
4.1.	Protein Purification	27
4.1.1.	His-tagged Proteins	27
4.1.2.	GST-tagged Proteins	27
4.1.3.	Protein Labeling	28
4.1.4.	Activity Assay of Labeled Proteins	29
4.1.5.	Active Site Titration of FKBP51	29
4.2.	HTRF	30
4.3.	Cell Culture	30
4.3.1.	Growth Conditions and Passaging	30
4.3.2.	Surface Coating	31
4.3.3.	Storage	31
4.3.4.	Cell Counting	31
4.3.5.	Jurkat Cell Culture	31
4.4.	Reporter Gene Assays	32
4.4.1.	Glucocorticoid Receptor Signaling	32
4.4.2.	NF- κ B-Signaling	33
4.5.	PROTAC Treatment of Cells	33
4.6.	Cell Lysis	34
4.7.	Protein Quantification via BCA Assay	34
4.8.	SDS-PAGE	34
4.9.	Coomassie Staining and Gel Drying	35
4.10.	Western Blotting	35
4.11.	Western Blot Data Processing for Signal Strength Analysis	36
4.12.	Degradation of Nanoluc-tagged FKBP51	36
4.13.	Calcium Influx Assays	37
5.....	Results	38
5.1.	FKBP51 PROTACs	38
5.1.1.	Endogenous FKBP51	38
5.1.2.	Exogenous FKBP51	44

5.1.3.	Degradation of Nanoluc-FKBP51	44
5.2.	FKBP51 in reporter gene assays	47
5.2.1.	Assay Setup	47
5.2.2.	Establishing the Assay Window and the Effect of Normalization	48
5.2.3.	Overexpression of FKBP51	49
5.2.4.	Effects of Different FKBP51 Mutants	50
5.2.5.	FKBP52 in the Reporter Gene Assay	51
5.2.6.	Impact of FKBP51 Ligands in the Reporter Gene Assay	53
5.2.7.	Overexpression of Glomulin	54
5.2.8.	FKBP51 in NF- κ B Signaling	55
5.3.	Glomulin – FKBP HTRF	60
5.3.1.	Assay Setup	60
5.3.2.	Assay development	61
5.3.3.	Active site titrations of FKBP51	61
5.3.4.	Binding site specificity	63
5.3.5.	Comparison of different FKBP51	65
5.3.6.	Characterization of FKBP51FK1 F67D and FD67/68DV mutants	68
5.3.7.	Competition of other FKBP51 constructs	70
5.3.8.	Impact of Rbx1 in this HTRF setup	70
5.4.	FKBP51 and Calcium Influx	73
6.....	Discussion	78
6.1.	Summary	78
6.2.	FKBP51 PROTACs	79
6.3.	FKBP51 in Glucocorticoid Receptor Signaling	80
6.4.	FKBP51 in NF- κ B Signaling	81
6.5.	FKBP51 and Glomulin	82
6.6.	FKBP51 in Calcium Signaling	84
6.7.	The FKBP51 interactome	85
6.8.	Perspectives for ligand development	88
7.....	Supplemental Information	92
7.1.	Chemical Knockdown of FKBP51 library	92
7.2.	MTQ202 / MTQ416	109

7.3.	Reporter Gene Assays	110
7.4.	HTRF	111
7.5.	Protein Purification - FPLC	113
7.6.	Active Site Titrations of HTRF used FKBP12 and FKBP12.6	118
7.7.	Tracer Structures	118
7.8.	HTRF Glomulin Titration	119
8.....	Abbreviations	120
9.....	Bibliography	1
10. ..	Acknowledgements	2
11. ..	Curriculum Vitae	4
12. ..	References	6

1. Abstract

1.1. Zusammenfassung

Das FK506-bindende Protein (FKBP51) wurde als Risikofaktor für diverse psychiatrische Erkrankungen wie beispielsweise Depression und andere Erkrankungen wie Fettleibigkeit und chronischem Schmerz identifiziert. FKBP51 ist enzymatisch aktiv, seine FK1-Domäne ist eine Prolyl-peptidyl-isomerase. FK506, ein natürlicher und immunsuppressiver Ligand, bindet an diese Tasche. Mittlerweile wurden verschiedene neue Klassen an FKBP51-Liganden entwickelt. Diese Moleküle sind nicht mehr immunsuppressiv, besitzen eine höhere Affinität zu FKBP51 und sind teilweise selektiv gegenüber anderen FKBP5s. Der „Selective Antagonist of FKBP51 by Induced Fit 1“ (SAFit1) ist hochselektiv für FKBP51 gegenüber seinem engen Homolog und in Teilen funktionellem Gegenspieler FKBP52. Liganden mit SAFit-Struktur wirken dem Effekt von FKBP51 entgegen, die Ausdifferenzierung neuronaler Zellen zu inhibieren. Außerdem zeigen sie diverse Effekte in verschiedenen Mausmodellen. Mäuse, die mit SAFit2 behandelt werden, passen sich besser an Stress an, bleiben schlanker bei fetthaltiger Ernährung und weisen abgeschwächte Symptome bei chronischem Schmerz auf. Die am besten beschriebene Aktivität auf molekularer und zellulärer Ebene von FKBP51 wird mit dem Glucocorticoid Rezeptor (GR) assoziiert. Dieser ist ein zentraler Regulator der Reizweiterleitung bei Stress. Mutationen im *fkbp5*-Gen wurden mit erhöhter FKBP51-Expression und Glucocorticoidresistenz assoziiert. Neben dem GR wurden noch viele weitere Proteine als FKBP51-Interaktoren beschrieben, u.a. innerhalb des NF- κ B und Akt-Signalweges. Obwohl FKBP51 ein attraktives Drugtarget von stetig steigendem Interesse ist, sind die zugrundeliegenden molekularen und zellulären Funktion von FKBP51-Liganden und des Proteins selbst kaum aufgeklärt. Diese Dissertation trägt dazu bei, die Kluft zwischen Molekularbiologie und klinischen Befunden zu schließen. In einem ersten Ansatz wird die Erforschung einer neuen Klasse von FKBP51-Liganden, entwickelt von Tianqi Mao in der Arbeitsgruppe Hausch, beschrieben. Diese FKBP51-PROTACs (proteolysis targeting chimeras) sollen einen chemischen Knockdown ihres Targets bewirken. Die PROTACs wurden gescreent. Eine vielversprechende Struktur, die die Menge an zellulär endogenem FKBP51 heruntersetzt, wurde mittels Western Blotting identifiziert. Dieser Befund wurde sowohl durch die reduzierte Aktivität eines FKBP51-Luciferase-Konstrukts als auch durch die PROTAC-Wirkung in einem GR Reporterassay bestätigt. Dieser Assay bestätigt zudem das Modell, dass FKBP51 den GR-Signalweg inhibiert und FKBP52 dem entgegenwirkt. Dennoch zeigten in diesem Assay konventionelle Liganden keinen Effekt. In einem zweiten Ansatz wurde die Interaktion von FKBP5s und dem E3-Ligaseregulator Glomulin detailliert untersucht. FKBP12.6 wurde als neuer Bindepartner mittels HTRF-Methodik (Homogeneous Time Resolved Fluorescence) identifiziert. Dies ist der erste *in-vitro*-Assay, der die Bindung von FKBP51 an andere Proteine auf molekularbiologischer Ebene untersucht. Die Aminosäuren F67 und D68 sind essentiell, damit Glomulin an die FK1 Domäne von FKBP51 binden kann. Letztendlich beschreibt die Glomulin-FKBP51-Interaktion den allerersten Proteinkomplex, der sensitiv für verschiedene Klassen

von FKBP51 Liganden ist. Zusammenfassend deuten meine Ergebnisse darauf hin, dass FKBP51 zwei grundverschiedene Wirkungsweisen aufzeigt. Einer ist sensitiv für Liganden und abhängig von einer intakten PPlase-Domäne und der andere nicht. Diese Arbeit weist damit auf die Wichtigkeit der Erforschung definierter FKBP51-Protein-Interaktionen hin und unterstreicht das Ziel, Liganden zu entwickeln, die beide Wirkungsweisen von FKBP51 beeinflussen.

1.2. Abstract

The FK506 Binding Protein 51 (FKBP51) is an identified risk factor for a variety of psychiatric disorders such as major depressive disorder as well as obesity and chronic pain. Enzymatically, FKBP51 exhibits prolyl-peptidyl-isomerase activity located within a pocket in its FK1 domain. The natural ligand and immunosuppressive drug FK506 binds to this pocket. Nowadays, several new classes of FKBP51 ligands have been developed. These compounds that lack the immunosuppressive feature, show higher affinity for FKBP51 and partial selectivity towards other FKBP family members. The Selective Antagonist of FKBP51 by Induced Fit 1 (SAFit1) is highly selective for FKBP51 compared to FKBP52, a close homolog and partial functional counterplayer of FKBP51. Ligands of the SAFit class have been shown to reverse FKBP51 induced inhibition of neurite development of neuronal cells and are active in various mouse models. Mice treated with SAFit2 have an improved stress coping behavior, remain leaner during a high-fat diet and show decreased symptoms in a chronic pain state. The best described molecular and cellular activity of FKBP51 is linked to the Glucocorticoid Receptor (GR), a key player in the stress signaling cascade. Mutations of the *fkbp5* gene were linked to increased FKBP51 levels and glucocorticoid resistance. Beside the GR, FKBP51 has been described as the interactor of many other proteins e.g. within the NF- κ B and Akt signaling pathway. Although FKBP51 is an attractive drug target of continuous rising interest, the underlying molecular and cellular functions of FKBP51 ligands and the protein itself remain to be elucidated. This thesis contributes in closing the gap between molecular biology and clinical findings regarding FKBP51 and its ligands. The first approach was the investigation of a new class of FKBP51 ligands developed by Tianqi Mao in the Hausch lab. These FKBP51 PROTACs (proteolysis targeting chimeras) aim to chemically knock down their target. These PROTACs were screened and a promising structure was identified, which resulted in decreased endogenous FKBP51 levels in cells detected through Western blotting. This finding was confirmed by a decreased FKBP51-Luciferase fusion protein signal and the PROTACs action in a GR reporter gene assay. The later assay supports the model of FKBP51 inhibiting and FKBP52 enhancing GR signaling. However, conventional ligands did not impact the FKBP51 effect. The second approach elucidated the interaction of FKBP51 and the E3 ligase regulator Glomulin (Glmn) in detail. FKBP12.6 has been identified as novel interactor of this protein utilizing the HTRF (Homogeneous Time Resolved Fluorescence) methodology. This is the first *in-vitro* assay, which addresses the binding of FKBP51 and a protein interactor on the molecular biological level. The amino acids F67 and D68 have been identified to be essential to establish the binding of Glmn to FKBP51s FK1 domain. At last, the FKBP51-Glmn complex is the first discovered interaction that is sensitive to multiple classes of FKBP51 ligands. In conclusion, my findings indicate two distinct modes of action of FKBP51. One is ligand-dependent and PPIase-domain-dependent while the other is independent. My thesis points out the importance to increase the focus on the investigation on defined FKBP51 interactions and to raise the efforts to develop FKBP51 ligands that address both FKBP51 action modi.

2. Introduction

2.1. FK506 Binding Proteins

FK506 binding proteins are clustered according to their ability to bind the immunosuppressive natural ligand FK506 and therefore, belong to the family of immunophilins along with cyclosporin-binding cyclophilins. Many members of both families are enzymatically active, exhibiting prolyl-peptidyl-isomerase activity. The structures of FKBP are versatile, but all members have at least one FK domain, a typical fold of five β -sheets palming an α -helix. The smallest family member, the archetypical FKBP12, comprises solely just this very domain. The FKBP motif can be found in all kingdoms of life, FKBP51 itself is present in all mammals (as investigated thus far). Cellular functions and distribution of human FKBP are various: FKBP12, 12.6, 51 and 52 can be localized in the cytoplasm; FKBP13 and 65 can be found in the endoplasm and FKBP25 in the nucleus. This already points out the multitude of molecular processes involved: FKBP51 and 52 serve as cochaperones of Hsp90 and modulate steroid receptor signaling (2.5.2), FKBP65 is involved in collagen folding [1] and calcium channels of the TRPC family are regulated by FKBP12 and 12.6 [2], just to name a few.

2.2. FKBP51 – a disease relevant protein

FKBP51 is a known interactor of the glucocorticoid receptor, a steroid hormone receptor and central player in stress procession and final attenuation of the hormonal stress reaction (see 2.5.2). It gained significant importance, as the correlation between single nucleotide polymorphisms (SNPs) and the recurrence of depressive episodes and rapid response to antidepressant treatment of major depressive disorder was discovered [3]. Some of those SNPs have been linked to altered methylation and expression patterns of the *fkbp5* gene [4], with an increasing number of associated psychiatric disorders [4-6]. There is indeed fundamental proof of the involvement of FKBP51 for the neuroendocrinology of stress and stress coping behavior in mice [7-11].

The genetics of FKBP51 is furthermore reported to be associated with insulin resistance and energy metabolism [12,13] as well as trauma related chronic pain [14,15]. On the one hand, data obtained from *fkbp5*^{-/-} mice is widely supporting genetic findings and detrimental effects of this knockout have not been observed thus far [10]. On the other hand, a row of phenomenological benefits can be found: improved sleep profile [16], resistance towards diet induced obesity [17,18], resistance against artificially induced chronic pain [19,20] and resistance against glucocorticoid induced skin atrophy [21]. Treatment of wild type mice with SAFit2 (Selective Antagonist of FKBP51 by induced fit) enhanced feedback inhibition of the hypothalamus-pituitary-adrenal axis [22], various behavioral stress coping mechanism [22,23] and glucose tolerance [18]. It acted anxiolytic [23,24], protected from weight gain

[18] and positively dampened mechanical hypersensitivity in inflammatory, neuropathic and chemotherapy-induced pain states [19,20].

Taken together, within the last 15 years FKBP51 emerged as an interesting and promising drug target.

2.3. Structure of FKBP51 ligand development

FKBP51 contains three domains: The *N*-terminal FK1 domain, the central FK2 domain and its *C*-terminal tetratricopeptide repeat (TPR) domain, which serves as attachment site for Hsp90s MEEDV motif (**Figure 1**) [25]. The FK1 domain displays prolyl-peptidyl-isomerase (PPIase) activity and is capable of binding ligands, such as the name-giving FK506 ($K_i = 100 \pm 10$ nM) and the second natural compound, Rapamycin ($K_i = 3.7 \pm 0.9$ nM) [26]. It comprises five antiparallel β strands, which are wrapped around a central α helix. Although the FK2 domain exhibits a similar structure to the FK1 domain, it is thought to neither be enzymatically active nor capable of ligand binding. The PPIase deficiency was justified by its structure [27]. The FK2 domain of FKBP52 was also found deficient [28,29]. The inability to bind ligand was thus far just shown for FKBP52s FK2 domain [30], where FK506 could be detected in the binding pocket of the FK1 but not the FK2 domain (PDB-ID: 1LAX).

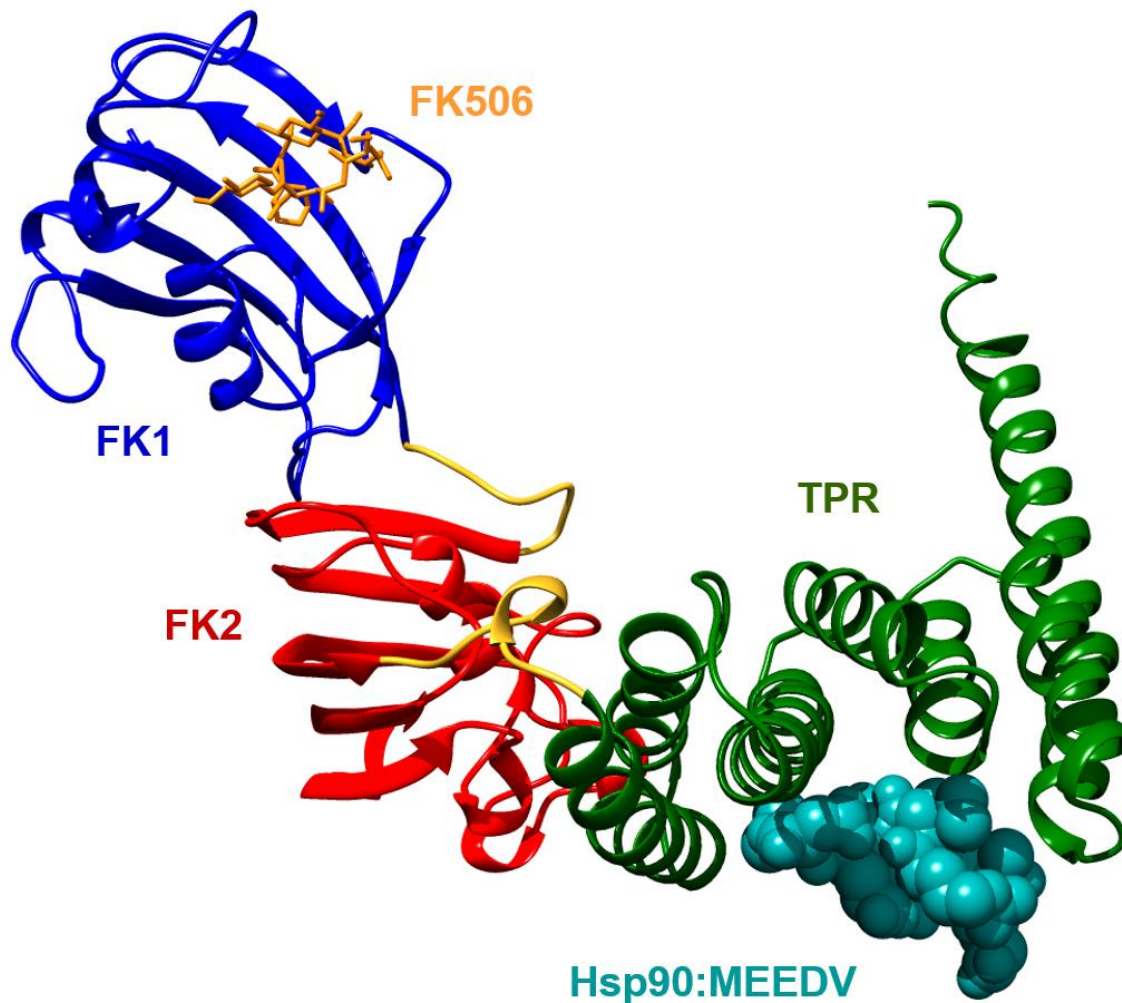


Figure 1 Full length FKBP51 (PDB-ID: 1KT0) [27] bound to the MEEDV motif derived from the Hsp90 C-terminus (PDB-ID: 5NJX) [31]. FK506 bound to the FK1 domain is superimposed from PDB-ID: 3O5R. Figure taken from [25].

FKBP51 shares 60% sequence identity and 78% similarity with its homologue FKBP52. Their overall structure is similar, but the relative orientation of FK1 and FK2 domain is twisted [32]. This could be a potential explanation for their differing effects on the glucocorticoid receptor [33,34] and non-identical interactomes. BioGRID.com (May 2019) lists 20 confirmed (≥ 2 independent methods and/or publications) interactors for FKBP52 and 69 for FKBP51.

Most important for binding of small molecules such as FK506 are the H-bond donors tyrosine 113 and isoleucine 87 within the FK1 domain [35,36]. Great efforts of ligand development were spent towards the development of selective ligands. Due to a highly conserved binding pocket shared with its close homologue FKBP52 ligands often exhibit similar binding affinities. Selectivity is important to achieve, since FKBP51 and FKBP52 act antagonistically in steroid hormone receptor signaling (see 2.5.2) and neuritotrophic differentiation [22,37]. Additionally, FKBP52 knockout mice display a strongly impaired phenotype regarding their reproductive tissue development and fertility [38], making it an

antitarget. Gaali and Kirschner overcame this obstacle by serendipity in their discovery of SAFit (Selective Antagonist of FKBP51) class ligands [22].

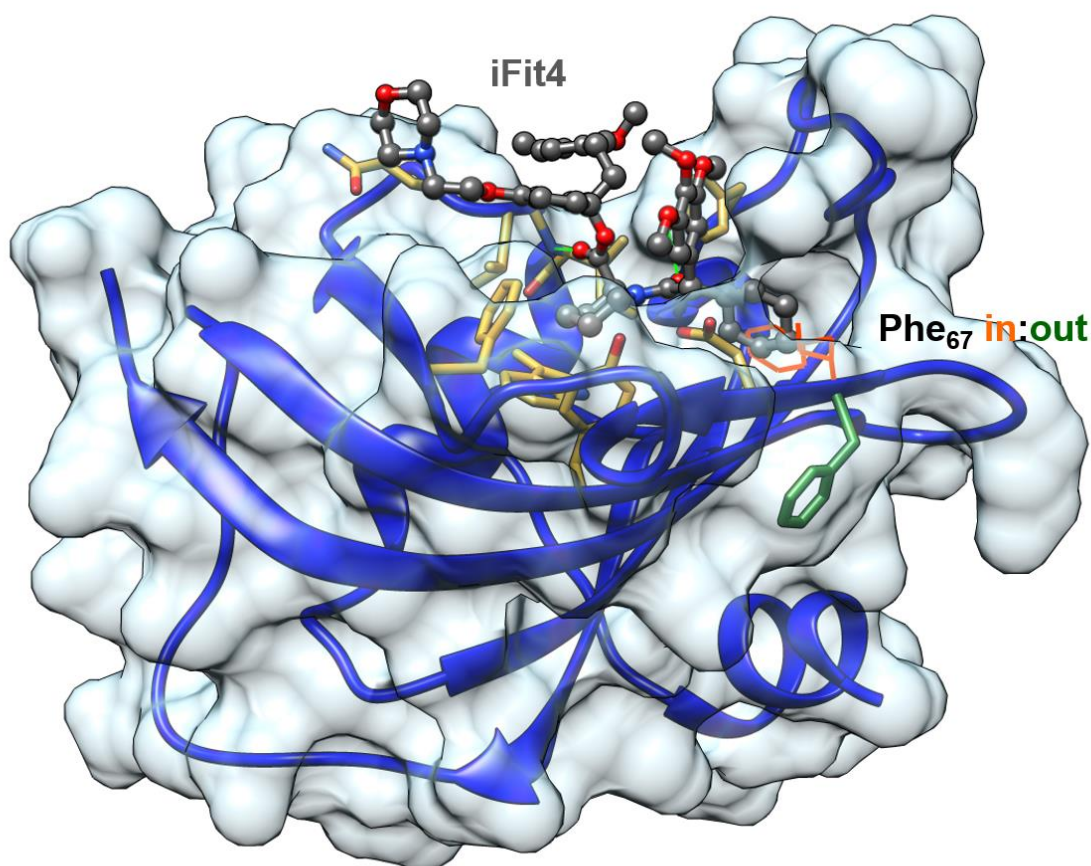


Figure 2 FK1 domain bound to the selective ligand iFit4 (PDB-ID: 4TB7). The Phe67-in state is superimposed from PDB-ID: 5OBK. Taken from [25].

The selectivity is achieved either by induced fit [22] or conformational selection [39][Jagtap et al. *Angew Chem*, 2019, in press] of a Phe67 out state, which is sterically possible for FKBP51 but not FKBP52 (**Figure 2** FK1 domain bound to the selective ligand iFit4 (PDB-ID: 4TB7)). The Phe67-in state is superimposed from PDB-ID: 5OBK. Taken from [25]. The best binding was achieved by SAFit1, which binds to FKBP51 with $K_i = 4$ nM and 10,000 fold stronger than to FKBP52. Yet another class of FKBP ligands are [4.3.1]-aza-bicyclic sulfonamides, which are unable to discriminate between FKBP51 and FKBP52. However, their affinity reach high picomolar range for FKBP12 and low nanomolar range for FKBP51 and FKBP52, serving as more powerful tools for *in vitro* assays [40,41]. An overview on those ligands is given in **Figure 3**.

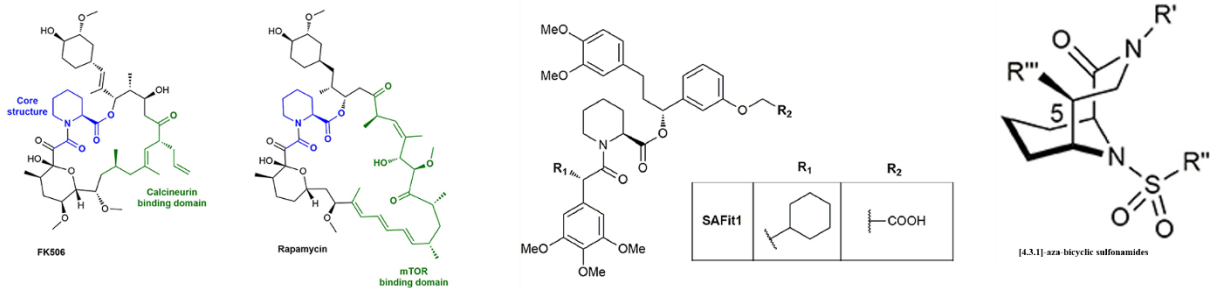
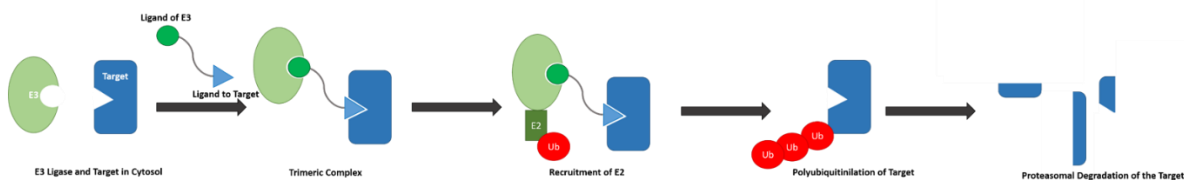


Figure 3 FKBP ligands: The natural compounds FK506 and Rapamycin, SAFit series structure and [4.3.1]-aza-bicyclic sulfonamides, adapted from [42].

2.4. PROTACs

The development of PROteolysis-TARgeting Chimeras (PROTACs) is a recently emerging concept of ligand development in order to achieve chemical knockdown of a target protein, which has yet to prove its applicability in drug development. The basic concept of PROTACs is the heterobifunctional connection of a target ligand (warhead) and an E3 ligase ligand connected via a linker (**Figure 4 A**).

A Working Principle of PROTACs



B Limitations of small molecular inhibitors

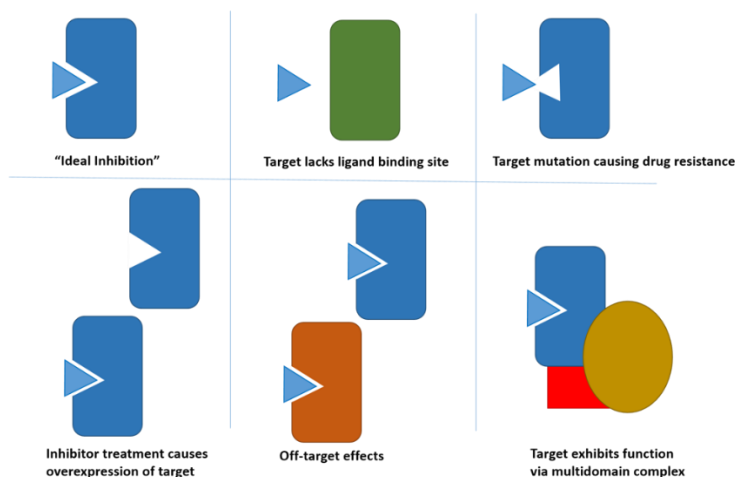


Figure 4 A) Action principle of PROTACs: By bringing target and E3 ligase into close proximity, polyubiquitination on the target followed by proteasomal degradation can be achieved. **B)** Overview on the limitations of conventional small molecular inhibitors. Inspired by [43].

The PROTAC principle was firstly developed in 2001 targeting peptidases by linking a phosphopeptide moiety and a small molecule moiety binding TrCP leading to the ubiquitination and degradation of the peptidase MetAP-2 [44]. In 2008 the first non-peptide based, cell permeable PROTAC consisting of a non-steroidal androgen receptor ligand and nutlin, a ligand of the E3 ligase MDM2, successfully knocked down its target in HeLa cells [45]. Within the last years the E3 ligases Von-Hippel-Lindau (VHL) and cereblon (CRBN) [43] became most common to exploit. Example ligands, also used in our research, of both E3 ligases are (S,R,S)-AHPC or VH032 for VHL [46] and pomalidomide for CRBN [47], respectively.

PROTACs have been shown to overcome certain limitations conventional ligands face (**Figure 4 B**) *in vitro*. Since PROTACs can exhibit their catalytic function for the degradation of multiple targets, their potential efficacy can be exhibited sub-stoichiometrically [43,47,48]. On top of that, it was shown that some PROTACs have lower half-maximal values for target degradation (DC_{50}) than the half-maximal inhibitory effect of their corresponding target ligand moiety (IC_{50}) [49,50]. A prominent readout in this field of research is the induction of apoptosis, due to the fact, that many cancers are caused by overexpression of certain factors. The inhibition of apoptosis via the bromodomain extraterminal protein (BETP) was with 16 nM for the PROTAC ARV-825 significantly higher than for the conventional inhibitor OTX015 with 398 nM [51]. Excitingly, the same study observed target overexpression induced by OTX015 treatment in Mino cells, which is a common escape mechanism of many cancer cell lines, which did not occur during PROTAC exposition. It was shown, that PROTACs can have both a quick onset (1 h) and long lasting effect up to 48 h, which could be even achieved by a single injection in a mouse xenograft model [52]. By developing conventional small molecules, drug discovery faces its limitations concerning certain proteins, which either lack an active site or contain an active site, which has no impact on its related pathology. Similar difficulties are encountered for multi-domain protein complexes, which serve as scaffolding platform for example in signal transduction, such as receptor tyrosine kinases (RTKs). In a recent case study, a PROTAC targeting the RTK epidermal growth factor receptor (EGFR), was introduced, which led to a more robust and rapid downstream inhibition and anti-proliferative effect compared to the classical inhibitor [53]. Additionally, it was found that PROTACs can feature altered selectivity patterns [54,55], which is especially interesting in order to hit protein families with highly conserved binding pockets, such as kinases or FKBP. It was even shown that PROTACs can have an improved efficacy against mutated targets [50], which is prominent escape mechanism in many cancers.

The successful development of PROTACs usually requires an empirical approach and the synthesis of a small library to achieve the desired chemical-induced protein degradation. For the conception of PROTACs, one needs to address the following attributes: designated E3 ligase, constitution of the linker (length and chemical nature), chemical nature of warhead, attachment point of linker at the warhead (examples: [49,56,57]). Especially the nature and length of the linker is not predictable, as the only available crystal structure of the artificial ternary complex, finds it folded in

between target and E3 ligase (**Figure 5**)[46]. This indicates a potentially essential enhancement of a stable and cooperative complex by the linker, rather than a simple distance definition.

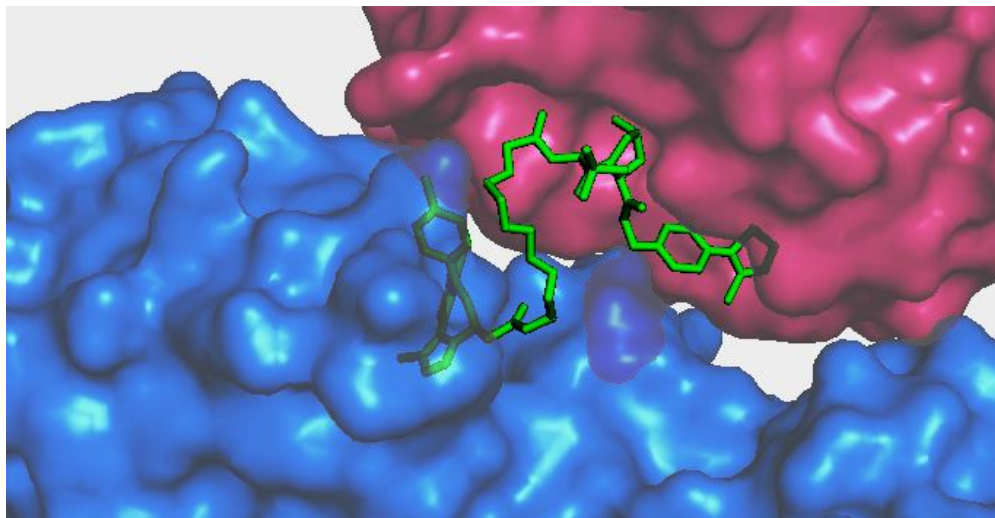


Figure 5 Ternary structure of human VHL (blue), Brd4 (pink) and the PROTAC MZ1 (green). Linker describes a turn between both binding moieties. PDB: 5T35

It has to be noted, that high throughput screening assays for PROTACs, especially with respect to concentration dependence and time course of the degradation, are hardly available so far, but first steps have been made by genetically labeling the protein of interest with a luciferase fragment tag [58].

Taken together, PROTACs are a promising concept of drug development. Besides conventional small molecules and monoclonal antibodies, PROTACs exhibit an often unpredictable difference regarding selectivity, efficacy and applicability compared to its small molecule warhead. Although they are proven to be powerful tools in molecular and cellular biology, clinical administration is in its earliest stage of development. Just recently, the first phase I study started by Arvinas to test *in vivo* degradation of the androgen receptor by their substance ARV-110 in stage 4 prostate cancer patients [59]. Due to the fact, that FKBP51 related pathologies are connected to elevated expression levels [3], the model of FKBP51 as scaffolding protein and a number of FKBP51 interactions, that have been found to be ligand insensitive [25], the research of FKBP51 PROTACs is promising to elucidate the biological role of this protein.

2.5. Interactome of FKBP51¹

FKBP51 has a rather vast interactome with more than 60 associated proteins reported (**Figure 6**). Many of the proposed interactors have been discovered through CoIP experiments and sometimes lack independent confirmation. Because FKBP51 binds to Hsp90, it is naturally part of large protein

¹ This content is taken from my review with slight changes "The Many Faces of FKBP51" 25. Hausch, F. The Many Faces of FKBP51. *Biomolecules* **2019**, *9*, doi:10.3390/biom9010035.

Hahle, A.; Merz, S.; Meyners, C.;

complexes for example steroid hormone receptors [60]. Therefore, FKBP51 can be considered to be rather “sticky” and claims of interactors should be evaluated with caution.

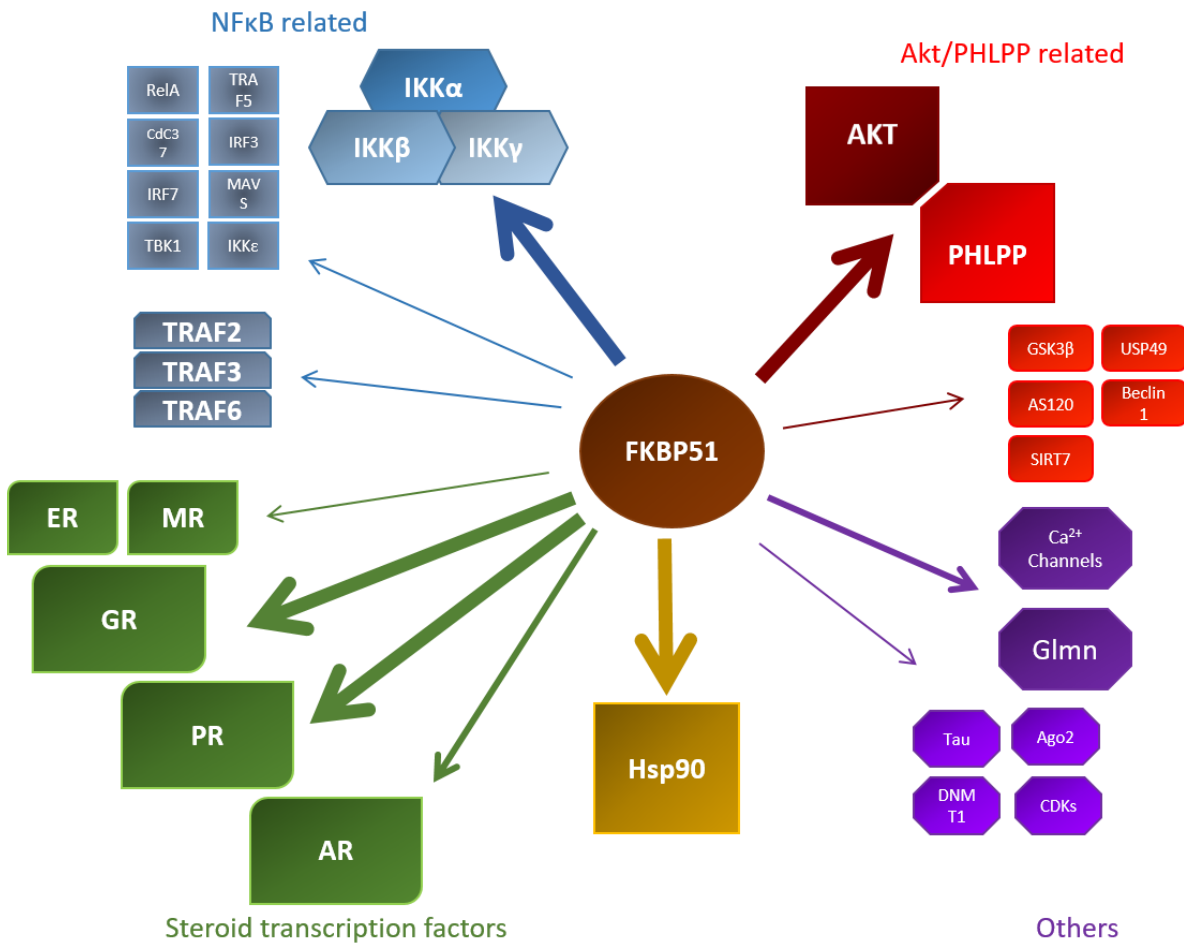


Figure 6 Overview of known FKBP51 interactors within their respective field of discovery. Stronger arrows indicate a larger data set of this specific interaction. Taken from [25].

2.5.1. Hsp90

The heat shock protein 90 (Hsp90) is a highly abundant and ubiquitously expressed chaperone in most mammalian cells. It is a central player in protein folding, stabilization, mediator of protein complex formation and involved in protein degradation, with hundreds of client proteins and therefore involved in a plethora of cellular pathways and processes [61]. In early studies on steroid hormone receptors, FKBP51 and 52 (“p50/p54”) were successfully co-purified along with Hsp90 and the progesterone receptor [62] and later on identified as immunophilins of the FKBP family [63]. FKBP51 and Hsp90 interact via their respective C-terminal domains. The FKBP51 TPR-domain binds the highly conserved MEEDV motif of Hsp90 [34]. The Hsp90 complex can be dissociated by the selective Hsp90 inhibitor Geldanamycin, which also interrupts the attachment of immunophilins to the complex [64].

About nine TPR domain-containing proteins have been identified and confirmed to bind to Hsp90, such as the Hsp70-Hsp90 Organizing Protein (HOP), the serine/threonine protein phosphates 5 (PP5) and the E3 ubiquitin ligase CHIP (C terminus of HSC70-Interacting Protein), which is explicitly reviewed

[61,65,66]. All of them share a 20 amino acid consensus sequence, which is required for Hsp90 recognition [67,68]. Cochaperones are thought to compete for Hsp90 association which was shown to be important for the regulation of steroid receptor signaling [69]. The differences in binding affinity and concentration of various TPR-domain proteins [28] reflects one layer to regulate the action of FKBP51 [60]. The dynamic association and dissociation of cochaperones, including PPIases, have been shown to be essential for the progression and fine-tuning of the conformational cycle of Hsp90 [61,70]. While it is clear that FKBP51 can associate with Hsp90, the involvement of Hsp90 as mediating factor in the action of FKBP51 within many pathways is often unclear.

2.5.2. Steroid Hormone Receptors

Both discovery and research motivation to study FKBP51 and other TPR-domain proteins is tightly connected to the investigation of steroid hormone receptors (SHR). The members of the SHR family are the Androgen Receptor (AR), the Estrogen Receptor (ER), the Mineralcorticoid Receptor (MR), the Progesterone Receptor (PR) and the Glucocorticoid Receptor (GR). SHRs are located in the cytosol and translocate into the nucleus upon hormone binding serving as transcription factors. Most SHR are clients of the Hsp90 chaperone machinery, which is essential for receptor maturation, hormone binding and translocation to the nucleus [71]. In a comprehensive study, Schülke *et al.* performed reporter gene assays and co-immunoprecipitations to investigate the impact of TPR proteins on SHRs [69]. GR and PR were shown to be most sensitive towards the presence of TPR proteins, including FKBP51, while AR was only mildly affected and MR and ER were found to be largely unresponsive to TPR proteins. Both FKBP51 and its PPIase-deficient mutant (FD67/68DV) are preferentially associated with PR and GR [72]. The *fkbp5* gene itself is inducible by glucocorticoids [73-76], progesterone [75,77-79] and androgenic hormones [80-82] leading to both elevated mRNA and protein levels. The *fkbp5* gene contains several glucocorticoid receptor response elements and GR attachment mediates PolIII loading and DNA methylation [83]. Soon it became clear, that FKBP51 and especially the glucocorticoid receptor constitute an ultrashort negative feedback loop: Induced by steroid hormone receptors, elevated expression of FKBP51 reduces the transcriptional activity of those receptors. It was first shown in yeast, that FKBP51 blocks the FKBP52-induced potentiation of the GR [84]. In mammalian cells, FKBP51 reduces GR reporter activity, which was connected in part to a reduced dynein binding of the receptor-chaperone-complex and henceforth a dampened translocation rate of the GR into the nucleus [33]. The PPIase activity seems not to be required for this mode of action since the FD67/68DV mutant, that has no PPIase activity on peptide substrates, retains GR inhibitory activity. However, amino acid 119 was found to be important in the different activity of FKBP51 and FKBP52. Pro119 as in FKBP52 supported receptor activation whereas L119 as in FKBP51 displayed an inhibitory effect [85]. Mass spectrometry studies reveal similar complexes of GR/Hsp90/Hsp70/ATP with FKBP51 and FKBP52 as interchangeable factors in the early stages of complex formation. In those complexes, FKBP51

stabilizes the binding of the cochaperone p23, while FKBP52 leads to a release of p23, which primes the complex for nuclear translocation [86].

There might be other forms of GR and FKBP51 crosstalk. One study found that FKBP51 expression leads to GR subform α -mediated adipogenesis [87]. Regulation by posttranslational modification has also been described for FKBP51. The attachment of SUMO at lysine 422, which was shown *in vitro*, was claimed to be important for GR inhibition in a reporter gene readout in hippocampal neuronal cells [88]. Recently, benztropine was claimed to diminish the inhibitory effect of FKBP51 on GR, but the molecular mechanism of this remains to be elucidated [89]. GR itself is part of the hypothalamic pituitary adrenal (HPA) axis, which is the neuroendocrine stress response. Upon an external stimulus, the hypothalamus releases the corticotropin-releasing factor (CRF). Upon binding of CRF to CRF receptors on the anterior pituitary gland, adrenocorticotrophic hormone (ACTH) is secreted. ACTH itself is perceived by the adrenal cortex and stimulates the release of cortisol. Cortisol finally activates the GR, which coordinates the final step of stress response and exerts a negative feedback on CRF and ACTH release, leading back to systemic homeostasis in the magnitude of hours. Several factors, such as repeating and continuous stress, certain drugs and age influence the sensitivity towards cortisol. Many patients suffering from major depressive disorder exhibit “cortisol resistance”, being unable to regain homeostasis (for recent reviews see [90-92]). Since FKBP51 is a negative regulator of the GR, its impact on various psychiatric disorders is mainly theorized to be GR-mediated.

AR has largely been investigated in prostate cancer models. Contrary to GR, where FKBP51 has repeatedly been described as an inhibitory factor, two studies in 2010 reported an activation of AR by FKBP51 [93,94]. However, since those initial studies, no further confirmation of these findings has been published and the role of FKBP51 in prostate cancer biology remains controversial. The involvement of FKBP51 in steroid hormone signaling leads to numerous associations in physiological and pathological pathways involving a fine-tuned and cross-regulated interactome, intensively studied and reviewed [95].

2.5.3. Akt and NF κ B

Besides steroid hormone signaling, FKBP51 is described as actor in the important pathways of Akt and NF κ B.

The kinase Akt serves as a central node to regulate various signaling pathways in growth and proliferation. Akt activity strongly depends on the phosphorylation of its Serine 473, which is thought to be regulated by the PH domain and Leucine rich repeat Protein Phosphatases (PHLPP). FKBP51 is believed to serve as a scaffolding protein that recruits PHLPP to Akt to facilitate dephosphorylation [96,97]. In support for this model, overexpression of FKBP51 was shown to reduce phosphorylation of both Akt S473 [8,96-98] and the Akt downstream targets GSK3 β and FOXO1. Conversely, FKBP51 knockdown or knockout led to an enhanced S473 phosphorylation of Akt. Truncation studies suggest that the FK1 domain of FKBP51 is mainly required to recruit Akt [99] and the TPR domain to recruit

PHLPP [96]. Further investigations revealed that the FK1 domain alone can bind Akt, as well as their respective PPlase mutants without being impacted by the presence of FKBP ligands [18,99], suggesting a competitive binding model for several FKBP51 towards Akt. Not all studies could confirm the impact of FKBP51 overexpression on Akt [99]. Another study found that FKBP51 overexpression enhanced GSK3 β phosphorylation in HEK293 cells, which is counterintuitive to the suggested role FKBP51 on Akt/PHLPP [100]. In the context of Akt regulation, the ubiquitin specific peptidase 49 (USP49) could be co-purified with FKBP51. This deubiquitinase was claimed to stabilize FKBP51 and to enhance the dephosphorylation of Akt via PHLPP [97]. Moreover, the Akt-FKBP51-interaction was recently suggested to be regulated by acetylation of FKBP51 [98]. Six acetylation sites were reported, of which two are regulated by the deacetylase Sirtuin 7 (SIRT7). Acetylation on the sites K28 and K155 were proposed to enhance FKBP51-Akt interaction, S473 dephosphorylation of Akt reduced phosphorylation of Akt downstream targets such as GSK3 β . In 2017, the Akt substrate 160 (AS160) was coimmunoprecipitated along with FKBP51, Akt and PHLPP [18]. Its phosphorylation status could be disrupted by the selective FKBP51 ligand SAFit2, both *in vitro* and *in vivo*.

On the other hand, FKBP51 was also described as a regulator of NF- κ B (nuclear factor binding near the κ light-chain in B cells) signaling in different cell types. For this reason, FKBP51 has been suggested as a drug target for the treatment of NF- κ B-mediated inflammation and cancer [101-106]. NF- κ B is a family of transcription factors affecting multiple cellular processes such as inflammation, proliferation, maturation, differentiation, survival and apoptosis [107-109]. As a key factor, NF- κ B regulates the innate and adaptive immune response. In the last 15 years, several studies aimed to elucidate the role of FKBP51 in NF- κ B pathways and the underlying mechanisms [101-106,110-113]. Different FKBP51 interaction partners involved in NF- κ B pathways have been identified. Among them, members of the IKK complex, namely IKK α [101,102,104,111,113], IKK β [102,104,113] and IKK γ [102,104,110,113] belong to the most prominent interaction partners shown in various cell lines. The FK1 and TPR domain of FKBP51 both appeared to be required for its interaction with IKK γ in HEK293 cells [104]. Jiang et al. proposed that the FK1 domain is involved in the interaction with IKK α in human glioma cells (U87) [101]. The data indicated that the PPlase-inactive double-point mutation FD67DV of the FK1 domain reduced the interaction of FKBP51 with IKK α [101]. In contrast, Romano et al. did not observe any impact of the FD67DV mutation on either the FKBP51/IKK α/β or the IKK γ /IKK α/β interaction in HEK293 cells [104]. In accordance with these results, FK506, a FKBP51 isomerase inhibitor, did not affect the FKBP51/IKK α interaction [104]. Instead, a TPR domain mutant with diminished Hsp90 binding seemed to impair the interaction of IKK α/β with FKBP51 as well as with IKK γ in HEK293 cells [104]. The involvement of Hsp90 in FKBP51-mediated NF- κ B signaling is still under discussion [102,112,113].

The effect of FKBP51 on NF- κ B activation is also controversially discussed. On the one hand, various studies demonstrated that FKBP51 enhances NF- κ B activation [104,105,111]. On the other

hand, Erlejman et al. described the opposite effect of FKBP51 and concluded that NF- κ B activation is regulated by the FKBP51/FKBP52 ratio [112]. Reporter gene assays implicated that FKBP51 impaired, whereas FKBP52 enhanced, PMA (phorbol 12 myristate 13 acetate) as well as TNF α induced NF- κ B activation in HEK293T cells overexpressing either FKBP51 or FKBP52, respectively. Both effects seemed to be reversed by the expression of the corresponding TPR peptide. A competition assay with FKBP51 and FKBP52 using the transcriptional activity of NF- κ B as readout led to the conclusion, that FKBP52 could act as an FKBP51 antagonist, reversing its inhibitory effect on NF- κ B activation.

Taken together, it can be concluded that FKBP51 is connected to both pathways, but the extend and significance is unclear due to strong controversing findings.

2.5.4. Glomulin

Glomulin (Glmn) has been identified as a binding partner of FKBP12 and FKBP52 in a Y2H screen [114,115]. Initially, Glmn has been described as FKBP Associated Protein (called FAP48 or FAP68) [114,116]. More recently, a link between FKBP51 and Glmn was described in a high-throughput interactome network study [60].

Glmn has been discussed as E3 ligase regulator. Eukaryotic cells utilize a system of three enzymes (E1 to E3) and ubiquitin to prime proteins for proteosomal degradation. One of the most studied examples of the E3 ligase family is CRL1^{Fbw7} [117,118]. Glomulin (Glmn) binds to this complex by intercalating between Cullin1 (Cul1) and RING-box protein 1 (Rbx1) (**Figure 7**). Henceforth, Glmn masks the interaction surface of Rbx1 towards the E2 ubiquitin-conjugating enzyme Cdc34, leading to an inhibition of the ligase activity, because activated ubiquitin becomes unavailable [119,120]. This is also thought to prevent an overshooting ubiquitylation reaction, which is mediated by Rbx1 binding to cullins and which would lead to a degradation of CRL1^{Fbw7} itself [120]. Later, an interaction of Glmn with cellular inhibitors of apoptosis proteins 1 and 2 (cIAP1 and cIAP2), which regulate E3 ligases, was discovered [121]. Additionally, most recently Glmn was associated with the infectious mechanism of Shigella [121,122], where Glmn was claimed to be hijacked by a bacterial E3 ligase to promote inflammation. Mutations in the Glomulin gene lead to Glomuvenous malformation [116,123,124]. Point mutants and truncation mutants lacking Proline219 of Glomulin showed significantly reduced β -galactosidase activity in a Y2H screen [115]. However, the detailed mechanism and regulation of this reaction is still poorly understood. A potential regulation by FKBP51 in this context has not been investigated.

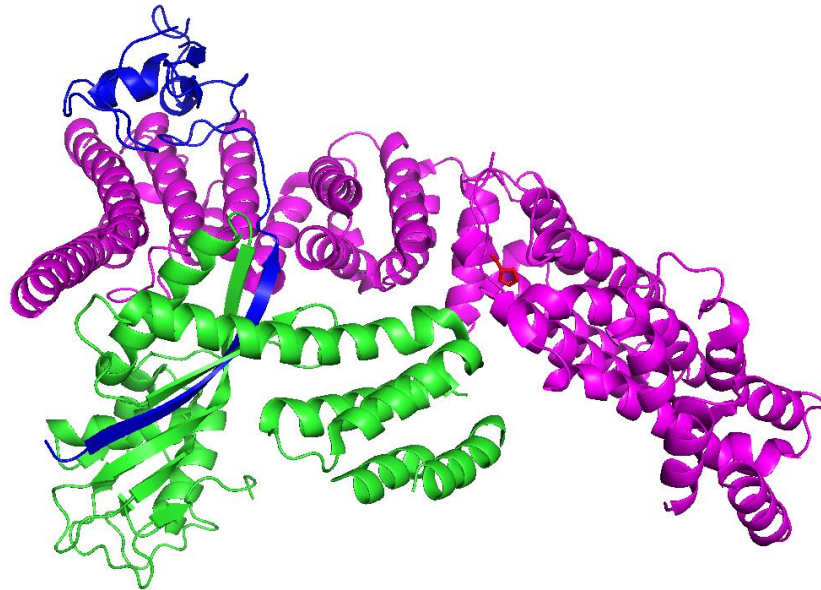


Figure 7 Crystal structure of Glomulin (pink) with Cullin1 (green) and Rbx1 (blue). Proline219 is indicated in red.

2.5.5. Other pathways and interactors associated with FKBP51

FKBP51 has been associated with a great number of other proteins. In a comprehensive interactome study addressing the Hsp90 complex and its cochaperones, numerous interaction partners of FKBP51 were described [60]. Among those findings are kinases such as the cyclin dependent kinases (CDK1, 4, 9 and 11A) as well as kinases involved in cytoskeleton formation (Aurorakinase B, Fer). Furthermore, MYND-domain proteins, associated with transcriptional repression, minichromosome maintenance (MCM) complex proteins, helicase subunits and the argonaut proteins Ago1 and 2, essential components of the RNA-induced silencing complex (RISC) were identified as potential interactors. For CDKs, an antagonizing action mode of FKBP51 and 52 was described for their respective impact on DNA methylation [125]. Both immunophilins were copurified with the cyclin dependent kinase (CDK5) and its downstream target DNA methyltransferase 1 (DNMT1) [100,125]. Higher FKBP51 expression was linked to decreased DNMT1 phosphorylation levels and reduced methylation levels of the brain-derived neurotrophic factor locus in human blood samples. Accordingly, FKBP52 was suggested to exhibit opposite effects [125]. In addition, FKBP51 was also found to bind to CDK4, a known oncogene, where FKBP51 knockdown led to decreased CDK4 expression [126].

Although, the evidence of FKBP51 being involved in cytoskeletal processes accumulates, an overall model for its action mode is still lacking. The microtubule forming monomer Tau is linked to plaque formation in Alzheimer's Disease (AD). In 2010 it was claimed, that overexpression of FKBP51 increases Tau concentration and FKBP51 knockdown reduces it. Both proteins could be copurified.

FKBP51 seemed to protect Tau from ubiquitination potentially acting as a chaperone, since Hsp90 was found in this complex as well. An active PPIase pocket was required for binding Tau [127]. In the same year, FKBP51 and its partial counter player FKBP52 were linked to another process involving microtubule arrangements. FKBP51 dampens while FKBP52 enhances neurite outgrowth during neuronal differentiation [22,37] which requires elevated expression of cytoskeletal proteins. The anti-neuritotrophic activity of FKBP51 could be blocked by FKBP51 ligands which increases neurite outgrowth in neuroblastoma cell lines and in primary embryonic neurons [22,41,128]

Interestingly, the connection of FKBP51 and microtubule formation via tau dephosphorylation was recently proposed to be PP5C mediated, a TPR-domain containing phosphatase [129]. Furthermore, expression levels of both proteins impact the store-operated calcium entry current in pulmonary artery endothelial cells and HEK293 cells. Additionally, store-operated channels have been reported to be desensitized by FKBP51. FKBP52 was shown to antagonize this effect [130]. Immunophilins, such as the FKBP5s 52, 12, 25 and 38 have generally been associated with calcium ion channels especially of the TRPC family and effects of high concentrations of FK506 on calcium flux have been reported [2,131-133].

The RISC protein complex shows elevated expression with increased FKBP51 and 52 levels in mural embryonic stem cells and is less abundant, if one or both immunophilins are knocked down. Interestingly, less Ago2 can be found if the cells are treated with FK506 [97,134].

It can be summarized that research on FKBP51 faces many (yet) loose ends and the findings are partially controversial or are lacking independent confirmations. A general concept bringing together all potential interactors and phenotypes has yet to be defined.

2.6. Objectives of the work

It becomes clear, that FKBP51 is an important protein factor in multiple cellular pathways and associated with many more other proteins. Side by side, there is continuous growing proof of FKBP51's disease relevance in multiple fields, including psychiatric disorders, obesity, chronic pain and some cancers [25].

The aim of this work was to contribute towards two goals, back to back:

1. Elucidate the molecular and cellular mechanisms of FKBP51 ligands.
2. Utilize FKBP51 ligands to create an improved understanding of FKBP51's action modes itself.

Selective FKBP51 ligands such as SAFit1 and SAFit2 have been shown to be active in various murine models for the previously named pathologies [18,20,23,24,104]. The underlying mechanisms are overall unclear. To address this problem, a first focus has been set to the action of FKBP51 in GR context. A reporter gene assay was established to research the effects of FKBP51 and its mutants overexpression on GR signaling strength, as well as the impact of FKBP51 ligands within this setup. In close cooperation with Tianqi Mao, a novel class of FKBP ligands – PROTACs – with the purpose to induce

chemical knockdown, were screened by Western Blotting and tested in the reporter gene assay. Besides the gain-of-function effects of FK506 and Rapamycin, no specific protein-protein interaction is described thus far which is altered by the presence of FKBP51 ligands. During the course of my work, some unpublished results indicated a tight and promising interaction of FKBP51 and Glmn. To investigate this interaction *in vitro* a HTRF setup was developed. Multiple FKBP51 mutants have been examined, as well as FKBP ligands.

In this work, I present a new functional readout for GR signaling that confirms the FKBP action. Conventional ligands and a PROTAC exhibit different effects in this assay. Furthermore, two unprecedented protein-protein interactions are discovered and the very first ligand-sensitive interaction is described.

3. Materials

All materials are listed with their name as indicated by their provider label, their provider and the providers catalog number.

3.1. General Chemicals

4-(6-methyl-1,3-benzothiazol-2-yl)aniline (dissolved in DMSO, Santa Cruz Biotechnology, sc-276812), Acetic acid 99-100% (C. Roth, 7332.2), Adenosin-5'-triphosphat disodium salt (C. Roth, HN35.1), Agar-Agar, Kobe I (C. Roth, 5210.3), Albumin, Fluorescein isothiocyanate Conjugate bovine (Sigma, A9771), Ampicillin sodium salt (C. Roth, K09.5), Bovine Serum Albumin (Sigma, A7030), Brilliant Blue G250 (C. Roth, 9598.1), Charcoal Activated (C. Roth, X865.1), Carbachol (Alfa Aesar, L06674), Coelenterazine h (dissolved in Ethanol, AAT Bioquest, 21159), Coenzyme A free acid (AppliChem, A0812), cOmplete Mini Protease inhibitor cocktail (Roche, 11836153001), Coomassie Brilliant Blue R250 (C. Roth, 9598.1), D-Luciferin (C. Roth, CN24.1), Deoxyribonuclease I from bovine pancreas (DNAse I) (Sigma, DN25-1G), Dexamethasone 21-phosphate disodium salt (dissolved in DMSO, Sigma, D1159), Dimethylsulfoxid (DMSO) (C. Roth, 4720.4), Dithiothreitol (DTT) (C. Roth, 6908.1), di-Potassium hydrogen phosphate (C. Roth, P749.1), Dual-Glo® Stop & Glo® Substrate (Promega, E313B), Ethanol 70% pure (Krankenhaus Apotheke Schwabing, UN 1170), Ethanol denatured (C. Roth, K928.4), FK506 Tacrolimus (Beta Pharma, 56-01267), Fluorescein-5-Maleimide (ThermoScientific, 62245), Glycerol 86% (C. Roth, 4043.2), Glycine (C. Roth, 3908.2), Glutathione (reduced) (Merck, K46409890 514), Hepes (C. Roth, 9105.3), Hyperforin, Hyperforin derivatives, OAG (Friedland group, Universität Mainz), Imidazole (Fluka, 56750), Insulin solution from bovine pancreas (Sigma, I0516-5mL), IPTG (C. Roth, CN08.3), Kanamycin sulphate (C. Roth, T832.1), LB Broth (Luria/Miller) (C. Roth, X968.2), Lysozym (C. Roth, 8259.3), Magnesium chloride hexahydrate (Merck, Q649033 524), Magnesium sulphate heptahydrate (C. Roth, P027.2), mTNF- α aa80-235 E.coli derived (R&D Systems, 410-MT) Nano-Glo® Luciferase Assay (Promega, N112B), Nickel II Sulphate 6-hydrate (C. Roth, T111.1), Nonidet® P-40 substitute (VWR Life Science, E109-50mL), Passive Lysis Buffer 5x (Promega, E194A), Phenylmethyl sulphonyl fluoride (C. Roth, 6367.2), Phorbol 12-myristate 13-acetate (Enzo, BML-PE 160), Ponceau S (C. Roth, 5938.2), Potassium dihydrogen phosphate (C. Roth, 3904.1), Potassium hydroxide (C. Roth, 6751.1), Powdered mil (C. Roth, T145.3), Propan-2-ol (AppliChem, 603-117-00-0), Protein degrader 1 hydrochloride (VHL ligand) (MedChemExpress, HY-101763A), Rapamycin (Alfa Aesar, J62473), Rotiophorese® Gel 30 (37.5:1) (C. Roth, 3029.1), SDS (C. Roth, 0183.3), Sodium Chloride (C. Roth), Sodium acetate anhydrous (Fluka, 71183), TECEP hydrochloride (trc Canada, 249283), TEMED (C. Roth, 2367.3), tetra-Sodium pyrophosphate decahydrate (Na₄PPi) (Fluka, 71515), Trichloroacetic acid (C. Roth, 8789.2), TRIS (C. Roth, 4855.2), TRIS hydrochloride (C. Roth, 9090.3), Triton X-100 (C. Roth, 3051.4), Tween 20 (C. Roth, 9127.2)

3.2. General Plastics and Materials

Eppendorf Tubes 5.0 mL (Eppendorf, 0030119401), Micro tube 1.5 mL (Sarstedt, 72.690.001), Microtube 1.5 mL protein LB (Sarstedt, 72.706.600), Micro tube 2.0 mL (Sarstedt, 72.691), Micro tube 2.0 mL LB (Sarstedt, 72.695.600), Pipette Tips – various volumes (Sarstedt), ProteinLoBind Tubes 5.0 mL (Eppendorf, 003010832), white 96-well half-area plate (Greiner bio-one, 392-0287), gel drying frame and cellophane (C. Roth), Amersham™ Protran™ 0.2 µm Nitrocellulose (GE Healthcare Life Sciences, 10600001), Rotilabo®-Blottingpapiere, 0.35 mm (C. Roth, CL65.1),

3.3. Cell Culture Plastics

TC Dish 100 Standard (Sarstedt 83.3902), Combitips advanced 1.0 mL (Eppendorf BIOPUR 0030 089.642), Combitips advanced 5 mL (Eppendorf BIOPUR 0030 089.669), CryoPure Tubes 1.8 mL white (Sarstedt, 72.379), TC Testplate 96F (TPP, 92096), TC Plate 24 Well Standard F (Sarstedt, 83.3922.005), 12 Well Cell Culture Plate (Greiner bio-one, 665 180), TC – Plate sterile with lid single packed (Greiner bio-one, 657 160), Greiner CELLSTAR® 96 well plates wells V-bottom (with lid) (M9686 Sigma), Cell Culture Microplate 96 well PS, F-bottom (CHIMNEY WELL) µCLEAR® black cellstar® TC lid with condensation rings (Greiner Bio-one, 655090), Adhesive Black Light-Absorbing Film (VWR, 391-1291)

3.4. HTRF Material

384 well plate Assay Plate 384 Well No Lid Flat Bottom Low Flange Non-Binding-Surface Black Polystyrene (CORNING, 3575), Mab Anti GST-Tb cryptate (Cisbio, 61GSTTLA)

3.5. Devices

Biofuge Pico (Heraeus), Electrophoresis Powersupply (EPS series, Amersham), CVC 3000 Vacuum pump (vacuubrand), DS11+ Spectrophotometer (Denovix), Duomax 1030 and Polymax 1040 (Heidolph), EMB500-1 scale (KERN), IKA Kombimak REO stirring device, RM5 Rollenmischgerät, Light Microscope WILVERT S (Leica), Microwave (Samsung), Mixing Block MB-102 (BIOER) Multichannel Pipette 8 – 100µL (Eppendorf), Pipette Matrix Multichannel 16 – 125µL (Thermo Scientific), Pipettes – various volumes (Gilson), Reax 1 Vortexer (Heidolph), Rotilabo-Block-Heater H250 (Roth), RS-T170S Rollenmischgerät (PHOENIX Instrument), Sartorius Analytic Scale, Sprout Minifuge (Biozym), Waterbath-GFL-Typ-1002

3.6. Readers

Genios Pro (Tecan), Infinite M1000 with dual injection module (Software: i-control 1.11), Berthold TriStar² LB 942

3.7. Software

Graphpad Prism6, ImageJ, Microsoft Office Suite 2016, Sigmaplot 11.0

3.8. List of used group internal ligands

Internal Nomenclature	Published Name	Publication
AV075	Unpublished	Dissertation AV
CK182	2b	[26]
MTQ238	16j	[40]
JK096	16g	[40]
MB53, THe10, SG770	SAFit1	[22]
MTQ202 / MTQ416	unpublished	Dissertation MTQ
Other PROTACs	unpublished	Dissertation MTQ

3.9. Primary Antibodies

Name	IgG Subtype, Species	Dilution	Manufacturer
Flag(HRP), A8592	mono, mouse	1:10000, 5% milk in TBS	Sigma-Aldrich
FKBP51 A301-430A	poly, rabbit	1:500, TBS	Bethyl
GAPDH A300-641A	poly, rabbit	1:1000, 5% milk in TBS	Bethyl
Glomulin A304-940A	poly, rabbit	1:1000, 5% milk in TBS	Bethyl
HA(HRP) 3F10	mono, rat	1:10000, 5% milk in TBS	Roche
Hsp90 PA5-27410	poly,rabbit	1:2500, 5% milk in TBS	Thermofisher

3.10. Secondary Antibodies

Name	IgG Subtype, Species	Dilution	Manufacturer
Rabbit IgG A120-112P	poly, goat	1:1000, 5% milk in TBS	Bethyl

3.11. Bacterial Strains

Two fundamental *Escherichia coli* strains were used, both purchased from Invitrogen (Karlsruhe). DH5 α (Genotype: F' Phi80dlacZ Δ M15 Δ (lacZYA-argF)U169 deoR recA1 endA1 hsdR17(rK-mK+)phoA supE44 lambda- thi-1) for molecular cloning, site-directed mutagenesis and preparation of plasmid DNA. BL21(DE3)pLysS (Genotype: F⁻, ompT, hsdS_B (r_B⁻, m_B⁻), dcm, gal, λ (DE3), pLysS, Cm^r) for the heterologous production of protein.

3.12. Expression Plasmids

Proteintags are indicated ahead of the protein name if they are located N-terminally and after the protein name if they are located C-terminally of the protein sequence.

3.12.1. Bacterial expression

Internal Reference Number	Insert	Backbone	Created by
HG 21	His-FKBP12	pProEx-HTA	CKo, 08.09.2005
HG 49	His-FKBP51FK1 (1-140)	pProEx-HTA	CKo, 09.03.2006
HG 92	His-FKBP52FK1 (1-140)	pProEx-HTA	Andreas, 10.04.2006
HG 116	His-FKBP51-Strep	pProEx-HTA	Steffen, 15.01.2008
HG 118	His-FKBP52-Strep	pProEx-HTA	Steffen, 15.01.2008
HG 156	His-FKBP12.6	pProEx-HTA	CIS, 2005
HG 306	His-FKBP51FK1 (1-140) F67V	pProEx-HTA	Bas
HG 365	His-FKBP51FK1 (1-140) FD67/68DV	pProEx-HTA	Veronika Kupfer, 19.07.2010
HG 633	His-FKBP51FK1 (16-140), A19T	pET30b	CIS, 16.02.2015
HG 653	His-FKBP51FK1-MonoCys (1-140, C103A, C107I, E140C)	pET30b	CIS, 02.09.2016
HG 656	His-FKBP12-MonoCys (C23V, E108C)	pET30b	CIS, 07.09.2016
HG 660	GST-Glmm	pGex	AHa, 08.07.2016 obtained from Schulman group, Memphis)

HG 661	GST-Rbx1	pGex	AHa, 08.07.2016 obtained from Schulman group, Memphis)
--------	----------	------	--

3.12.2. Eukaryotic expression

Internal Reference number	Insert	Backbone	Created by
HG 124	HA-GR	pRK5	AHa, 13.07.2018 (AG Rein, MPIPpsych)
HG 206	FKBP52-Flag	pRK5	AF, 2008 (AG Rein, MPIPpsych)
HG 207	FKBP51-Flag	pRK5	AF, 2008 (AG Rein, MPIPpsych)
HG 302	FKBP51- Flag TPR* (K352A/R356A)	pRK5	SC, 02.12.2009 (AG Rein, MPIPpsych)
HG 382	FKBP51-Flag PPlase (FD67/68DV)	pRK5	AK, 23.11.2011
HG 473	hRLuc/TK (pGL4.74)	pGL4	AK, 23.08.2011 (Promega, 9PIE692)
HG 490	HA-FKBP51	pRK5	AK, 17.10.2011
HG 498	MmFKBP51-HA	pRK5	CKo, 3.11.2011
HG 591	FKBP51-Flag (L119P)	pRK5	CIS
HG 598	RT-233-2/TRPC6-YFP	pcDNA3.1	AG Leuner, FAU Erlangen
HG 600	FKBP51-Flag Triple mut (K58T, K60W, F129V)	pRK5	CIS, 25.06.2013
HG 628, pGRE4luc2P	Three copies of tandem GRE [135]	pGL4.27	AHa, 01.09.2014 (Dvorak Group, University Olomouc)
HG 644	3xFlag-Glmn	pcDNA3.1	AHa, 11.01.2016 (Taipale Group, Toronto University)
HG 645	Glmn-3xFlag	pcDNA3.1	AHa, 11.01.2016 (Taipale Group, Toronto University)
HG 658	TRPC6 YFP SDM C1	pcDNA3.1	AHa, 08.07.2016
HG 680	Nluc-FKBP51	pNLF1	NGu, Master Thesis

HG813 p1242	Firefly-Reporterplasmid, canonical NF- κ B pathway	pGL2	Nils Gassen, MPIPsych, Promega product
HG814 pNF- κ B2	Firefly-Reporterplasmid, non-canonical NF- κ B pathway	pGL2	Nils Gassen, MPIPsych, [136]

3.13. Mammalian Cell Lines

Name	Description	Origin	Provided by	ATCC No.
A375	malignant melanoma skin cells	<i>H. sapiens</i>	AG Boßerhoff (FAU Erlangen)	CRL-1619
HEK293-T	Embryonic kidney cells	<i>H. sapiens</i>	Dr. T. Rein (MPI for Psychiatry, Munich)	CRL-1573
HEK TRPC6-HA #4	Embryonic kidney cells, stable transfection with TRPC6	<i>H. sapiens</i>	Jana Demleitner (LMU Munich)	
HeLa	Cervix adenocarcinoma cells	<i>H. sapiens</i>	Dr. T. Rein (MPI for Psychiatry, Munich)	CCL-2
Jurkat	peripheral blood T Lymphocyte	<i>H. sapiens</i>	Anthony Zannas, Nils Gassen (MPI for Psychiatry, Munich)	CRL-2899
MEF	Embryonic fibroblast cells	<i>M. musculus</i>	Dr. M. Cox (University of Texas, El Paso)	CRL-2991
Neuro2a	Brain neuroblastoma cells	<i>M. musculus</i>	Dr. J. Deussing (MPI for Psychiatry, Munich)	CCL-131
PC12	Pheochromocytoma cell, adrenal gland	<i>R. norvegicus</i>	AG Friedland (Universität Mainz)	CRL-1721

3.14. Cell Culture Media and Additives

Name	Contents	Used for	Manufacturer
Sterile Water Art.- Nr. 3256.1		Plasmid Dilution, Plate coating	C. Roth (Karlsruhe)
Dulbecco's Modified Eagle Medium C4207.0500	4.5g/L glucose, L- glutamine, sodium pyruvate, w/o phenol red, 3.7g/L NaHCO ₃	Reporter Gene Assays	GENAXXON bioscience (Ulm)
Dulbecco's Modified Eagle Medium 41966- 029	4.5g/L glucose, L- glutamine, sodium pyruvate, phenol red	Most cell lines	Gibco-Invitrogen (Karlsruhe)
Advanced RPMI 1640 Medium, 12633012	glucose, non essential amino acids, sodium pyruvate, phenol red	Jurkat, PC12	Gibco-Invitrogen (Karlsruhe)
Dulbecco's Phosphate Buffered Saline 14190-094		All cell lines	Gibco-Invitrogen (Karlsruhe)
Heat Inactivated Fetal Bovine Serum 10500-064		All cell lines	Gibco-Invitrogen (Karlsruhe)
Poly-L-Lysine P4707	0.01% PLL		Sigma LifeScience (Steinheim)
Opti-MEM Reduced Serum Medium, 11058- 021	L-Glutamine, HEPES, w/o phenol red	All cell lines	Gibco-Invitrogen (Karlsruhe)
Pen Strep 15140-122	10,000 Units/mL Penicillin 10,000 µg/mL Streptomycin	All cell lines	Gibco-Invitrogen (Karlsruhe)

Lipofectamine 2000, 11668-019		All cell lines	Invitrogen (Karlsruhe)
0.25% Trypsin- EDTA, 25200-056		All cell lines	Gibco-Invitrogen (Karlsruhe)
Trypan Blue Stain (0.4%), 15250- 061		All cell lines	Gibco by Life Technologies

4. Methods

4.1. Protein Purification

4.1.1. His-tagged Proteins

Proteins were expressed in *E.coli* BL21(DE3) cells. All incubation steps were performed at approximately 200 rpm in a heatable shaker. 3 mL LB media and the according antibiotic were inoculated with a scratch of glycerol stock by a steril pipette tipp to obtain the preculture and grown at 37 °C overnight. The next day, 200 mL media + antibiotic were inoculated with 1 mL preculture and treated similar. 4 L of the main culture were inoculated with 120 mL of the second preculture and distributed into four time 1 L in a 2 L glass Erlmeyer flask. The cultures were grown to an $OD_{600}=0.5$, induced with 600 μ M IPTG (final) and grown for 4 h at 37 °C (Monocys variants 4 h 30 °C). The culture was spun down (4 °C, 6,000 g, 10 min, Sorvall RC5B), resuspended in lysis buffer (20 mM Hepes, 200 mM NaCl, 200 mg/mL lysozyme, 2.5 mM PMSF, 0.1 mg/mL DNase I, pH 8.0) and subjected to sonication (Branson SONIFIER cell disruptor B15, 20% output, 60% duty cycle, two times 5 min). After that, the lysis mixture was centrifuged (35,000 xg, 4 °C, 30 min, Sorvall RC5B). 6 mL Nickel-NTA bead slurry (Machery Nagel) were equilibrated in washing buffer (20 mM Hepes, 200 mM NaCl, 40 mM imidazole, pH 8.0, two times 10 mL), added to the lysis supernatant and incubated for 2h on a rolling device at 4°C. After that, the beads were spun down (100 xg, 2 min, Eppendorf Centrifuge 5804 R), the supernatant was removed, and the beads were washed two times with 30 mL washing buffer. The beads were added to a column (Biorad) and washed again. Elution was performed with elution buffer (20 mM Hepes, 200 mM NaCl, pH 8.0, 300 mM imidazole). Elution progress was monitored via qualitative Bradford assay (5 μ L elution fraction added to 100 μ L 1x Roti®-Nanoquant, C. Roth, in a transparent 96-well plate). Protein-containing fractions were pooled, centrifuged (14,000 xg, 4 °C, 20 min, Eppendorf Centrifuge 5804 R), and the supernatant was subjected to size exclusion chromatography (FPLC buffer: 20 mM Hepes, 20 mM NaCl, 5%(v/v) glycerol, pH 8.0, HiLoad™ 26/600 SuperDex™ 200pg on an ÄKTA Pure chromatography system by GE Healthcare). Resulting protein fractions were quantified, frozen in liquid nitrogen and stored at -80 °C. All buffers used for the purification of MonoCys mutants additionally contained 5 mM DTT.

4.1.2. GST-tagged Proteins

Proteins were expressed in *E.coli* BL21(DE3) cells. All incubation steps were performed at approximately 200 rpm in a heatable shaker. 3 mL LB media and the according antibiotic were inoculated with a scratch of glycerol stock by a steril pipette tipp to obtain the preculture and grown at 37 °C overnight. The next day, 200 mL media + antibiotic were inoculated with 1 mL preculture and

treated similar. 4 L of the main culture were inoculated with 120 mL of the second preculture and distributed into four times 1 L in a 2 L glass Erlenmeyer flask. The cultures were grown to an $OD_{600}=0.5$, induced with 600 μ M IPTG (final) and grown at 15 °C overnight). The culture was spun down (4 °C, 6,000 g, 10 min, Sorvall RC5B), resuspended in lysis buffer (20 mM Hepes, 200 mM NaCl, 200 mg/mL lysozyme, 2.5 mM PMSF, 0.1 mg/mL DNase I, 5mM DTT, pH 8.0) and subjected to sonication (Branson SONIFIER cell disruptor B15, 20% output, 60% duty cycle, two times 5 min). After that, the lysis mixture was centrifuged (35,000 xg, 4 °C, 30 min, Sorvall RC5B). 7 mL Glutathion bead slurry (Glutathion Sepharose 4 FastFlow, GE Healthcare, 17-5132-01) were equilibrated in washing buffer (20 mM Hepes, 200 mM NaCl, 5 mM DTT, pH 8.0, two times 10 mL), added to the lysis supernatant and incubated for 2 h on a rolling device at 4 °C. After that, the beads were spun down (100 xg, 2 min, Eppendorf Centrifuge 5804 R), the supernatant was removed, and the beads were washed two times with 30 mL washing buffer. The beads were added to a column (Biorad) and washed again. Elution was performed with elution buffer (20 mM Hepes, 200 mM NaCl, 5 mM DTT, pH 8.0, 10 mM glutathione). Elution progress was monitored via qualitative Bradford assay (5 μ L elution fraction added to 100 μ L 1x Roti®-Nanoquant, C. Roth, in a transparent 96-well plate). Protein-containing fractions were pooled, centrifuged (14,000 xg, 4 °C, 20 min, Eppendorf Centrifuge 5804 R), and the supernatant was subjected to size exclusion chromatography (FPLC buffer: 20 mM Hepes, 20 mM NaCl, 5% glycerol, 5 mM DTT, pH 8.0, HiLoad™ 26/600 SuperDex™ 200pg on an ÄKTA Pure chromatography system by GE Healthcare). Resulting protein fractions were quantified, frozen in liquid nitrogen and stored at -80 °C. Previous to size exclusion chromatography GST-Rbx1 was digested with TEV-protease to remove the GST-tag (20 U/ μ L = 3.5 μ g/ μ L TEV Protease (MPI for Biochemistry, Munich, Dr. B. Suppmann) added to pooled Elution fractions, incubated at 4 °C overnight).

4.1.3. Protein Labeling

2 mL (up 2.5 mg protein) of FKBP51FK1-MonoCys and FKBP12-MonoCys were dialysed for 5 cycles (approximately 30 min / 1 / 2 / 4 h and overnight) at 4 °C in a Dialyse Slide-A-Lyzer 3.5k MWCO (ThermoFisher) in 20 mM Hepes, 20 mM NaCl, 5%(v/v) glycerol, 10 mM TCEP pH 8.0 with 45 mL buffer per cycle in order to remove DTT. The rebuffed protein was added to 500 μ L equilibrated Ni-NTA slurry (4.1.1). After 2 h, a 20-fold molar excess of fluorescein-maleimide "5-MF" (TRC, F489500) was added and incubated for 2 h. The mix was transferred to a column (Biorad) and washed with buffer (20 mM Hepes, 20 mM NaCl, 5%(v/v) glycerol, pH 8.0, 5 mM DTT) until the flowthrough became colorless. Elution was performed with elution buffer (20 mM Hepes, 200 mM NaCl, pH 8.0, 300 mM imidazole, 5 mM DTT). The elution was ended as the eluate became colorless. In order to remove remaining unreacted fluorescein-maleimide, the first 3 mL of eluted, labeled protein were dialysed for 5 cycles in a Dialyse Slide-A-Lyzer 3.5k MWCO (ThermoFisher, #88403) in 20 mM Hepes, 20 mM NaCl,

5% glycerol, 5 mM DTT as described before. The protein concentration was determined by measuring OD₂₈₀ and OD₄₉₅. Calculation protocol by ThermoFisher:

$$C_{\text{Protein}} = (\text{OD}_{280} - (\text{OD}_{495} * 0,3)) / \epsilon_{\text{Protein}}$$

$$\text{Labeling efficiency} = (\text{OD}_{495} / (\epsilon_{\text{Fluorescein}} * C_{\text{Protein}})); \epsilon_{\text{Fluorescein}} = 68000 \text{ M}^{-1} \text{ cm}^{-1}$$

Washing and elution of FKBP12-MonoCys with 5-MF are visualized in Suppl. Fig. 63.

4.1.4. Activity Assay of Labeled Proteins

Compound FK[4.3.1]-16g [40] (**Figure 8**) was diluted in 15 one-to-one dilution steps ranging from 25 μM to 1.5 nM in DMSO. 1 μL of each dilution step was added to a black 384 well plate (Corning 3575). 50 μL of a 5 nM 5-MF labeled protein dilution in FP-Assay buffer (20 mM Hepes, 0.002% Triton X-100, pH 8.0) were added to each tracer containing well. Fluorescence (Ex: 485 \pm 20 nm, Em: 520 \pm 10 nm) was measured with a Tecan Genios Pro plate reader. Data was processed with GraphPad Prism 6 and curves were fitted via a one-site-ligand depletion curve ($Y = A / E * 0.5 * (X + E + 1 / K - \text{sqrt}(\text{sqrt}(X + E + 1 / K) - 4 * E * X)) + B$).

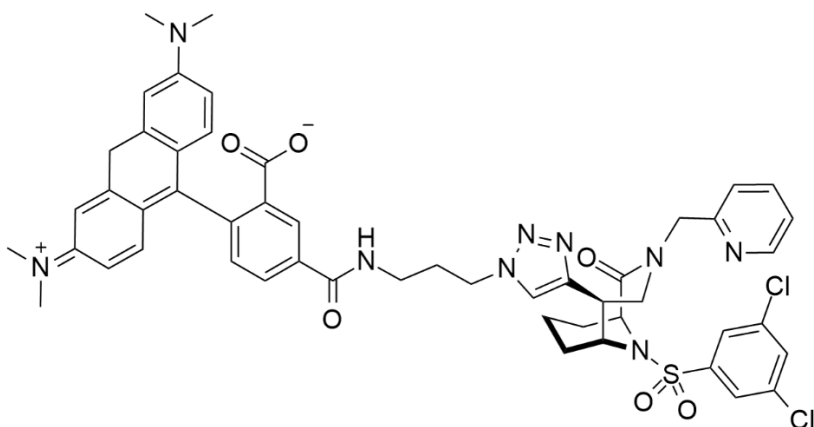


Figure 8 Structure of FK[4.3.1]-16g.

The TAMRA fluorescence was not obtained.

4.1.5. Active Site Titration of FKBP

All unlabeled FKBP have been quantified by active site titration [26]. Proteins were diluted in 15 one-to-one dilution steps in FP-assay buffer and equally mixed with a 100 nM solution of compound FK[4.3.1]-16 g in FP-Assay buffer (20 mM Hepes, 0.002% Triton X-100, pH 8.0) in a black 384 well plate (Corning 3575). Fluorescence polarization was measured with a Tecan Genios Pro plate reader (Ex: 485 \pm 20 nm, Em: 535 \pm 25 nm), plotted against the UV concentration (DevNovix,

D11+Spectrophotometer) and subjected to a four parameter fit using GraphPad Prism6: $Y=Bottom + (Top-Bottom)/(1+10^{((LogIC50-X)*HillSlope)})$. Concentration of active protein was calculated: $c_{AST} = ((0.5 \times c_{Tracer} + K_D) / EC_{50}) \times c_{UV}$.

4.2. HTRF

All components were diluted in HTRF-Assay-Buffer (20 mM Hepes, 20 mM NaCl, 5% Glycerol, 10 mM DTT, pH 8.0). The assay mix consists of four fractions of equal volume: binding partner I and II, Tb – cryptate coupled antibody and competitor. Therefore, 4x predilutions dilutions of all fractions were prepared (if not indicated differently) in low binding tubes: 120 nM Glmn-GST, 120 nM FKBP51FK1MonoCys-5MF, 40 ng /well Mab Anti GST-Tb cryptate monoclonal antibody (Cisbio) (approximate final concentration of 0.8 nM) and competitor as indicated. FKBP51FK1MonoCys-5MF, competitor and Glmn-GST (each 20 μ L) were pre-incubated in a 384 well plate for 1 h at RT. Mab Anti GST-Tb cryptate (20 μ L) was added and incubated for 2 h at. Fluorescence at Em: 340 \pm 10 nm / Ex: 520 \pm 10 nm and Em: 340 \pm 10 nm / Ex 620 \pm 10 nm was measured sequentially for all wells in a Tecan Genios Pro Reader. The 520 nm signal of each well was normalized over its corresponding 620 nm signal. All assays were measured with the “Gain Optimal” setting, potentially leading to variations of absolute fluorescence values in between separate assays. Data was processed with GraphPad Prism6 and competition curves fitted using a four parameter fit: $Y=Bottom + (Top-Bottom)/(1+10^{((LogIC50-X)*HillSlope)})$

4.3. Cell Culture

All incubation steps took place in a HERAcell 160vi (ThermoFisher) at 37 °C and 5% CO₂, if not indicated differently. All media and reagents are listed in section 3.14. All work was performed using sterility guidelines. Cell culturing and cellular assays were generally accompanied by the observation of the cells via light microscopy to assure confluency, cell shape, surface effects and the absence of contaminations. The adherent cell lines Neura2a (N2a), HEK293T and HeLa as well as Jurkat cells, which grow in suspension were used. Protocol deviations for Jurkat cells are described in 4.3.5.

4.3.1. Growth Conditions and Passaging

Cells were grown in 10 cm TC-dishes for 3 to 5 days. After that, the cell culture media was aspirated and the cells were washed with 5 mL PBS. 1 mL of prewarmed Trypsin-EDTA solution was added and equally distributed on the surface. The dish was placed in the incubator for 5 min. Cells were removed from the surface by resuspension in 5 mL culture media and spun down for 2 min at 1000 rpm. The supernatant was removed and cells were resuspended with 5 mL culture growth media. For cells of 80

– 95% confluency, 250 μ L of this suspension were added to 10 mL cell culture media in a fresh plate (1 to 20 passage).

4.3.2. Surface Coating

If indicated, cell culture dishes and multiwell plates used for assays were coated with poly-L-Lysine (PLL, 0.002%(v/v), 1:50 dilution in water). Half of the volume of the recommended culture volume was added to each cavity and placed in the incubator for 2 h up to 24 h. Afterwards, the solution was removed and all cavities were washed with an equal amount of water. Plates were dried in a sterile bank for 1 h and stored tape sealed at 4 °C until usage. Surface coating was performed for all cell culture assay experiments such as PROTAC treatment and reporter gene assays and to culture N2a and MEF cells.

4.3.3. Storage

In order to store cells, they were resuspended after passaging in cell culture media containing 10% (v/v) sterile filtered DMSO. The suspension was added to Cryo Pure tubes (Sarstedt, 72.379) and frozen to -80 °C in Cryo 1 °C Freezing Container (NALGENE). After 1 day, the tubes were transferred to a liquid nitrogen container (Locator 5 Plus, Thermo Scientific). In order to regain fresh cells, a 10 cm petri dish was filled with 20 mL media. An aliquoted cryotube of cells was removed from the liquid nitrogen tank and thawed in a 37 °C warm water bath under mild shaking. Cell suspension was then added to the prepared petri dish. After one day the media was exchanged and on the second day, cell passaged. Usually 30 to 100% of the cells were reseeded at this point, depending on their confluency.

4.3.4. Cell Counting

As the cells were passaged in order to transfer them to any assay, they were counted after resuspension. For this, 10 μ L of cells and 10 μ L Trypan Blue solution were mixed in a tube. 10 μ L were then transferred to a Neubauer Counting Chamber (Marienfeld). All non-blue cells in the four major quadrants were counted. Cell count in resuspension was calculated: 1 Neubauer count \approx 5,000 cells / mL in the primary resuspension.

4.3.5. Jurkat Cell Culture

Jurkat cells are a non-adherent T lymphocyte cell line. They are cultured in RPMI 1640 media, supplemented with 10% FBS. Passaging was performed by simply transferring 10% of the current

passage and add it to fresh media. In reporter gene assays non-coated, V-shaped well 96well plates were used. Each step, which required exchange of media, was preceded by a centrifugation step (1000 rpm, 2 min) and followed by mildly tapping the plate to assure resuspension. A successful centrifugation and resuspension of Jurkat cells in V-shaped wells can be monitored via light microscopy.

4.4. Reporter Gene Assays

4.4.1. Glucocorticoid Receptor Signaling

Reporter gene assays were performed using media without phenol red and with 10% charcoal stripped FCS. 10,000 cells in media were seeded into a PLL-coated 96 well plate in a volume of 50 μ L/well. Plates were incubated for 24 h. The transfection mix was prepared according to Lipofectamine 2000 (Invitrogen) protocol: Plasmids (solved in sterile water) were diluted in Opti-MEM (45 ng/well pGRE4Luc2P, 5 ng/well pGL4.74, 0.5 ng/well HA-GR, different amounts of FKBP51, FKBP52 and Glmn). Maximum transfection doses varied from assay to assay but were equalized within an assay by the addition of mock plasmid (pRK5). Transfection doses always remained beneath 100 ng/well as recommended. A 1.67% (v/v) dilution of Lipofectamine in Opti-MEM was prepared and incubated for 5 min at RT. After that, both Lipofectamine 2000 and plasmid dilutions were mixed equally and incubated for 20 to 25 min at RT. During that time, media was removed from the seeded cells and 80 μ L of fresh media were added to each well. 20 μ L of the final transfection mix were added to each well and the cells were incubated for 24 h. After that, each well was washed once with 50 μ L media and 50 μ L media were added to the wells. An incubation period of 30 to 60 min followed. Consecutively, the cells were treated with small molecules, which were added in a volume of 50 μ L solved in media (4x concentration of the final concentration). All used compounds were dissolved and prediluted in sterile DMSO and the final DMSO content of the cell culture media remained below 0.2%. Treatment time extended up to 24 h. After that, the stimulation mix in a volume of 100 μ L was added on top. This mix consisted of Dexamethasone dissolved and prediluted in sterile DMSO, diluted in cell culture media to a final concentration ranging from 0 to 100 nM. Here as well, the DMSO content in the cell culture media did not exceed 0.2% (v/v). Stimulation time extended up to 24 h. Subsequently, the cells were washed with 100 μ L/well cold PBS and lysed in 50 μ L 1x "Passive Lysis Buffer" (Promega, E1910) on ice for 30 min. The plates with lysed cells were stored at - 20 °C.

Preceding measurement, plates were thawed and 20 μ L lysate of each well transferred to a white 96-well half-area plate (Greiner bio-one, 392-0287). Measurement buffers were prepared as published in "A protocol for combined Photinus and Renilla luciferase quantification compatible with protein assays" by Hampf, M. and Gossen, M., *Anal Biochem*, **2006** [137]. Measurement was performed with a Berthold TriStar² LB 942 (indicated in figure description) or a Tecan Infinite M1000 connected to a dual injection

module. Both lines were washed with 80% EtOH and water and primed with 0.5 mL of the corresponding substrate solution. 20 μ L of firefly luciferase substrate solution (Photinus Buffer: 200 mM Tris-HCl, 15 mM MgSO₄, 0.1 mM EDTA, pH 8, plus freshly added: 25 mM DTT, 1 mM ATP, 0.2 mM CoA, 0.2 mM Luciferin) were injected to one well (speed: 200 μ L/s) and luminescence measured for 5 s after a delay of 2 s. Afterwards, the same procedure was repeated in the same well with the gaussia substrate solution (Renilla Buffer: 25 mM Na₄PP_i, 10 mM NaOAc, 15 mM EDTA, 500 mM Na₂SO₄, 500 mM NaCl, pH 5, plus freshly added: 4 μ M benzylcoelenterazine, 50 μ L 4-(6-methylbenzothiazol-2-yl)-aniline). Both buffers were prepared and stored at 4 °C without the components indicated as “freshly”. After the measurement of a single well, the measurement proceeded to the next well. Data were processed as following: 1) Normalization of the firefly signal over the gaussia signal. 2) Averaging the quadruplicate or hexaplicate values of firefly, gaussia and normalized signal and calculation of the standard error of the mean using excel. Data was transferred to GraphPad Prism6 and graphically edited.

4.4.2. NF- κ B-Signaling

Reporter gene assays measuring the reporter activity of NF- κ B-plasmids were generally performed in a similar fashion as GR reporter gene assays. Instead of pGRE4luc2P, the reporter plasmids p1242 for the canonical pathway and pNF- κ B2 for the non-canonical NF- κ B pathway were used at the concentration of 45 ng/well. A GR expression plasmid was not transfected. No experiment with ligand treatment was performed. Therefore, 24 h transfections were directly followed by stimulation with TNF α or PMA (phorbol 12-myristate 13-acetate) for 20 h. The stimulants were used up to a concentration of 20 ng/ μ L for TNF α (stock dissolved in sterile PBS with 0.1% BSA) and 80 nM for PMA (stock dissolved sterile DMSO). For concentration equal and greater than 40 nM PMA massive cell death was observed (HEK293T and A375). Up to 15 nM PMA cells appeared to be fine in light microscopic observation.

4.5. PROTAC Treatment of Cells

Cells were seeded at a concentration of 35,000 per well in a 24 well TC-plate and incubated for 24 h. Medium was removed and 250 μ L fresh medium were added to each well. PROTACs (Stock 1 to 5 mM in DMSO) were diluted in medium at 2x concentration. Usually a 1:1 dilution series was performed in DMSO containing medium to achieve a constant final DMSO content of 0.2% (v/v). 250 μ L of the respective dilution was added to the according wells and incubated for the indicated time. After that, cells were lysed.

4.6. Cell Lysis

To analyse expression levels of certain cellular proteins, medium was removed and cells were washed with 4 °C cold PBS: 50 µL for reporter gene assay in 96 well format, 1 mL for a PROTAC in 24 well format. Then an appropriate amount (e.g. 70 µL for a single well of a 24 well plate) of NETN buffer (100 mM NaCl, 20 mM Tris-Cl pH 8.0, 0.5 mM EDTA, 0.5% (v/v) Nonidet P-40 (NP-40), 1% Protease inhibitor, 1 mM PMSF) was added. Cell plates were incubated for at least 30 min on ice on a shaking device. Cells were scratched off with a bended 100 µL pipette tipp (1 per well) and the fluid suspension was transferred to an Eppendorf tube. Lysates were centrifuged for 20 min at 16,000 xg at 4 °C (Eppendorf Centrifuge 5804 R) and the supernatants transferred to a fresh tube.

4.7. Protein Quantification via BCA Assay

In order to quantify protein amounts via Western Blot detection, the total protein content of lysates was normalized. The relative quantity of protein was obtained using a Pierce® BCA Protein Assay Kit (Thermo Scientific, 23227). 5 µL of centrifuged lysate sample were added to a transparent 96 well plate and 100 µL BCA reagent mix added. The plate was closed with a lid and incubated at 37 °C in a water bath above the water level for 30 min. The bottom of the plate was dried. The absorbance of each well at 590±20 nm was measured with a Tecan Genios Pro device. Data was processed using Excel. All samples which were going to be added to the same SDS-gel were normalized to an equal total protein concentration with 4xLämmli buffer of the sample of the least protein content: 15 µL of lysate mixed with at least 15 µL 4xLämmli buffer.

4.8. SDS-PAGE

SDS-PAGEs were performed using 1.0 mm disposable cassettes (Novex, NC2010) and mini gel tanks (Invitrogen by Thermo Fisher Scientific). In order to cast two gels, the separation gel was prepared as following:

Amounts in mL	8%	10%	12%	14%	16%
Acrylamide / Bisacrylamide 30% / 0.6%	3.80	4.75	5.70	6.65	7.60
Aqua dest.	4.87	3.92	2.97	2.02	1.07

Table 1 Variable components of acrylamide gels. Values are not rounded, since often a multitude of those amounts were calculated and pipetted

Independent of the acrylamide concentration: 5.34 mL 1 M Tris pH 8.8, 140 μ L 10% SDS, 84 μ L 10% APS, 17 μ L TEMED. The mixture was poured into the cassettes (filling 3 / 4) and was overlaid with ca. 250 μ L isopropanol. After polymerization, isopropanol was poured out and collection gel filled in to the top (for three gels: 5 mL stacking gel buffer containing, 25 μ L 10% APS, 10 μ L TEMED).

Stacking Gel Buffer (250 mL): 44 mL Acrylamide /Bisacrylamide 30% / 0,6%, 188.5 mL aqua dest, 15 mL 1 M Tris-HCl pH 6.8, 2.5 mL 10% SDS.

Gel combs were added right afterwards. After polymerization, gels were stored wrapped in wet tissue at in a plastic back at 4 °C.

Protein samples were prepared with at least 25% 4xLämmli (amounts vary, especially since Lämmli buffer was used to normalize protein concentration) and boiled at 96 °C for at least 5 min. 1 L 4xLämmli buffer contains: 80 g SDS, 320 mL, 1 M Tris pH 6.8, 400 mL glycerol, 400 mg brom phenol blue, aqua dest add 1 L. Before usage 14 μ L β -Mercaptoethanol were added per 1 mL Lämmli. Afterwards, the samples were spun down (13.000 rpm, 3 min) and added to the gel (3 to 15 μ L). 3 μ L marker solution were used (Page Ruler™, Prestained Protein Ladder, Thermo Scientific, #26616).

Gels were run at 15 / 25 mA for the stacking phase and 25 / 45 mA for the separation phase, depending if one or two gels were loaded in a tank module using 1x SDS-Page buffer (500 mL 10x buffer contain: 15 g Tris base, 72 g glycin, 5 g SDS, pH 8.3, in aqua dest). SDS-Pages performed for protein level quantification to analyse chemical knockdown by PROTACs were loaded with equal sample volume (15 μ L) of equal total protein concentration.

4.9. Coomassie Staining and Gel Drying

SDS-page gels, which were not transferred for Western Blotting, were stained in Coomassie stainer (40% v/v ethanol, 10% v/v acetic acid, 1 g/L Coomassie Brilliant Blue R250) for at least 15 min. Destaining was performed in two steps: 1) at least 30 min in destaining solution (40% v/v ethanol, 10% v/v acetic acid) and 2) in water at 4 °C overnight. Additional steps in either liquid could be added for optimized contrast. Subsequently, gels were dried for at least two days in cellophane using a gel drying frame.

4.10. Western Blotting

Western blot sandwiches consisting of sponge, whatman paper, SDS-gel, nitrocellulose membrane, whatman paper and another sponge were prepared. All components were previously soaked in western blot buffer (1x SDS buffer, 20% (v/v) EtOH). The blotting sandwich was transferred to a blotting chamber and added to a mini gel tank (Invitrogen, various models). Transfer was performed at 30 V for one and

60 V for two sandwiches per chamber for 75 min. Afterwards, the nitrocellulose membrane was stained with Ponceau S solution (0.1%(w/v) Ponceau S in 5%(v/v) acetic acid) to verify transfer and subsequently destained in water. The membrane was blocked in 5% skimmed milk in TBS (50 mM Tris, 150 mM NaCl, pH 7.4) for at least 30 min. The membranes were incubated with the primary antibody in the indicated dilution overnight at 4°C on a rolling device. Afterwards, the membrane was washed in TBS, TBS-T (0.1% Tween-20 added) and TBS for 5 min each under mild, constant swiveling. The membrane was added to the secondary antibody dilution and incubated for at least 1 h at room temperature on a rolling device. Washing procedure was repeated similarly. A mixture of equal parts HRP substrate solutions (“Immobilon Western”, Millipore) was prepared, added to the membrane placed in a transparent foil, equally distributed and measured until a decent chemiluminescence signal was detected (LAS-3000, Fujifilm).

4.11. Westen Blot Data ProceSSION for Signal Strength Analysis

This procedure was developed by Thomas Geiger, during his research internship under my supervision in order to analyse chemiluminescence signals for chemical knockdown by PROTACs.

Images of the blots were (colour) inverted using Paint (Version 1803). Afterwards, the FKBP51 and GAPDH band intensities were quantified using the “Analyze” tool of ImageJ. The area of interest was constant for all protein bands. The intensity of the FKBP51 band was normalized by the corresponding GAPDH intensities. The normalized intensities were divided by the normalized intensity of the according DMSO control (DMSO value is set to 1). This value indicates the endogenous FKBP51 level relative to the DMSO control. Data was processed using GraphPad Prism6.

4.12. Degradation of Nanoluc-tagged FKBP51

10,000 cells in media were seeded into each well of a polylysine coated 96 well plate in a volume of 50 µL each. Plates were incubated for 24 h. The transfection mix was prepared according to the Lipofectamine 2000 (Invitrogen) protocol. Transfection was performed as described in 4.4 Reporter Gene Assays with HG 680 (*N*-terminally Nanoluc tagged FKBP51) in amounts indicated in the experiment. At the end of the transfection, the supernatant of each well was removed and fresh 50 µL media were added per well. Consecutively, the cells were treated with small molecules, which were added in a volume of 50 µL dissolved in media (2x concentration of the final concentration). All used compounds were dissolved and prediluted in sterile DMSO and the final DMSO content of the cell culture media remained below 0.2%. Treatment time extended up to 24 h. Subsequently, the cells were washed with 100 µL/well cold PBS and lysed in 50 µL 1x “Passive Lysis Buffer” (Promega, E1910) on ice for 30 min. The plates with lysed cells were stored at - 20 °C.

Preceding readout measurement, plates were thawed and 20 μ L lysate of each well were transferred to a white 96-well half-area plate (Greiner bio-one, 392-0287). Nano-Glo[®] Luciferase Assay (Promega, N1120) was prepared by adding 45 μ L substrate to 2250 μ L assay buffer and 2250 μ L PBS. 20 μ L of this mixture were added to each lysate-containing well using a dispenser. These plates were incubated for 5 min at RT and measured in a Tecan Genius Pro (automatic signal reduction mode). Obtained data was processed using GraphPad Prism6.

4.13. Calcium Influx Assays

Calcium Influx Assays were performed using a Fluo-4 Direct Calcium Assay Kit (Invitrogen, F14201, containing assay buffer, calcium reagent and probenecid). In preparation one vial probenecid (77 mg) was dissolved in 1 mL assay buffer to obtain a 250 mM stock solution. The 2x calcium loading solution consisted of 10 mL assay buffer and 200 μ L probenecid added to one bottle of calcium reagent. Cells were seeded at a density of 80,000 cells per 50 μ L per well in a black 96 well plate with transparent bottom (655090) if no transfection step is indicated and 40,000 cells, if a transfection was performed prior to measurement. Transfection was performed as described in 4.4 Reporter Gene Assays with the plasmids indicated in the experiments. Cells were allowed to attach for 24 h. Afterwards, the assay was performed under non-tissue culture conditions and the bottom of the plate sealed with adhesive black light-absorbing film. 50 μ L of 2x calcium loading solution were added to each well and incubated 30 to 60 min at 37° C for dye loading. After that time, plates were kept at room temperature until measurement (Kit protocol notes assay stability up to 4 h at RT). Stimulation solutions containing OAG, Carbachol, Hyperforin, Hyp1 (stocks prepared in DMSO under excess of light) or DMSO were prepared in assay buffer. ATP served as positive control and was prepared as 10 mM stock in water. The Berthold TriStar² LB 942 injectors were primed with the solutions. The background of each well was measured (RLU₀). 50 μ L were injected into three adjacent wells (medium speed setting). Plate was shaken by the device for 2 s. The wells were measured for up to 200 s, Ex: 530 \pm 15 nm and Em: 585 \pm 15 nm. Data was processed with SigmaPlot 11 and the fluorescence intensity (RLU) was corrected by the well background plotted against the time.

5. Results

5.1. FKBP51 PROTACs

Thus far, several series of PROTACs aimed to target endogenous FKBP51 were generated in the Hausch lab. Out of these, 62 different compounds [PhD Thesis Mao Tianqi] were tested in several cell lines (HeLa, HEK293T, N2a) and the levels of FKBP51 have been monitored via Western Blotting (**Table 2**). Yannick Kristiansen and Thomas Geiger contributed to this project as students under my supervision. The experiments performed by them are labeled with “Lab book: YK #” and “Lab book: TGe #”.

Linker Length	SAFit based structure			Bicyclic structure			
1	199	328	338	498	508	518	VHL
2	200	329	339	499	509	519	
3	201	330	340	500	510	520	
4	202 / 416	331	341	501	511	521	
5	203	332	342	502	512	522	
0	229						CRBN
1	204	333	343	503	513	523	
2	205	334	344	504	514	524	
3	206	335	345	505	515	525	
4	207	336	346	506	516	526	
5	208	337	347	507	517	527	
0	235						
Attachment Point	1	2	3	Substituent	none	X	Y

Table 2 Overview of tested PROTACs. PROTACs are named as their respective "MTQ" number according to the following features: 1) SAFit-like or bicyclic structure, 2) linker length, 3) attachment point or substituent and 4) targeted E3 ligase (VHL or CRBN)

5.1.1. Endogenous FKBP51

The expression of GAPDH usually served as reference. Among the tested PROTACs only MTQ202 and its second batch MTQ416 robustly decreased levels of FKBP51. The structure of this PROTAC is depicted in Suppl. Fig. 61. Western Blot figures of all other PROTACs can be found in 7.1. The PROTAC MTQ202 was able to knockdown the levels of FKBP51 in HEK293 cells after 24 h with maximum efficacy with concentration ranges between 63 and 500 nM (Figure 9).

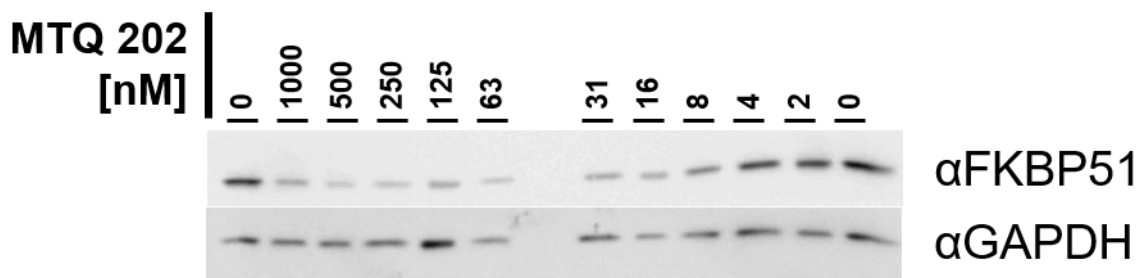


Figure 9 Incubation of HEK293T cells with the PROTAC MTQ202, 35,000 cells per well in a 24 well format. Upper blot: Endogeneous FKBP51. Lower blot: GAPDH. Cells are treated with the compound for 24 h before lysis. All samples have exposed to a constant DMSO concentration. Lysate protein concentration was quantified via BCA assay and normalized with Lämmli buffer. Equal amounts of total protein were subjected to SDS-Page and Western Blot afterwards. Lab book: TGe13

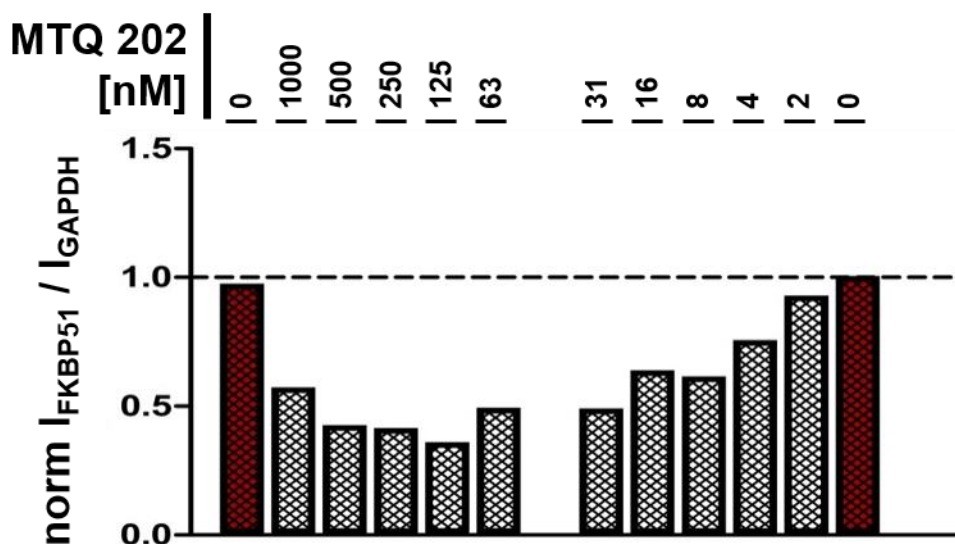


Figure 10 Quantification of Figure 9. Normalized Intensities of FKBP51 over GAPDH signal. Ration of the last lane (DMSO control) is set to 1. Intensities were analyzed using ImageJ. Masterthesis TGe

The quantification of the same blot shows that FKBP51 levels go down to 40% (**Figure 10**)

The very same compound is also active in HeLa cells with minimum FKBP51 concentrations after 24h of 250 nM (**Figure 11**). Since the antibody used for FKBP51 detection showed clearer signals in HEK293 lysats compared to HeLa cell lysats, I mainly focused on that cell line. The antibody was not reactive to mouse derived cell lines such as Neuro2a and MEF.

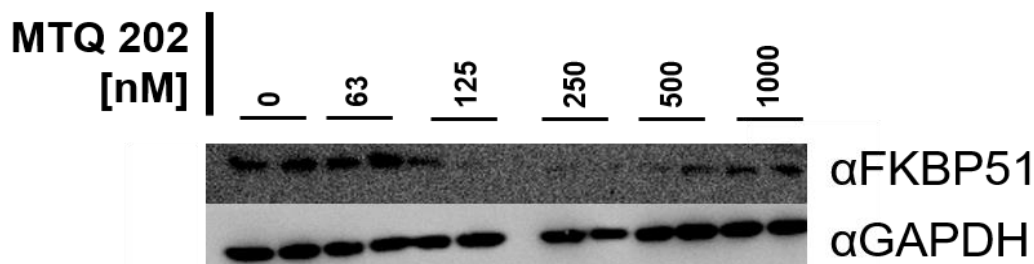


Figure 11 Incubation of HeLa cells with the PROTAC MTQ202. 35,000 cells per well in a 24 well format. Upper blot: Endogeneous FKBP51. Lower blot: GAPDH. Cells are treated with the compound for 24 h before lysis. All samples have exposed to a constant DMSO concentration. Lysate protein concentration was quantified via BCA assay and normalized with Lämmli buffer. Equal amounts of total protein were subjected to SDS-Page and Western Blot afterwards. This blot shows duplicates. Lab book: AHa388

During the course of this thesis, a second batch of MTQ202, MTQ416, was synthesized. This batch was tested as well and showed a strong chemical knockdown of FKBP51 after 48 h incubation in the range of 60 and 1000 nM (**Figure 12**).

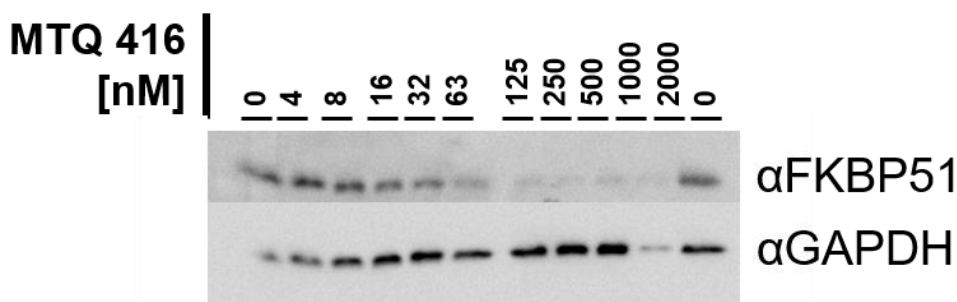


Figure 12 Incubation of HEK293T cells with the PROTAC MTQ416. 35,000 cells per well in a 24 well format. Upper blot: Endogeneous FKBP51. Lower blot: GAPDH. Cells are treated with the compound for 48 h before lysis. All samples have exposed to a constant DMSO concentration. Lysate protein concentration was quantified via BCA assay and normalized with Lämmli buffer. Equal amounts of total protein were subjected to SDS-Page and Western Blot afterwards. This blot shows duplicates. Lab book: AHa456

To elucidate the time course of the chemical knockdown of MTQ202, a similar experiment was performed on several plates which were incubated with the PROTAC (**Figure 14**) or DMSO (**Figure 13**) for the indicated time prior to lysis.

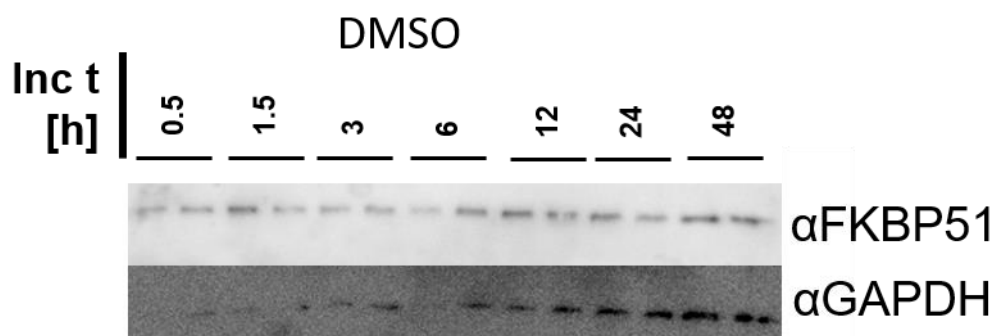


Figure 13 Incubation of HEK293T cells with DMSO. 35,000 cells per well in a 24 well format. Upper blot: Endogeneous FKBP51. Lower blot: GAPDH. Cells were seeded in separate 24well plates and treated with DMSO containing media. Cells were lysed after indicated incubation time ranging from 30 min to 48 h. Experiment shows duplicates for each point of time. Although there is an instable GAPDH signal, no effect of DMSO was observable in other experiments for the time points of 24 and 48 h. Lab book: AHa428.

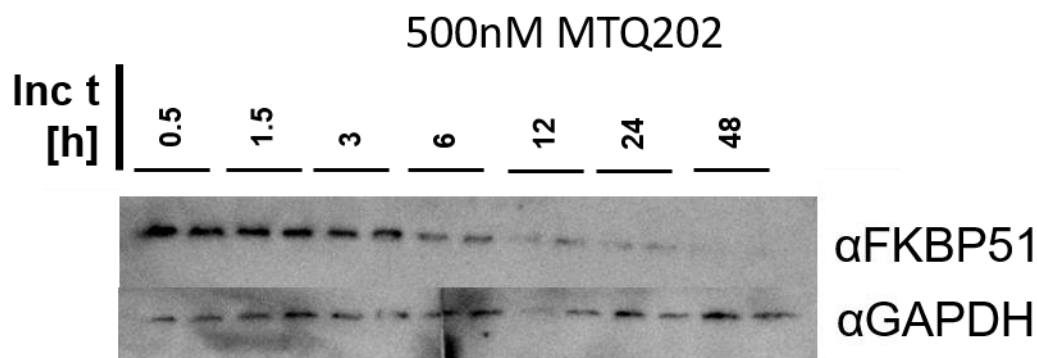


Figure 14 Incubation of HEK293T cells with the PROTAC MTQ202. 35,000 cells per well in a 24 well format. Upper blot: Endogeneous FKBP51. Lower blot: GAPDH. Cells were seeded in separate 24 well plates and treated with DMSO containing media. Cells were lysed after indicated incubation time ranging from 30 min to 48 h. Experiment shows duplicates for each point of time. While the FKBP51 signal gradually decreases over time, the GAPDH signal remains rather stable. Lab book: AHa428.

MTQ202 continuously decreases the levels of FKBP51 for up to 48h, while the DMSO control showed no effect over time. Although many PROTACs show a limited action window for intracellular chemical knockdown, MTQ202 remained active for 48 h.

In order to obtain more information on the the PROTACs activity time course, a lower amount of cells was seeded and incubated with MTQ416 up 72 h. After 24 h incubation, the media was exchanged in some wells to provide a PROTAC-free growth environment. 24 h incubation without PROTAC led to a recovery of the FKBP51 signal (**Figure 15**).

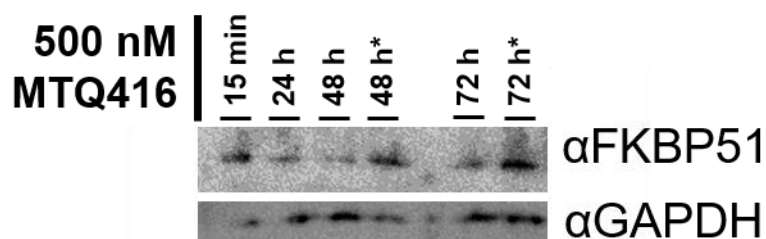


Figure 15 Incubation of HEK293T cells with the PROTAC MTQ416. 15,000 cells per well in a 24 well format. Upper blot: Endogeneous FKBP51. Lower blot: GAPDH. Cells were seeded in separate 24 well plates (one per point of time) and treated with media containing 500 nM MTQ416. Cells were lysed after indicated incubation time ranging from 15 min to 72 h. For some wells liquid was exchanged after 24 h with compound free media, indicated with a *. The FKBP51 signal decreased for 24 / 48 and 72 h, while media exchange leads to signal recovery. The GAPDH signal fluctuates. The quality of these blots are low due to low protein amount loaded. Protein concentrations were normalized to the first sample (15,000 cells, which grew for 24 h, instead of 35,000 cells growing for usually at least 48 h. Lab book: AHa490.

Finally, a competition experiment was performed to investigate the chemical knockdown effect of MTQ416 in presence of either 2 μ M SAFit1 or 2 μ M VHL-ligand (Protein degrader 1 hydrochloride, dissolved in DMSO + 10% water). In the 24 h incubation blot the presence of both ligands seem to increase FKBP51 levels. At least for SAFit1 also GAPDH gives a stronger signal indicating a higher protein load for this sample. The FKBP51 levels after 48 h remain unaffected, neither did they dampen the chemical knockdown by MTQ416. Due to solubility limitations, an 8-fold excess of competitor (250 nM vs. 2 μ M) was the highest possible (**Figure 16**).

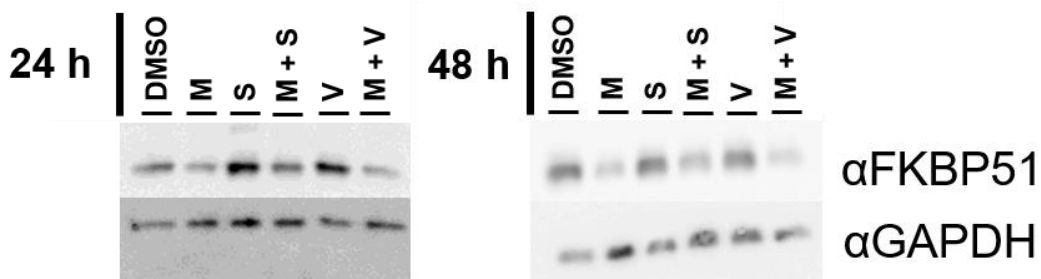


Figure 16 Incubation of HEK293T cells with the PROTAC MTQ416 (M), SAFit1/THe10 (S) or VHL-ligand (V). 35,000 cells per well in a one 24 well format. Upper blot: Endogeneous FKBP51. Lower blot: GAPDH. Cells were seeded in separate

24 well plates (one per point of time) and treated with media containing either 250 nM MTQ416, 2 μ M SAFit1 or 2 μ M VHL-ligand. Cells were lysed after indicated incubation time of either 24 or 48 h. All samples containing the PROTAC show a decreased FKBP51 signal independent of the presence of SAFit1 or VHL-ligand. SAFit1 and VHL-ligand alone have no impact on FKBP51 levels. The GAPDH signal is rather stable. Lab book: AHa491.

5.1.2. Exogenous FKBP51

The detection of endogenous FKBP51 was limited to human FKBP51. Other antibodies tested showed no reactivity towards mouse FKBP51 (data not shown, AHa375, AHa384). MTQ202 was capable to both knock-down mouse FKBP51 with a C-terminal HA-tag transfected in HeLa cells (**Figure 17**) and human FKBP51 with a N-terminal HA-tag in murine N2a cells (**Figure 18**).

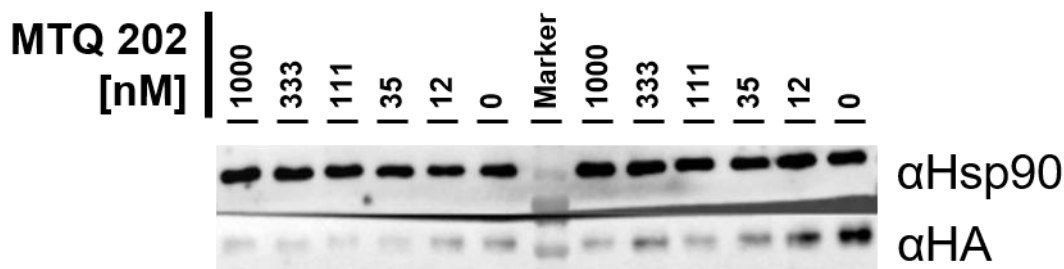


Figure 17 Incubation of HeLa cells with the PROTAC MTQ202. 35,000 cells per well in a 24 well format and transfected with 100 ng/well mouse FKBP51-HA (HG498) for 24 h. Upper blot: Hsp90. Lower blot: HA-tag. Cells were seeded in separate 24 well plates and treated with DMSO containing media. Cells were lysed after 24 h. Experiment shows duplicates for each concentration. While the FKBP51 signal gradually decreases over time, the Hsp90 signal remains stable. Lab book: YK Bachelorthesis

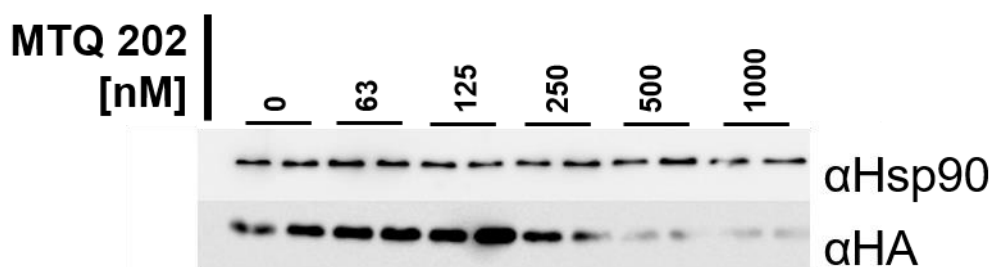


Figure 18 Incubation of murine N2a cells with the PROTAC MTQ202. 35,000 cells per well in a 24 well format and transfected with 100 ng/well human HA-FKBP51 (HG490). Upper blot: Hsp90. Lower blot: HA-tag. Cells were seeded in separate 24 well plates and treated with DMSO containing media. Cells were lysed after 24 h. Experiment shows duplicates for each concentration. While the FKBP51 signal gradually decreases over time, the Hsp90 signal remains stable. Lab book: AHa380

5.1.3. Degradation of Nanoluc-FKBP51

The screening of the PROTAC library via Western Blot required a high work and time load. In a side-project a screening method was investigated featuring a higher throughput. In order to do so, HEK293T and N2a cells were seeded in a 96 well plate and transfected with an N-terminally Nanoluc®-tagged FKBP51 expression construct (HG 680). Transfected cells were treated with MTQ202 and the luciferase activity was read out after lysis. It was assumed that degradation of FKBP51 by MTQ202 also leads to degradation of the Nanoluc tag. It could be shown that, MTQ202 was capable to reduce luciferase

signal for the transfection amount of 1 ng/w HG 680 (**Figure 19**). Increasing amounts of transfected plasmid increased general signal strength from 10^4 RLU background to 10^8 for 10 ng/w. While no clear trend can be observed for 0 and 10 ng/w, the signal reduces with increasing amounts of MTQ202 on both cell lines by approximately 50% (125 nM for N2a and 500 to 1000 nM for HEK293T cells). The competition of 1000 nM MTQ202 with 1000 nM SAFit1 (MB53) did not lead to a significant change of the signal, likely because the lower plateau was already reached. High amounts of transfected plasmid could lead to an unaffected signal due to high expression levels.

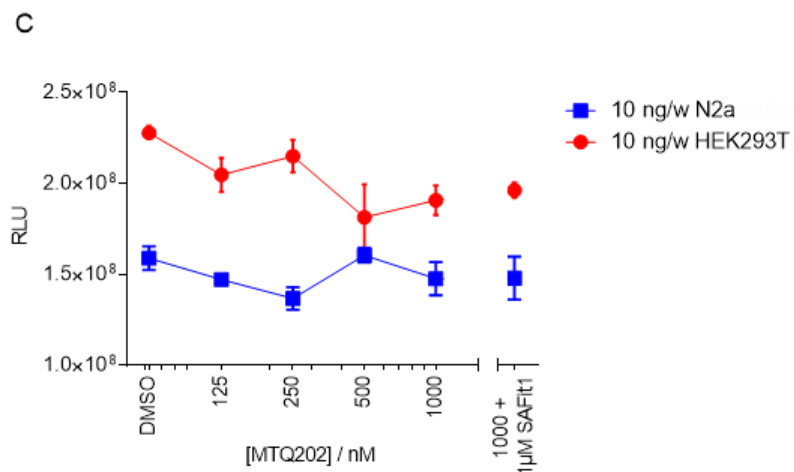
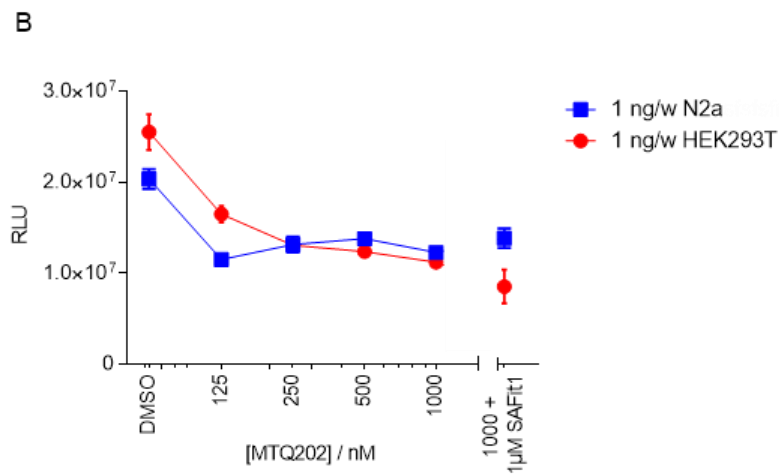
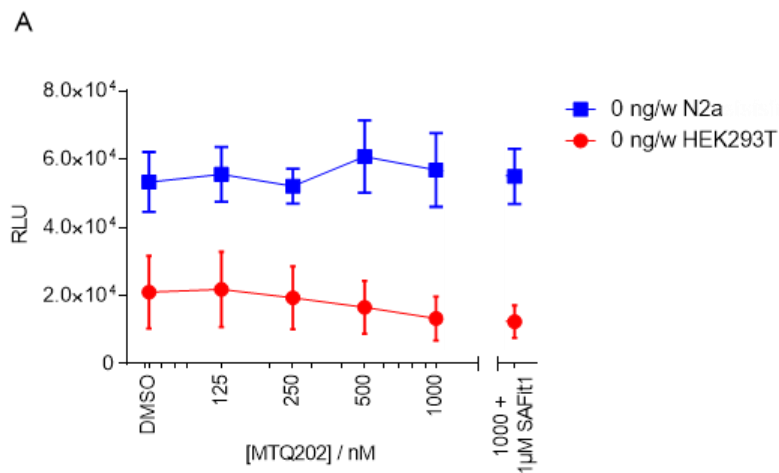


Figure 19 HEK293T (red) and N2a (blue) cells transfected with 0 (A), 1 (B) or 10 ng/w HG680 and treated with MTQ202.

10,000 cells were seeded in a 96 well plate, settled for 24

This assay system has not been persuaded further.

5.2. FKBP51 in reporter gene assays

5.2.1. Assay Setup

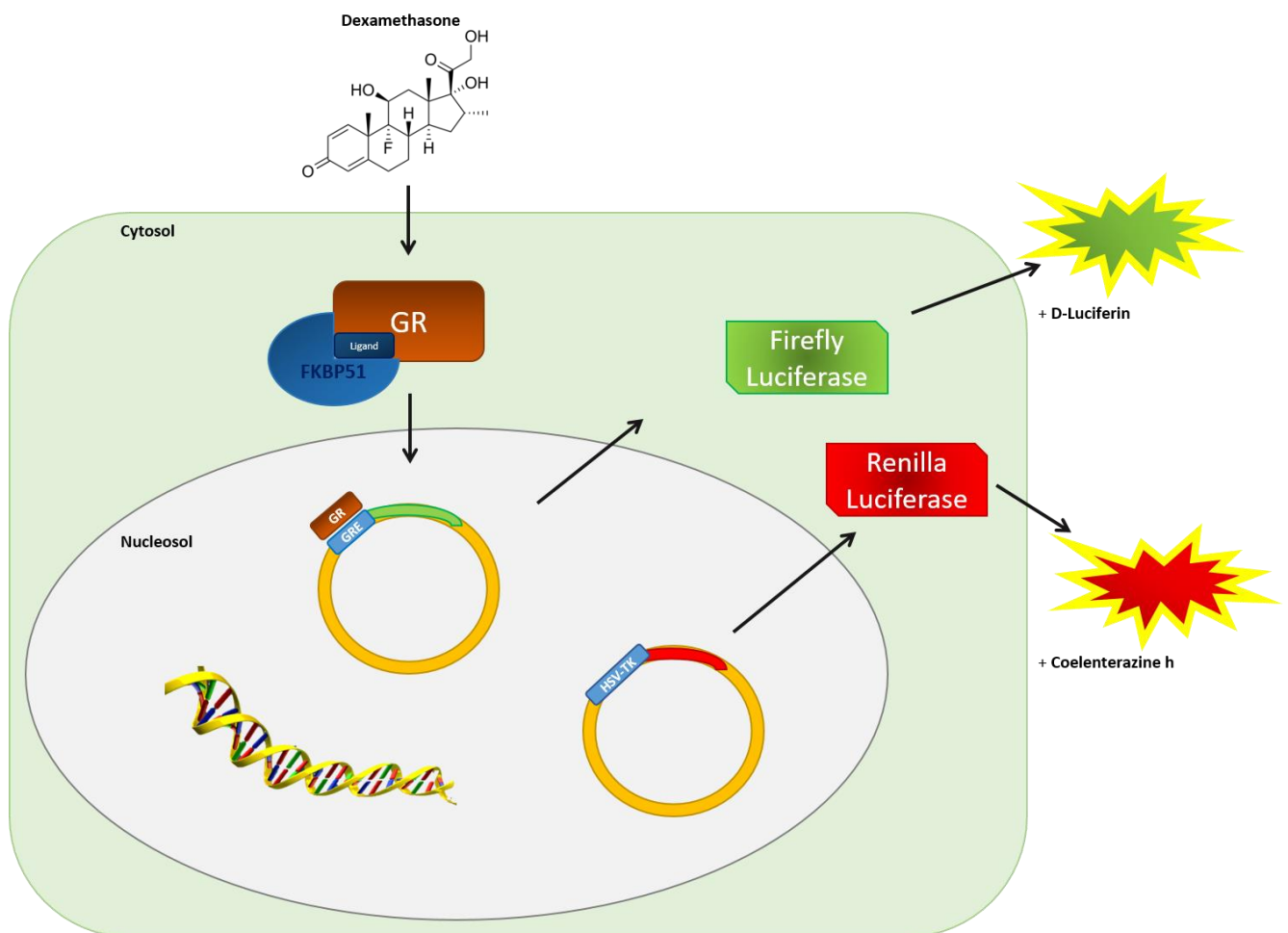


Figure 20 Working principle of the GR reporter gene assay used here. Cell, which are exogenously transfected with a mix of plasmids including two reporters as well as GR and FKBP51 expression plasmids are stimulated with dexamethasone. The reporter plasmid containing GREs (triple tandem repeat) is expressed upon GR activation. The amount of transcribed firefly luciferase depends on the GR signaling strength, which might be impacted by the amount of FKBP51 present and potentially by FKBP ligands. The second reporter transcribes renilla luciferase and is neither activated nor repressed by GR, FKBP51 or ligands (herpes simplex virus thymidine kinase promoter – HSV-TK). Its expression levels serve as signal normalization tool. The GR is stimulated by Dexamethasone, inducing a reporter plasmid expressing the firefly luciferase. This induction might be dependent on the levels of FKBP51 present and its ligands. A second plasmid, expressing the Renilla luciferase is independent of external stimuli. The expression strength of both luciferases can be read out independently by the addition of their respective substrates and the measurement of the resulting luminescence. The assay principle is graphically depicted in **Figure 20**. It was observed that absolute luminescence value varied in between assays for various reasons. Therefore, stimulation controls were included.

5.2.2. Establishing the Assay Window and the Effect of Normalization

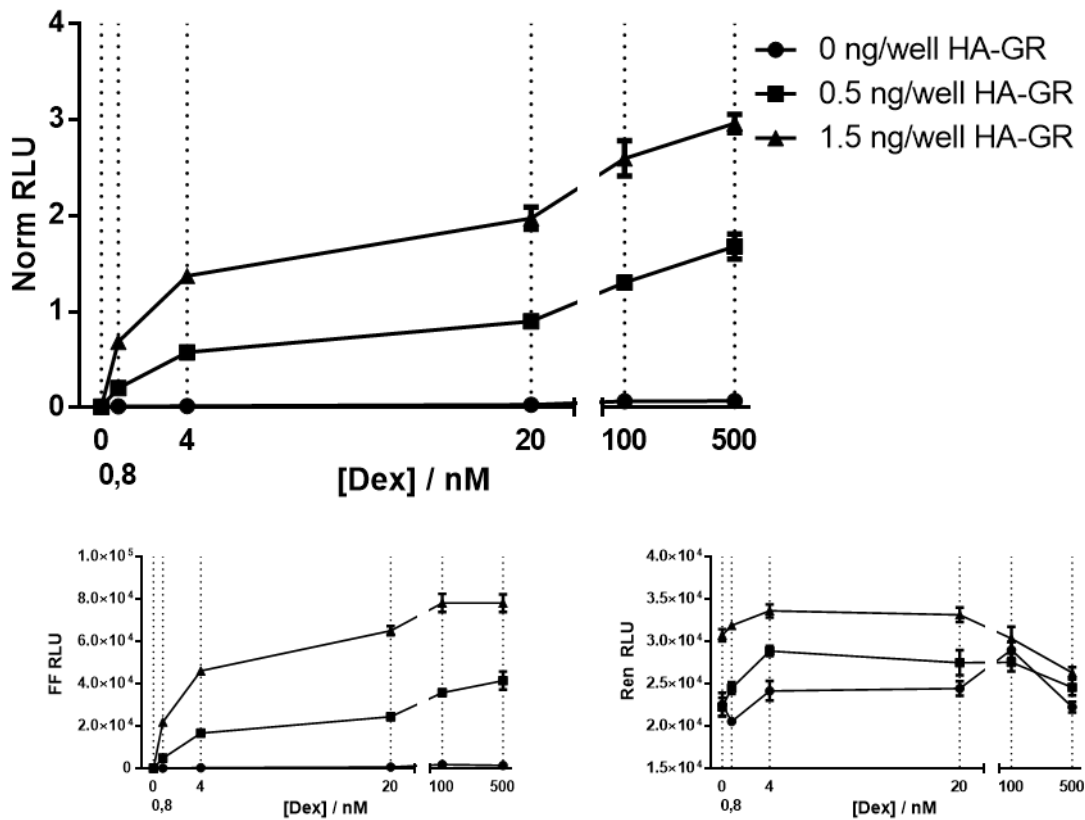


Figure 21 Graph shows the normalized signal of N2a cells transfected with different amounts of HA-GR by increasing Dex concentrations. 10,000 cells per well in a 96well plate were used. Lower panels show the respective Firefly and Renilla signal. Each data point represents a quadruplicate and SEM. Lab book: AHa426

During the establishment of the assay in N2a cells an insufficient assay window was observed. Therefore, a plasmid carrying HA-GR was cotransfected. 0.5 ng/well of this plasmid were sufficient to increase the signal from 0 to 4 nM Dex about 15-fold and with 100 nM Dex 30-fold (**Figure 21**). This effect is based on the signal change within the Firefly signal. The Renilla signal remains rather independent of Dexamethasone and serves as normalization basis to normalize occurring variables within and between assays, such as a fluctuating cell growth rate. All later described effects were observed at a stimulation of 4 nM Dexamethasone. 0 nM and 100 nM Dexamethasone served as stimulation control.

5.2.3. Overexpression of FKBP51

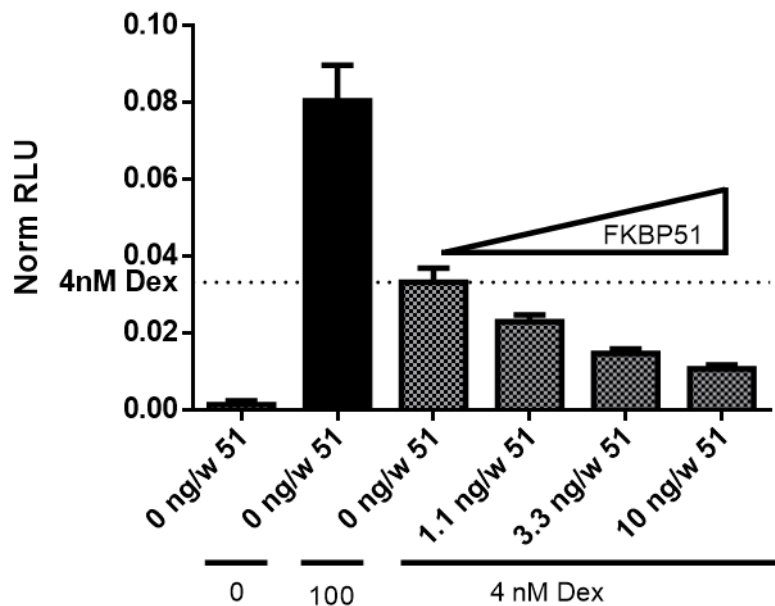


Figure 22 Effect of increasing transfection amounts of FKBP51 on GR signaling stimulated by 4 nM Dex. Normalized signal of N2a cells transfected with different amounts of FKBP51 at constant Dex concentrations. 10,000 cells per well in a 96well plate were used, transfected with plasmid mix (Firefly reporter, Renilla Reporter, GR, FKBP51) for 24 h. 0 and 100 nM Dex serve as controls. Dexamethasone stimulation started 24 h prior to lysis. DMSO concentration and total plasmid load are kept constant for all conditions. Lysates were transferred and handled as described in methods section 4.4.1 to be read out with a Tecan Infinite M1000. Each bar represents mean values of a quadruplicate and SEM. Lab book: AHa439

At a constant stimulation of the N2a cells an increasing transfection dose of FKBP51 is lowering the read out signal indicating an active repression of GR signaling by FKBP51 (**Figure 22**). Each condition contained the same amount of plasmid to exclude transfection stress induced effects. The following assays used transfection amounts of either 3.3 or 10 ng/well FKBP51 plasmid (if not indicated differently: FKBP51-FLAG, HG207).

5.2.4. Effects of Different FKBP51 Mutants

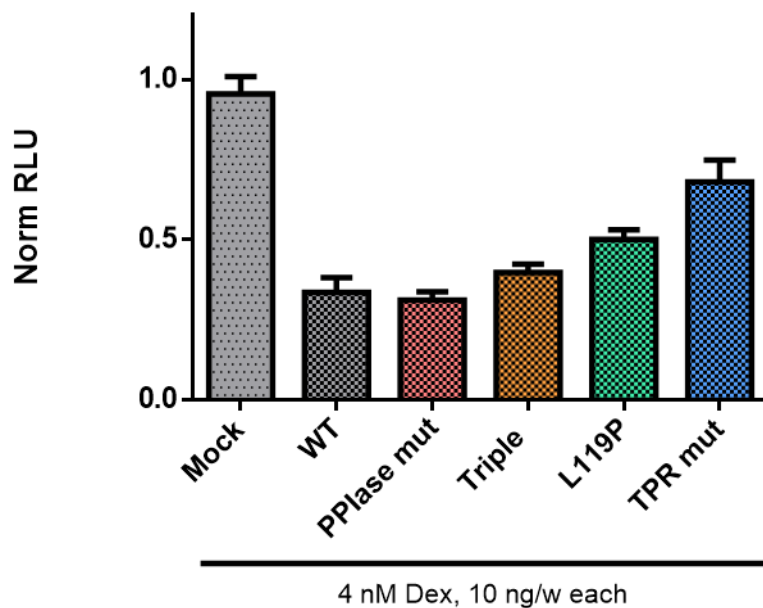


Figure 23 Effect of different FKBP51 mutants at 4 nM Dex stimulation: WT – wild type, PPlase mut = FD67/68DV; Triple = K58T/K60W/F129V, L119P, TPR mut = K352A/R356A. Normalized signal of N2a cells transfected with different mutants of FKBP51 at constant Dex concentrations. 10,000 cells per well in a 96well plate were used, transfected with plasmid mix (Firefly reporter, Renilla Reporter, GR, FKBP) for 24 h. Total plasmid load are kept constant for all conditions. Stimulation took place 24 h prior to lysis. Lysates were transferred and handled as described in methods section 4.4.1 to be read out with a Berthold TriStar² LB 942. Each bar represents mean values of a quadruplicate and SEM. Lab book: AHa125

Different FKBP51 constructs have been cotransfected in a dose of 10 ng/well. Wild type FKBP51 reduced the GR reporter strength at 4 nM Dex, as well as the PPlase deficient mutant (FD67/68DV) and the triple mutant, containing three amino acids of the homologues FKBP52 (K58T/K60W/F129V). The L119P mutant, another FKBP51-52 swap and especially the TPR mutant (K352A/R356A), which is unable to bind Hsp90 proved to be weaker inhibitors of the GR.

5.2.5. FKBP52 in the Reporter Gene Assay

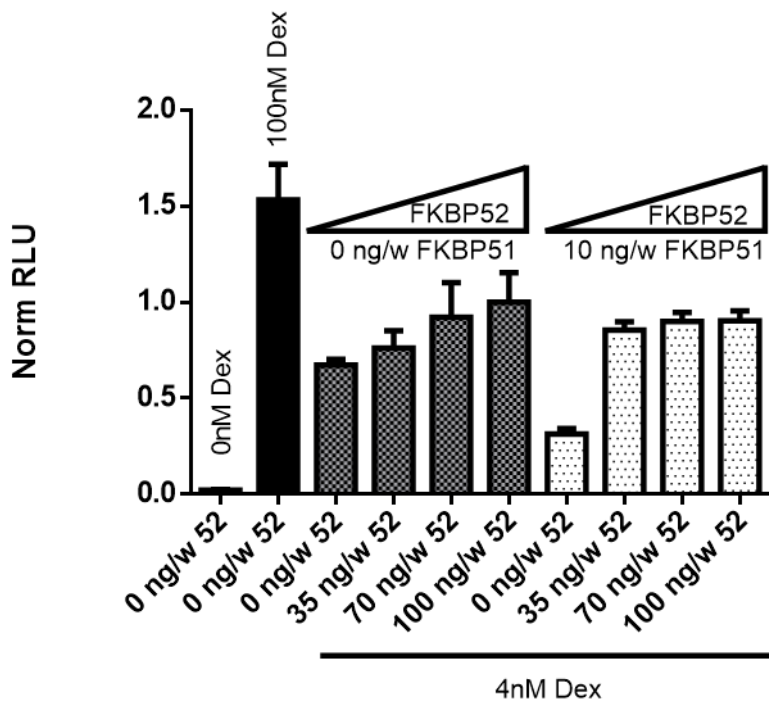


Figure 24 Effect of the titration of FKBP52 with and without the cotransfection of FKBP51. Normalized signal of N2a cells transfected with different amounts of FKBP52 at constant Dex concentrations. 10,000 cells per well in a 96well plate were used, transfected with plasmid mix (Firefly reporter, Renilla Reporter, GR, FKBP) for 24 h. Total plasmid load are kept constant for all conditions. 0 and 100 nM Dex serve as controls. Stimulation took place for 8 h prior to lysis. Lysates were transferred and handled as described in methods section 4.4.1 to be read out with a Berthold TriStar² LB 942. Each bar represents mean values of a quadruplicate and SEM. Lab book: AHa126

FKBP52 is described as functional counter player of FKBP51 in the GR context, enhancing GR signaling. An increasing amount of FKBP52 added to the transfection mix enhanced GR signaling both in the presence and absence of exogenous FKBP51. FKBP52 is able to completely overrule FKBP51 inhibition. This effect was only observable after 8 h and not after 24 h stimulation time in the incubator (**Figure 24**).

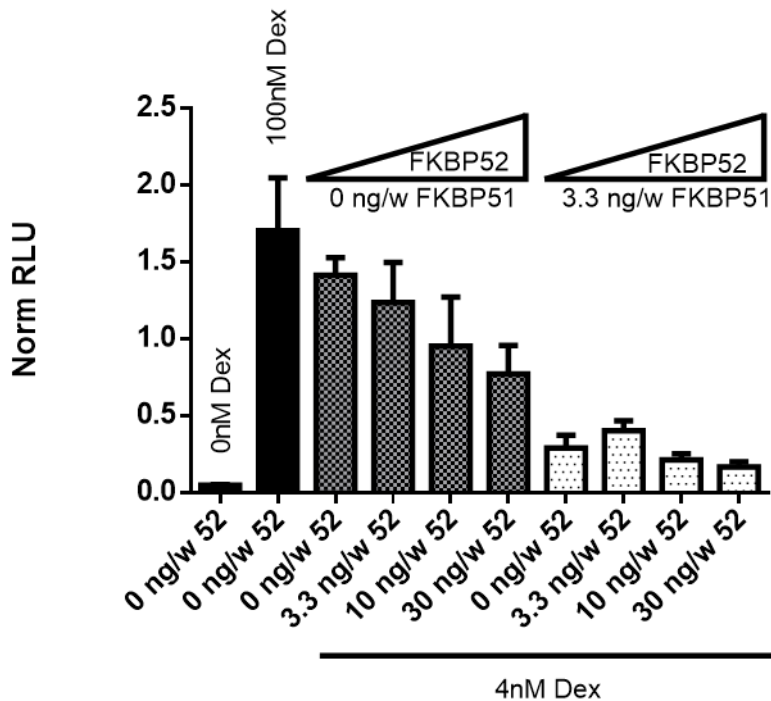


Figure 25 Effect of the titration of FKBP52 with and without the cotransfection of FKBP51. Normalized signal of N2a cells transfected with different amounts of FKBP52 at constant Dex concentrations. 10,000 cells per well in a 96well plate were used, transfected with plasmid mix (Firefly reporter, Renilla Reporter, GR, FKBP) for 24 h. Total plasmid load are kept constant for all conditions. 0 and 100 nM Dex serve as controls. Stimulation took place for 24 h prior to lysis. Lysates were transferred and handled as described in methods section 4.4.1 to be read out with a Tecan Infinite M1000. Each bar represents mean values of a triplicate and SEM. Lab book: AHa458

After 24 h of stimulation, increasing amounts of FKBP52 expression plasmid transfected further reduced the luminescence, which could be caused by degradation of FKBP52 and increasing cellular translational stress (**Figure 25**).

5.2.6. Impact of FKBP51 Ligands in the Reporter Gene Assay

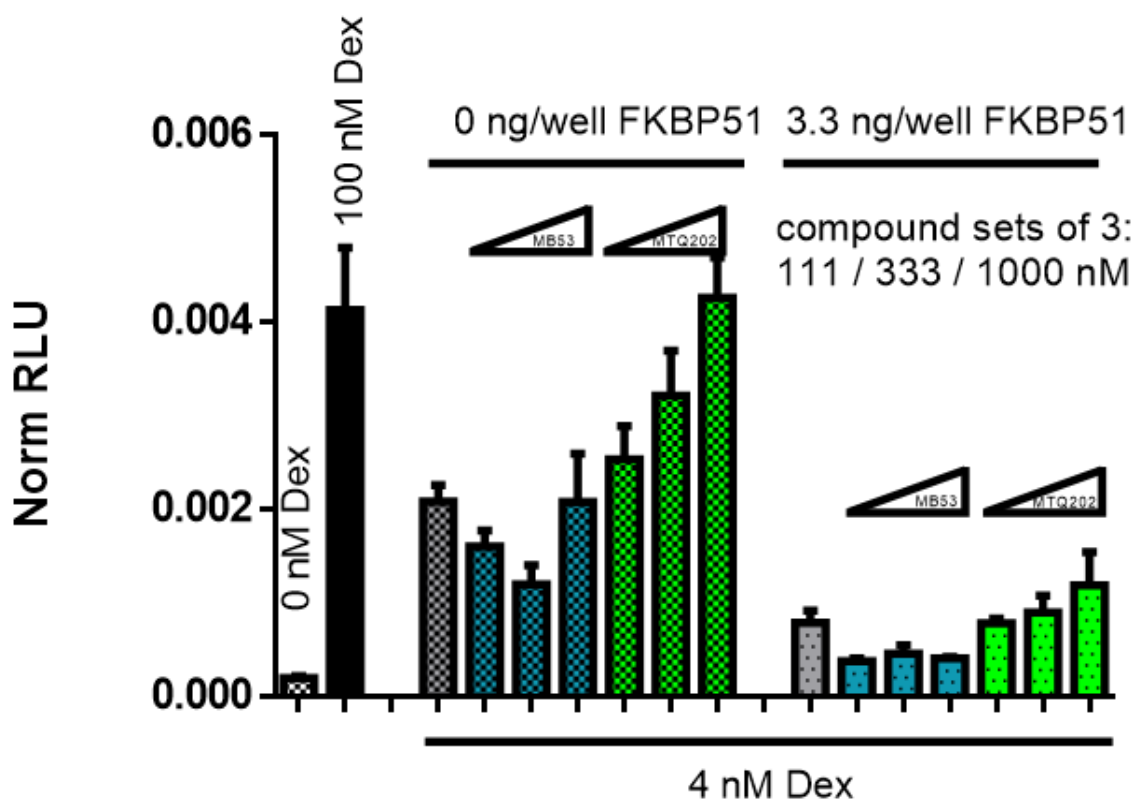


Figure 26 Addition of two FKBP51 ligands at the indicated concentrations with and without overexpression of FKBP51. Normalized signal of N2a cells. 10,000 cells per well in a 96well plate were used, transfected with plasmid mix (Firefly reporter, Renilla Reporter, GR, FKBP51) for 24 h. Cells were treated for 8 h with MB53 (SAFit1) in blue or MTQ202 in green. Stimulation mix was added on top without removing treatment mix. 0 and 100 nM Dex serve as controls. Dexamethasone stimulation took 24 h prior to lysis. DMSO concentration and total plasmid load are kept constant for all conditions. Lysates were transferred and handled as described in methods section 4.4.1 to be read out in a Tecan Infinite M1000. Each bar represents mean values of a quadruplicate and SEM. Lab book: AHa453

The effects of FKBP51 ligands present in the assay have been tested as well. After transfection, ligand containing-medium was added to the cells. Then, the cells were incubated for 8 h. After that, stimulation was performed without removing the ligand solution. **Figure 26** shows three concentrations of MB53 (SAFit1 blue) and MTQ202 (green) added in the presence and absence of exogenous FKBP51. While MB53 seems to have a negative impact on GR signaling, MTQ202 increases the signal under both conditions in a dose-dependent manner. The negative impact of SAFit not always occurred. Especially here, the highest concentration of SAFit has no effect in absence of exogenous FKBP, indicating an unspecific artifact.

5.2.7. Overexpression of Glomulin

Due to the fact, that Glmn emerged as interesting interactor of FKBP51 during the course of this thesis, a similar reporter gene assay was performed to investigate any effect by the overexpression of Glmn. Two eukaryotic expression plasmids carrying Glmn tagged with three FLAG-peptides either *N*-terminally (HG 644) or *C*-terminally (HG 645) were cotransfected. Interestingly, 3x-FLAG-Glmn (*N*-term.) overexpression shows no effect for both amounts (10 and 30 ng/well) (**Figure 27**), while Glmn-3xFLAG (*C*-term) does increase reporter strength for the transfection load of 30 ng plasmid per well, but not for 10 ng/well. This effect is even stronger, if FKBP51 is co-overexpressed. How and if this effect is related to FKBP51 cannot be concluded, but Glomulin has a strong impact on GR signaling if its *N*-terminus remains unlabeled.

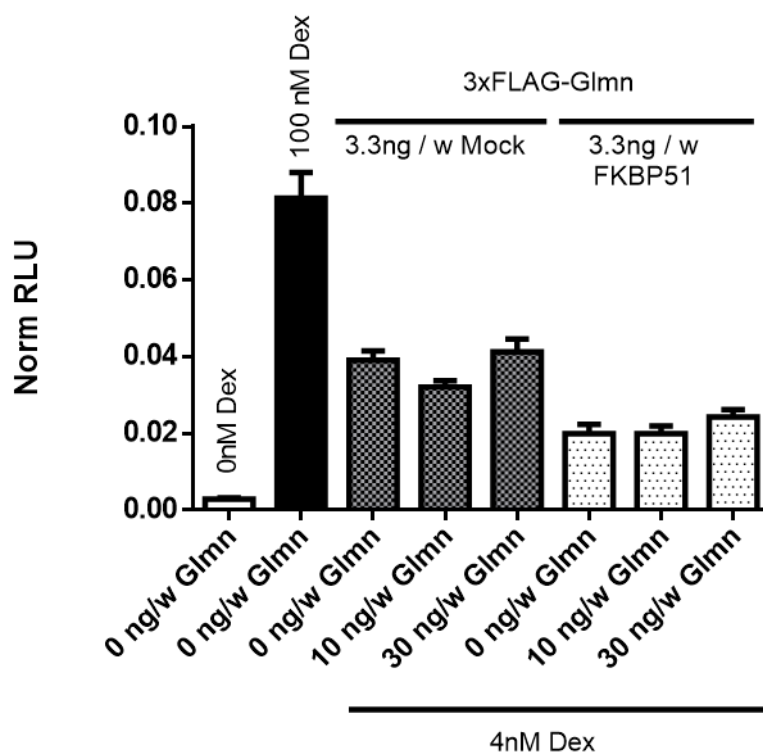


Figure 27 The effect of overexpression of 3xFLAG-Glmn in presence and absence of cotransfected FKBP51 at the stimulation of 4 nM Dex. Normalized signal of N2a cells transfected with two amounts of 3xFLAG-Glmn at constant Dex concentrations. 10,000 cells per well in a 96well plate were used, transfected with plasmid mix (Firefly reporter, Renilla Reporter, GR, FKBP, Glmn) for 24 h. 0 and 100 nM Dex serve as controls. Dexamethasone stimulation was performed for 24 h prior to lysis. DMSO concentration and total plasmid load are kept constant for all conditions. Lysates were transferred and handled as described to be read out in methods section 4.4.1 in a Tecan Infinite M1000. Each bar represents mean values of a hexaplicate and SEM. Lab book: AHa464

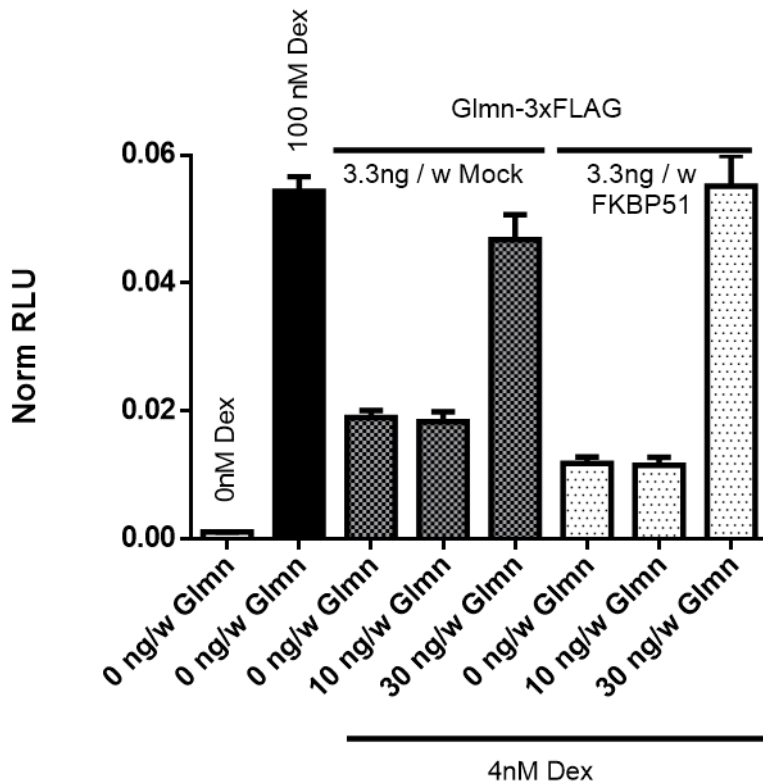


Figure 28 The effect of overexpression of Glmn-3xFLAG in presence and absence of cotransfected FKBP51 at the stimulation of 4 nM Dex. Normalized signal of N2a cells transfected with two amounts of 3xFLAG-Glmn at constant Dex concentrations. 10,000 cells per well in a 96well plate were used, transfected with plasmid mix (Firefly reporter, Renilla Reporter, GR, FKBP, Glmn) for 24 h. 0 and 100 nM Dex serve as controls. Dexamethasone stimulation took 24 h prior to lysis. DMSO concentration and total plasmid load are kept constant for all conditions. Lysates were transferred and handled as described in methods section 4.4.1 to be read out in a Tecan Infinite M1000. Each bar represents mean values of a hexaplicate and SEM. Lab book: AHa464

The according Firefly and Renilla signals can be found in Suppl. Fig. 62.

5.2.8. FKBP51 in NF-κB Signaling

Via an internal cooperation within the MPI for Psychiatry, reporter gene assays were performed to investigate the effect of FKBP51 on NF-κB Signaling as a side project. Two different reporter plasmids were used: p1242 addressing the canonical and pNF-κB2 addressing the non-canonical pathway. The assay principle is depicted in **Figure 29**.

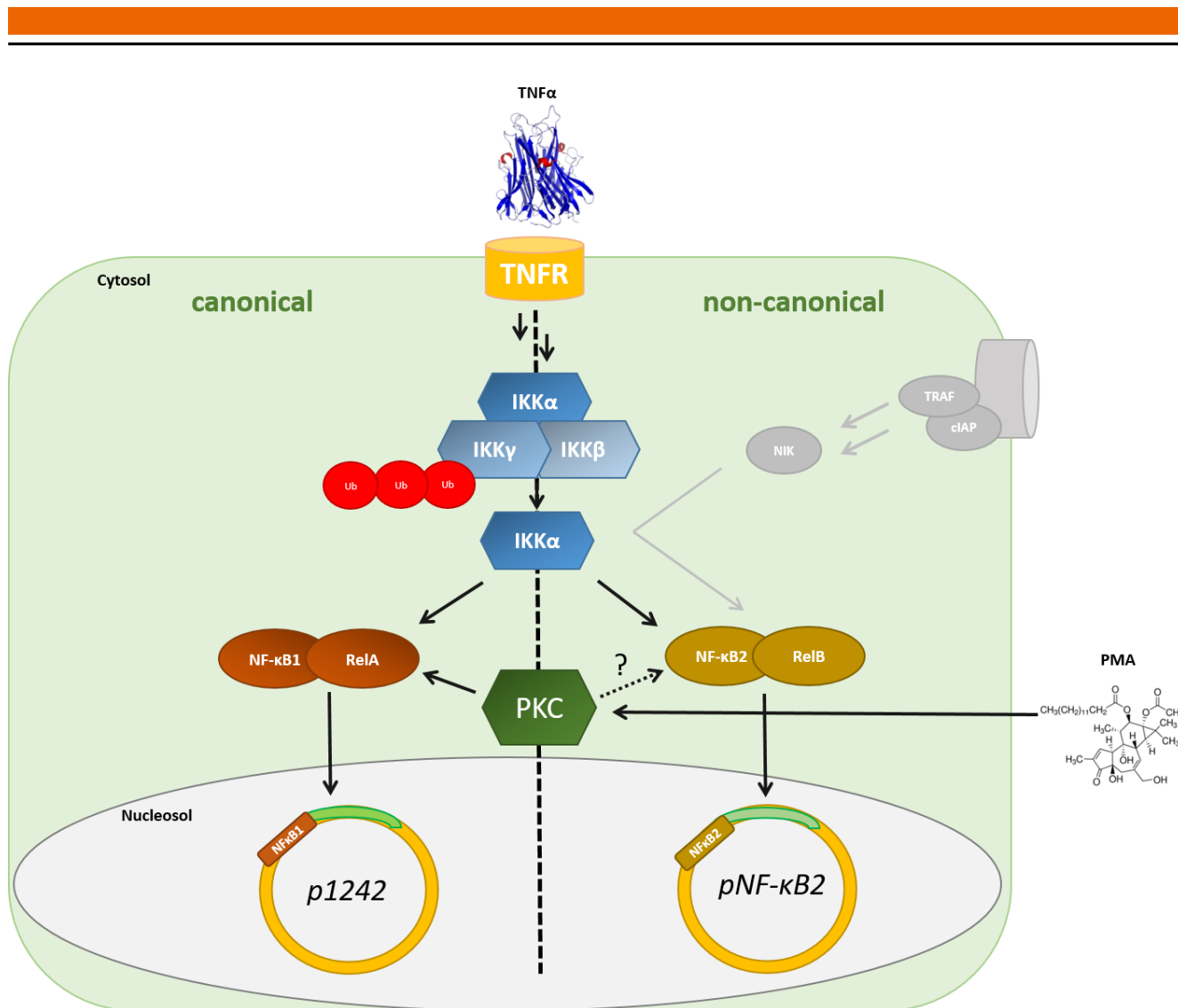


Figure 29 Schematic depiction of the assay principle. A signaling cascade, which is induced by TNF α , leads to the release of IKK α from the IKK complex. IKK α phosphorylates the NF- κ B precursors, which triggers proteolytic cleavage of the precursors and the formation of the transcription factor complexes. NF- κ B can also be primed by PKC upon its activation by PMA. How PKC interacts with NF- κ B2 is uncertain. The non-canonical pathway is stimulated by other signaling cascades as well, which are excluded here. This is a very strong simplification of the signaling pathway.

Those firefly luciferase carrying reporters were transfected into different cell lines: the standard system HEK293T (**Figure 30**), the melanoma derived A375 line (**Figure 31**) and Jurkat T cells (**Figure 32**). A375 and Jurkat cells are commonly used to investigate the NF- κ B pathway. Overall, experiments were performed similar to GR reporter gene assays. Stimulation was performed with either TNF α or PMA. It is speculated that PMA activates the non-canonical pathway via a limited set of PKC isoforms [138]. Optimal stimulation by PMA was reported for 15 nM [136,139,140]. Therefore, two concentrations higher and two concentrations lower have been chosen to stimulate the reporters as well. However, PMA treatment with 40 nM and more led to massive cell death of HEK293T and A375 cell (not tested for Jurkat). For lower PMA concentrations no detrimental effect was observed.

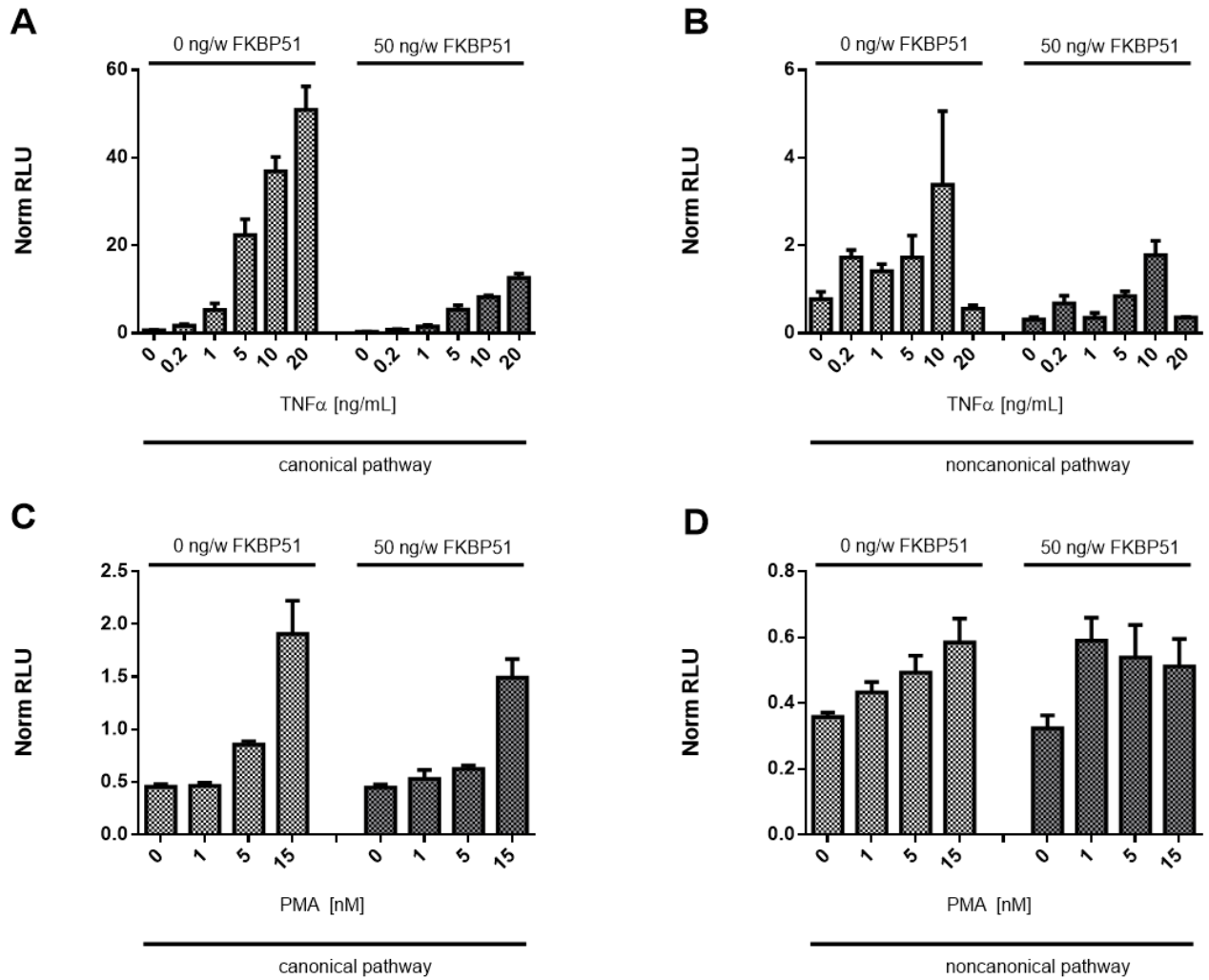


Figure 30 The effect of overexpression of FKBP51 and the stimulation of the NF- κ B Pathway in HEK293T cells. Normalized signal of HEK293T cells transfected with or without exogenous FKBP51 at increasing stimulant concentration. Two different reporter plasmids have been used: p1242 (A and C) and pNF- κ B2 (B and D). Stimulation was performed either with TNF α (A and B) or PMA (C and D). 10,000 cells per well in a 96well plate were used, transfected with plasmid mix (NF- κ B reporter, Renilla Reporter, FKBP) for 24 h. Stimulation took 20 h prior to lysis. DMSO concentration and total plasmid load are kept constant for all conditions. Lysates were transferred and handled as described to be read out in a Berthold TriStar² LB 942. Each bar represents mean values of a hexaplicate and SEM. Lab book: AHa109 (analog in AHa94, 97, 103)

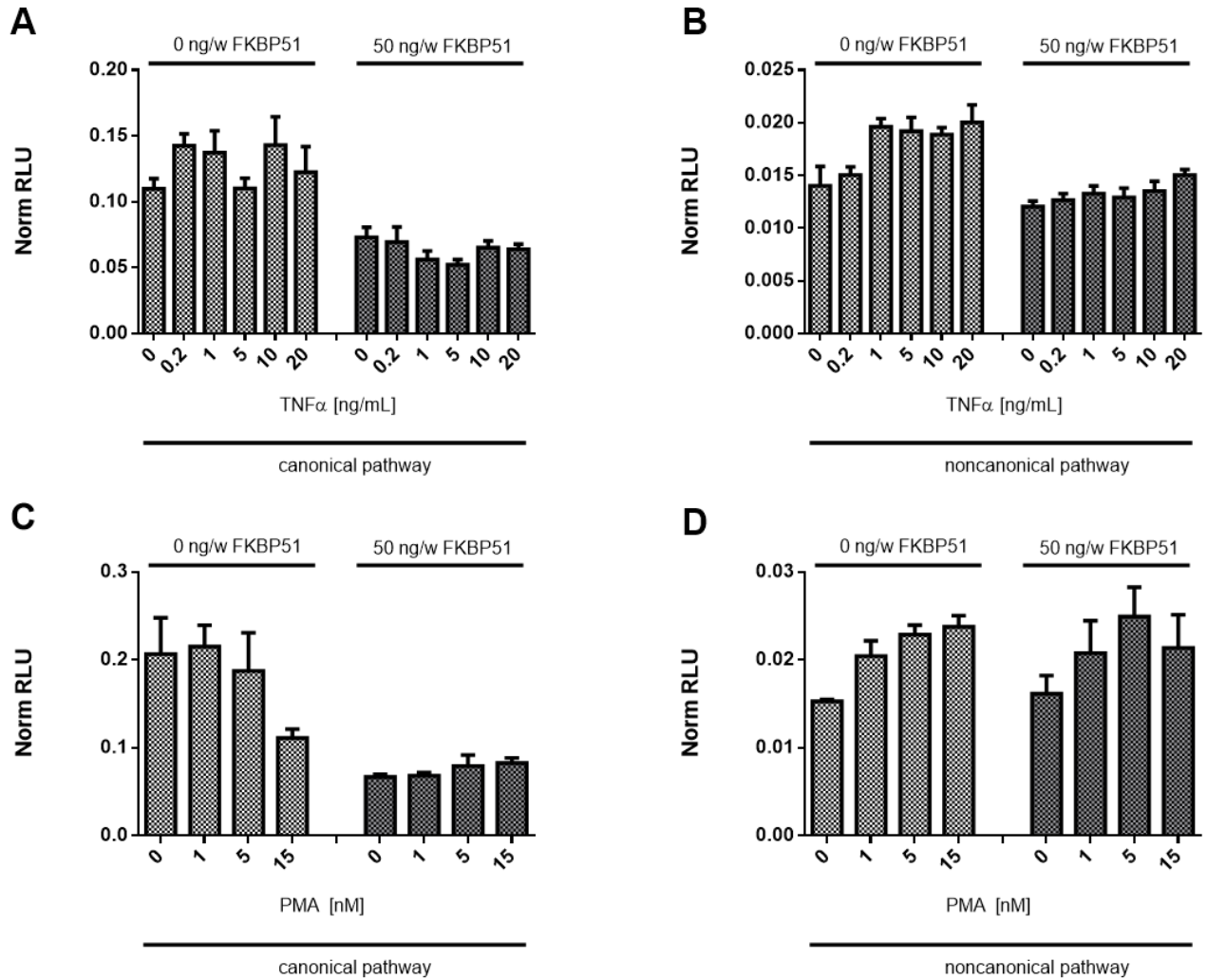


Figure 31 The effect of overexpression of FKBP51 and the stimulation of the NF- κ B Pathway in A375 cells. Normalized signal of A375 cells transfected with or without exogenous FKBP51 at increasing stimulant concentration. Two different reporter plasmids have been used: p1242 (A and C) and pNF- κ B2 (B and D). Stimulation was performed either with TNF α (A and B) or PMA (C and D). 10,000 cells per well in a 96well plate were used, transfected with plasmid mix (NF- κ B reporter, Renilla Reporter, FKBP) for 24 h. Stimulation took 20 h prior to lysis. DMSO concentration and total plasmid load are kept constant for all conditions. Lysates were transferred and handled as described to be read out in a Berthold TriStar² LB 942. Each bar represents mean values of a hexaplicate and SEM. Lab book: AHa117

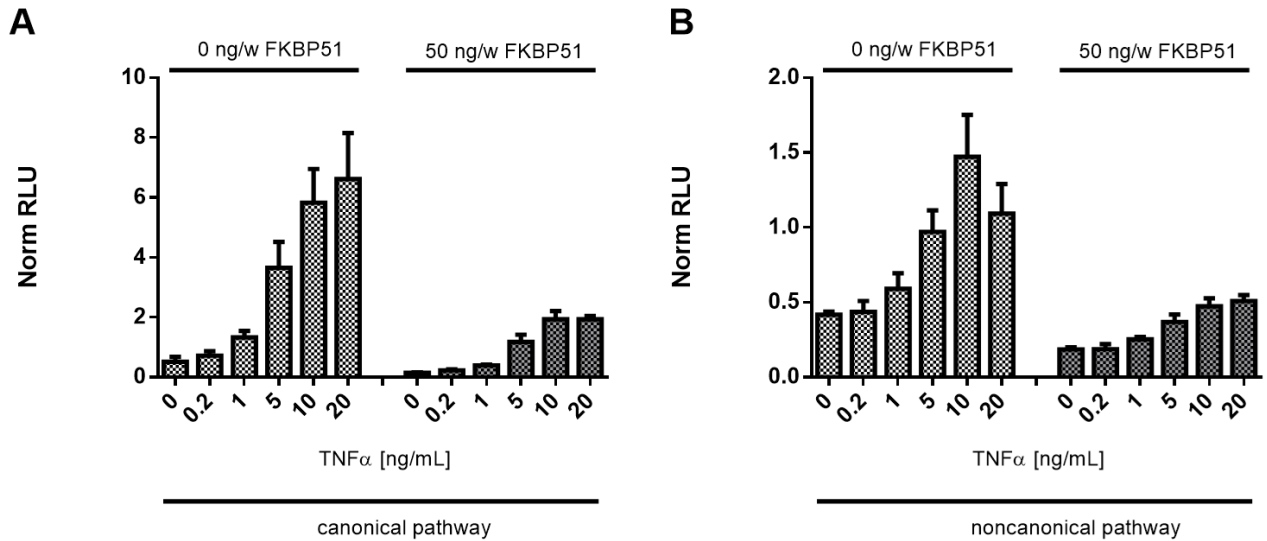


Figure 32 The effect of overexpression of FKBP51 and the stimulation of the NF-κB Pathway in Jurkat cells. Normalized signal of Jurkat cells transfected with or without exogenous FKBP51 at increasing stimulant concentration. Two different reporter plasmids have been used: p1242 (A and C) and pNF-κB2 (B and D). Stimulation was performed either with TNFα (A and B) or PMA (C and D). Bars indicated by with a * have been omitted due to cell death at those conditions. 10,000 cells per well in a 96well plate were used, transfected with plasmid mix (NF-κB reporter, Renilla Reporter, FKBP) for 24 h. Stimulation took 20 h prior to lysis. DMSO concentration and total plasmid load are kept constant for all conditions. Lysates were transferred and handled as described to be read out in a Berthold TriStar² LB 942. Each bar represents mean values of a hexaplicate and SEM. Lab book: AHa124

The canonical pathway could be stimulated with TNFα in HEK293T and Jurkat cells and PMA in HEK293T cells. The non-canonical pathway responded to TNFα in Jurkat cells and weakly to PMA in A375 and HEK293T cells only. The overexpression of FKBP51 at 50 ng/well leads to a reduced signal for most stimutable conditions. This assay has not been optimized with respect to transfection amounts and stimulation time. Further follow up would require and optimization of the assay window and address the issue if the FKBP51 overexpression effect is robust.

5.3. Glomulin – FKBP HTRF

During the course of this PhD it several indicators (unpublished) arose, that FKBP51 might be an interactor of Glomulin. To address and quantify the Glmn – FKBP-Interaction a homogenous time-resolved fluorescence (HTRF) assay was developed. The experiments were partly performed by Thomas Geiger, a master student under my supervision. His data is labeled with “Lab book: TGe #”. Over the time of the experiments two batches of Glmn have been purified and are indicated here as B1 and B2.

5.3.1. Assay Setup

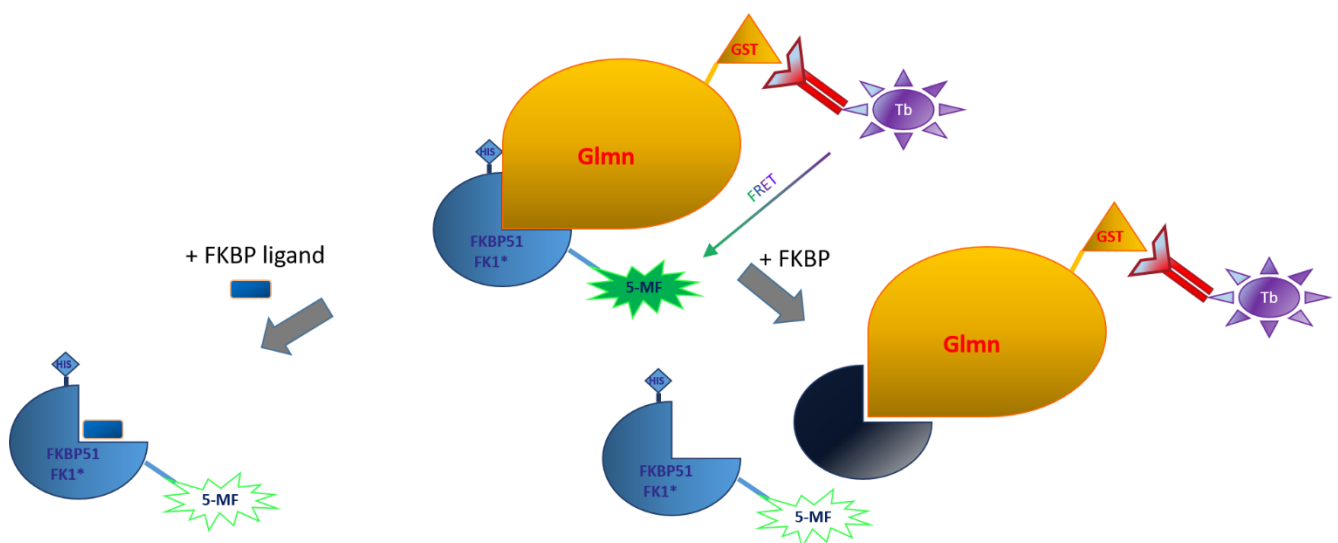


Figure 33 HTRF Setup. Binding of Glmn-GST and FKBP51FK1-5-MF brings both fluorophores (Terbium cryptate and Fluorescein) in close proximity and enables FRET. The disruption of this interaction by FKBP ligands or unlabeled FK1 domains can be tested in a competitive setup.

The constitution of the assay is depicted in **Figure 33**. For this assay, protein binding partners were heterogeneously expressed and purified. Purity was confirmed via SDS-Page (Suppl. Fig. 64). Size exclusion chromatograms can be found in Suppl. Fig. 65 to Suppl. Fig. 69. The Glmn construct contains a C-terminal GST-Tag. A C-terminal MonoCystein mutant of the FK1 domain of FKBP51 was covalently labeled with Fluoresceinmaleimide (5-MF). A Tb-cryptate conjugated antibody binds to the Glmn construct. If Glmn and FKBP51FK1 bind in close proximity excitation of the Tb will lead to emission of 5-MF: Specificity and binding site can be probed with an excess of unlabeled FKBP51FK1 and FKBP51 ligands.

5.3.2. Assay development

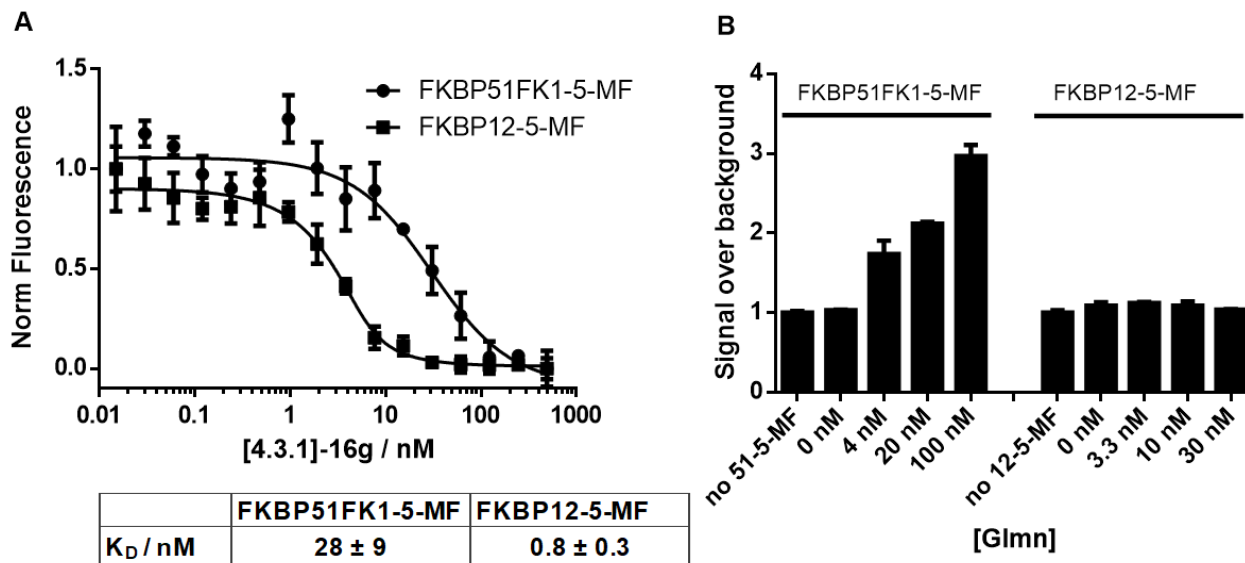


Figure 34 Establishing the HTRF (A) Activity test of labeled proteins by destructive FRET: Labeled proteins (5 nM) were incubated with the TAMRA based fluorescent tracer [4.3.1]-16g /MTQ238. Fluorescence (Ex: 485±20 nm, Em: 520±10 nm) of 5-MF is quenched for higher tracer concentration. Data points (triplicates) are normalized to the “no tracer” value and fitted with a one-site-ligand depletion curve. Lab book: AHa485 (B) Assay window depending on Glmn concentration in presence of 30 nM 5-MF labeled FKBP. Labeled FKBP, increasing concentrations of Glmn B1 and 0.8 nM α GST-Tb-Cryptate are incubated together and FRET was measured. Data (triplicates) is normalized to the corresponding no FKBP control (first bar of each set). Suppl. Fig. 72 shows the same data plotted against the respective normalized fluorescence. Lab book: AHa382+407.

In order to check the activity of the 5-MF labeled proteins, an activity assay was performed. An increasing amount of fluorescent tracer [4.3.1]-16g quenched the signal of the conjugated 5-maleimide fluorescein in a dose-dependent manner via a destructive FRET (**Figure 34 A**). This can only be achieved, if the tracer binds to the fluorescein labeled protein, indicating that its binding pocket is still active and no denaturation of the pocket took place during the labeling. 30 nM of the respective FKBP was incubated with increasing concentrations of Glmn. It was possible to observe a FRET signal with FKBP51FK1-5-MF to a factor of three above background. This could not be achieved with FKBP12-5-MF (**Figure 34 B**).

5.3.3. Active site titrations of FKBP

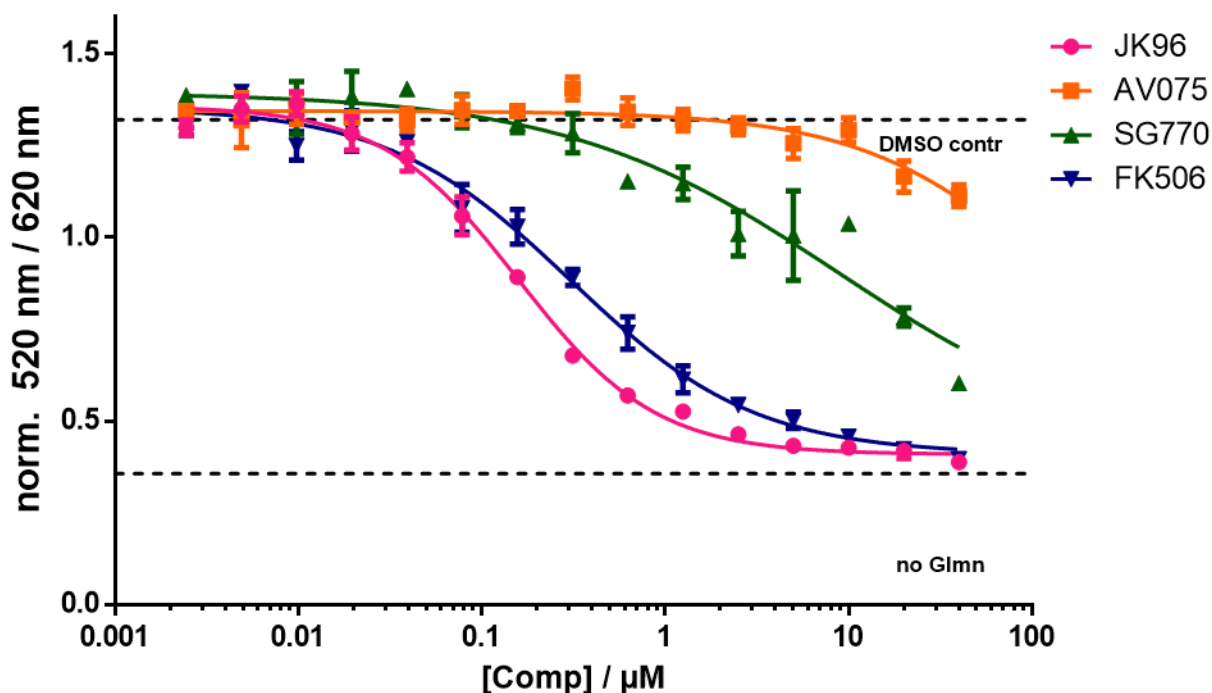
The concentration of each unlabeled FKBP used in the HTRF assay was validated via active site titration (AST). This is an almost stoichiometric titration since the tracer concentration used is 10 to 100 times higher than its respective K_D . ASTs show a steep hillslope. At their EC_{50} s (half rise to maximum), 50% of the tracer molecules are equimolar bound to protein. Suppl. Fig. 70 shows the ASTs of FKBP12

and FKBP12.6 which exhibit a very different binding affinity towards Glmn. ASTs confirm the determined affinities within the HTRF by excluding inactive or denatured proteins within the batch. Since the tracer concentration is defined, the protein concentration can be calculated. Proteins were prepared and quantified by different people in the lab. An overview of all used FKBP is given in **Table 3**. ASTs have been performed by different people in the lab, as the reference indicates. The structure of MTQ238 can be found in Suppl. Fig. 71.

Protein	Tracer	[Tracer] / nM	c _{UV} / μM	c _{AST} / μM	Ref
FKBP51FK1 (16-140)	MTQ238	50	102	120	AHa463
FKBP51FK1 (1-140)	CK97	50	223	456	AHa186
FKBP51FK1 (1-140) F67V	CK97	50	113	167	AHa186
FKBP51FK1 (1-140) FD67/68DV	CK97	50	141	106	AHa186
FKBP52FK1	CK97	50	136	209	CIS231
FKBP12 B1	CK97	50	600	498	CIS203
FKBP12 B2	MTQ238	50	150	130	CMe291
FKBP12.6 B1	CK97	50	88	16	CIS238
FKBP12.6 B2	MTQ238	50	20	17	CMe362
FKBP51FL	MTQ238	50	41	136	AHa405
FKBP52FL	MTQ238	50	9	25	AHa401

Table 3 Overview of FKBP is used in HTRF assays. All FKBP is characterized via active site concentration with the indicated tracer in the indicated experiment. CK97 is a rapamycin derived tracer.

5.3.4. Binding site specificity

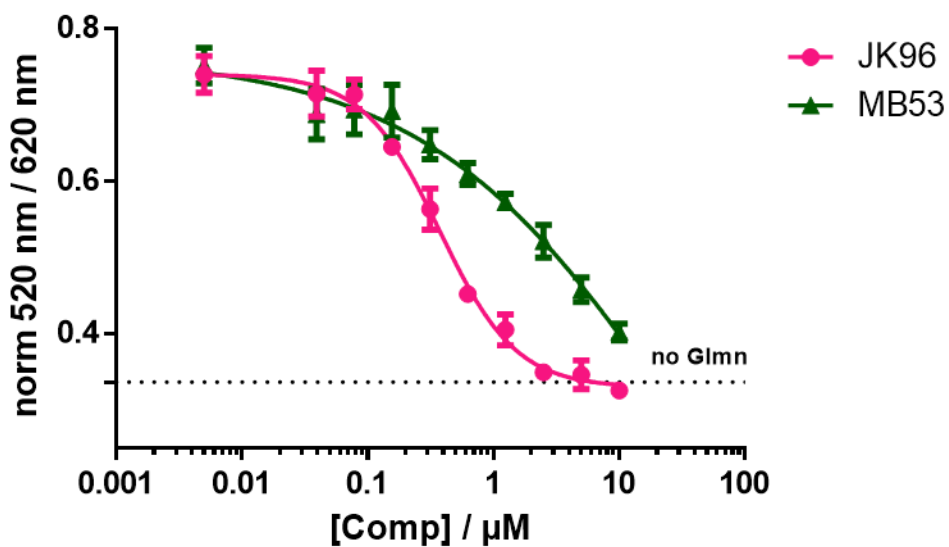


	JK96	AV075	SG770	FK506
IC ₅₀ / μM	0.16 ± 0.01	150 ± 60	9 ± 1	0.31 ± 0.03

Figure 35 Four FKBP51 ligands compete with the interaction of Glmn and FKBP51FK1. 30 nM FKBP51-5-MF, increasing amounts of compounds (up to 40 μM), 30 nM Glmn B2 and 0.8 nM αGST-Tb-Cryptate are incubated together and FRET was measured. Data (triplicates) is normalized, plotted in GraphPad Prism6 and fitted to a non-linear regression curve. Lab book: AHa487

FKBP51 ligands were tested for their potential to compete with Glmn binding to FKBP51FK1. **Figure 35** shows four competition curves of the ligands SG770 (SAFit1), JK96, FK506 and AV075 which are capable to quench the FRET signal. All curves are fitted with a four parameter fit. The half maximal inhibitory concentration (IC₅₀) is the high nanomolar for JK96 and FK506 respectively and low micromolar range for SG770. The value for AV075 is extrapolated. Higher concentrations for this ligand could not be tested due to solubility limitations.

A similar experiment was performed using a different a different batch Glmn and SAFit1 (MB53) (**Figure 36**). Although JK96 binds weaker by a factor of 2 and SAFit by a factor of 4 in that assay under slightly different conditions (10 nM Glmn), it confirms the difference of competitive potential of both ligands.



	JK96	MB53
IC₅₀ / μM	0.37 ± 0.03	35 ± 2

Figure 36 Two FKBP51 ligands compete with the interaction of Glmn and FKBP51FK1. 30 nM FKBP51-5-MF, increasing amounts of compounds (up to 10 μM), 10 nM Glmn B1 and 0.8 nM $\alpha\text{GST-Tb-Cryptate}$ are incubated together and FRET was measured. Data (triplicates) is normalized, plotted in GraphPad Prism6 and fitted to a non-linear regression curve. Lab book: AHa387

5.3.5. Comparison of different FKBP

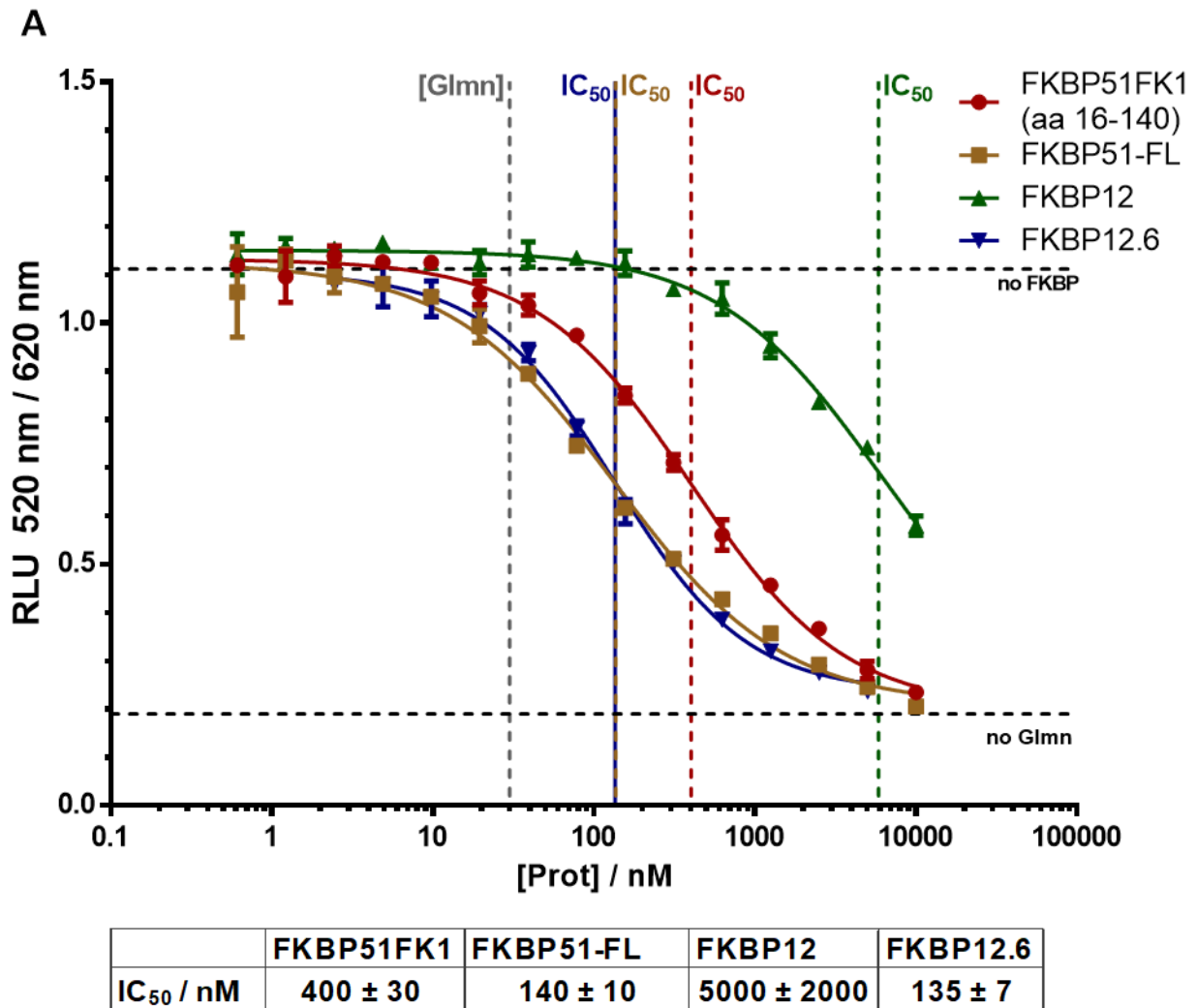
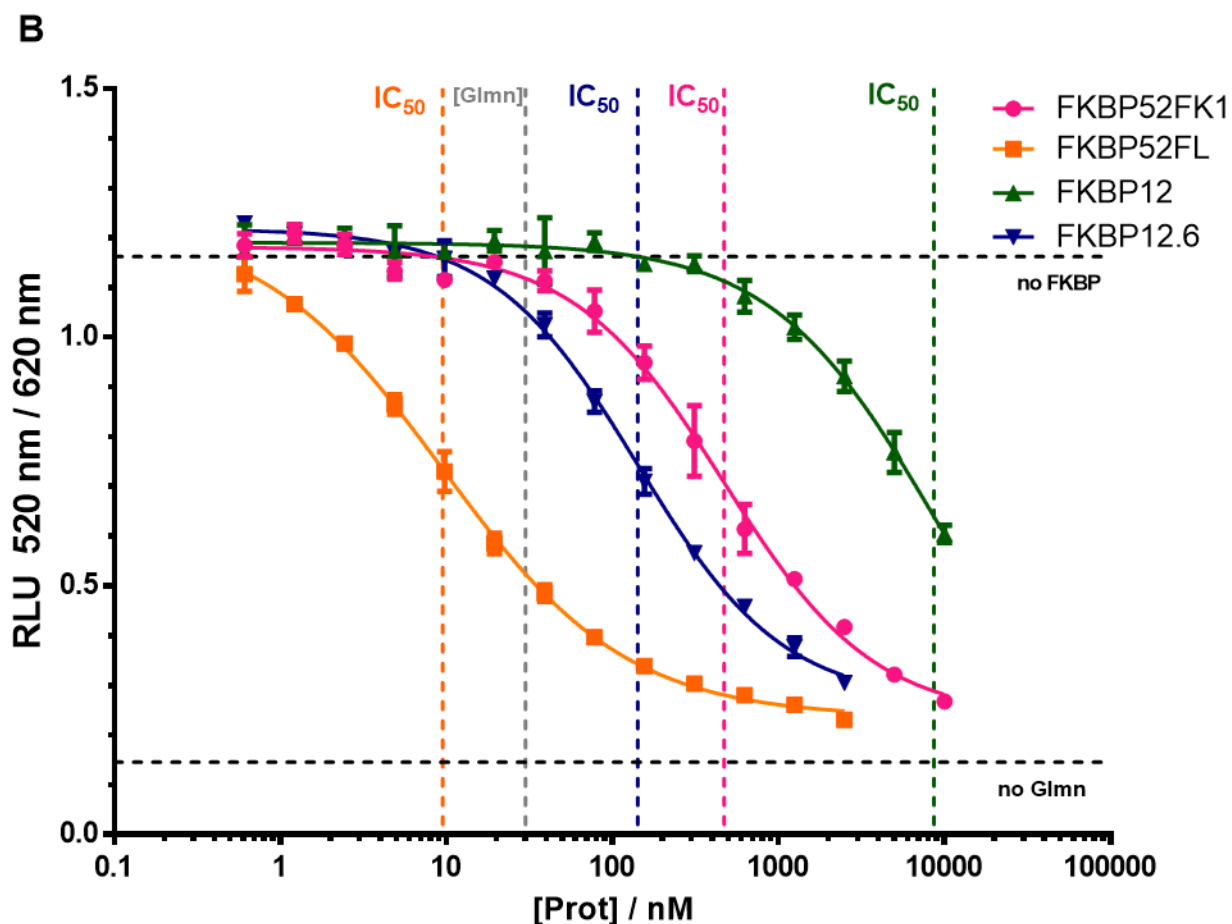


Figure 37 Competition of several FKBP with FKBP51FK1-5-MF for Glmn binding. 30 nM FKBP51-5-MF, increasing amounts of the competing proteins FKBP51FK1, FKBP51-FL, FKBP12 (B2) and FKBP12.6 (B2) (up to 10 μ M), 30 nM Glmn B2 and 0.8 nM α GST-Tb-Cryptate are incubated together and FRET was measured. Data (triplicates) is normalized, plotted in GraphPad Prism6 and fitted to a non-linear regression curve. Lab book: TGe71

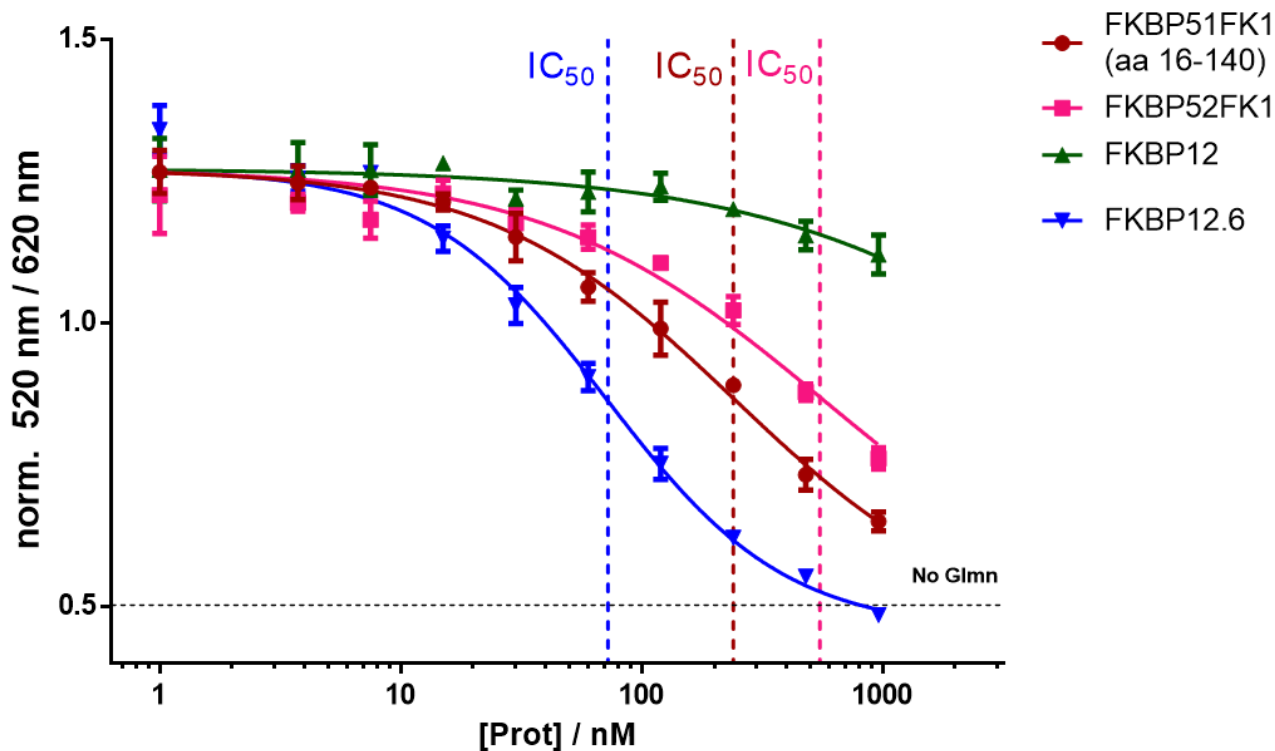
The same setup was used to investigate the competitive capabilities of other FKBP and their potential to sequester Glmn and henceforth, lower the FRET signal (**Figure 37** and **Figure 38**). The FK1 domains of FKBP51 and 52 showed comparable affinities (400 nM, 470 nM). Although, FKBP12 is the best described interactor of Glmn [114,115] it exhibited the weakest competitive capabilities with IC_{50} s in micromolar range. On the other side, its close homologue FKBP12.6 proved to bind rather strong with around 140 nM. Interesting as well is the fact, that both full-length proteins show improved binding compared to their respective FK1 domains. FKBP51 is three-times stronger and FKBP52 almost by a factor 50.



	FKBP52FK1	FKBP52-FL	FKBP12	FKBP12.6
IC_{50} / nM	470 ± 40	9.5 ± 0.6	9000 ± 6000	143 ± 7

Figure 38 Competition of several FKBP proteins with FKBP51FK1-5-MF for Glmn binding. 30 nM FKBP51-5-MF, increasing amounts of the competing proteins FKBP52FK1, FKBP52-FL, FKBP12 (B2) and FKBP12.6 (B2) (up to 10 μ M), 30 nM Glmn B2 and 0.8 nM α GST-Tb-Cryptate are incubated together and FRET was measured. Data (triplicates) is normalized, plotted in GraphPad Prism6 and fitted to a non-linear regression curve. Lab book: TGe76

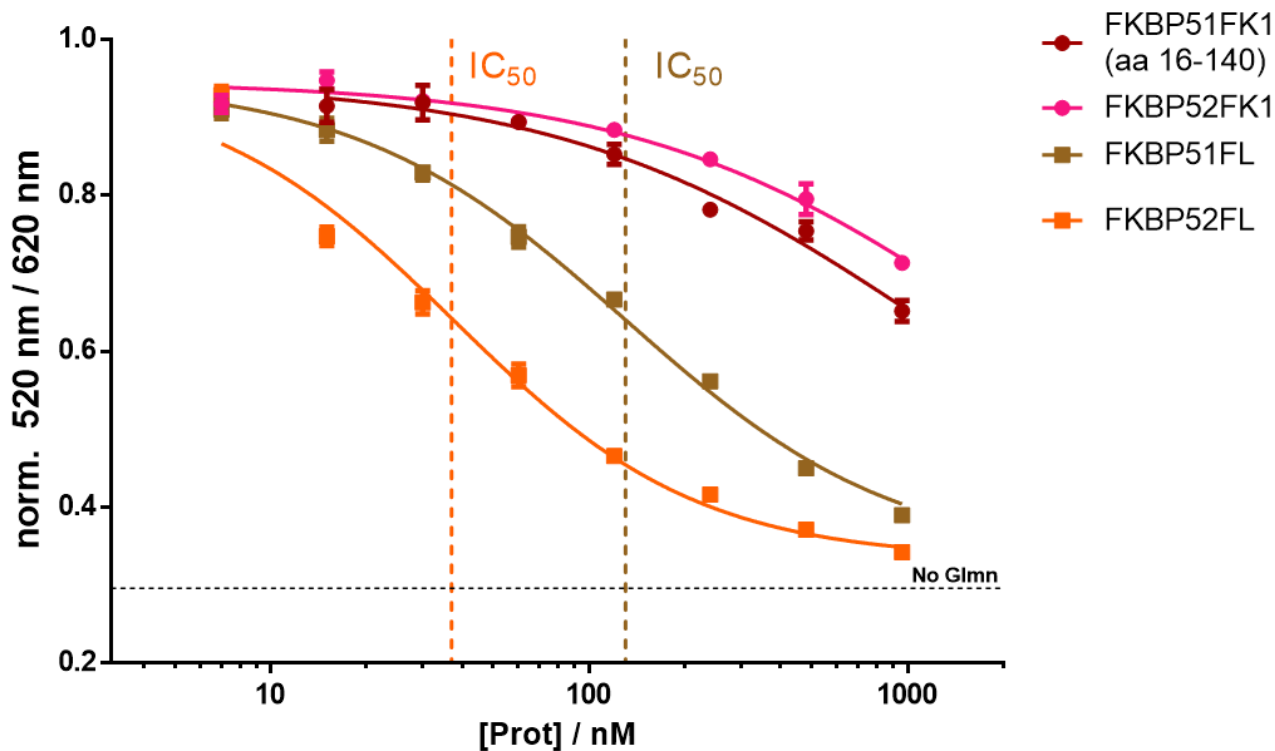
These findings were confirmed in another set of experiments, where the assay was performed with a different batch of Glmn, in the concentration of 10 nM final instead of 30 nM, and different batches of FKBP12 and 12.6 (**Figure 39**). This assay showed comparable results in the respective IC_{50} values: 400 vs. 240 nM for FKBP51FK1, 470 vs. 560 nM for FKBP52FK1, 9,000 vs. 10,000 nM for FKBP12 and 140 vs. 72 nM for FKBP12.6. This points out a general robustness of this assay towards changes of protein batches and Glmn concentration.



	FKBP51FK1	FKBP52FK1	FKBP12	FKBP12.6
IC ₅₀ / nM	240 ± 30	560 ± 90	10000 ± 9000	72 ± 8

Figure 39 Competition of several FKBP proteins with FKBP51FK1-5-MF for Glmn binding, control with different batches Glmn, FKBP12 and FKBP12.6. 30 nM FKBP51-5-MF, increasing amounts of the competing proteins FKBP51FK1, FKBP52FK1, FKBP12 (B1) and FKBP12.6 (B1) (up to 1 μM), 10 nM Glmn B1 and 0.8 nM αGST-Tb-Cryptate are incubated together and FRET was measured. Data (triplicates) is normalized, plotted in GraphPad Prism6 and fitted to a non-linear regression curve. Lab book: AHa393

The differences of competitive binding capability of full length and their respective FK1 domains was also confirmed with this batch of Glmn (**Figure 40**). The IC₅₀s of all tested proteins were about a factor 3 higher but for FKBP51FL, it still confirms the general trend seen so far: FKBP52FL >FKBP51FL > FKBP51FK1 >FKBP52FK1.

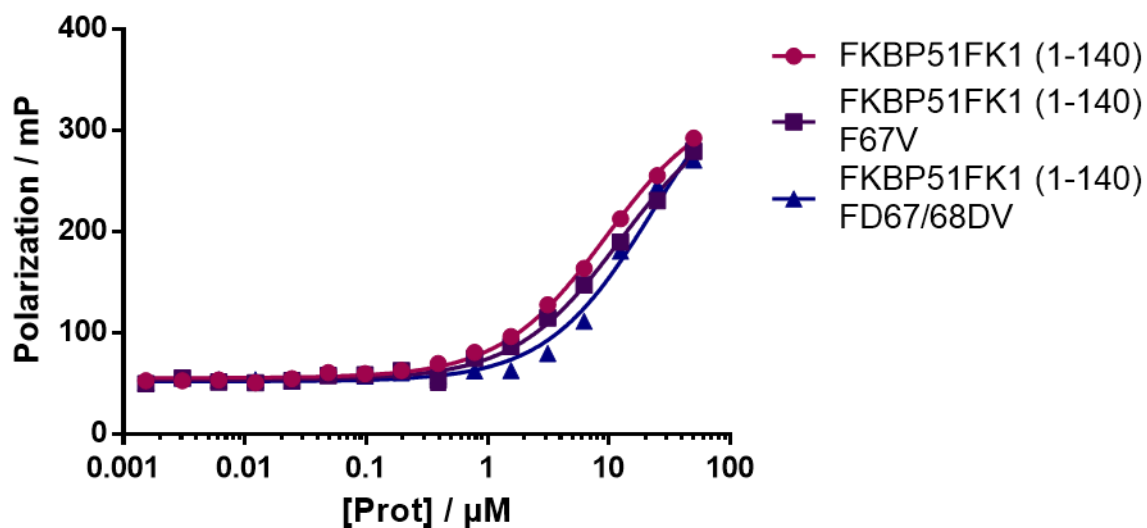


	FKBP51FK1	FKBP52FK1	FKBP51FL	FKBP52FL
IC_{50} / nM	1100 ± 200	1900 ± 500	130 ± 10	37 ± 4

Figure 40 Competition of several FKBP51FK1-5-MF for Glmn binding, control with different batches Glmn. 30 nM FKBP51-5-MF, increasing amounts of the competing proteins FKBP51FK1, FKBP51-FL, FKBP52FK1 and FKBP52-FL (up to 1 μ M), 10 nM Glmn B1 and 0.8 nM α GST-Tb-Cryptate are incubated together and FRET was measured. Data (triplicates) is normalized, plotted in GraphPad Prism6 and fitted to a non-linear regression curve. Lab book: AHa406

5.3.6. Characterization of FKBP51FK1 F67D and FD67/68DV mutants

In order to investigate potential binding sites within the FK1 domain of FKBP51, two mutants showing decreased (F67V) and completely blunted PPlase activity (FD67/68DV) were purified. The K_D of the low affine tracer CK182 (Structure: Suppl. Fig. 71) of wild type and mutant FK1 domains is in the same order of magnitude (**Figure 41**) indicating that the binding pocket remains intact and capable to bind small molecular ligands.



	FKBP51FK1 (1-140)	FKBP51FK1 (1-140) F67V	FKBP51FK1 (1-140) FD67/68DV
$K_D / \mu\text{M}$	9.4 ± 0.5	12 ± 1	22 ± 4

Figure 41 Binding curves of the three different FKBP51FK1 domains with the low affine tracer 20 nM CK182. FKBP51FK1 (1-140) and mutants F67V and FD67/68DF bind to the tracer with similar affinity in fluorescence binding assay. K_D s are obtained using GraphPad Prism6 and an one-site depletion fit: $Y = A / E * 0.5 * (X + E + 1 / K - \text{sqrt}(\text{sqr}(X + E + 1 / K))) + B$.

Lab book: AHa187

5.3.7. Competition of other FKBP51 constructs

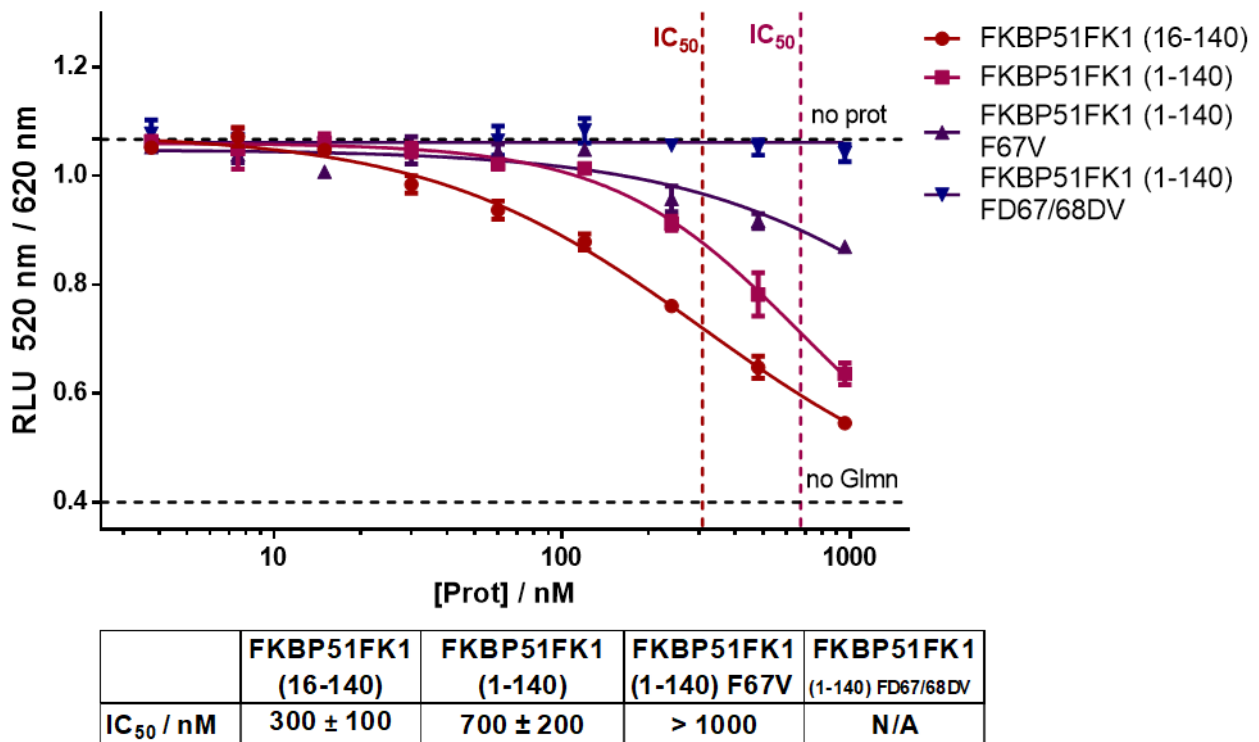
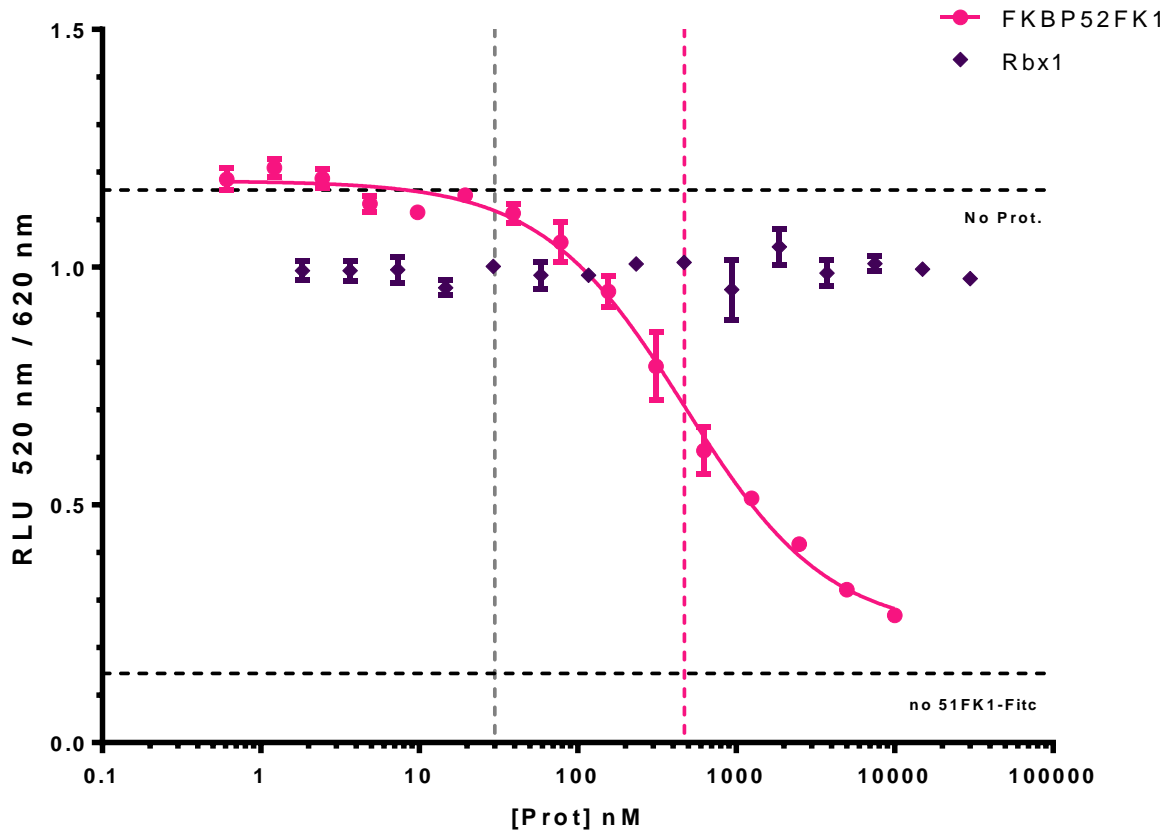


Figure 42 Competition of various FKBP51FK1 constructs. 30 nM FKBP51-5-MF, increasing amounts of the competing proteins FKBP51FK1 (16-140), FKBP51FK1 (1-140), FKBP51FK1 (1-140) F67V and FKBP51FK1 (1-140) FD67/68DV (up to 1 μ M), 10 nM Glmn B1 and 0.8 nM α GST-Tb-Cryptate are incubated together and FRET was measured. Data (triplicates) is normalized, plotted in GraphPad Prism6 and fitted to a non-linear regression curve. Lab book: AHa397

Similar to previous results different FK1 domains of FKBP51 were investigated for their competitive binding capability (**Figure 42**). The *N*-terminal shortened construct (aa 16-140, red circles) exhibits a slightly increased binding compared to the whole FK1 domain. Furthermore, the single respectively double point mutations of the FK1 domain of FKBP51 are not or just hardly able to break up the bound complex.

5.3.8. Impact of Rbx1 in this HTRF setup

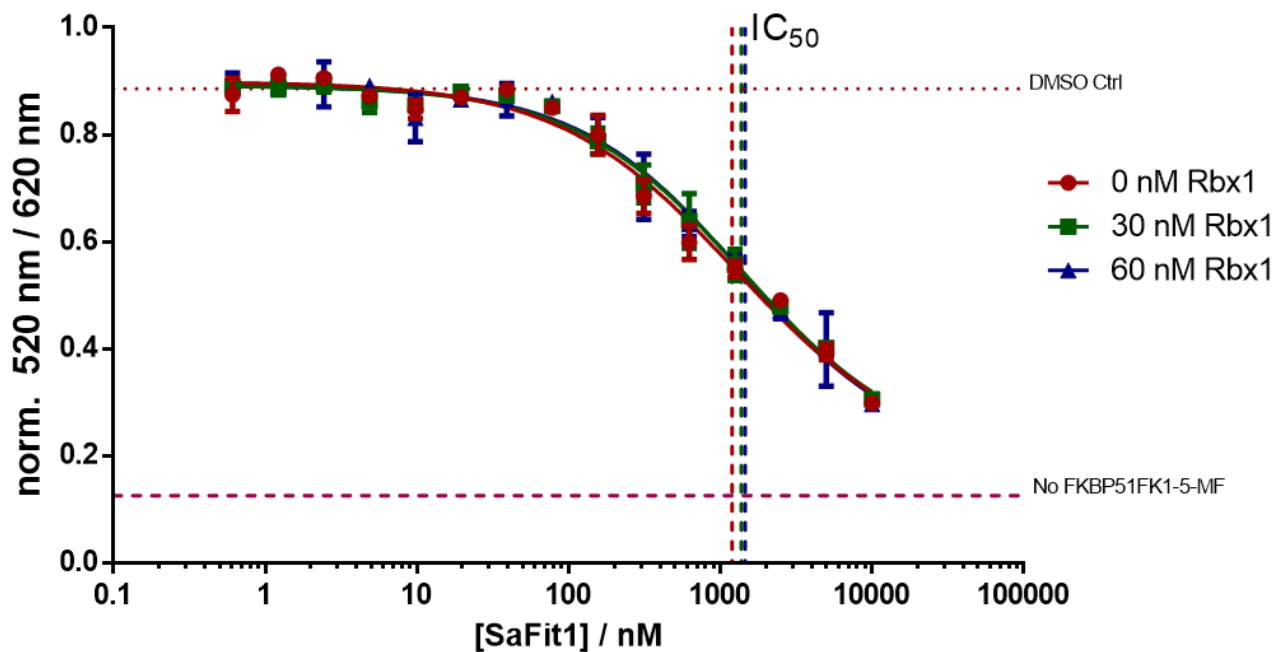
Under my supervision Thomas Geiger performed competitive HTRF assays also testing Rbx1. Rbx1 did not show any competition for Glmn binding up to a concentration of 40 μ M (**Figure 43**), while FKBP52FK1 did.



	FKBP52FK1
IC ₅₀ / nM	470 ± 40

Figure 43 Competition of Rbx1 with the interaction of Glmn and FKBP52FK1. FKBP52FK1 serves as control. 30 nM FKBP51-5-MF, 30 nM Glmn, increasing amounts of competing protein (up to 40 μ M) and 0.8 nM α GST-Tb-Cryptate are incubated together and FRET was measured. Data (triplicates) is normalized, plotted in GraphPad Prism6 and fitted to a non-linear regression curve. Data was obtained in the same assay as **Figure 38**. The shown FKBP52FL is identical Lab book: TGe76

We then tested, if the presence of Rbx1 has an impact on the competition of the FKBP51 ligand SAFit 1 (**Figure 44**). The addition of 30 and 60 nM respectively, did not alter the IC₅₀ of SAFit1 significantly. Interestingly, the IC₅₀ in this experiment was with 1 to 2 μ M way lower than in previous experiment. A dilution error has to be assumed.



	0 nM Rbx1	30 nM Rbx1	60 nM Rbx1
IC ₅₀ / nM	1200 ± 300	1400 ± 300	1500 ± 400

Figure 44 Competition of the FKBP51 ligand SAFit1 with the interaction of Glmn and FKBP51FK1. 30 nM FKBP51-5-MF, 30 nM Glmn, increasing amounts of SAFit1 (up to 10 μ M), 0.8 nM α GST-Tb-Cryptate and 0 / 30 / 60 nM Rbx1 are incubated together and FRET was measured. Data (triplicates) is normalized, plotted in GraphPad Prism6 and fitted to a non-linear regression curve. Lab book: TGe78

5.4. FKBP51 and Calcium Influx

FKBPs are described as regulators of calcium channels such as RyR1 and TRPC6 [2,141]. Hyperforin, a small molecule found in the popular herbal St. Johns wort, which is claimed to be mood enhancing, was described both as activator of TRCP6 calcium channels and neurite outgrowth regulator [142-144]. In order to investigate a potential impact of FKBP51 on TRPC6, it was tried to set up a calcium uptake assay utilizing the Fluor4 assay kit by Invitrogen. In all assays, fluorescence increased upon injection independent of the injected solution, which might be due to the chemical shift around the cells and detachment from the surface. Stably transfected HEK293 cells expressing TRPC6 and PC12 cells, which endogenously express this channel, were stimulated with ATP, DMSO, Hyperforin and the Hyperforin derivative Hyp1 (**Figure 45**). Only the positive control, ATP, which is an unspecific stimulator of Ca²⁺-channels, lead to a quick exponential rise followed by a slow sigmoidal decay. All others remained at a rather constant level.

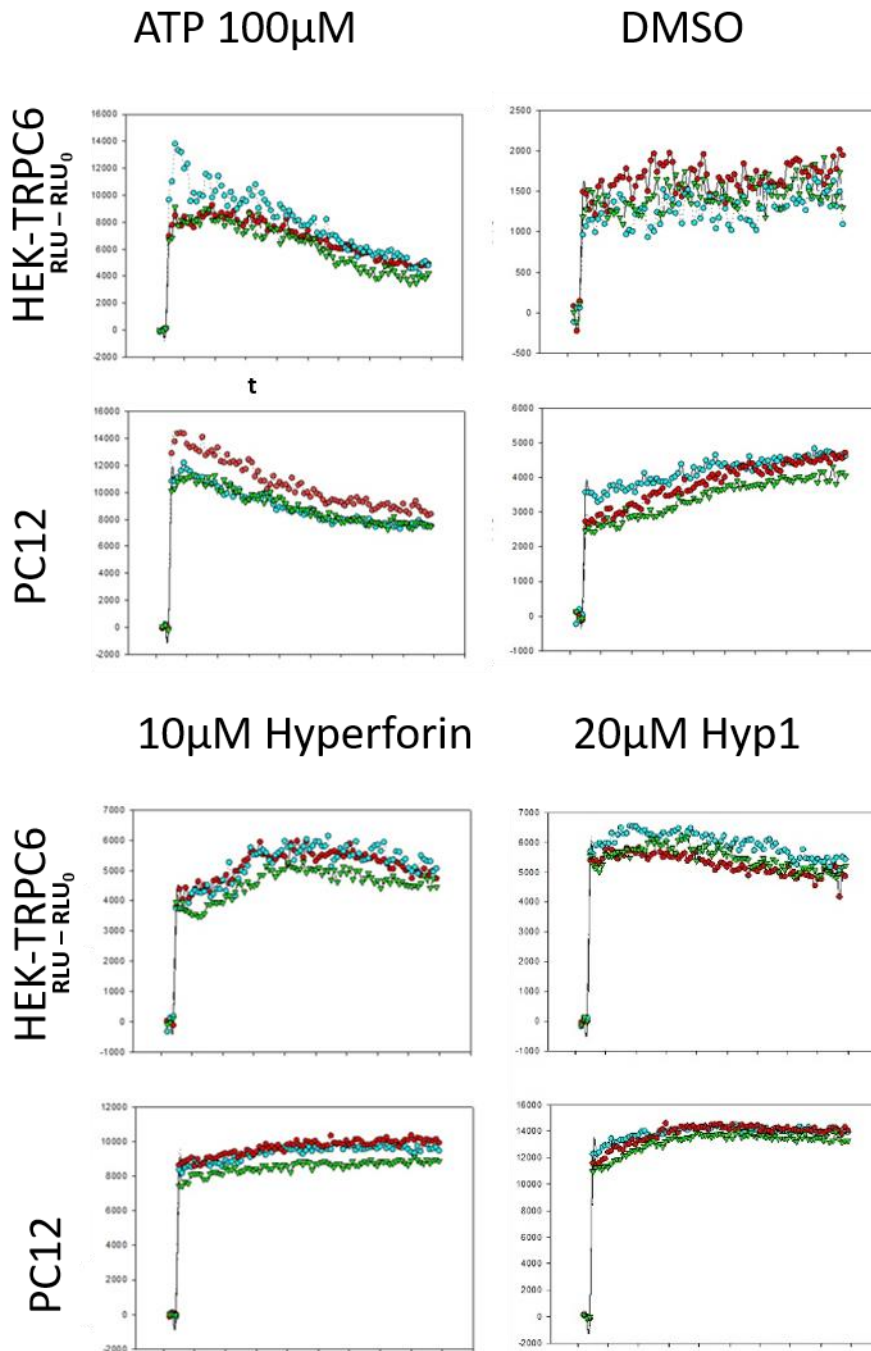


Figure 45 Calcium influx into HEK293 cells expressing TRPC6 and PC12 cells. Baseline-corrected fluorescence intensity ($RLU - RLU_0$) over time. Time course of 3 min, six wells measured simultaneously, measurement per well every 2.13s. 50,000 cells per well seeded 24 h prior to measurement and loaded with Fluor-4 dye. Stimulation solution either contained 100 μ M ATP, DMSO, 10 μ M Hyperforin or 20 μ M Hyp1. 1st and 3rd row represent each three wells of TRPC6 stable transfected HEK. 2nd and 4th row represent three wells of PC12 cells. Lab book: AHa160

To verify the functionality of the assay, a similar experiment was performed injecting a 5% SDS solution into dye loaded HEK-TRPC6 and PC12 cells. Two conditions have to be met in order to constitute an active fluorophore: 1) intracellular cleavage and 2) binding of Ca^{2+} . SDS leads to cell lysis and the

exposure of the dye to elevated calcium concentrations in the surrounding media. If the dye was taken up by the cells and cleaved, SDS would lead to a signal increase. The addition of EDTA will complex Ca^{2+} and inactivated the dye again. Such an assay was performed (**Figure 46**) and the principal functionality of the assay proven.

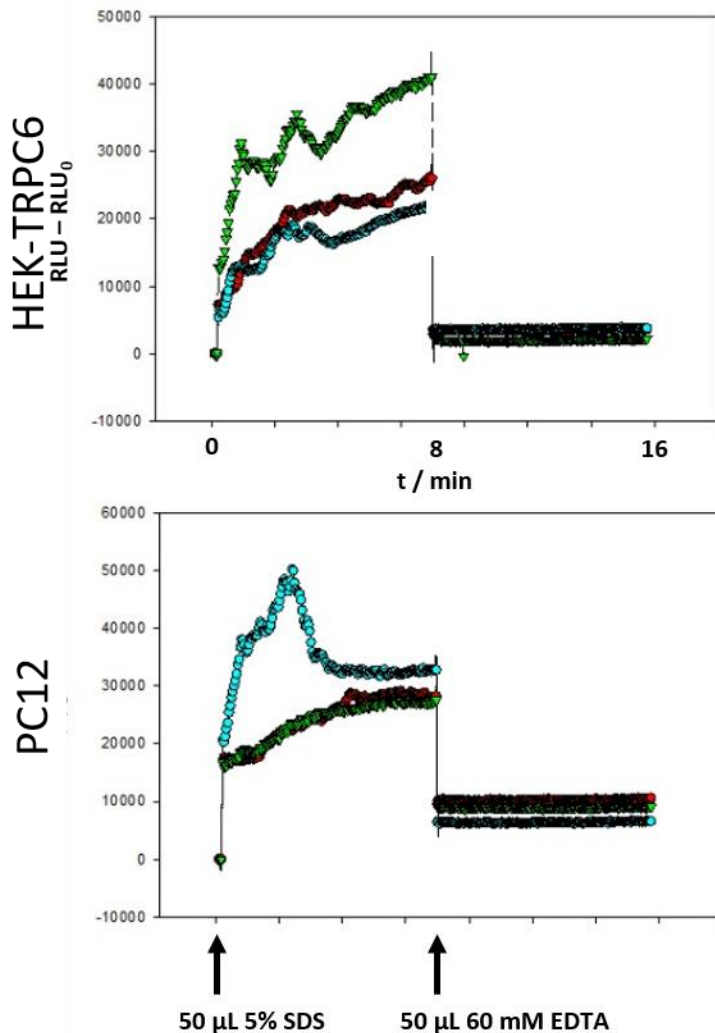


Figure 46 Calcium influx into HEK293 cells expressing TRPC6 and PC12 cells. Baseline-corrected fluorescence intensity (RLU-RLU₀) over time. Time course of 16 min, six wells measured at once, measurement per well every 2.13s. 50,000 cells per well seeded 24 h prior to measurement and loaded with Fluor-4 dye. Instead of stimulant, 50 µL 5% SDS solution was added. After 8 min 50 µL of a 60 mM EDTA solution were injected on top (200 µL final volume). Labbok: AHa161

Since the reported TRPC6 stimulants did not show the expected effect in the mentioned cell lines, additional substances, namely the activator of phospholipid-dependent protein kinase C 1-oleoyl-2-acetyl-glycerol (OAG) and the cholinergic agonist carbachol were tested. HEK293T cells were transiently transfected with either TRPC6 or mock plasmid and treated with OAG and Carbachol (**Figure 47**). While

ATP served as robust positive control, OAG did not show any effect at the two used concentrations. Using Carbachol, it was possible to stimulate both TRPC6 overexpressing and Mock transfected cells.

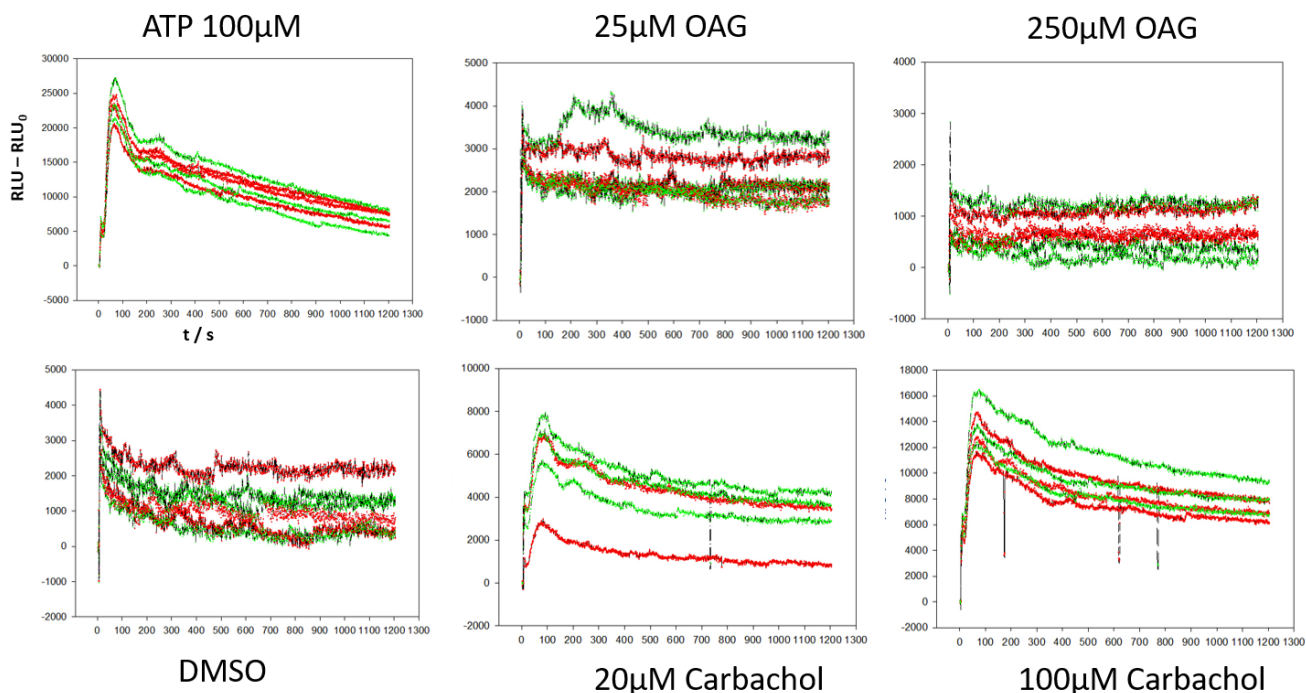


Figure 47 Calcium influx into transient TRPC6 (green) or mock (red) transfected HEK293T. Baseline-corrected fluorescence intensity ($RLU - RLU_0$) over time. Time course of 2 min, measurement interval of 0.1 s. 50,000 cells per well seeded 24 h prior to transfection with 100 ng/w (HG598 or HG30) for 24 h. Afterwards, cells were loaded with Fluor-4 dye. Stimulation solution either contained 100 μ M ATP, DMSO, 25 μ M OAG, 250 μ M OAG, 20 μ M Carbachol or 100 μ M Carbachol. Lab book: AHa180

To exclude artifacts introduced by the transfection and in order to check other stimulants as well, HEK293T cells were transfected with either TRPC6 or TRPC6 mutant (Leuner group, FAU Erlangen), which is expressed but incapable of Ca^{2+} transport. The cells have been subjected to a Calcium-Uptake Assay using ATP, DMSO, Hyperforin, Hyp1 and OAG (**Figure 48**). Again, only ATP lead to Ca^{2+} influx.

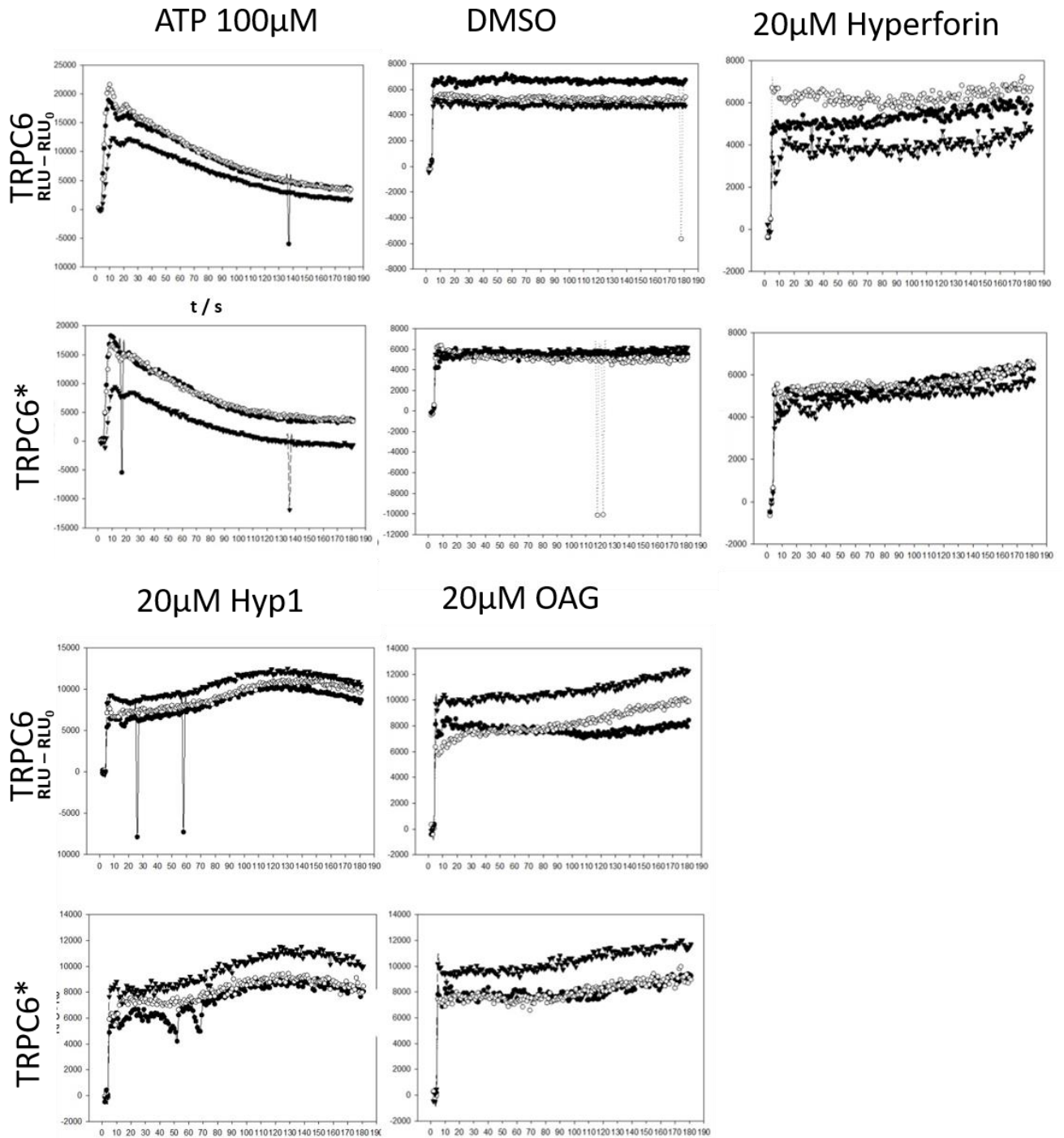


Figure 48 Calcium influx into transient TRPC6 (upper row) or TRPC6 mutant (lower row) transfected HEK. Baseline-corrected fluorescence intensity (RLU-RLU₀) over time. Time course of 3 min, measurement interval of 0.5 s. 50,000 cells per well seeded 24 h prior to transfection with 100 ng/w (HG598 or HG658) for 24 h. Afterwards, cells were loaded with Fluor-4 dye. Stimulation solution either contained 100 µM ATP, DMSO, 20 µM Hyperforin, 20 µM Hyp1 or 20 µM OAG. Lab book: AHa210

6. Discussion

6.1. Summary

In this thesis I present data that further elucidates both the action modes of FKBP51 and the effects of FKBP51 ligands. With MTQ202, I identified a PROTAC which robustly knocks down FKBP51 expression levels in three different cell lines (HEK293, HeLa and N2a), both endogenous and transiently overexpressed. Using Western Blot protein detection, MTQ202 shows activity in concentrations higher than 60 nM which is confirmed by a reduced luminescence signal of an overexpressed Nanoluc-FKBP51 fusion protein. The effect of MTQ202 is strongest after 48 h treatment. A competition of 250 nM MTQ202 with an 8-fold excess of either SAFit1 or VHL-ligand did not show a reduction of PROTAC activity.

In order to investigate FKBP51 in its role as cochaperone and regulator of glucocorticoid signaling, I successfully established a dual-luciferase-flash reporter gene assay in N2a cells. This assay required the cotransfection of a small amount GR in order to establish a sufficient assay window. The overexpression of FKBP51 reduced the expression of firefly luciferase in a dose-dependant manner without impacting the second luciferase signal. Several mutants of FKBP51 have been tested. A major impact was only exhibited by the TPR mutation but not by its active site mutations. The overexpression of FKBP52 increased GR signaling after 8 h stimulation but not 24 h. The reporter activity remained unaltered by the addition of SAFit1 but could be increased by MTQ202.

To investigate the FKBP-Glmn interaction, I developed a competitive HTRF binding setup. This HTRF assay confirmed the previously described binding of Glmn towards FK1 domains. Excitingly, other FKBP5s and FKBP constructs were identified as interactors as well, discovering the novel interaction of Glmn and FKBP12.6. The known binder FKBP12 was shown to be a very weak interactor within this setup. Full-length FKBP51 and FKBP52 bind stronger than their respective FK1 domains. Within the FK1 domains two amino acids, F67 and D68, were identified, which are essential for the FKBP51-Glmn interaction. At last, I could demonstrate that this interaction is ligand sensitive, showing the very first biochemical activity of synthetic FKBP51 ligands.

6.2. FKBP51 PROTACs

Testing 62 different PROTACs for FKBP51 revealed a single compound (MTQ202/MTQ416) which induced a chemical knockdown in the range of 60 to 2000 nM after 6 h as long as 72 h down to 40% compared to FKBP51 levels in untreated cells. This effect was confirmed by the PROTACs action in the knockdown of a Nanoluc-FKBP51 construct and its effect in a GR reporter gene assay. Although, all SAFit and most bicyclic PROTACs are binding FKBP51 in the low nanomolar range (unpublished, PhD Thesis MTQ), their target affinity clearly cannot be translated into knockdown efficacy [43]. This phenomenon is commonly seen during the development of PROTACs, which often requires the synthesis of a small library to obtain a successful lead compound. The PROTACs developed by Tianqi Mao vary in linker length and linker attachment point. The formation of the trimeric complex is thus far unpredictable, but the linker is likely involved in mediating contacts instead of just a simple space keeper [46]. Therefore, the crystallization of the trimeric FK1-PROTAC-VHL complex might give valuable insights into the future development of FKBP-PROTACs.

Although, HEK293T cells have been treated with up to 2 μ M PROTAC, no hook effect was observable. The hook effect describes the phenomenon of decreased chemical knockdown at high PROTAC concentrations which is believed to be caused by the preferred formation of dimeric complexes (Figure 49). The absence of the hook effect is not unprecedented and some PROTACs are only able to knock down their target at relatively high concentration in μ M-range (see for example [145]).

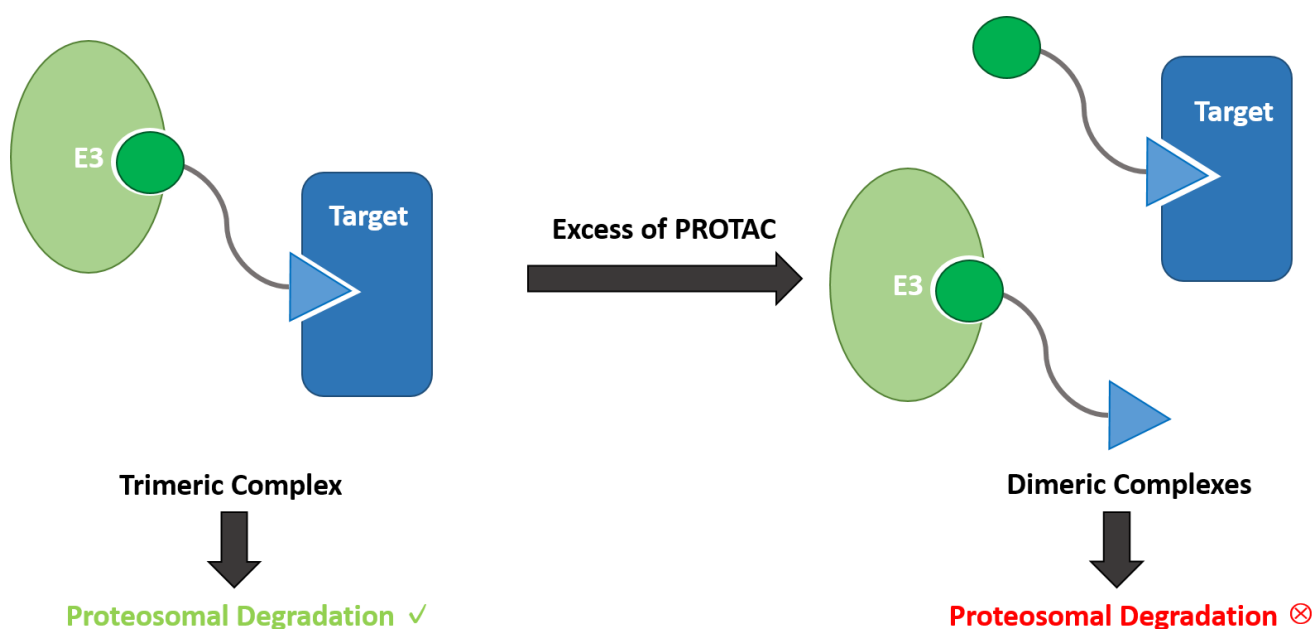


Figure 49 Hook effect of PROTACs. The excess of PROTACs leads to an increased formation of dimeric complexes, where the PROTAC binds either its target or the E3 ligase. The dimeric complexes

In order to obtain decent Western Blot results, I experienced the importance of the normalization of the samples according to their total protein concentration and a careful removal of media prior to lysis and

washing step, since leftover media distorts the BCA assay. Additionally, the solubility of many PROTACs have to be carefully observed during the experiment. Many of the here tested compounds precipitated at concentration $>4 \mu\text{M}$ in cell media as they precipitated during the assay preparation. This limitation also prevented the observation of a competition effect by either free SAFit or VHL-ligand added. An 8-fold excess of both factors did not dampen the knockdown induced by 250 nM MTQ202, which is in line with the fact that at maximum tested PROTACs concentration of $2 \mu\text{M}$ no hook effect occurred. An overall challenge was the detection of the GAPDH control band. No systematic cause for partial altered GAPDH bands could be identified. The switch to another control would benefit the result quality, yet many of them run close FKBP51. In my experience, Hsp90 gives a decent control signal but is a rather uncommon loading control and also strongly associated with FKBP51.

At last, I want to point out a certain possibility, that more than one PROTAC is active, but the chemical knockdown was not observable under the applied assay conditions. Recently, Riching, et. al. showed in their efforts to develop high-throughput PROTAC-screening methods that especially time and concentration will strongly effect knockdown strength [58]. They were able to label target BRD proteins in cells. A newly constituted luciferase-tag provided a luminescence readout in presence of stabilized substrate. The indirectly measured protein concentration varied strongly depending on the assay condition and the time of the readout.

Generally, the development of PROTACs would greatly benefit from high-throughput screening methods, enabling investigators to vary time, concentration and compounds within the same experiment without the workload of Western Blot detection.

6.3. FKBP51 in Glucocorticoid Receptor Signaling

In order to investigate the role of FKBP51 and FKBP52 ligands in GR signaling a dual-luciferase-flash reporter gene assay was set up. The co-transfection of low amounts of a HA-GR construct (0.5 ng/well per 10,000 cells) was required to obtain a decent assay window, which underlines the low amount of endogenous GR present in N2a cells. This neuronal cell line was used for two reasons: On the one hand, stress-induced depression is linked to glucocorticoid resistance in the hypothalamus [146]. On the other hand, FKBP51-specific ligands showed an impact on the neurite formation of neuronal cells, including N2a cells [22]. Both firefly and normalized luciferase signal reached saturation as cells were stimulated with more than 100 nM Dexamethasone. The half-maximal signal was observed for concentrations around 4 nM. Henceforth, this concentration was used to investigate FKBP51 related effects. The titration of FKBP51 plasmid during the transfection led to a dose-dependant decrease of reporter signal saturated for concentrations $> 10 \text{ ng/well per } 10,000 \text{ cells}$. The overexpression of FKBP52 raised the signal and competed with the FKBP51-induced effect but only after 8 h stimulation time and not after 24 h. Those findings confirm the inhibitory model of FKBP51 in GR signaling and its functional counterplayer FKBP52. It can be speculated that FKBP52 overexpression raises intracellular

coping mechanisms, such as the induction of degradation of this protein, which level off its effects after 24 h stimulation time.

The reporter gene assay setup was also used to transfect different FKBP51 mutants. The PPIase mutant (FD67/68DV) had the same inhibitory potency as the wild type as well as the triple FKBP51-FKBP52 swap mutant. The L119P is a FKBP51/FKBP52 swap, which is located in a proline-rich loop on top of the active site. The position 119 is one of the few differences in the very conserved binding pocket. Still, this mutant inhibited GR signaling, only mildly weaker than the wild type. The TPR* mutant, which was shown not to bind Hsp90 [28], led only to a slightly decreased signal. Those observations indicated that an intact PPIase activity is not required for GR signaling and that Hsp90 binding enhances FKBP51 activity in GR signaling. Nevertheless, the TRP* mutant effect, which only dampens but not obliterates FKBP51 inhibition might indicate the presence of more interaction sites throughout the protein, concurring with the the model of FKBP51 serving as protein complex scaffold.

The presence of SAFit1 did not reverse FKBP51-induced GR inhibition. On the contrary, it weakly increases GR inhibition, which might be due to an unspecific side reaction. It has to be noted that SAFit1 concentrations greater 5 μ M lead to an artificial rise of the normalized signal, due to a decreased Renilla signal concomitant with observable cell rounding and detachment. The addition of the PROTAC MTQ202 antagonized FKBP51 inhibition independent of the presence of transiently transfected FKBP51. This supports the hypothesis, that FKBP51 acts independent of its active site and the presence of ligands attached to it. I consider it very likely, that the action of FKBP51 selective ligands in mouse model studies and in neuronal differentiation might be either hardly GR dependent or not represented within this reporter gene assay performed in the murine neoplastoma derived N2a cell line. This concurs with the observation that single mutations of FKBP51 swapping amino acids with FKBP52 hardly showed an impact. The triple mutant is unable to bind SAFit1 because it cannot adopt the Phe67-out conformation. To confirm this scaffold model, a domain swap mutant (FKBP52FK1-FKBP51FK2-TPR) should be tested in this assay.

The FKBP51 PROTAC MTQ202 acts differently compared to SAFit. Instead of a mere binding site occupation, it leads to proteasomal degradation of the protein reversing its expression – ligand induced removal instead of epitope inhibition. Overall, this assay has the potential to address the investigation of the effects of FKBP51 and FKBP52 mutants, but reaches its limitations to study FKBP51 ligands. In order to transfer this assay to other cellular systems, a certain amount of optimization efforts have to be invested with respect to transfection, treatment and stimulation conditions. Performing this assay in a human cell line would bear the advantage of creating a pure human system which might not require the overexpression of the GR. The FKBP51 constructs and GR used in my experimental setup are human and the ligands are generally tested for in-vitro affinity on human but not murine FKBP51s.

6.4. FKBP51 in NF- κ B Signaling

While setting up a reporter gene assay using two reporter plasmids for either the canonical or non-canonical NF- κ B pathway, several observations did not concur with previous reports. The non-canonical pathway was only inducible with TNF α in Jurkat cells providing a very limited assay window of a 3-fold induction. PMA proved to be a very weak, but toxic stimulant, only inducing the canonical pathway in HEK293 cells. The concentrations greater than 40 nM led to massive cell death of HEK293 and A375 cells. Since the maximum induction by PMA occurred at 15 nM, it has to be questioned, if this stimulation might be unspecific and an overall cellular stressor. My findings indicate, that PMA is not a suitable stimulant, contradicting several reports [136,140]. A375 cells are derived from a human malignant melanoma, but the primary reporter remained unable to express the firefly reporter in presence of stimulants. Due to the fact, that the Renilla reporter showed a decent signal, the preceding transfection was successful. It has to be assumed, that a general issue with this cell line occurred. A375 cells are a commonly used cancer cell line to investigate NF- κ B signaling [103,104,147]. All data presented here, which showed a decent reporter induction, had the same feature in common: Overexpression of FKBP51 resulted in a reduced reporter activity. This is the contrary effect as Zannas *et. al.* found recently [148], which used the same cell line and reporter constructs. There are a couple of differences in the performance of the assay:

	Hähle	Zannas, et. al.
Overall protocol	1) Seeding into 96 well plate 2) Transfection in 96 well plate	1) Transfection of the cell whole batch 2) Seeding into 96 well plate
Transfection amount of FKBP51	50 ng/well per 10 ⁵ cells	1 μ g per 10 ⁶ cells
Stimulation	0 to 20 ng/mL TNF α	25 ng/ml PMA (40 nM) 375 ng/ml Ionomycin

The co-stimulation with PMA and Ionomycin is widely used to stimulate both NF- κ B and NFAT pathway in order to study interleukin secretion. This was also represented in the paper for which the reporter gene assay was performed under similar stimulation conditions.

To further confirm any FKBP51 effect, several controls should be introduced into the assay. Especially the effect of a PPlase-deficient mutant, a Hsp90 binding disabled TPR mutant and FKBP52 should be cotransfected in order to exclude an assay artifact, such as translational stress.

6.5. FKBP51 and Glomulin

In my results, I show the binding of several FKBP5s and Glmn in a HTRF setup. Variations in the respective IC₅₀s occurred without altering the general trends of the different protein affinities. Those

shifts appear for all competing proteins or ligands indicating a general error. Generally, increased attention should be paid to the environmental conditions during the assay performance. Especially assays with purified proteins might be temperature and humidity sensitive if incubated in a lid closed but unsealed state at “room temperature”, which I experienced to vary between 12 and 40 °C. A higher temperature would affect the HTRF signal by altering the thermodynamics of the interaction. An increased concentration of labeled FKBP51FK1-5MF would bind to those competitors without a decrease of the HTRF signal. I identified FKBP12.6 as a novel interactor, while FKBP12 remained very weak. This novel example of difference can help to understand the difference of action mode of those two proteins despite their homology for example in RyR1 regulation. It has previously been proposed that a limited number of point mutations can reverse binding affinities to the ryanodine receptor [149]. A similar test as the HTRF setup might help to identify more amino acid sites, which contribute to the interaction. Furthermore, the enzymatic essential sites Phe67 and Asp68 of FKBP51 were shown to be required to bind Glomulin. In order to identify an overall FKBP interaction surface, those mutations should additionally be incorporated into FKBP52FK1 and FKBP12.6. Since full length FKBP51 and especially FKBP52 are binding Glmn 3-fold, respectively 50-fold better, the ability to blunt the FK1 domain might finally lead to an improved understanding of the function of the FK2 domain. If those mutated full-length proteins still bind Glmn, it is very likely that either the FK2 or the TPR domain positively contribute to the binding. This could also be verified by testing the competitive capability of the purified domains alone. Also the respective TPR domains which are overall less conserved as the FK1 domains might be of interest. Bracher et. al. showed that the linker between FK1 and FK2 domain is more flexible in FKBP52 than it is in FKBP51 [30]. They found two conformational orientations of both FKBP52 FK domains. One is “FKBP51-like” and the other one is twisted by 180° (**Figure 50**). It is possible that the twisted conformation makes the FK2 domain more accessible for interaction, which cannot occur in FKBP51 and leads to a strongly improved binding of FKBP52 compared to FKBP52FK1 and FKBP51.

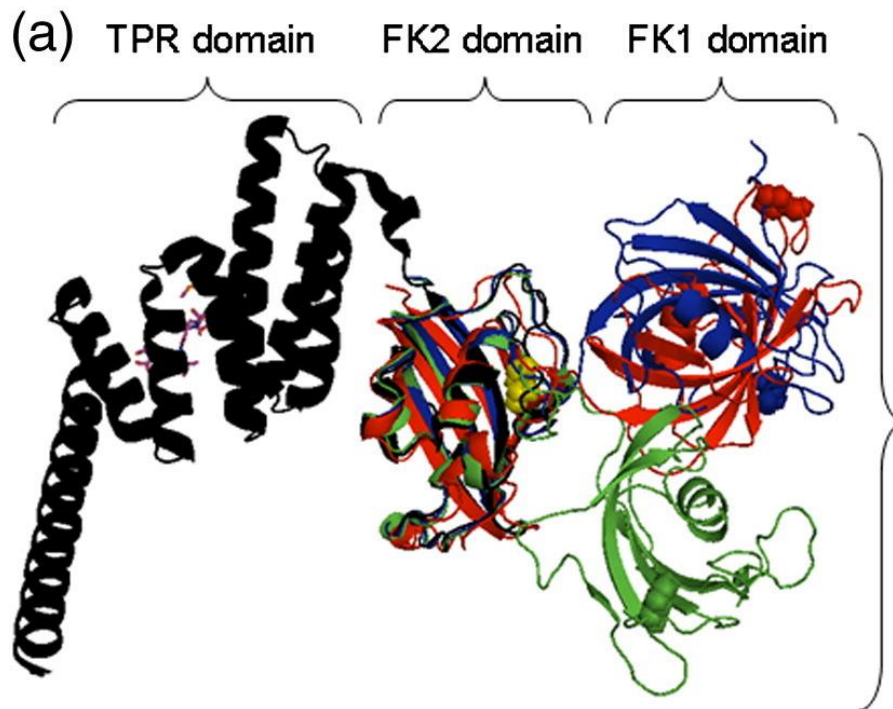


Figure 50 The interface between the FK1 and FK2 domains, overlay of FKBP51 (red) and two conformation of FKBP52: “FKBP51-like” (blue) and rotated by 180° (green). Taken from [30].

I hypothesize that FKBP5s represent an additional layer of E3 regulation and propose that FKBP5s affect Cul/Rbx1-type E3 ligases through sequestration of the Glmn and therefore affecting E3 ligase target levels. The overexpression of Glmn was shown to lead to an increase of Fbw7 E3 ligase targets such as Cyclin E and c-Myc [119]. If Glmn sequestration by FKBP5s would prevent Glmn from binding to the E3 complex, it should impact the target degradation. According to my results such sequestration might be FKBP5 ligand sensitive.

FKBP5 Inhibitors \downarrow FKBP5 \downarrow Glmn \downarrow Cul/Rbx1 \rightarrow Fbw7 self-ubiquitination and degradation \rightarrow Cyclin E/c-Myc abundance.

I propose that FKBP5 inhibitors, which disrupt the FKBP5-Glmn complex, will restore the regulatory role of Glmn on E3 ligases counteracting the effect of the known Glmn mutants. Investigating this hypothesis will improve our understanding of E3 regulation and might foster a novel therapeutic approach to target Glmn-associated disorders.

6.6. FKBP51 in Calcium Signaling

FKBPs are associated to calcium channels such as TRPC6 and RyR1. Therefore, a calcium influx assay was set up to test a potential impact. The calcium agonists are listed in **Table 4**. ATP treatment, which activates P2X and P2Y receptors, led to an increase of nucleosolic calcium concentrations, as did Carbachol, which leads to a release of intracellular stored calcium.

Stimulant	Mechanism	Reference
ATP	Activates P2X receptors for external influx Activates P2Y receptors for stored release	[150] [151]
Hyperforin and its derivatives	Specifically activates TRPC6	[142,143,152]
OAG	Derivative of DAG, both directly bind TRPC6	[153-155]
Carbachol	Agonist for muscarinic acetylcholine receptors, release of intracellular stored calcium	[156,157]

Table 4 Overview of tested stimulants

Cells treated with the DAG derivative OAG, Hyperforin and its derivative Hyp1 did not show a measurable calcium increase in the reported range of 10 to 30 μ M. There is a possibility, that the used drugs were degraded as Hyperforin and OAG is light and heat sensitive. Since the literature claimed stimulation was not observed, this assay was not pursued further.

6.7. The FKBP51 interactome

In this thesis, my results indicate that FKBP51 exhibits two different action modi. While FKBP51s binding to Glmn is mediated via Phe67 and Asp68 in its FK1 domain, their absence does not impact FKBP51s inhibitory effect on GR signaling. This concurs with the ligand sensitivity of the FKBP51FK1-Glmn interaction, while the presence of SAFit shows no major impact within the GR reporter gene assay. In order to elucidate the molecular mechanisms of FKBP51 more knowledge of the protein-protein-interaction sites needs to be acquired. Thus far, no cocrystal structure of FKBP51 with a potential client is available (except with Hsp90s MEEDV motif). Here, the homology with the FKBP family might be a guide for inspiration.

All published dimeric crystal structure of FKBP51 in complex with client proteins are listed in **Table 5**. The two available trimeric complexes of FKBP12 with the FRB of mTOR mediated by Rapamycin and Calcineurin mediated by FK506 are excluded. Interestingly, all four structures show a proline close to either FKBP12 or FKBP12.6s concurring phenylalanin and aspartic acid (**Figure 51** to **Figure 54**). Even the trimeric complex of FKBP12, Calcineurin and FK506 finds a proline at that position. I raise the hypothesis that those three amino acids might define a common FKBP-client interaction motif. The F-D sequence is present in many FK1 domains: FKBP51 Pos. 67-68, FKBP52 Pos. 67-68, FKBP12 37-38, FKBP12.6 Pos. 37-38, FKBP13 66-67, FKBP25 145-146, FKBP65 Pos. 79-80.

FKBP	Client	Remarks	Proline present near Phe - Asp	PDB
FKBP12	RyR1	Dimeric complex	YES	3J8H [158]
FKBP12	TGF β	Dimeric complex	YES	1B6C [159]
FKBP12	ACVR1	Dimeric complex	YES	3H9R [160]
FKBP12.6	ACVR1	Dimeric complex	YES	4C02 [10.2210/pdb4C02/pdb]

Table 5 Overview on published FKBP-client cocrystalstructures

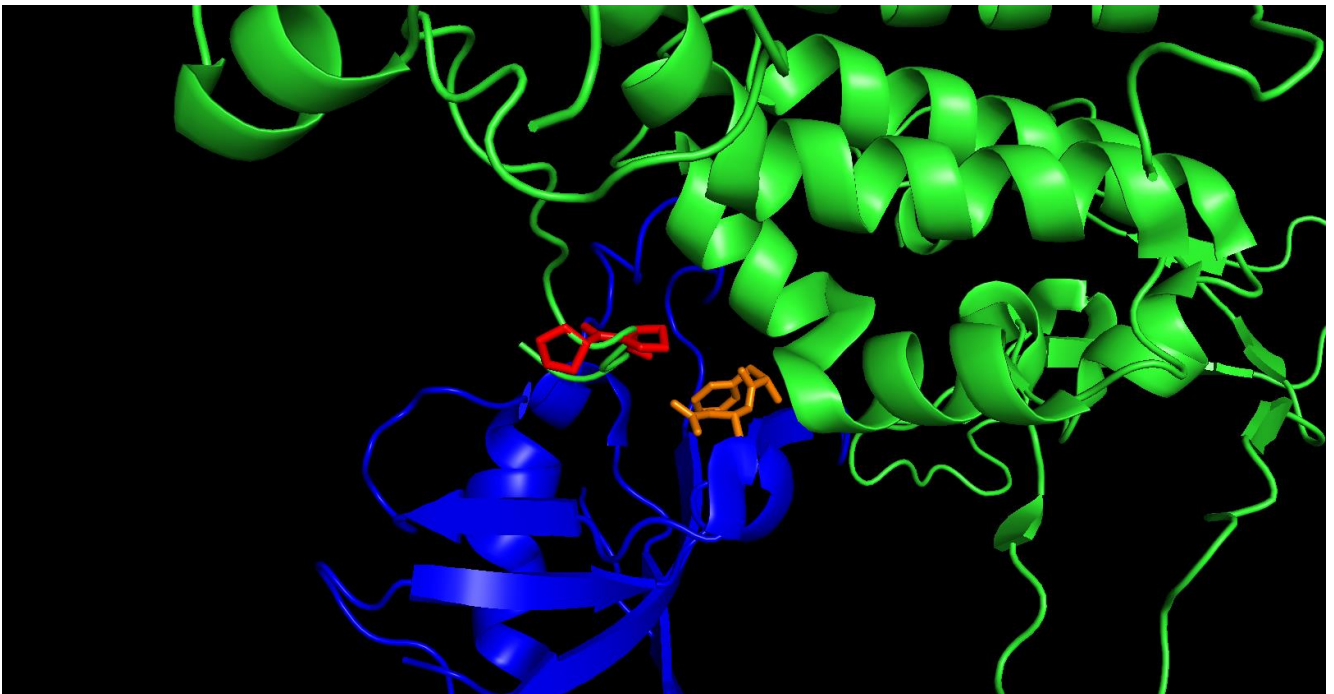


Figure 51 Cocrystalstructure of FKBP12 (blue) and RyR1 (green). Phe and Asp within the FKBP binding pocket are depicted in orange. Client prolines close to that pocket are depicted in red. PDB: 3J8H

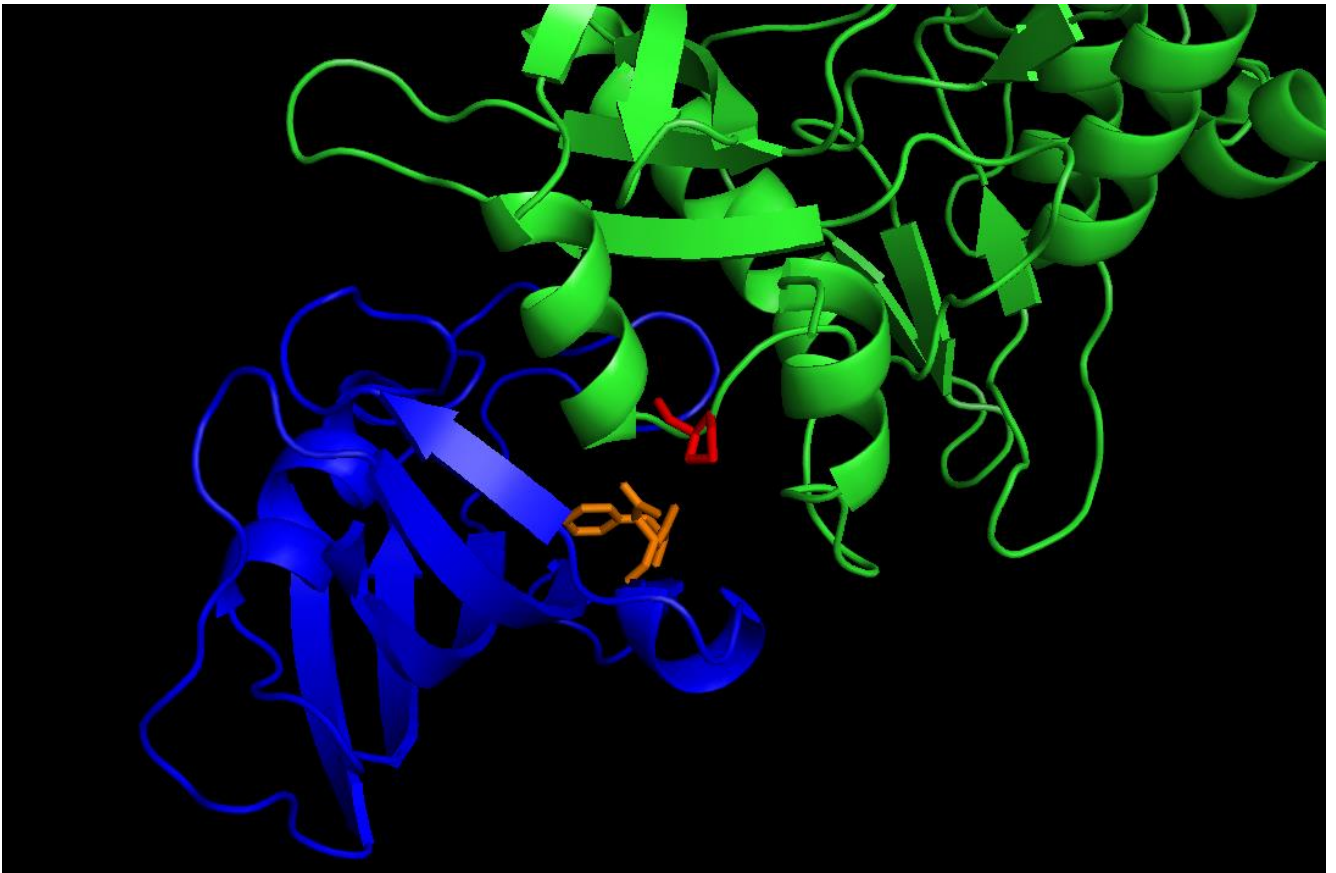


Figure 52 Cocrystalstructure of FKBP12 (blue) and TGFβ (green). Phe and Asp within the FKBP binding pocket are depicted in orange. Client prolines close to that pocket are depicted in red. PDB: 1B6C

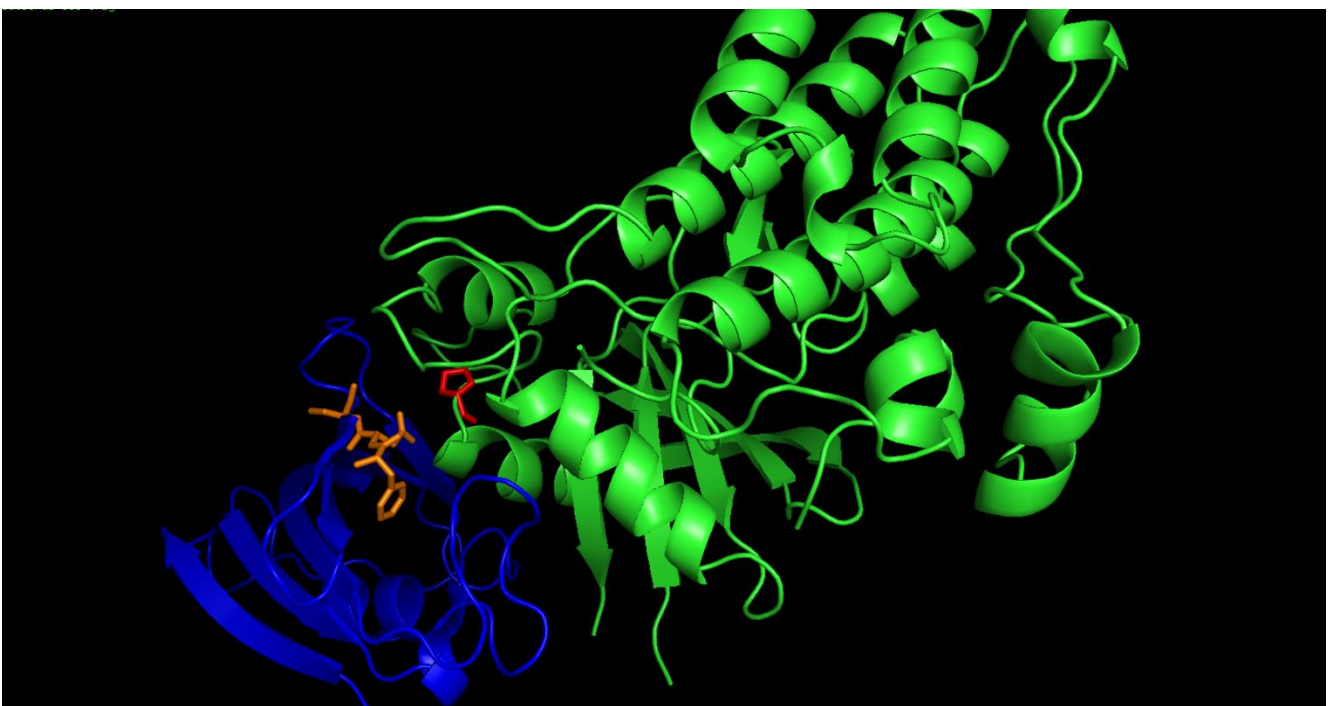


Figure 53 Cocrystalstructure of FKBP12 (blue) and ACVR1 (green). Phe and Asp within the FKBP binding pocket are depicted in orange. Client prolines close to that pocket are depicted in red. PDB: 3H9R

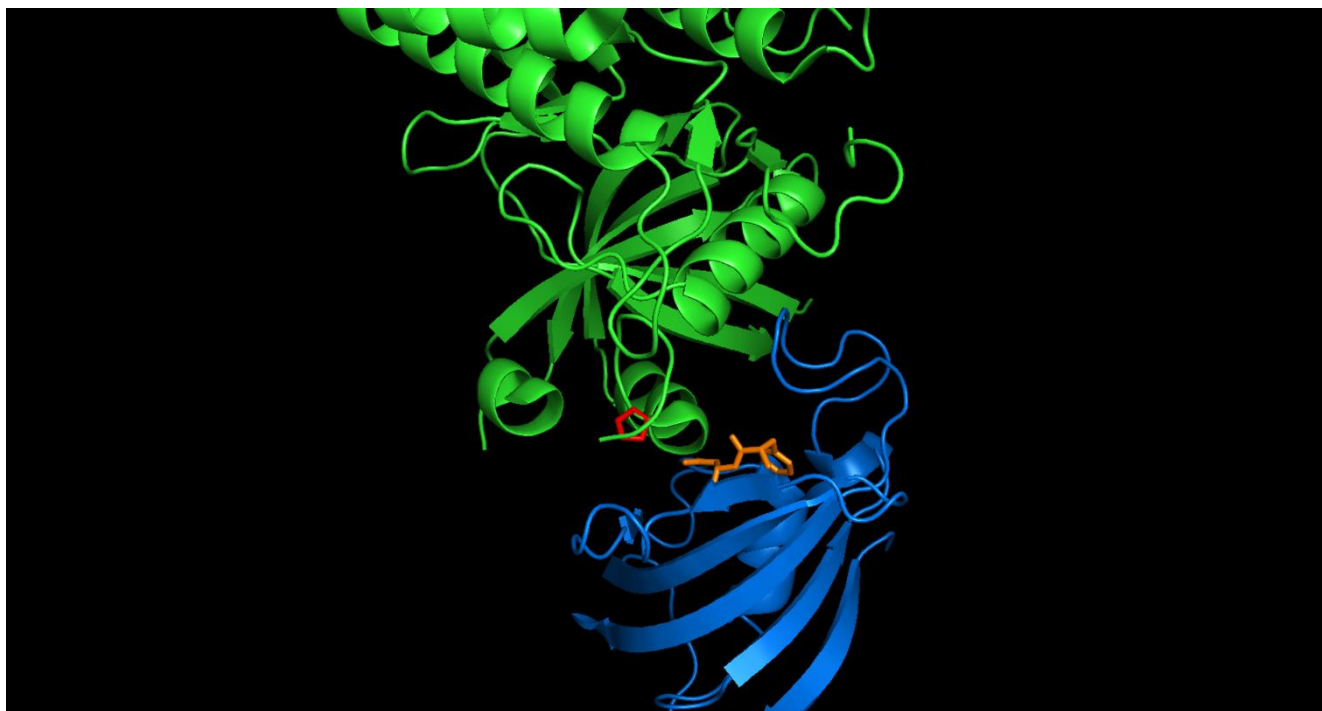


Figure 54 Cocrystal structure of FKBP12.6 (blue) and ACVR1 (green). Phe and Asp within the FKBP binding pocket are depicted in orange. Client prolines close to that pocket are depicted in red. PDB: 4DRI

An important follow-up towards the shown FKBP-Glcn interaction would be crystallization efforts, which not only give more insight into the interaction surface, but have direct implications for drug development aiming for a disruption of the interaction.

6.8. Perspectives for ligand development

In summary, I described two different potential modes of action for FKBP51 ligands: The FKBP51-Glcn interaction can be interrupted *in vitro* with different classes of ligands – the SAFit class ligand SAFit1, the bicyclic compound JK96, and the natural ligand FK506. In this kind of *in-vitro* assay using purified proteins, the addition of the PROTAC MTQ202 would not bear any benefit, since the assay mix does not contain the degradation-catalyzing enzymes. The inhibitory effect of FKBP51 in GR signaling could neither be obstructed by SAFit1 nor a blunted PPIase pocket. Here, FKBP51 likely serves as a part of a multi-protein complex exhibiting scaffold function which is independent enzyme pocket related activity. Nevertheless, MTQ202 impacted the reporter activity by degrading FKBP51. An overview can be found in **Figure 55**.

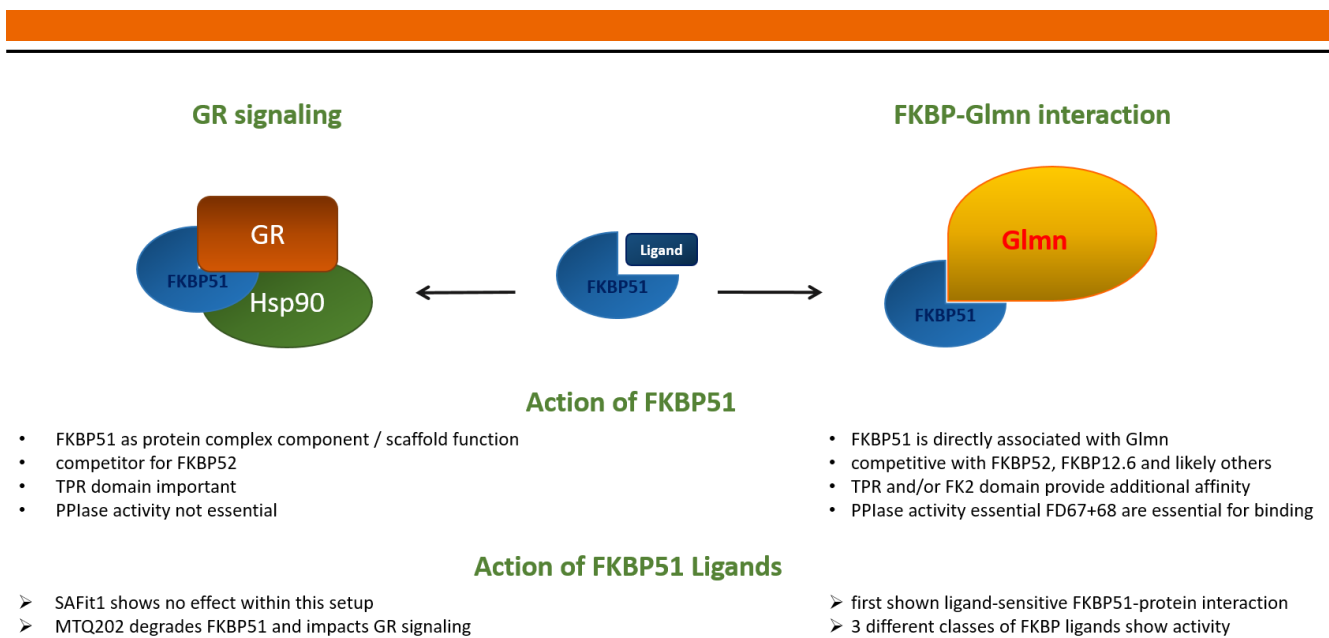


Figure 55 Summary of found FKBP51 ligand action in GR signaling and the FKBP-Glmn interaction

PROTACs and “conventional” ligands do not only distinguish from one another in their way of target inhibition but also in their chemical features.

Especially the development of *in-vitro* assays would benefit by overcoming the 4 μM limitation. More hydrophilic compound derivatives could be applied to both cellular and purified protein utilizing assays. With respect to the addition of ligands to cultured cells an increase hydrophilicity can cause a decreased uptake into the cytosol. A competitive BRET setup would be able to observe such a drawback. The use of more hydrophilic compounds in purified protein assays bears several advantages: 1) Higher concentrations of soluble compound has the benefit to allow a more accurate quantification by obtaining both plateaus within the compound titration series as shown in my HTRF setup. 2) Any assay based on a pulldown or fishing approach will benefit from better soluble ligands, since the HTRF setup e.g. identified the IC_{50} of SAFit1 in the low micromolar range in order to disrupt the Glmn-FKBP51FK1-5MF binding. In order to identify interaction partners of either FKBP51 or FKBP51 ligands in cell lysates, it might occur that ligands thus far are too weak to quantitatively disrupt an already established FKBP-protein interaction.

Table 6 lists the measured HTRF IC_{50} s and their FP-Assay K_D s on FKBP51FK1:

	HTRF IC_{50} in μM	FP-Assay K_D in nM	#-fold difference
SAFit1	9; 35	20 [40]	1000
JK96	0.16; 0.37	20 [40]	10
FK506	0.31	400 [40]	similar

Table 6 Comparison of compound affinities (rounded) in Glmn-HTRF setup and competitive FP-Assay on FKBP51FK1

It is obvious, that the values of both assays do not correlate. It has to be noted, that both assays utilize different FKBP51FK1 constructs: aa 1-140 C103A / C107I / E140C, 5-MF labeled (HTRF) and aa 16-

140 A19T (FP-Assay). Those different constructs unlikely impact ligand binding since the alterations are outside of the binding pocket and not conserved between FKBP51, FKBP52 and FKBP12. Still, a single mutation and especially the fluorescein maleimide labeling procedure can impact the overall structure. For this reason, we choose to label the C-terminus which is of greater distance from the binding pocket and more likely avoids structural interference. While the values for FK506 are in the same order of magnitude, synthetic ligands compete worse in the HTRF. The HTRF assay incubated at least for one hour and also overnight ligand affinities tend to get weaker. Therefore, a model of a kinetic inert FKBP51FK1-Glmn complex, which cannot be disrupted by ligands seems unlikely. It is more likely that the K_D of Glmn towards the FK1 domain is much lower than of the tested ligands, which would contradict the findings of FK506. To overcome this obstacle, simply more data is required, including the testing of more ligands and a similar HTRF with a different FKBP client protein. Different FK1 domains should also be utilized and fluorophore labeled as well as FK2 domains, as the respective Cysteins are not conserved within the FKBP family and usually not close to the ligand binding pocket. The creation of a labeled full-length FKBP51 or 52 might prove more sophisticated, as the greater number of Cysteins to mutate can affect the protein structure. The labeling position is of importance as well, as the FRET effect is strongly distance depending.

This is the first shown FKBP51-protein interaction disruptable by conventional ligands. Although those ligands did not impact GR signaling, their respective effects on neurite outgrowth and multiple mouse model phenotypes might be effected by one or more direct interactions. A promising target to follow up my findings seems to comprise components of the IKK complex. Despite the confusion on FKBP51s action within the NF- κ B pathway, the increasing amount of publications linked to it urgently require a revision via a clear breakdown into single interactions.

All in all, those findings encourage the development of conventional ligands striving for high-affinity and selectivity profiles. Nethertheless, relying on FP-Assay data to justify their investigation in cellular or even mouse models should be backed up by other *in-vitro* assays such as my HTRF.

Despite the conventional ligands, I showed the activity of the FKBP51 PROTAC MTQ202. PROTACs acts completely different by the induction of target degradation. This enables MTQ202 to decrease intracellular FKBP51 concentration and even target its PPIase pocket and conventional ligand insensitive functions, such as a scaffold providing platform. Henceforth, MTQ202 was active in my GR reporter gene assay. MTQ202 can serve as a great tool for any kind of cellular assay, since it provides the answer to a simple but important question: Do FKBP51 levels matter within a certain context? Therefore, PROTACs provide a potent and easy applicable alternative to gene editing and RNAi knockdown. The PROTAC is simply added to the cell media and the cells do not need to undergo a stressful transfection step, keeping their genome unaltered. MTQ202 seems especially promising, due to its long lasting effect. The concept of PROTACs always carried the flaw of being non-adaptive to mouse model studies for their comparable large molecular size and predicted ADME profile. This belief slowly changes. Some PROTACs carry the potential serving as more than “just” a chemical knockdown

tool. Recently, the first PROTAC went into clinical trial phase I [59] and a FKBP12 degrader was shown to be active in multiple tissues in mouse – after oral administration [161]. Parallel to the development of CRISPR and RNAi technology, PROTACs might have a future in clinics (**Figure 56**). Further increasing the lab internal PROTAC library might lead to a better PROTAC as MTQ202, although the outcome is not predictable. Discovery of PROTACs acting on other FKBP's could be a potential side effect.

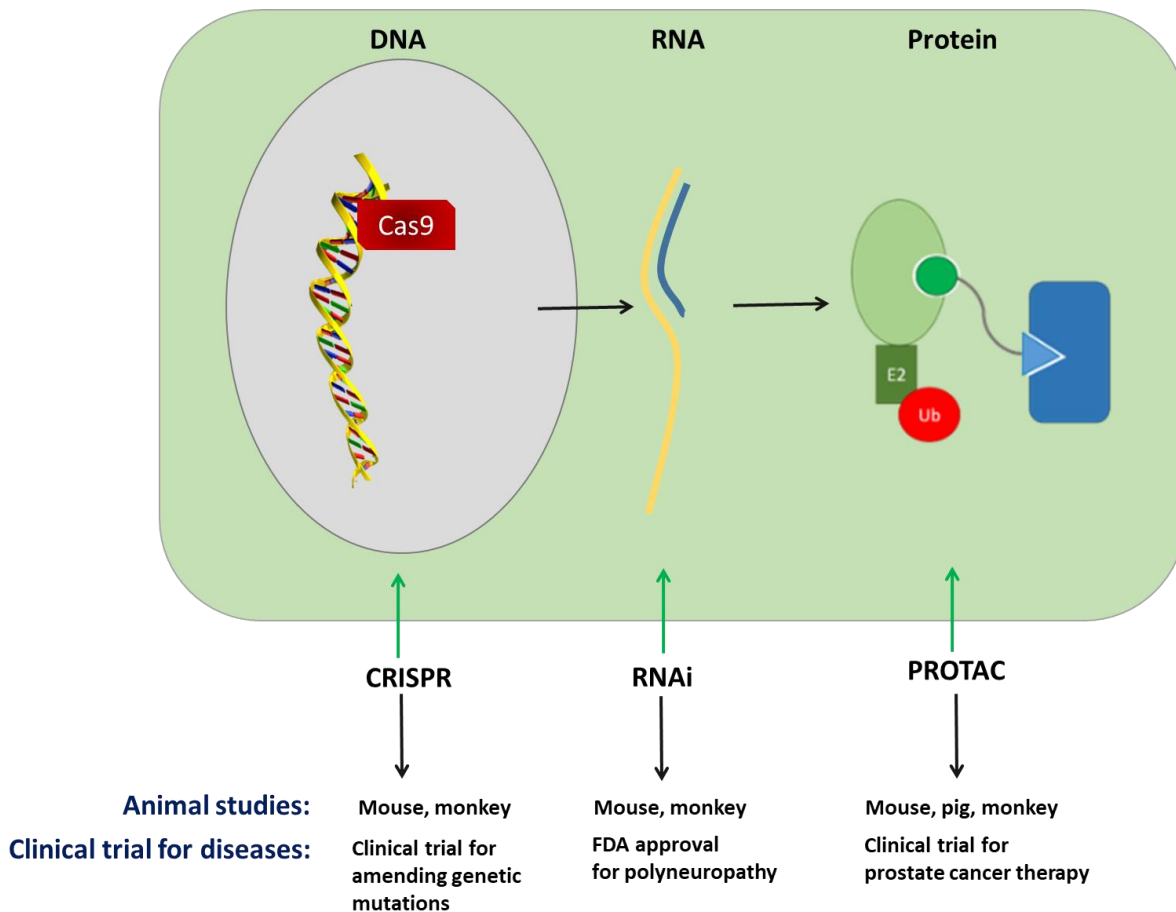
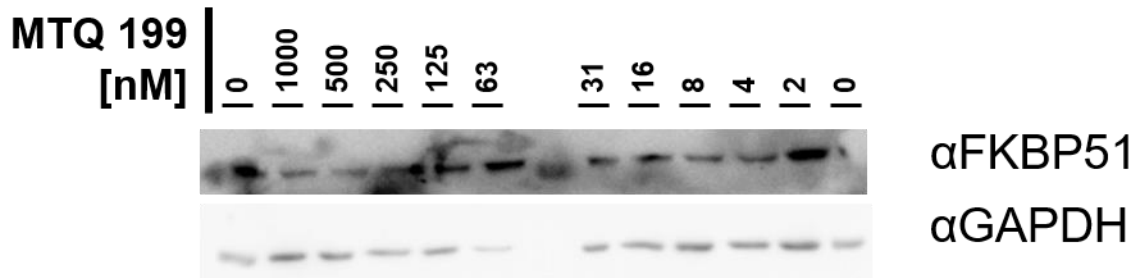


Figure 56 The schematic illustration of various strategies to inactivate an oncogene or other disease-causing genes at the DNA, RNA or protein level by CRISPR, RNAi or PROTAC, respectively. Adopted from [162].

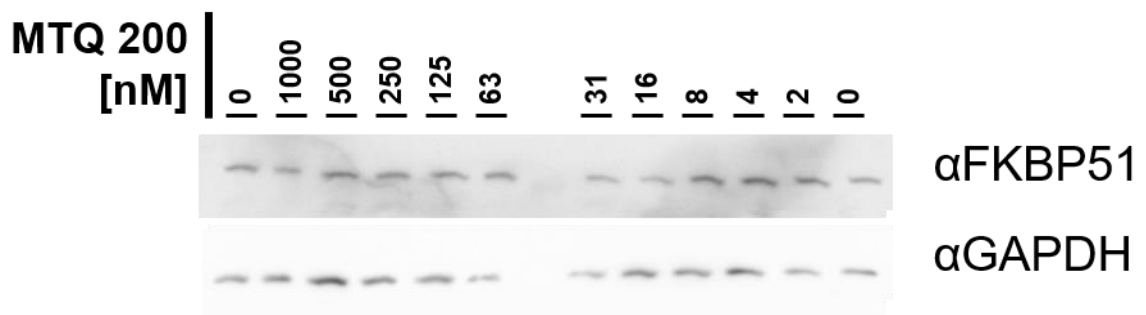
7. Supplemental Information

7.1. Chemical Knockdown of FKBP51 library

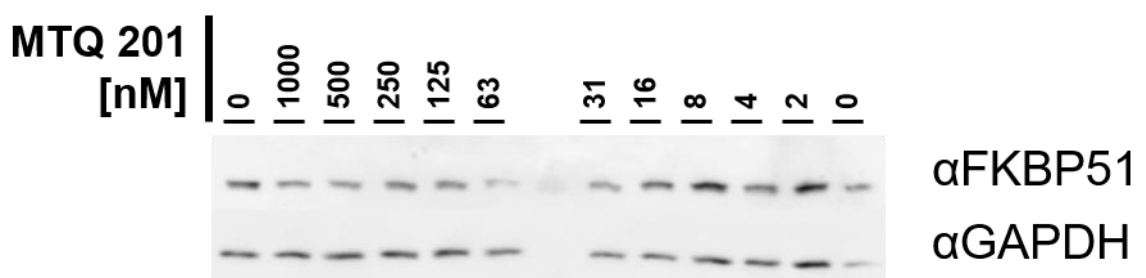
The first set of figures covers 11-point dilution series of the indicated compound. Upper panel FKBP51, lower panel GAPDH. Incubation time: 24h.



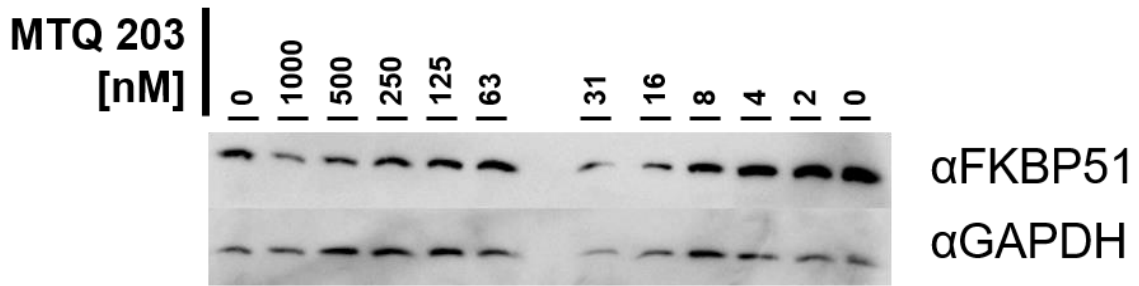
Suppl. Fig. 1 Western Blot of HEK293T cell lysates treated with different concentrations of MTQ199. Lab book: TGe14



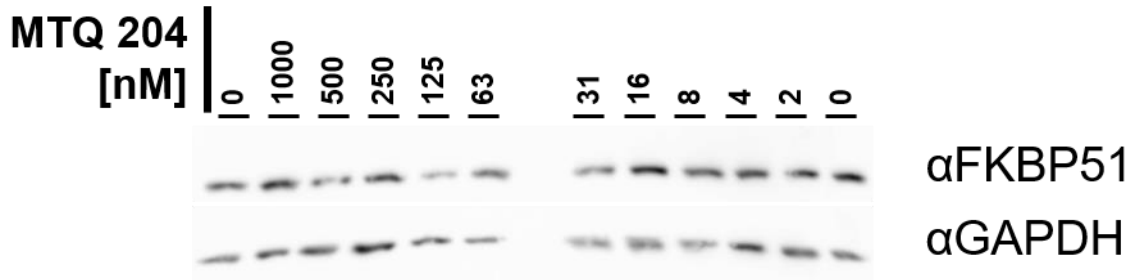
Suppl. Fig. 2 Western Blot of HEK293T cell lysates treated with different concentrations of MTQ200. Lab book: TGe14



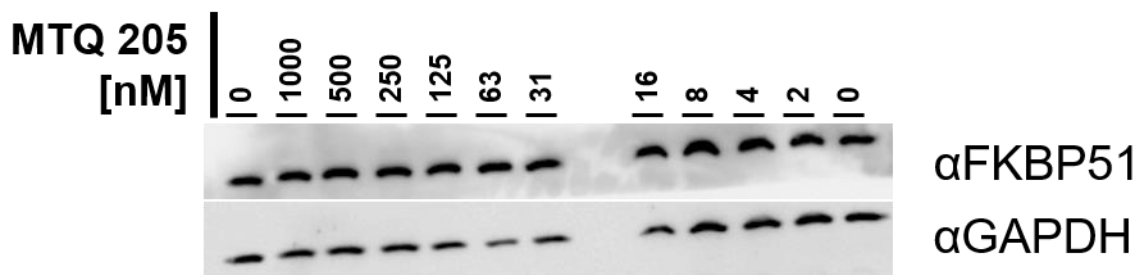
Suppl. Fig. 3 Western Blot of HEK293T cell lysates treated with different concentrations of MTQ201. Lab book: TGe15



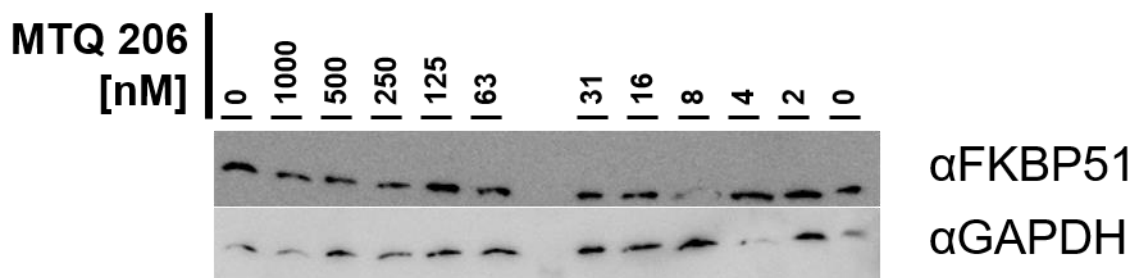
Suppl. Fig. 4 Western Blot of HEK293T cell lysates treated with different concentrations of MTQ203. Lab book: TGe21



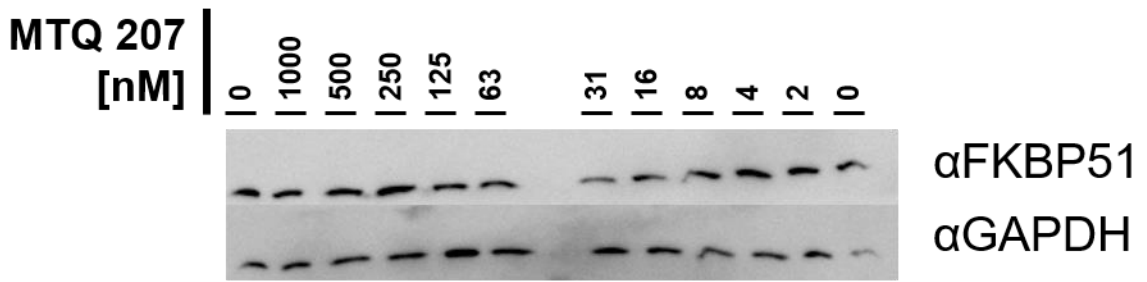
Suppl. Fig. 5 Western Blot of HEK293T cell lysates treated with different concentrations of MTQ204. Lab book: TGe18



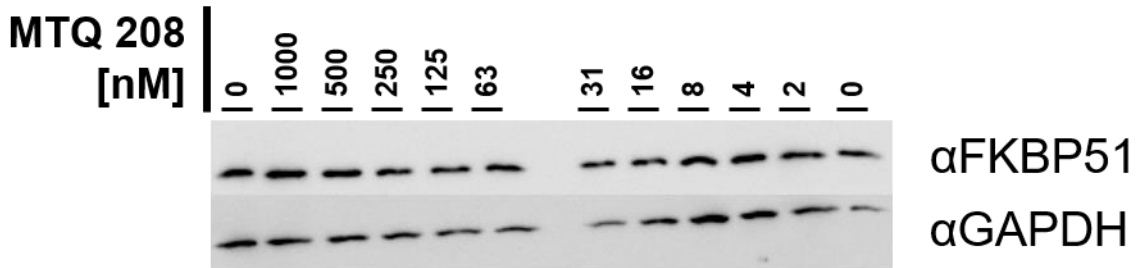
Suppl. Fig. 6 Western Blot of HEK293T cell lysates treated with different concentrations of MTQ205. Lab book: TGe18



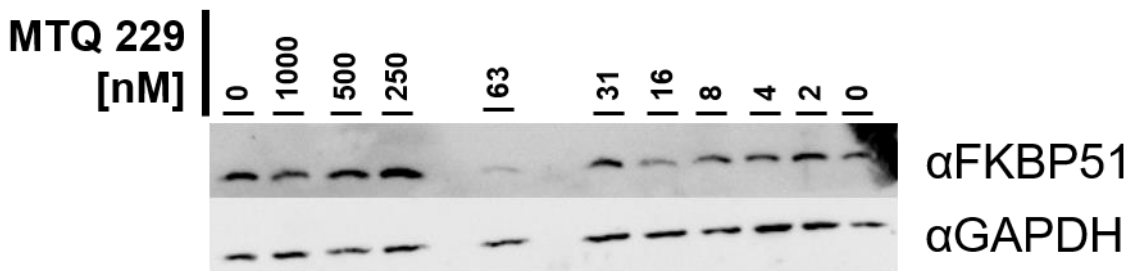
Suppl. Fig. 7 Western Blot of HEK293T cell lysates treated with different concentrations of MTQ206. Lab book: TGe19



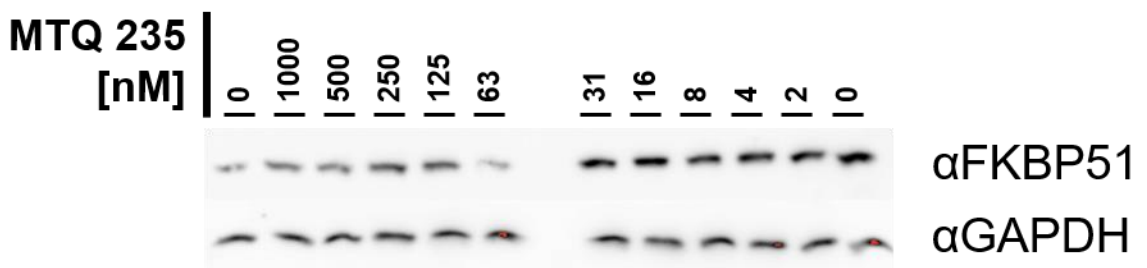
Suppl. Fig. 8 Western Blot of HEK293T cell lysates treated with different concentrations of MTQ207. Lab book: TGe19



Suppl. Fig. 9 Western Blot of HEK293T cell lysates treated with different concentrations of MTQ208. Lab book: TGe19

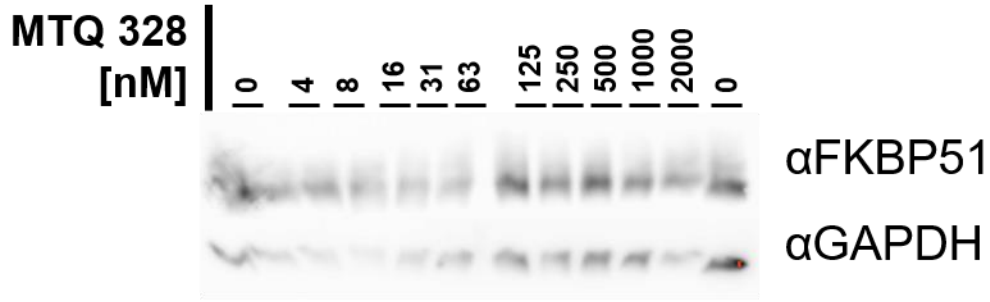


Suppl. Fig. 10 Western Blot of HEK293T cell lysates treated with different concentrations of MTQ229. Lab book: TGe19

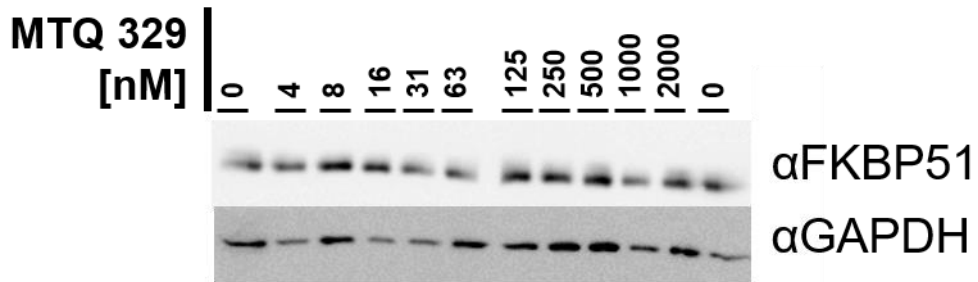


Suppl. Fig. 11 Western Blot of HEK293T cell lysates treated with different concentrations of MTQ235. Lab book: TGe18

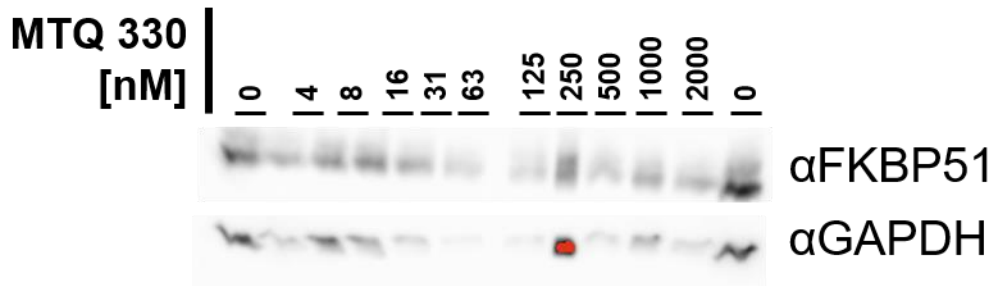
The next set of figures covers 11-point dilution series of the indicated compound. Upper panel FKBP51, lower panel GAPDH. Incubation time: 48h.



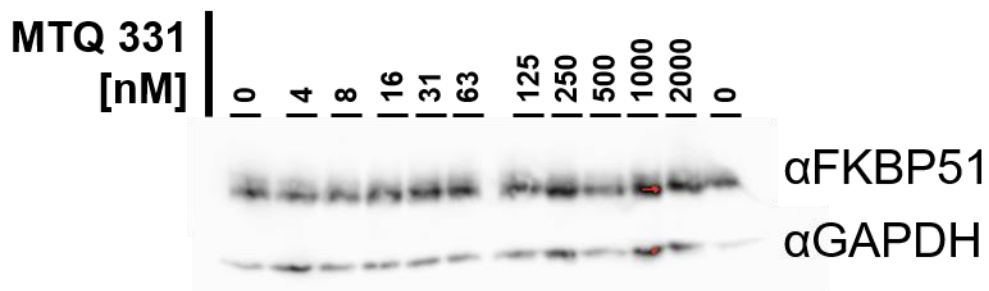
Suppl. Fig. 12 Western Blot of HEK293T cell lysates treated with different concentrations of MTQ328. Lab book: AHa447



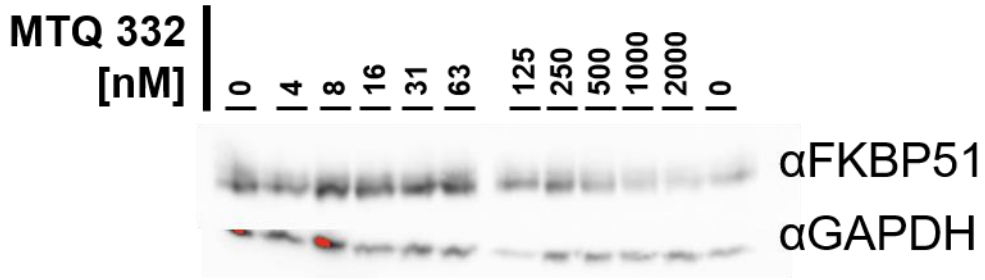
Suppl. Fig. 13 Western Blot of HEK293T cell lysates treated with different concentrations of MTQ329. Lab book: AHa442



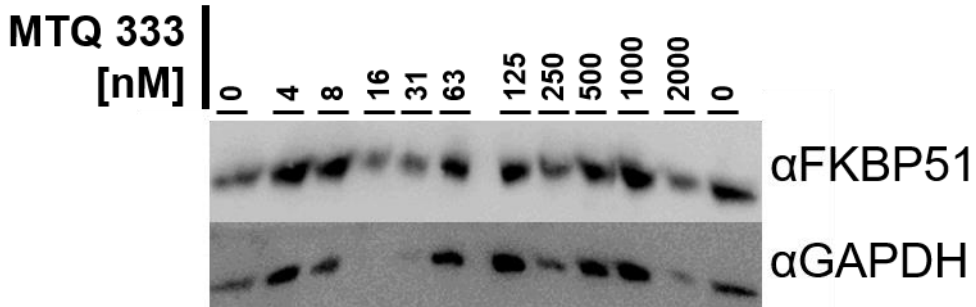
Suppl. Fig. 14 Western Blot of HEK293T cell lysates treated with different concentrations of MTQ330. Lab book: AHa447



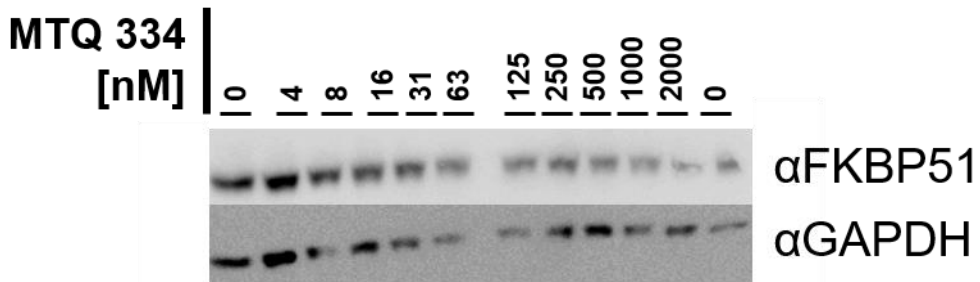
Suppl. Fig. 15 Western Blot of HEK293T cell lysates treated with different concentrations of MTQ331. Lab book: AHa447



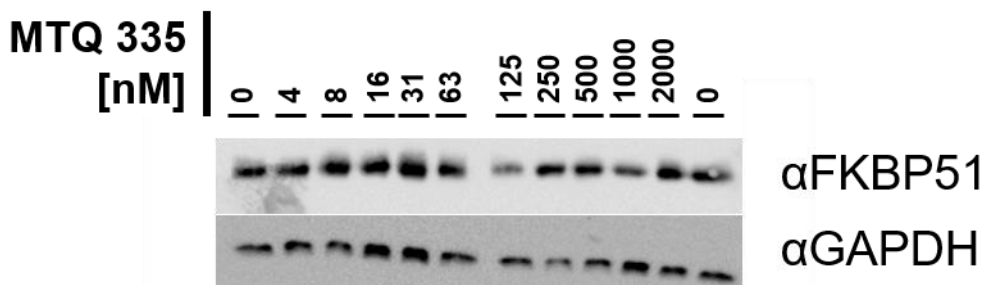
Suppl. Fig. 16 Western Blot of HEK293T cell lysates treated with different concentrations of MTQ332. Lab book: AHa447



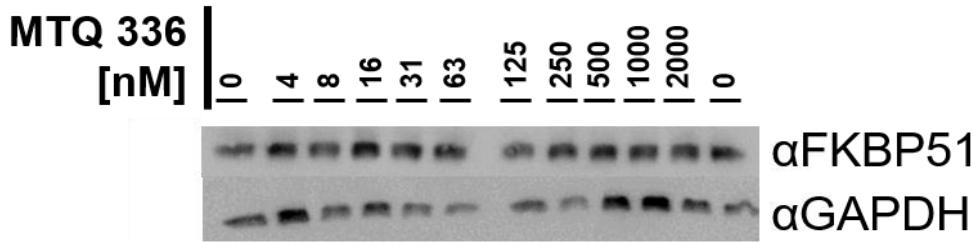
Suppl. Fig. 17 Western Blot of HEK293T cell lysates treated with different concentrations of MTQ333. Lab book: AHa448



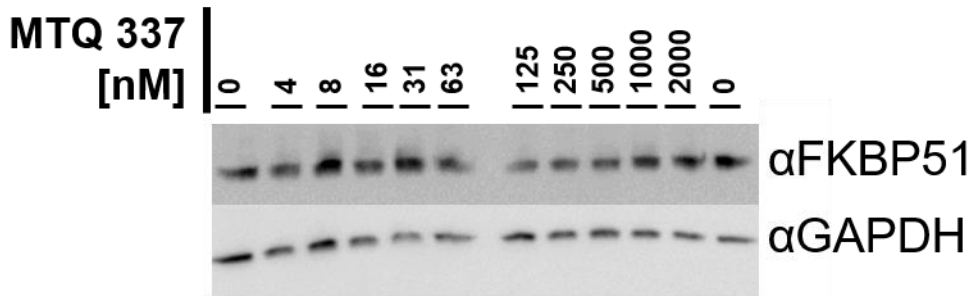
Suppl. Fig. 18 Western Blot of HEK293T cell lysates treated with different concentrations of MTQ334. Lab book: AHa448



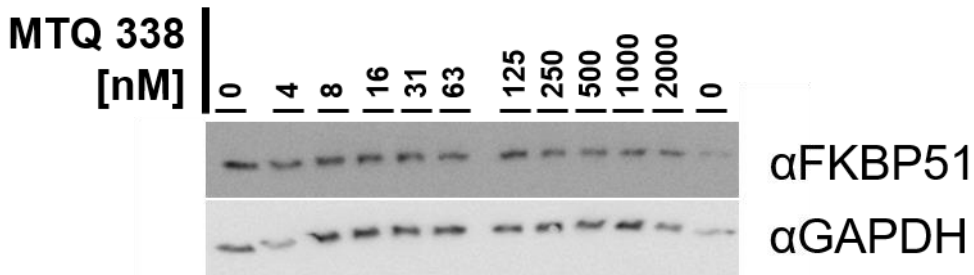
Suppl. Fig. 19 Western Blot of HEK293T cell lysates treated with different concentrations of MTQ335. Lab book: AHa442



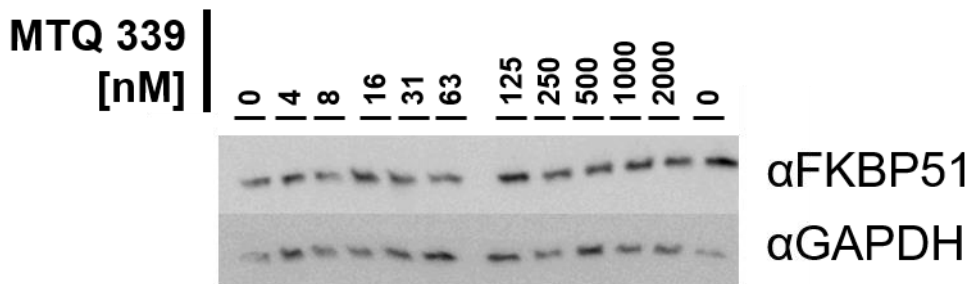
Suppl. Fig. 20 Western Blot of HEK293T cell lysates treated with different concentrations of MTQ336. Lab book: AHa448



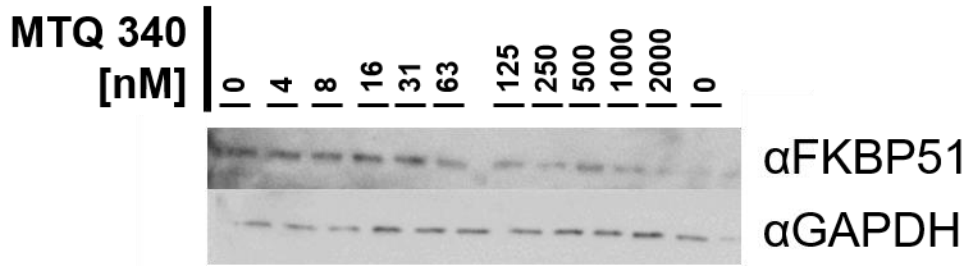
Suppl. Fig. 21 Western Blot of HEK293T cell lysates treated with different concentrations of MTQ337. Lab book: AHa448



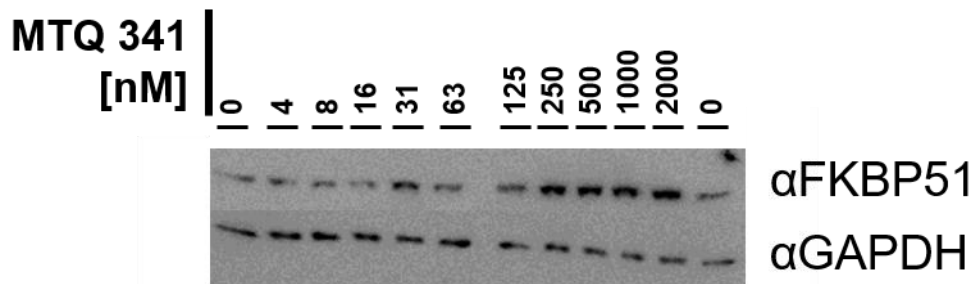
Suppl. Fig. 22 Western Blot of HEK293T cell lysates treated with different concentrations of MTQ338. Lab book: AHa450



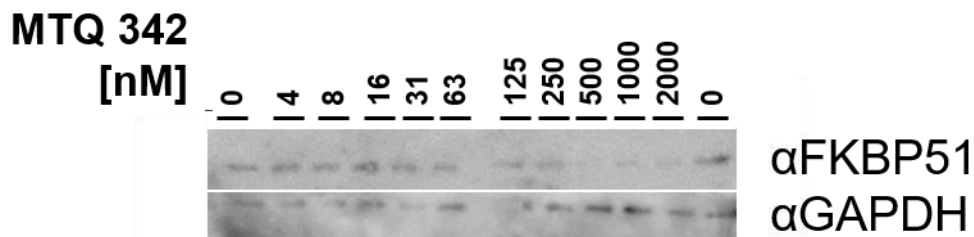
Suppl. Fig. 23 Western Blot of HEK293T cell lysates treated with different concentrations of MTQ339. Lab book: AHa450



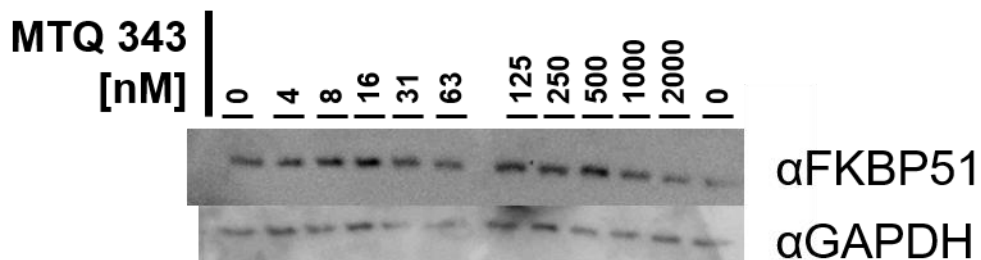
Suppl. Fig. 24 Western Blot of HEK293T cell lysates treated with different concentrations of MTQ340. Lab book: AHa455



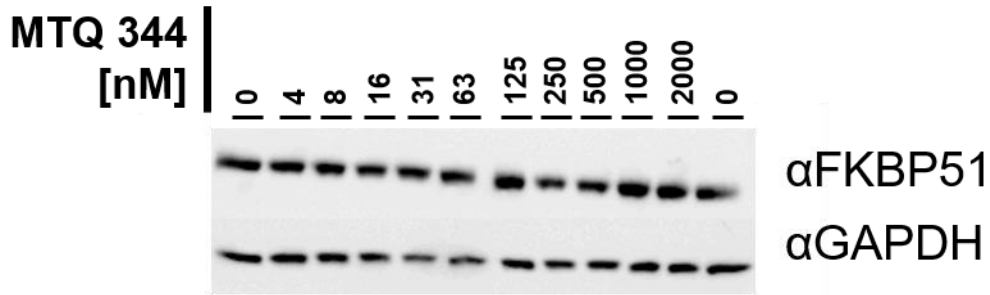
Suppl. Fig. 25 Western Blot of HEK293T cell lysates treated with different concentrations of MTQ341. Lab book: AHa450



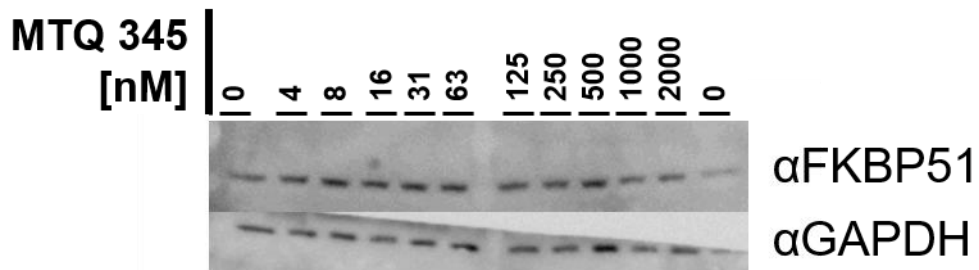
Suppl. Fig. 26 Western Blot of HEK293T cell lysates treated with different concentrations of MTQ342. Lab book: AHa452



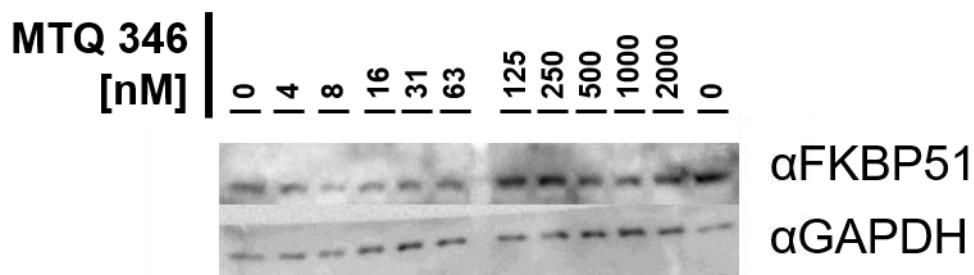
Suppl. Fig. 27 Western Blot of HEK293T cell lysates treated with different concentrations of MTQ343. Lab book: AHa452



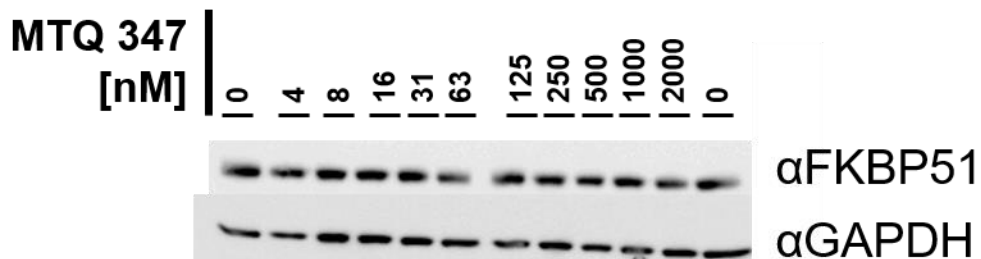
Suppl. Fig. 28 Western Blot of HEK293T cell lysates treated with different concentrations of MTQ344. Lab book: AHa344



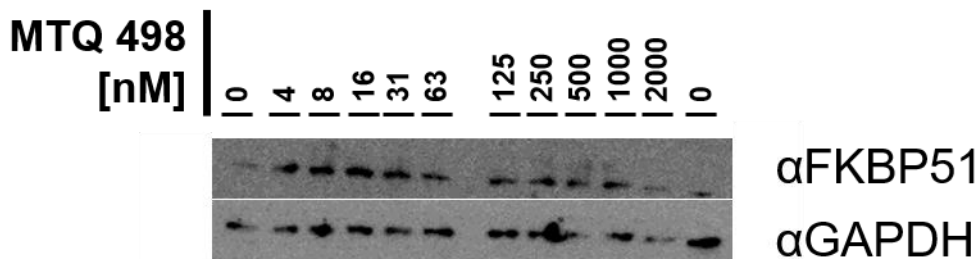
Suppl. Fig. 29 Western Blot of HEK293T cell lysates treated with different concentrations of MTQ345. Lab book: AHa452



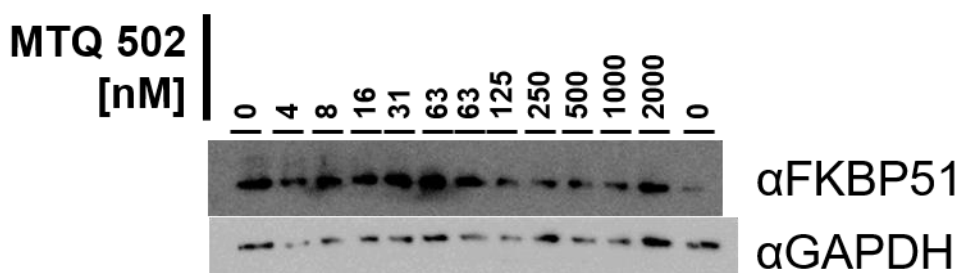
Suppl. Fig. 30 Western Blot of HEK293T cell lysates treated with different concentrations of MTQ346. Lab book: AHa452



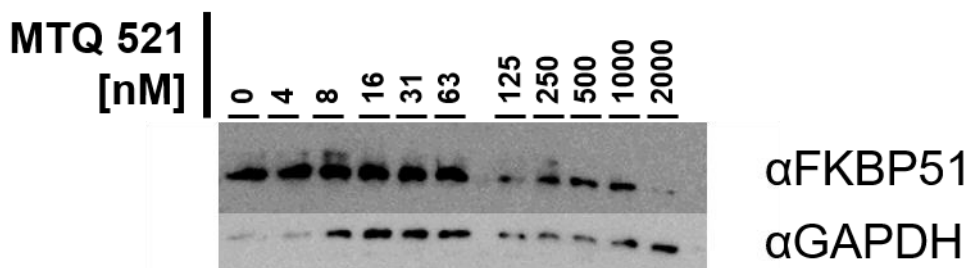
Suppl. Fig. 31 Western Blot of HEK293T cell lysates treated with different concentrations of MTQ347. Lab book: AHa442



Suppl. Fig. 32 Western Blot of HEK293T cell lysates treated with different concentrations of MTQ498. Lab book: AHa474

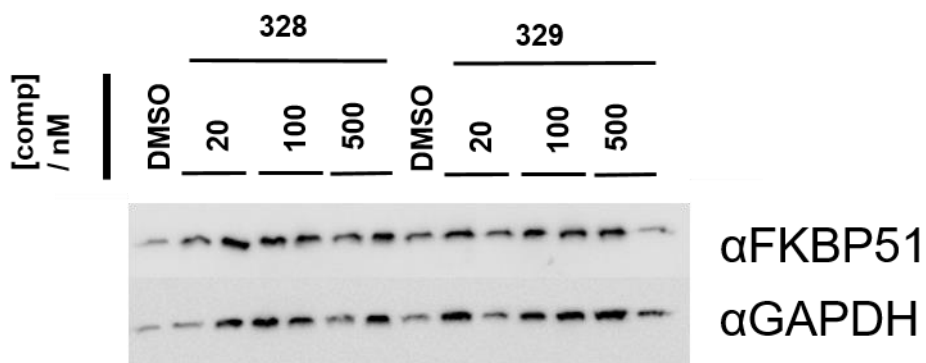


Suppl. Fig. 33 Western Blot of HEK293T cell lysates treated with different concentrations of MTQ502. Lab book: AHa474

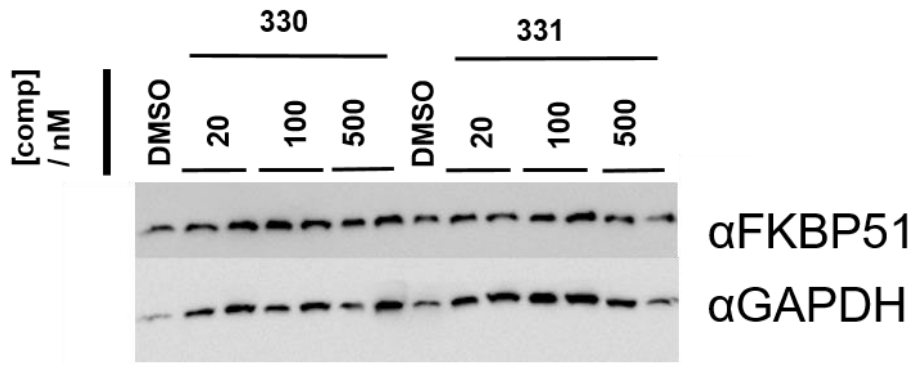


Suppl. Fig. 34 Western Blot of HEK293T cell lysates treated with different concentrations of MTQ521. Lab book: AHa474

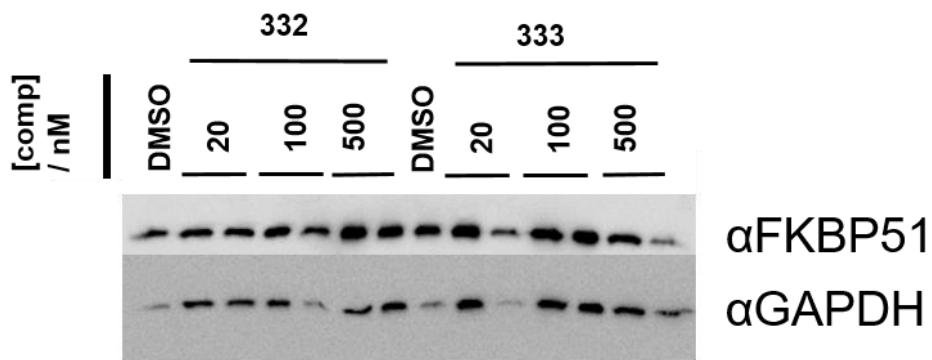
The next set of figures shows a “quicktest” of PROTACs of the second series. Upper panel FKBP51, lower panel GAPDH. Incubation time: 48h.



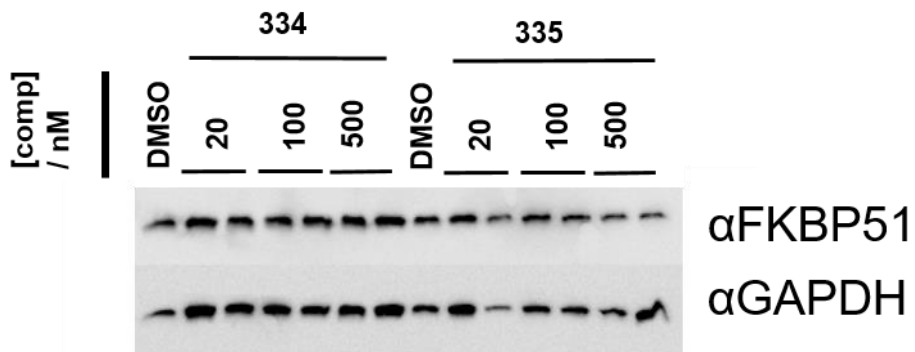
Suppl. Fig. 35 Western Blot of HEK293T cell lysates treated with three concentrations (duplicates) of MTQ328 and MTQ329



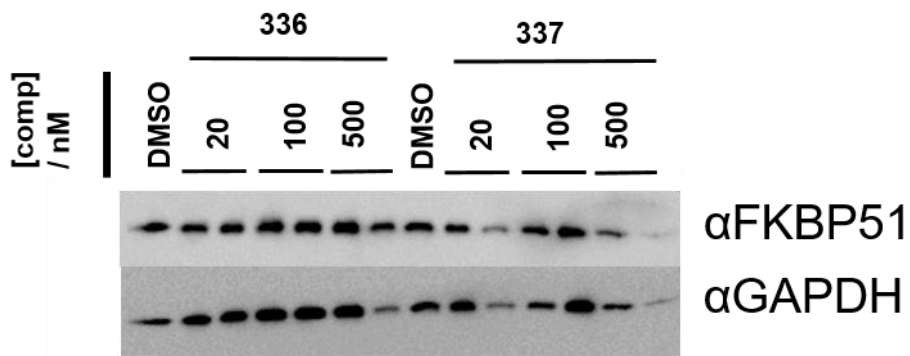
Suppl. Fig. 36 Western Blot of HEK293T cell lysates treated with three concentrations (duplicates) of MTQ330 and MTQ331



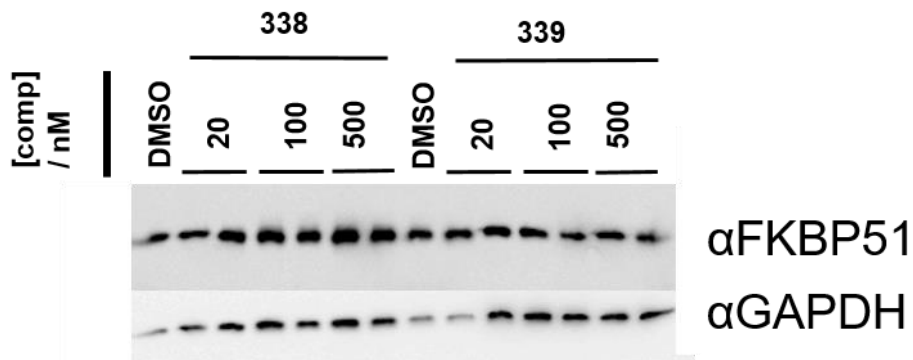
Suppl. Fig. 37 Western Blot of HEK293T cell lysates treated with three concentrations (duplicates) of MTQ332 and MTQ333



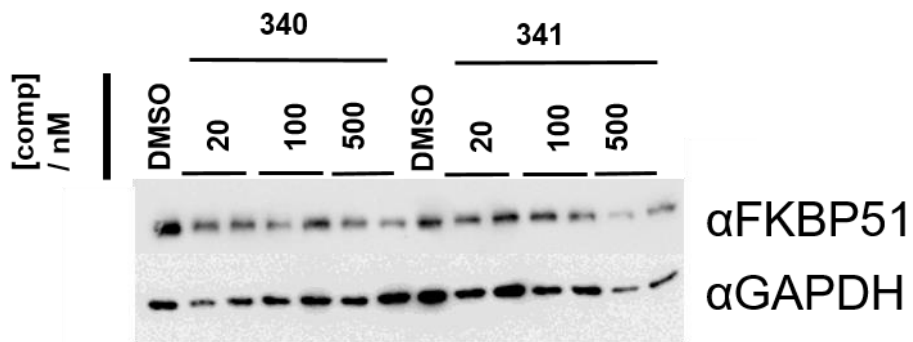
Suppl. Fig. 38 Western Blot of HEK293T cell lysates treated with three concentrations (duplicates) of MTQ334 and MTQ335



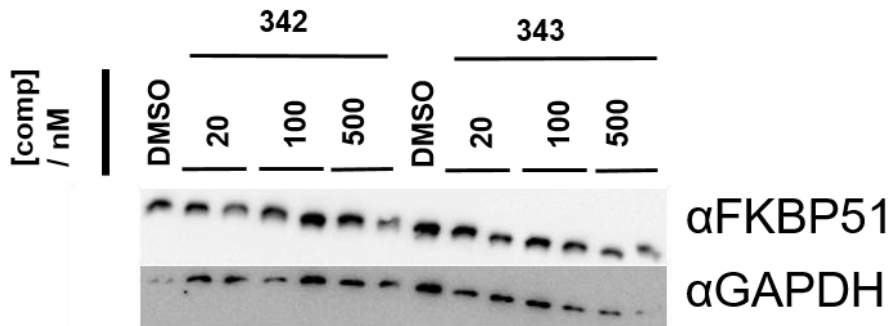
Suppl. Fig. 39 Western Blot of HEK293T cell lysates treated with three concentrations (duplicates) of MTQ336 and MTQ337



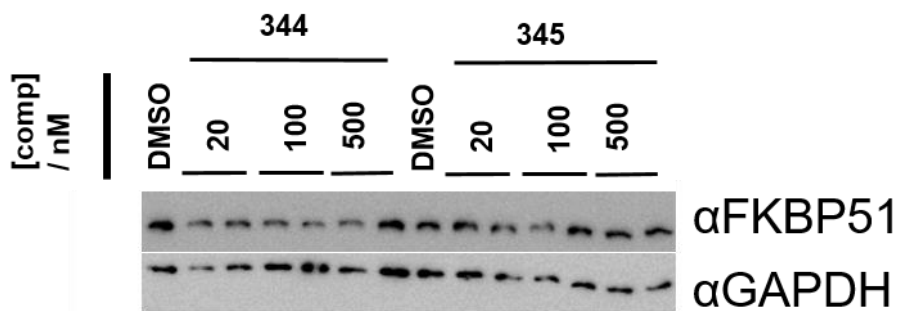
Suppl. Fig. 40 Western Blot of HEK293T cell lysates treated with three concentrations (duplicates) of MTQ338 and MTQ339



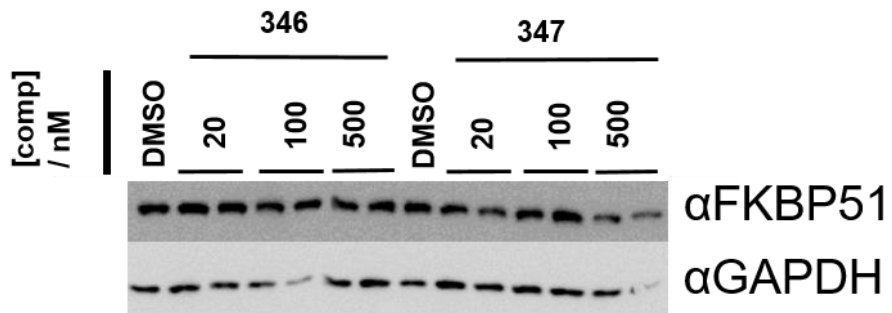
Suppl. Fig. 41 Western Blot of HEK293T cell lysates treated with three concentrations (duplicates) of MTQ340 and MTQ341



Suppl. Fig. 42 Western Blot of HEK293T cell lysates treated with three concentrations (duplicates) of MTQ342 and MTQ343

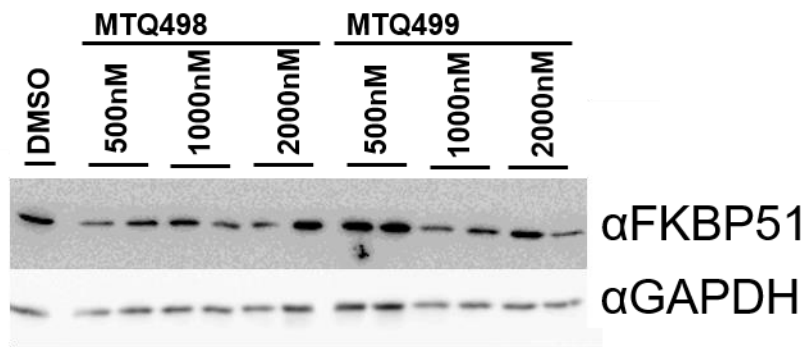


Suppl. Fig. 43 Western Blot of HEK293T cell lysates treated with three concentrations (duplicates) of MTQ344 and MTQ345

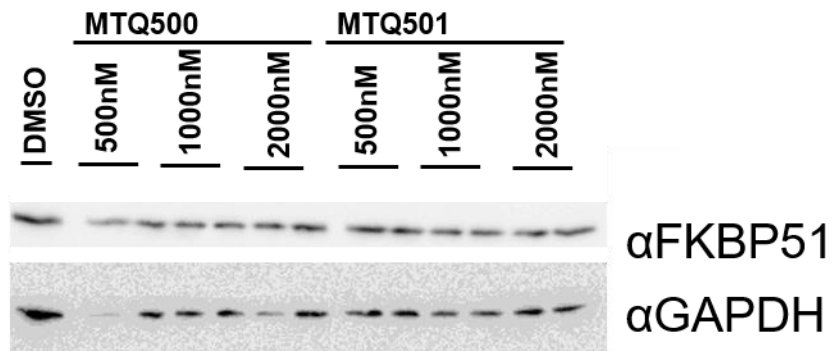


Suppl. Fig. 44 Western Blot of HEK293T cell lysates treated with three concentrations (duplicates) of MTQ346 and MTQ347

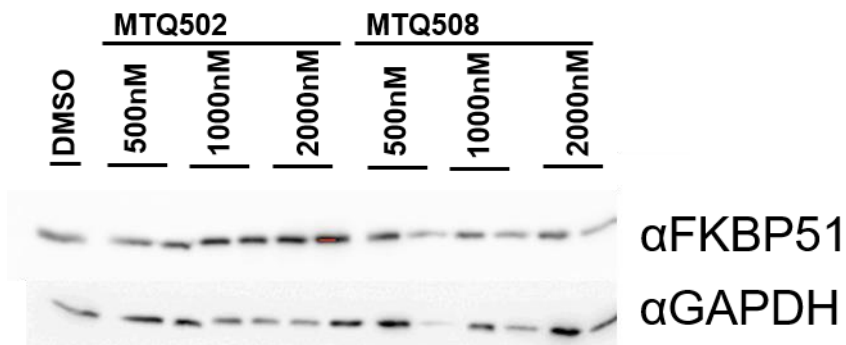
The next set of figures shows a “quicktest” of PROTACs of the third series. Upper panel FKBP51, lower panel GAPDH. Incubation time: 48h.



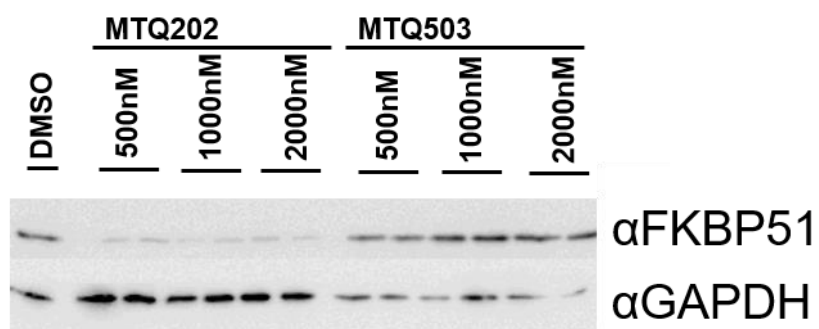
Suppl. Fig. 45 Western Blot of HEK293T cell lysates treated with three concentrations (duplicates) of MTQ498 and MTQ499



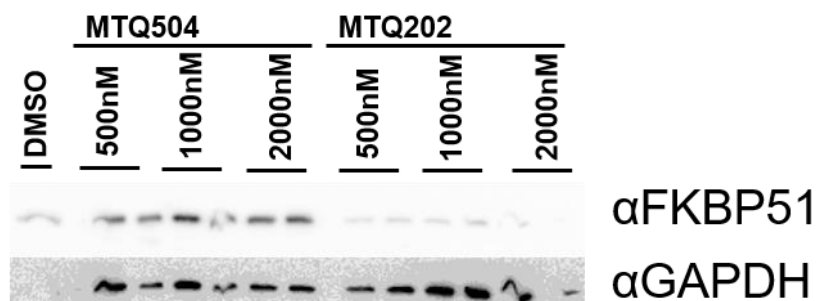
Suppl. Fig. 46 Western Blot of HEK293T cell lysates treated with three concentrations (duplicates) of MTQ500 and MTQ501



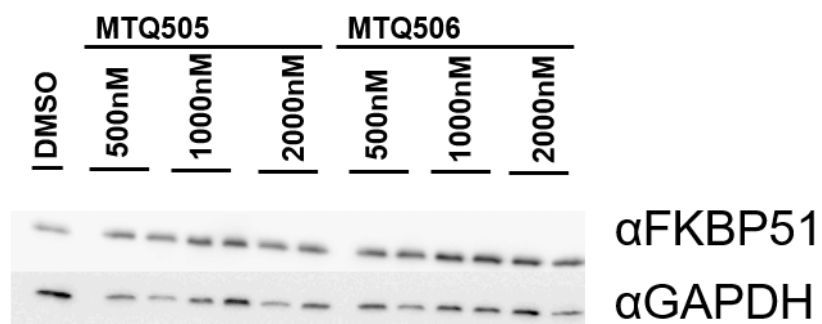
Suppl. Fig. 47 Western Blot of HEK293T cell lysates treated with three concentrations (duplicates) of MTQ502 and MTQ508



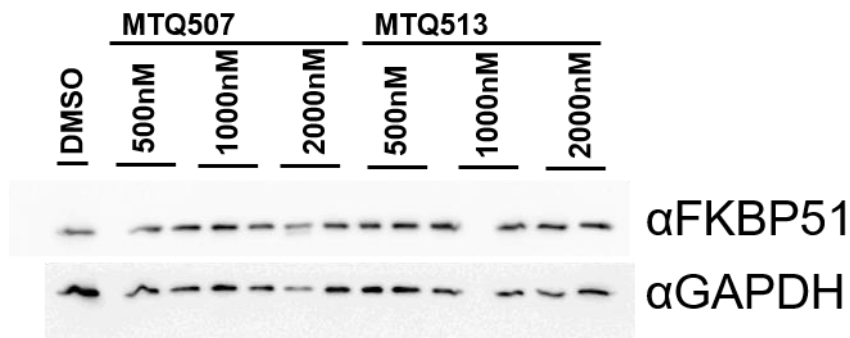
Suppl. Fig. 48 Western Blot of HEK293T cell lysates treated with three concentrations (duplicates) of MTQ202 and MTQ503



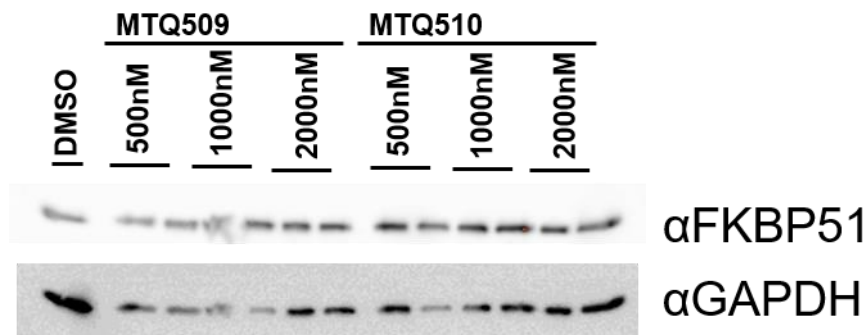
Suppl. Fig. 49 Western Blot of HEK293T cell lysates treated with three concentrations (duplicates) of MTQ504 and MTQ202



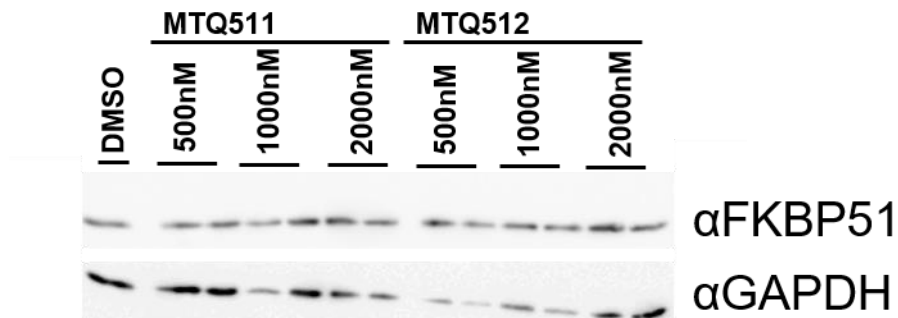
Suppl. Fig. 50 Western Blot of HEK293T cell lysates treated with three concentrations (duplicates) of MTQ505 and MTQ506



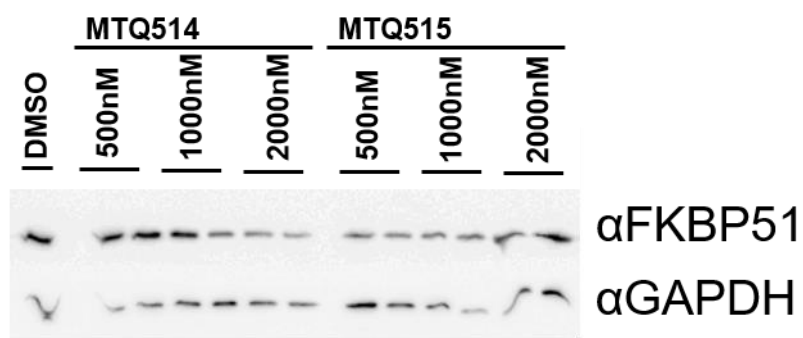
Suppl. Fig. 51 Western Blot of HEK293T cell lysates treated with three concentrations (duplicates) of MTQ507 and MTQ513



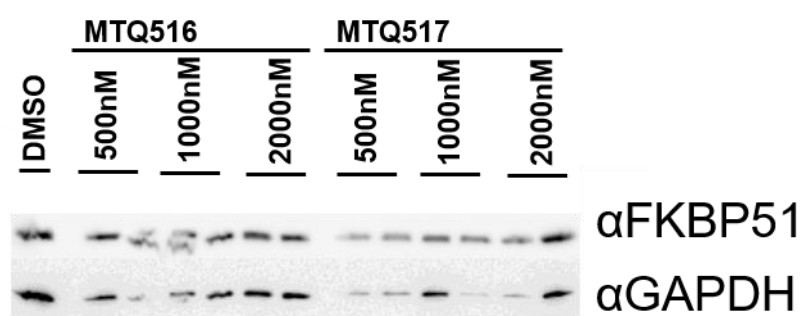
Suppl. Fig. 52 Western Blot of HEK293T cell lysates treated with three concentrations (duplicates) of MTQ509 and MTQ510



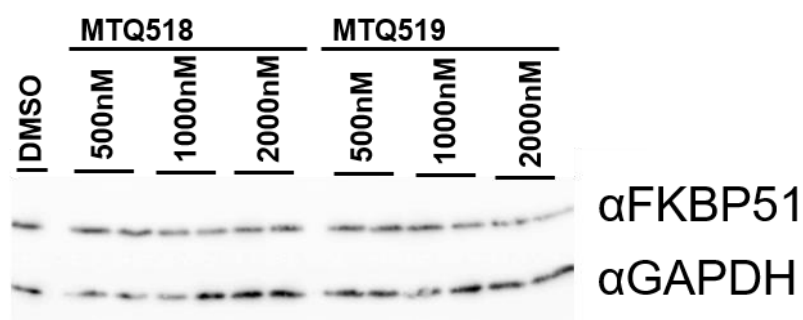
Suppl. Fig. 53 Western Blot of HEK293T cell lysates treated with three concentrations (duplicates) of MTQ511 and MTQ512



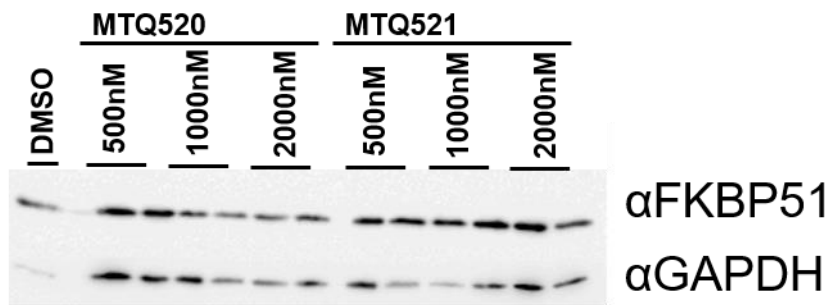
Suppl. Fig. 54 Western Blot of HEK293T cell lysates treated with three concentrations (duplicates) of MTQ514 and MTQ515



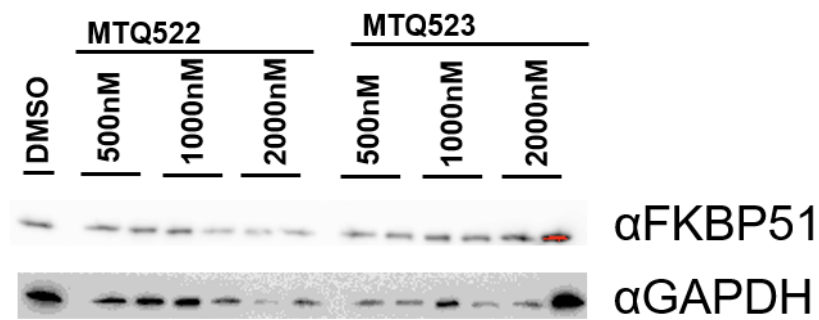
Suppl. Fig. 55 Western Blot of HEK293T cell lysates treated with three concentrations (duplicates) of MTQ516 and MTQ517



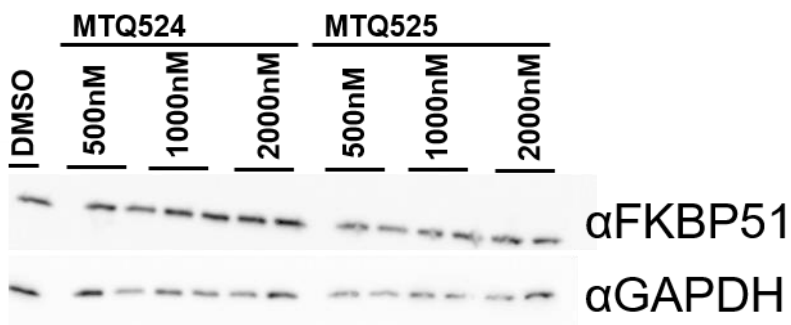
Suppl. Fig. 56 Western Blot of HEK293T cell lysates treated with three concentrations (duplicates) of MTQ518 and MTQ519



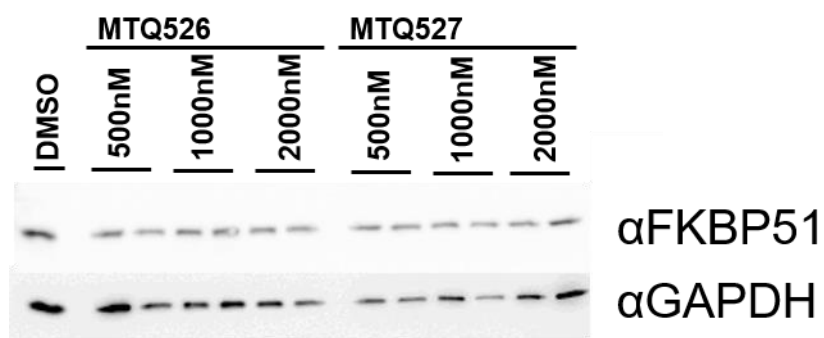
Suppl. Fig. 57 Western Blot of HEK293T cell lysates treated with three concentrations (duplicates) of MTQ520 and MTQ521



Suppl. Fig. 58 Western Blot of HEK293T cell lysates treated with three concentrations (duplicates) of MTQ522 and MTQ523

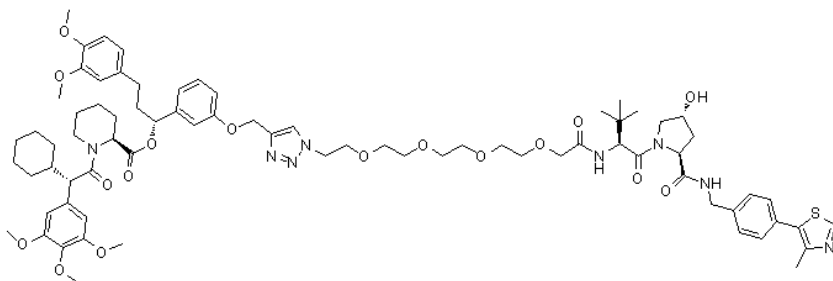


Suppl. Fig. 59 Western Blot of HEK293T cell lysates treated with three concentrations (duplicates) of MTQ524 and MTQ525



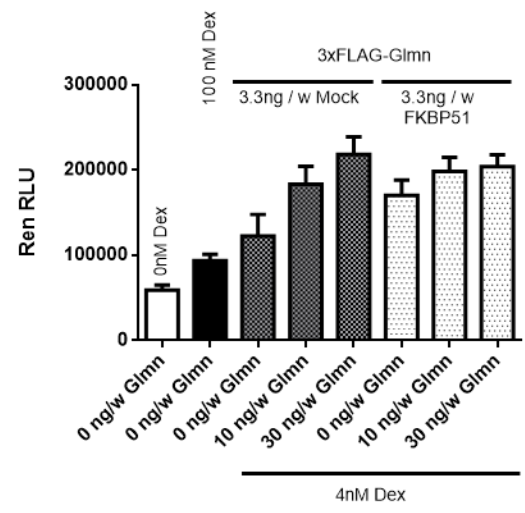
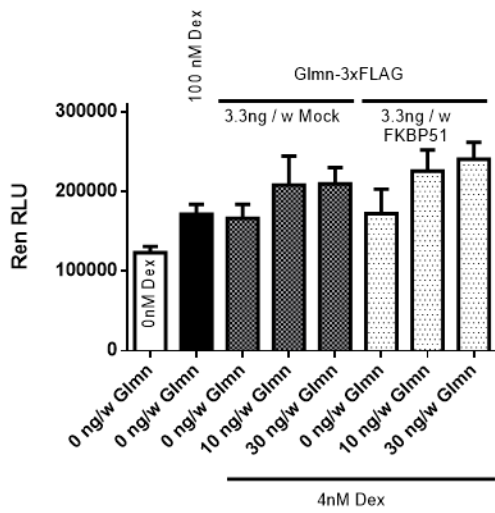
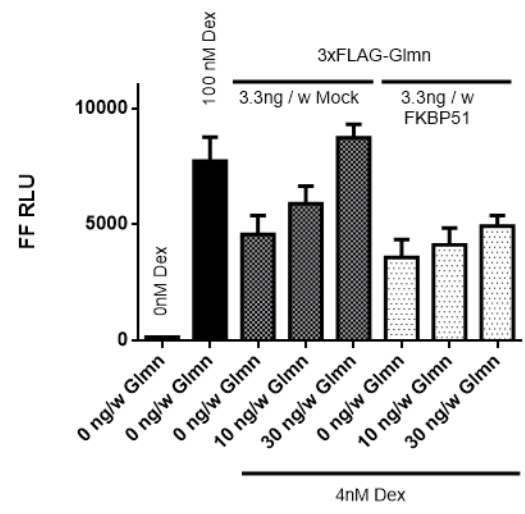
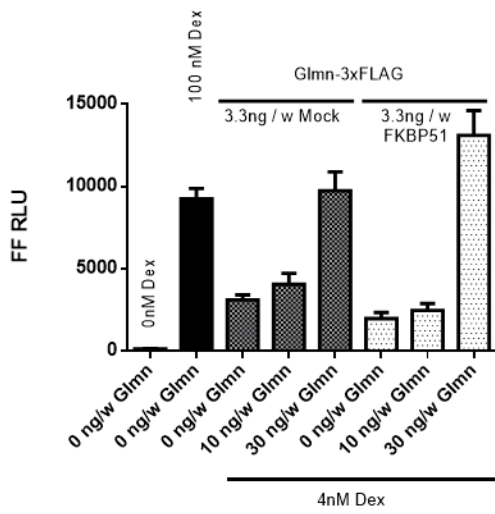
Suppl. Fig. 60 Western Blot of HEK293T cell lysates treated with three concentrations (duplicates) of MTQ526 and MTQ527

7.2. MTQ202 / MTQ416



Suppl. Fig. 61 Structure of the PROTAC MTQ202 / MTQ416

7.3. Reporter Gene Assays

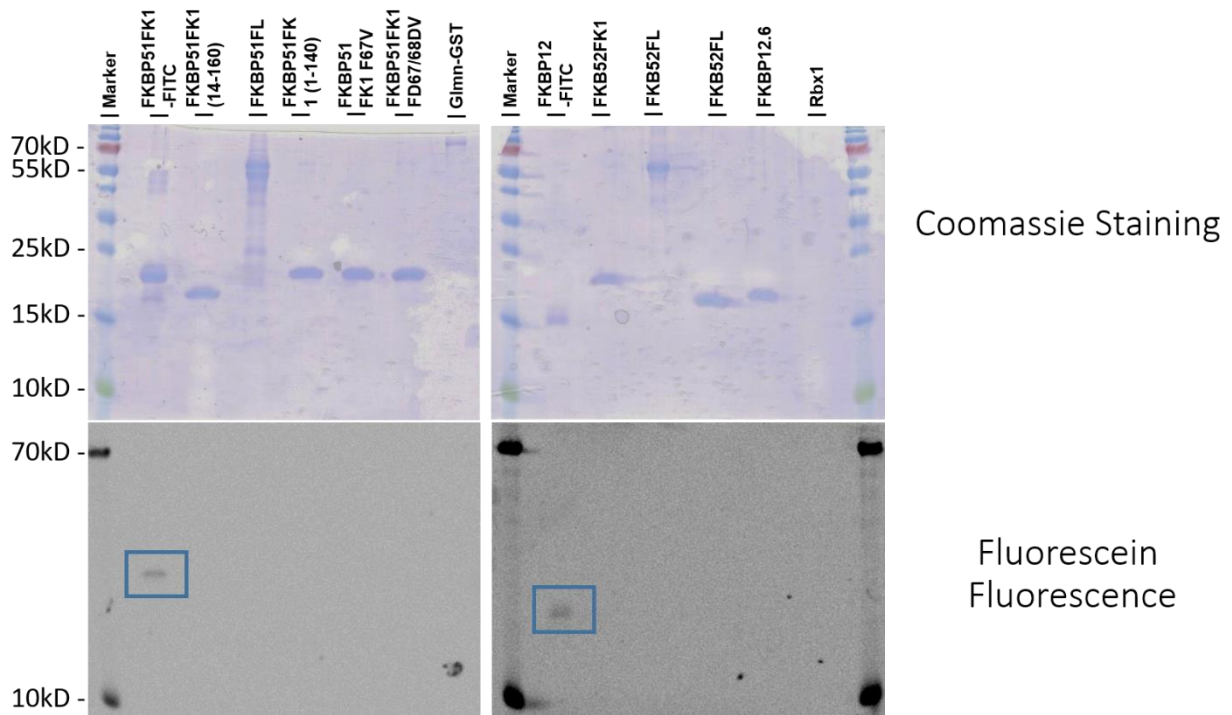


Suppl. Fig. 62 Firefly and Renilla signal for **Figure 27** and **Figure 28**.

7.4. HTRF

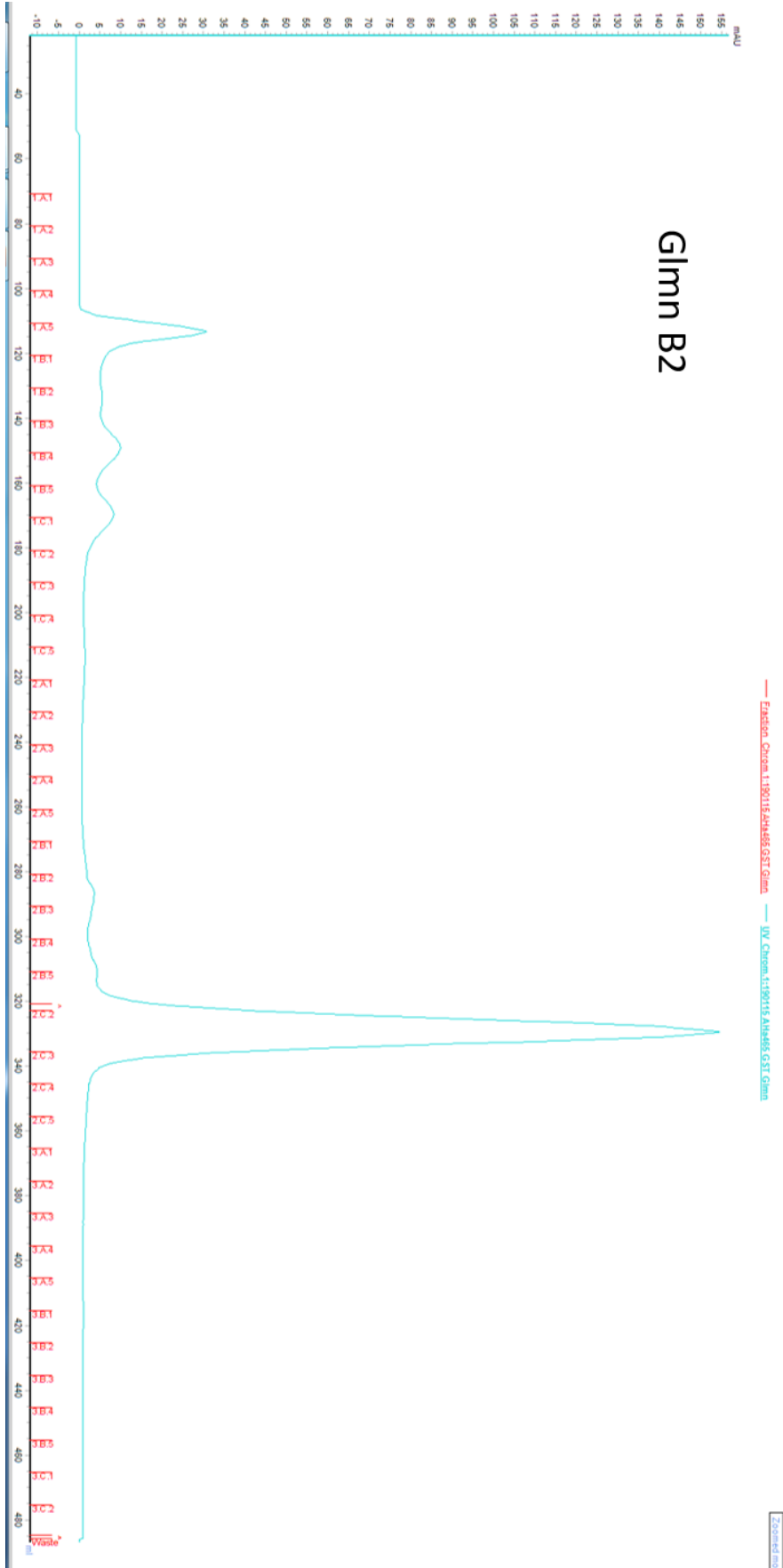


Suppl. Fig. 63 Labeling of FKBP12-MonoCys with 5-MF on Ni-NTA-Agarose. First row shows the fractions during the column wash. Second row shows the elution fractions.

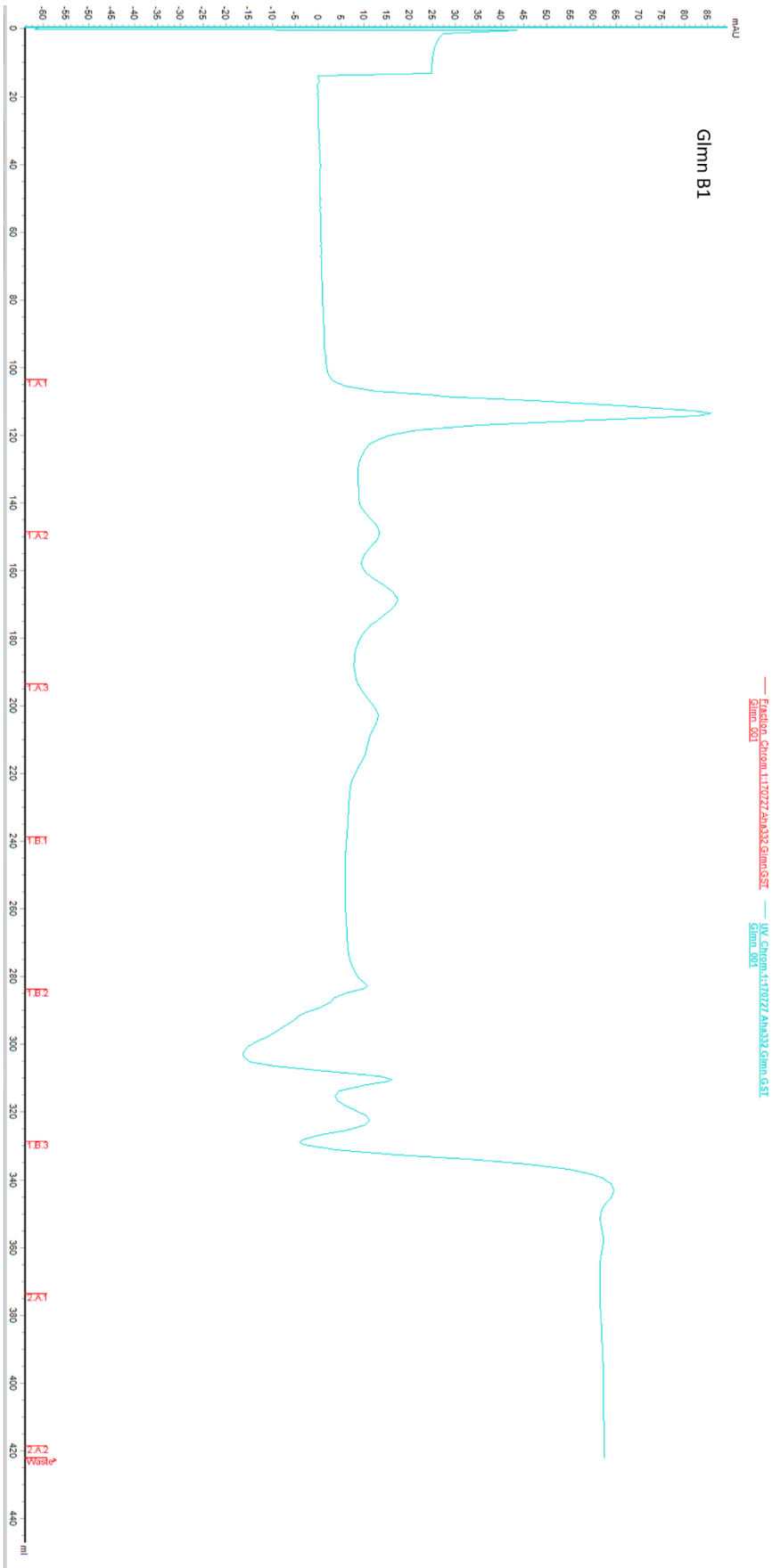


Suppl. Fig. 64 Purified proteins used in the HTRF Assay. Upper panel depicts the Coomassie staining of the indicated proteins. Lower panel shows the same SDS-Page gels in GFP-detection mode of LAS-3000, Fujifilm, detecting 5-MF label of FKBP51FK1 and FKBP12. Rbx1 is not visible in this scan but a clean band was observable by eye. Lab book: AHa483

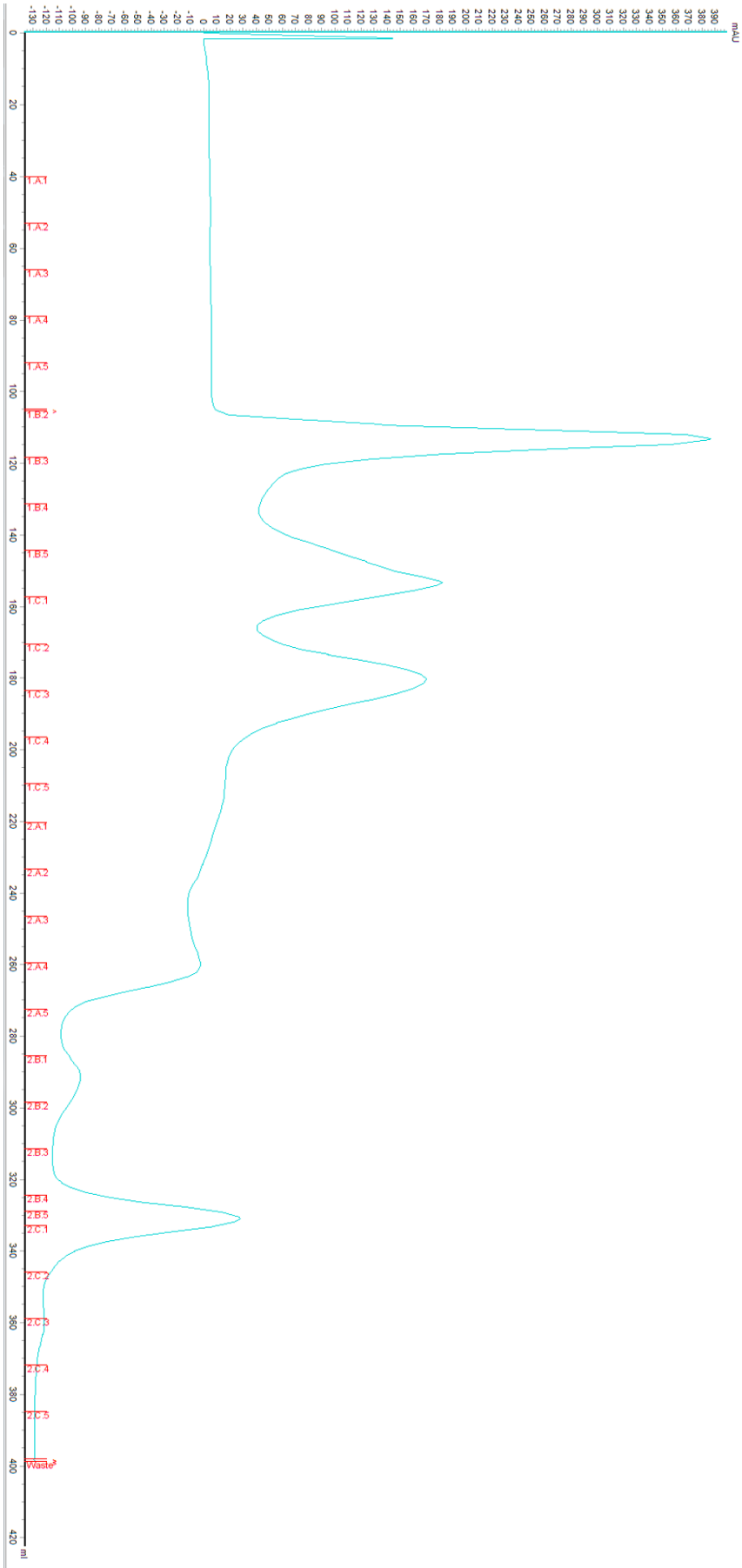
7.5. Protein Purification - FPLC



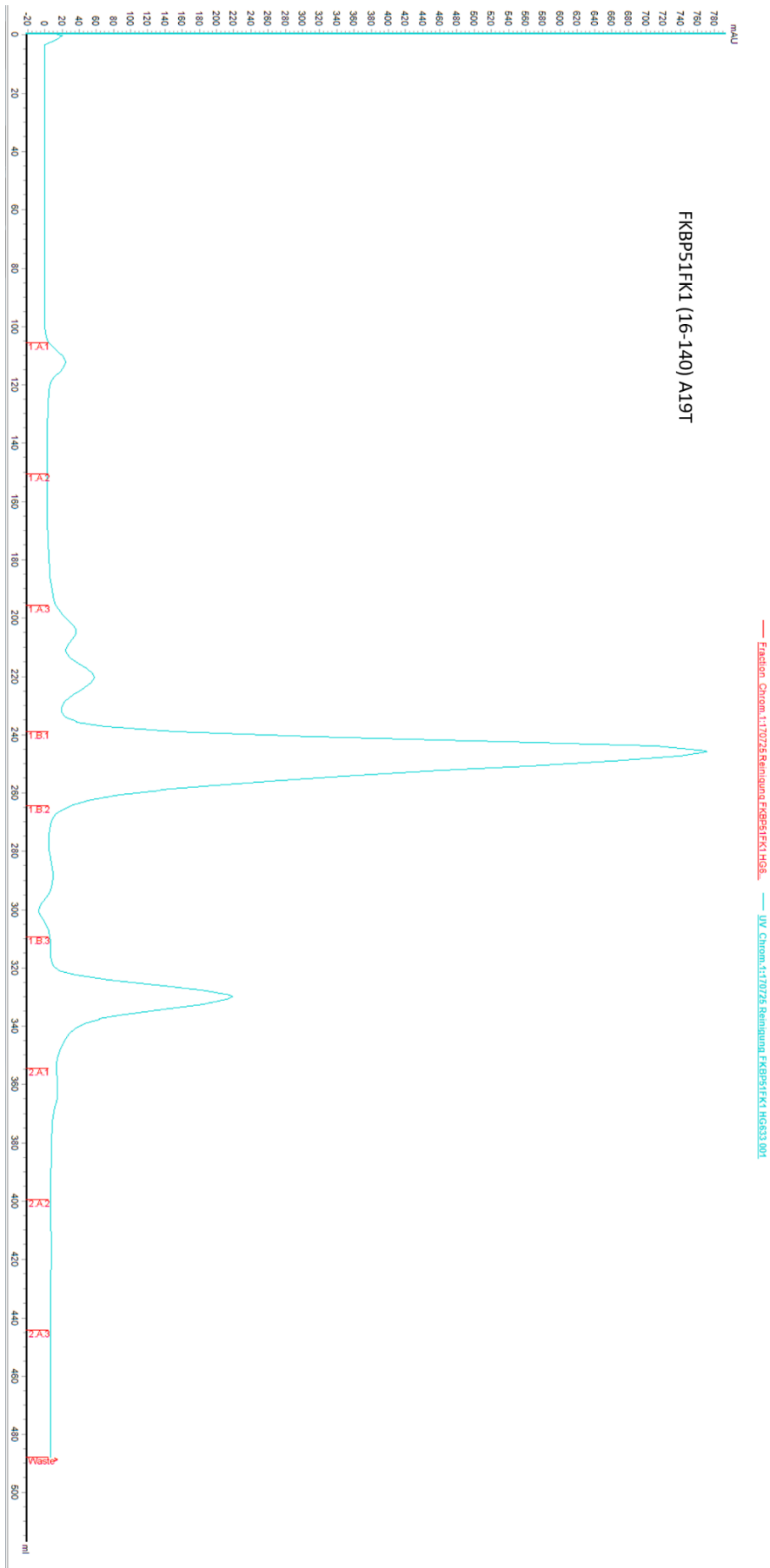
Suppl. Fig. 65 SEC of Glmn B2



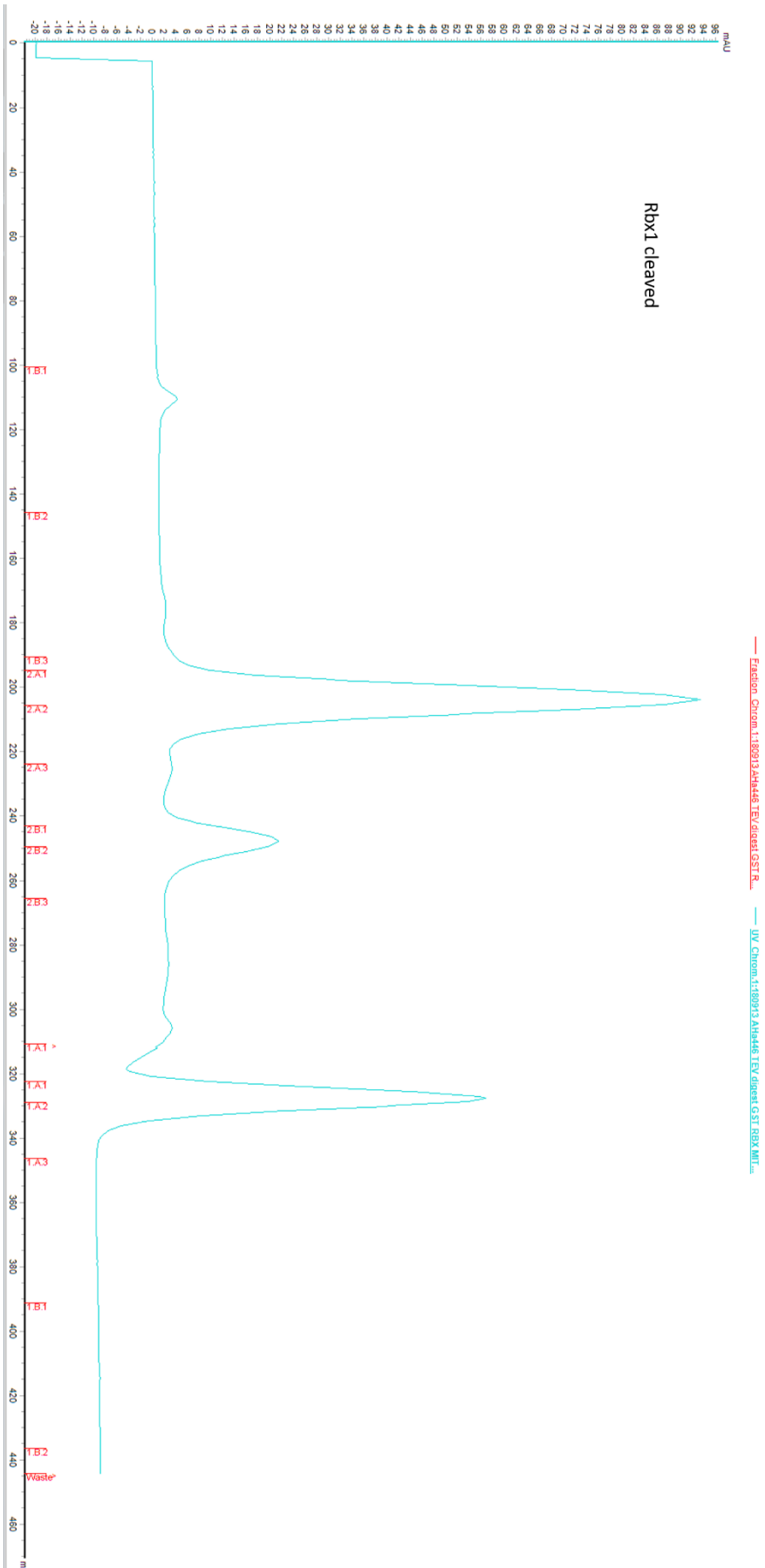
Suppl. Fig. 66 SEC of Glmn B1



Suppl. Fig. 67 SEC of FKBP52FL

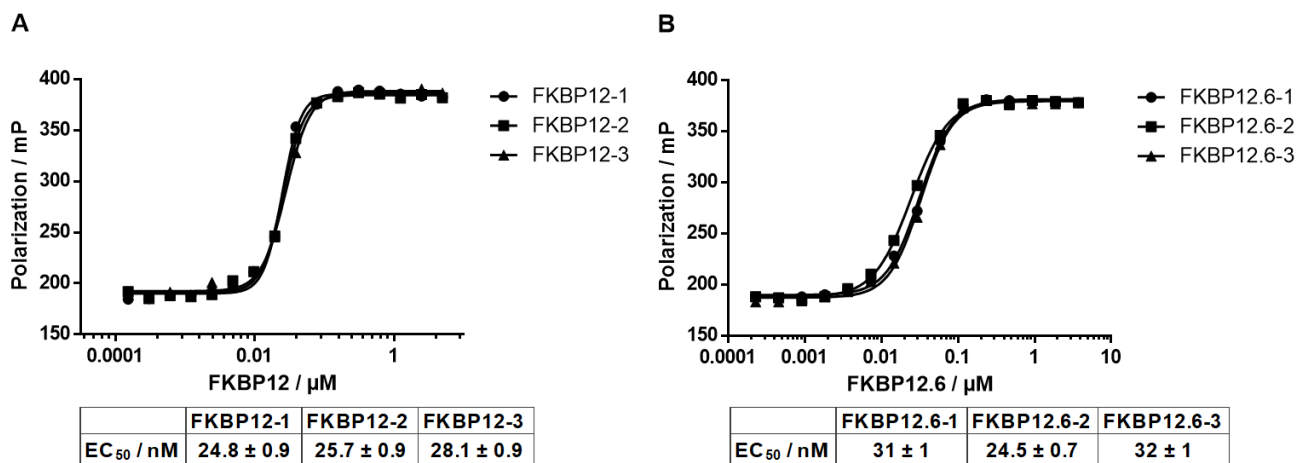


Suppl. Fig. 68 SEC of FKBP51FK1 (16-140) A19T



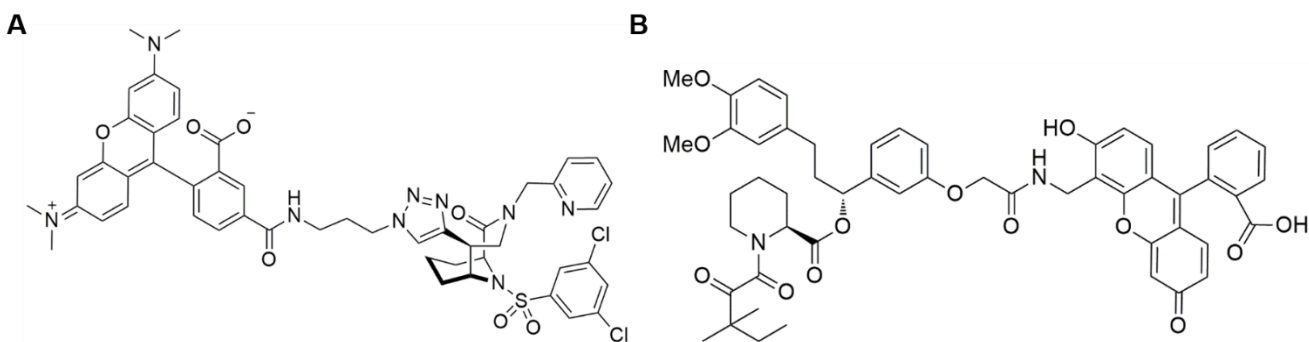
Suppl. Fig. 69 SEC of TEV cleaved Rbx1

7.6. Active Site Titrations of HTRF used FKBP12 and FKBP12.6



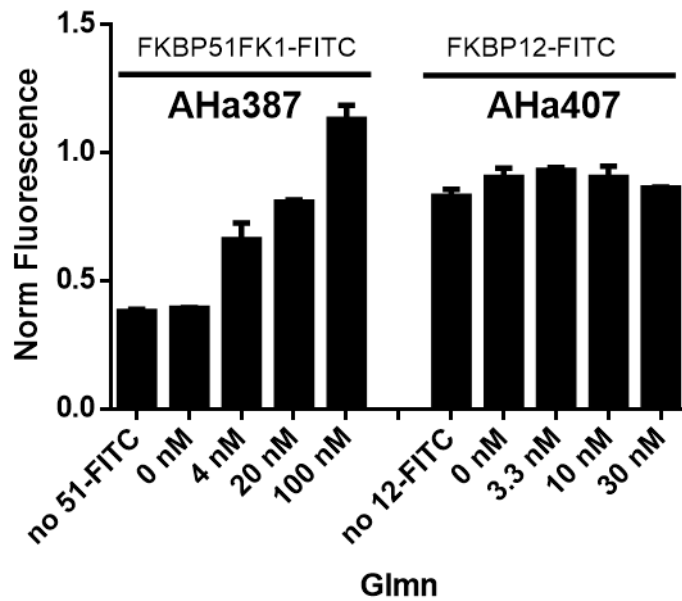
Suppl. Fig. 70 Active Site Titrations of (A) FKBP12 and (B) FKBP12.6 Assays were performed in triplicates with 50 nM MTQ238 /FK[4.3.1]-16g tracer. Active protein concentrations were calculated by $CAST = ((0.5 \times C_{Tracer} + K_D) / EC_{50}) \times C_{UV}$. Lab book: SME88 and CMe362. Data gratefully taken from Stephanie Merz and Christian Meyners.

7.7. Tracer Structures



Suppl. Fig. 71 (A) Structure of FK[4.3.1]-16g / MTQ238 and (B) 2b / CK182

7.8. HTRF Glomulin Titration



Suppl. Fig. 72 Titration of Glmn in the presence of labelled FKBP and Tb- α GST. Norm Fluorescence of 520/620 plotted. The two sets have been performed in two different experiments using the "Gain Optimal" setting that leads to different overall values in between different measurements

8. Abbreviations

5-MF	Fluorescein 5-Maleimide
ADME	Absorption, distribution, metabolism, and excretion
AF	Anne Fabian
APS	Ammonium persulfate
ATP	Adenintriphosphat
BCA	Bicinchoninic Acid
BRET	Bioluminescence Resonance Energy Transfer
Ca ²⁺	Calciumions
CKo	Christian Kozany
CIS	Claudia Sippel
CRISPR	Clustered regularly interspaced short palindromic repeats
C-terminus	Carboxy-terminus
DAG	Diacylglycerol
DMSO	Dimethylsulfoxid
DTT	Dithiothreitol
EC ₅₀	Concentration at which the effect is half maximal
EDTA	Ethylendiamintetraacetat
EtOH	Ethanol
Em	Emission
Ex	Excitation
FCS	Fetale Calf Serum
FKBP	FK506 binding Protein
FL	Full Length
FRET	Förster Resonance Energy Transfer
GAPDH	Glyceraldehyde 3-phosphate dehydrogenase
Glmn	Glomulin
GR	Glucocorticoid Receptor
GST	Glutathion S-Transferase
HEK	Human embryonal kidney cells
HTRF	Homogenous Time Resolved Fluorescence
Hsp90	Heat shock protein HSP 90
IC _{50#}	Concentration at which the inhibition is half maximal
IKK	I-κB kinase
IPTG	Isopropyl β-D-1-thiogalactopyranoside
MB	Compounds synthesized by Michael Bauder

MEF	Mouse embryonal fibroblasts
MTQ	Compounds synthesized by Tianqi Mao
N2a	Neuro-2a (ATCC® CCL-131™)
NaAc	Sodium acetate
NaPP _i	sodium pyrophosphate
NMR	Nuclear magnetic resonance spectroscopy
N-terminus	Amino-terminus
OAG	1-oleoyl-2-acetyl-sn-glycerol
PBS	Phosphate-buffered saline
PKC	Protein kinase C
PLL	poly-L-Lysine
PMA	Phorbol 12-myristate 13-acetate
PMSF	Phenylmethylsulfonylfluorid
PROTAC	proteolysis targeting chimera
SDS	Sodium dodecyl sulfate
Tb	Terbium
TBS(-T)	Tris-buffered saline (-Tween)
TC	Tissue Culture
TEMED	Tetramethylethylenediamine
TNF α	tumor necrosis factor α
TNFR	tumor necrosis factor receptor
TRPC6	Transient Receptor Potential Cation Channel Subfamily C Member 6
Y2H	Yeast2Hybrid

9. Bibliography

- “FKBP51 and FKBP12.6 – novel and tight interactors of Glomulin” **Hähle, A.**, Geiger, T., Merz, S., Meyners C., Mao, T., Kolos, J., Hausch, F., **in revision**
- “Epigenetic upregulation of FKBP5 by aging and stress contributes to NF-kappaB-driven inflammation and cardiovascular risk” Zannas, A. S., Jia, M., Hafner, K., Baumert, J., Wiechmann, T., Pape, J. C., Arloth, J., Kodel, M., Martinelli, S., Roitman, M., Roh, S., **Hähle, A.**, Emeny, R. T., Iurato, S., Carrillo-Roa, T., Lahti, J., Raikkonen, K., Eriksson, J. G., Drake, A. J., Waldenberger, M., Wahl, S., Kunze, S., Lucae, S., Bradley, B., Gieger, C., Hausch, F., Smith, A. K., Ressler, K. J., Muller-Myhsok, B., Ladwig, K. H., Rein, T., Gassen, N. C., Binder, E. B., *PNAS.*, **2019**
- “The Many Faces of FKBP51” **Hähle, A.**, Merz, S., Meyners C., Hausch, F. *Biomolecules*, **2019**
- “Chemogenomic Profiling of Human and Microbial FK506-Binding Proteins” Pomplun, S., Sippel, C. **Hähle, A.**, Tay, D., Shima, K., Klages, A., Unal, C. M., Riess, B., Toh, H. T., Hansen, G., Yoon, H. S., Bracher, A., Preiser, P., Rupp, J., Steinert, M., Hausch, F. *J. Med. Chem.*, **2018**
- “Rapid, Structure-Based Exploration of Pipecolic Acid Amides as Novel Selective Antagonists of the FK506-Binding Protein 51” Gaali S., Feng X., **Hähle A.**, Sippel C., Bracher, A., Hausch, F., *J. Med. Chem.*, **2016**
- “Crystal structures of the free and ligand-bound FK1-FK2 domain segment of FKBP52 reveal a flexible inter-domain hinge.” Bracher, A., Kozany, C., **Hähle, A.**, Wild, P., Zacharias, M., Hausch, F., *Journal of Molecular Biology*, **2013**

10. Acknowledgements

First and foremost, I am grateful to have been surrounded by so many kind, nice and caring people on both Munich and Darmstadt, both at work and in my off-time.

My family, especially my mother Kathrin, my father Jürgen and my dear sister Sabine deserve all my gratitude for their continuous support. Although it was difficult for them, to understand what I am doing, they helped me moving, listened to me and counselled me during my many fights for quality in teaching, lab management and opportunities for international students. Special thoughts are to my sister Sarah-Loreen. May my defeats and victories benefit her life.

I am thankful to my supervisor Prof. Dr. Felix Hausch, who provided me with the opportunity to dive deep into science. Through him, I was able to overcome the limitations of my body, mind and soul. This gratitude will even grow, as I will treasure the loss of my naivity as I mature in the real world.

Among my many colleagues, Stephanie Merz deserves the seat of honor in my heart: Friendship, shared laughter and tears, connected in winnings and losses, never rejecting, always caring. She has the greatest soul I was able to discover in those intense 5 years. Stephi, the world might be too heavy to move, but the good will continue pushing!


Special thanks deserve Sebastian Pomplun, Xixi Feng, Claudia Sippel, Tianqi Mao, Christian Meyners, Asat Baischew, Christine Schröpfer and Andreas Voll. Sebastian, Xixi and Claudia guided me at the beginning of my work and never fell short of their senior and useful advice. Christian and Asat always kept a positive mood in the biochemistry lab and provided tremendously needed scientific exchange. Tianqi was the salt in our rather monocultural department broth. Andreas gave me exciting and valuable insights into a life and character, which is very different from mine. I am especially grateful for his friendship. May it be lasting.

A great share of my gratitude goes to Ms. Beslek, the early morning sunshine every Tuesday and Thursday, as well as the team of Mr. Schädler. Without his essential skills of fixing urgently required infrastructure, most of the presented experiments never could have taken place.

I am grateful for Ms. Dr. Mada Mevissen, who gave me comfort, when as the situations became dire, over and over again.

My heart reaches out to the men, who teach me humility and an up-site-down view of the world. God bless you my dear friends in Guishan Prison Taiwan. I shall not stop reaching out to you.

The financial and intellectual this work was supported by the Hanns-Seidel Stiftung. Finally, I want to thank all the places outside of work where I met so many special, gifted, empathetic and passionate people: MPI for Psychiatry, Hochschulsportzentrum Darmstadt, Staatstheater Darmstadt, SMD International München, Internationaler Kreis Darmstadt, Bachchor Darmstadt und Münchenklang, Johanneskirche Darmstadt and Matthäusdienst München and especially my friends in mission in Taiwan.



Finally, to everybody who reads this, the most important question of all: What is love? The answer is more than “Baby, don’t hurt me”.

11. Curriculum Vitae

Personal information:

Name: Andreas Hähle

Date and place of birth: July 6th 1987, Rochlitz

Citizenship: German

Professional Experience:

Since 9/2014 – 06/2019

PhD studies starting at the Max-Planck-Institute for Psychiatry later at Technical University Darmstadt Research Group Prof. Hausch; Development of cellular and in vitro assays to elucidate protein-protein-interactions and protein-ligand-interaction

Volunteer Experience:

9/2013 – 7/2014

Volunteer Internship with Stiftung Marburger Mission in Taiwan

English- and German Teacher for students and migrant workers, as well as foreign inmate prison counselling

08/2006 – 07/2007

Volunteer Social Year (FSJ), CVJM Lüdenscheid-West

University Education and School:

7/2013

Degree Master of Science


10/2010 – 7/2013

Master studies Biochemistry at Ludwig-Maximilians-University Munich and Uppsala University (Erasmus semester, 03 – 08/2011)

10/2010

Degree Bachelor of Science

10/2007 Studies of Chemistry and Biochemistry an der Ludwig-Maximilians-University Munich



09/1998 – 07/2006

Johann-Mathesius-Gymnasium Rochlitz, High School Diploma: Abitur

Awards:

Promotionsstipendium Hanns-Seidel-Stiftung

Studienstipendium Konrad-Adenauer-Stiftung

Auszeichnung des Landes Sachsen „Abitur mit 1,0“

12. References

1. Gjaltema, R.A.; van der Stoel, M.M.; Boersema, M.; Bank, R.A. Disentangling mechanisms involved in collagen pyridinoline cross-linking: The immunophilin FKBP65 is critical for dimerization of lysyl hydroxylase 2. *Proc Natl Acad Sci U S A* **2016**, *113*, 7142-7147, doi:10.1073/pnas.1600074113.
2. Sinkins, W.G.; Goel, M.; Estacion, M.; Schilling, W.P. Association of immunophilins with mammalian TRPC channels. *J Biol Chem* **2004**, *279*, 34521-34529, doi:10.1074/jbc.M401156200.
3. Binder, E.B.; Salyakina, D.; Lichtner, P.; Wochnik, G.M.; Ising, M.; Putz, B.; Papiol, S.; Seaman, S.; Lucae, S.; Kohli, M.A., et al. Polymorphisms in FKBP5 are associated with increased recurrence of depressive episodes and rapid response to antidepressant treatment. *Nat Genet* **2004**, *36*, 1319-1325, doi:10.1038/ng1479.
4. Klengel, T.; Mehta, D.; Anacker, C.; Rex-Haffner, M.; Pruessner, J.C.; Pariante, C.M.; Pace, T.W.; Mercer, K.B.; Mayberg, H.S.; Bradley, B., et al. Allele-specific FKBP5 DNA demethylation mediates gene-childhood trauma interactions. *Nat Neurosci* **2013**, *16*, 33-41, doi:10.1038/nn.3275.
5. Zannas, A.S.; Wiechmann, T.; Gassen, N.C.; Binder, E.B. Gene-Stress-Epigenetic Regulation of FKBP5: Clinical and Translational Implications. *Neuropsychopharmacology* **2016**, *41*, 261-274, doi:10.1038/npp.2015.235.
6. Matosin, N.; Halldorsdottir, T.; Binder, E.B. Understanding the Molecular Mechanisms Underpinning Gene by Environment Interactions in Psychiatric Disorders: The FKBP5 Model. *Biol Psychiatry* **2018**, *83*, 821-830, doi:10.1016/j.biopsych.2018.01.021.
7. Touma, C.; Gassen, N.C.; Herrmann, L.; Cheung-Flynn, J.; Bull, D.R.; Ionescu, I.A.; Heinzmann, J.M.; Knapman, A.; Siebertz, A.; Depping, A.M., et al. FK506 binding protein 5 shapes stress responsiveness: modulation of neuroendocrine reactivity and coping behavior. *Biol Psychiatry* **2011**, *70*, 928-936, doi:10.1016/j.biopsych.2011.07.023.
8. Gassen, N.C.; Hartmann, J.; Zschocke, J.; Stepan, J.; Hafner, K.; Zellner, A.; Kirmeier, T.; Kollmannsberger, L.; Wagner, K.V.; Dedic, N., et al. Association of FKBP51 with priming of autophagy pathways and mediation of antidepressant treatment response: evidence in cells, mice, and humans. *PLoS Med* **2014**, *11*, e1001755, doi:10.1371/journal.pmed.1001755.
9. Hartmann, J.; Wagner, K.V.; Liebl, C.; Scharf, S.H.; Wang, X.D.; Wolf, M.; Hausch, F.; Rein, T.; Schmidt, U.; Touma, C., et al. The involvement of FK506-binding protein 51 (FKBP5) in the behavioral and neuroendocrine effects of chronic social defeat stress. *Neuropharmacology* **2012**, *62*, 332-339, doi:10.1016/j.neuropharm.2011.07.041.
10. Sabbagh, J.J.; O'Leary, J.C., 3rd; Blair, L.J.; Klengel, T.; Nordhues, B.A.; Fontaine, S.N.; Binder, E.B.; Dickey, C.A. Age-associated epigenetic upregulation of the FKBP5 gene selectively impairs stress resiliency. *PLoS One* **2014**, *9*, e107241, doi:10.1371/journal.pone.0107241.
11. O'Leary, J.C., 3rd; Dharia, S.; Blair, L.J.; Brady, S.; Johnson, A.G.; Peters, M.; Cheung-Flynn, J.; Cox, M.B.; de Erausquin, G.; Weeber, E.J., et al. A new anti-depressive strategy for the elderly: ablation of FKBP5/FKBP51. *PLoS One* **2011**, *6*, e24840, doi:10.1371/journal.pone.0024840.
12. Pereira, M.J.; Palming, J.; Svensson, M.K.; Rizell, M.; Dalenback, J.; Hammar, M.; Fall, T.; Sidibeh, C.O.; Svensson, P.A.; Eriksson, J.W. FKBP5 expression in human adipose tissue increases following dexamethasone exposure and is associated with insulin resistance. *Metabolism* **2014**, *63*, 1198-1208, doi:10.1016/j.metabol.2014.05.015.
13. Sidibeh, C.O.; Pereira, M.J.; Abalo, X.M.; G, J.B.; Skrtic, S.; Lundkvist, P.; Katsogiannos, P.; Hausch, F.; Castillejo-Lopez, C.; Eriksson, J.W. FKBP5 expression in human adipose tissue: potential role in glucose and lipid metabolism, adipogenesis and type 2 diabetes. *Endocrine* **2018**, *62*, 116-128, doi:10.1007/s12020-018-1674-5.
14. Bortsov, A.V.; Smith, J.E.; Diatchenko, L.; Soward, A.C.; Ulirsch, J.C.; Rossi, C.; Swor, R.A.; Hauda, W.E.; Peak, D.A.; Jones, J.S., et al. Polymorphisms in the glucocorticoid receptor co-chaperone FKBP5 predict persistent musculoskeletal pain after traumatic stress exposure. *Pain* **2013**, *154*, 1419-1426, doi:10.1016/j.pain.2013.04.037.

15. Linnstaedt, S.D.; Riker, K.D.; Rueckeis, C.A.; Kutchko, K.M.; Lackey, L.; McCarthy, K.R.; Tsai, Y.H.; Parker, J.S.; Kurz, M.C.; Hendry, P.L., et al. A Functional riboSNitch in the 3' Untranslated Region of FKBP5 Alters MicroRNA-320a Binding Efficiency and Mediates Vulnerability to Chronic Post-Traumatic Pain. *J Neurosci* **2018**, *38*, 8407-8420, doi:10.1523/JNEUROSCI.3458-17.2018.
16. Abu, S.; Romanowski, C.P.; Letizia Curzi, M.; Jakubcakova, V.; Flachskamm, C.; Gassen, N.C.; Hartmann, J.; Schmidt, M.V.; Schmidt, U.; Rein, T., et al. Deficiency of FK506-binding protein (FKBP) 51 alters sleep architecture and recovery sleep responses to stress in mice. *J Sleep Res* **2014**, *23*, 176-185, doi:10.1111/jsr.12112.
17. Stechschulte, L.A.; Qiu, B.; Warriar, M.; Hinds, T.D., Jr.; Zhang, M.; Gu, H.; Xu, Y.; Khuder, S.S.; Russo, L.; Najjar, S.M., et al. FKBP51 Null Mice Are Resistant to Diet-Induced Obesity and the PPARgamma Agonist Rosiglitazone. *Endocrinology* **2016**, *157*, 3888-3900, doi:10.1210/en.2015-1996.
18. Balsevich, G.; Hausl, A.S.; Meyer, C.W.; Karamihalev, S.; Feng, X.; Pohlmann, M.L.; Dournes, C.; Uribe-Marino, A.; Santarelli, S.; Labermaier, C., et al. Stress-responsive FKBP51 regulates AKT2-AS160 signaling and metabolic function. *Nat Commun* **2017**, *8*, 1725, doi:10.1038/s41467-017-01783-y.
19. Maiaru, M.; Tochiki, K.K.; Cox, M.B.; Annan, L.V.; Bell, C.G.; Feng, X.; Hausch, F.; Geranton, S.M. The stress regulator FKBP51 drives chronic pain by modulating spinal glucocorticoid signaling. *Sci Transl Med* **2016**, *8*, 325ra319, doi:10.1126/scitranslmed.aab3376.
20. Maiaru, M.; Morgan, O.B.; Mao, T.; Breitsamer, M.; Bamber, H.; Pohlmann, M.; Schmidt, M.V.; Winter, G.; Hausch, F.; Geranton, S.M. The stress regulator FKBP51: a novel and promising druggable target for the treatment of persistent pain states across sexes. *Pain* **2018**, *159*, 1224-1234, doi:10.1097/j.pain.0000000000001204.
21. Baida, G.; Bhalla, P.; Yemelyanov, A.; Stechschulte, L.A.; Shou, W.; Readhead, B.; Dudley, J.T.; Sanchez, E.R.; Budunova, I. Deletion of the glucocorticoid receptor chaperone FKBP51 prevents glucocorticoid-induced skin atrophy. *Oncotarget* **2018**, *9*, 34772-34783, doi:10.18632/oncotarget.26194.
22. Gaali, S.; Kirschner, A.; Cuboni, S.; Hartmann, J.; Kozany, C.; Balsevich, G.; Namendorf, C.; Fernandez-Vizarra, P.; Sippel, C.; Zannas, A.S., et al. Selective inhibitors of the FK506-binding protein 51 by induced fit. *Nat Chem Biol* **2015**, *11*, 33-37, doi:10.1038/nchembio.1699.
23. Pohlmann, M.L.; Hausl, A.S.; Harbich, D.; Balsevich, G.; Engelhardt, C.; Feng, X.; Breitsamer, M.; Hausch, F.; Winter, G.; Schmidt, M.V. Pharmacological Modulation of the Psychiatric Risk Factor FKBP51 Alters Efficiency of Common Antidepressant Drugs. *Front Behav Neurosci* **2018**, *12*, 262, doi:10.3389/fnbeh.2018.00262.
24. Hartmann, J.; Wagner, K.V.; Gaali, S.; Kirschner, A.; Kozany, C.; Ruhter, G.; Dedic, N.; Hausl, A.S.; Hoeijmakers, L.; Westerholz, S., et al. Pharmacological Inhibition of the Psychiatric Risk Factor FKBP51 Has Anxiolytic Properties. *J Neurosci* **2015**, *35*, 9007-9016, doi:10.1523/JNEUROSCI.4024-14.2015.
25. Hahle, A.; Merz, S.; Meyners, C.; Hausch, F. The Many Faces of FKBP51. *Biomolecules* **2019**, *9*, doi:10.3390/biom9010035.
26. Kozany, C.; Marz, A.; Kress, C.; Hausch, F. Fluorescent probes to characterise FK506-binding proteins. *Chembiochem* **2009**, *10*, 1402-1410, doi:10.1002/cbic.200800806.
27. Sinars, C.R.; Cheung-Flynn, J.; Rimerman, R.A.; Scammell, J.G.; Smith, D.F.; Clardy, J. Structure of the large FK506-binding protein FKBP51, an Hsp90-binding protein and a component of steroid receptor complexes. *Proc Natl Acad Sci U S A* **2003**, *100*, 868-873, doi:10.1073/pnas.0231020100.
28. Pirkl, F.; Buchner, J. Functional analysis of the Hsp90-associated human peptidyl prolyl cis/trans isomerases FKBP51, FKBP52 and Cyp40. *J Mol Biol* **2001**, *308*, 795-806, doi:10.1006/jmbi.2001.4595.
29. Chambraud, B.; Rouviere-Fourmy, N.; Radanyi, C.; Hsiao, K.; Peattie, D.A.; Livingston, D.J.; Baulieu, E.E. Overexpression of p59-HBI (FKBP59), full length and domains, and characterization of PPlase activity. *Biochem Biophys Res Commun* **1993**, *196*, 160-166.

30. Bracher, A.; Kozany, C.; Hahle, A.; Wild, P.; Zacharias, M.; Hausch, F. Crystal structures of the free and ligand-bound FK1-FK2 domain segment of FKBP52 reveal a flexible inter-domain hinge. *J Mol Biol* **2013**, *425*, 4134-4144, doi:10.1016/j.jmb.2013.07.041.
31. Kumar, R.; Moche, M.; Winblad, B.; Pavlov, P.F. Combined x-ray crystallography and computational modeling approach to investigate the Hsp90 C-terminal peptide binding to FKBP51. *Sci Rep* **2017**, *7*, 14288, doi:10.1038/s41598-017-14731-z.
32. Wu, B.; Li, P.; Liu, Y.; Lou, Z.; Ding, Y.; Shu, C.; Ye, S.; Bartlam, M.; Shen, B.; Rao, Z. 3D structure of human FK506-binding protein 52: implications for the assembly of the glucocorticoid receptor/Hsp90/immunophilin heterocomplex. *Proc Natl Acad Sci U S A* **2004**, *101*, 8348-8353, doi:10.1073/pnas.0305969101.
33. Wochnik, G.M.; Ruegg, J.; Abel, G.A.; Schmidt, U.; Holsboer, F.; Rein, T. FK506-binding proteins 51 and 52 differentially regulate dynein interaction and nuclear translocation of the glucocorticoid receptor in mammalian cells. *J Biol Chem* **2005**, *280*, 4609-4616, doi:10.1074/jbc.M407498200.
34. Chen, S.; Sullivan, W.P.; Toft, D.O.; Smith, D.F. Differential interactions of p23 and the TPR-containing proteins Hop, Cyp40, FKBP52 and FKBP51 with Hsp90 mutants. *Cell Stress Chaperones* **1998**, *3*, 118-129.
35. Wilson, K.P.; Yamashita, M.M.; Sintchak, M.D.; Rotstein, S.H.; Murcko, M.A.; Boger, J.; Thomson, J.A.; Fitzgibbon, M.J.; Black, J.R.; Navia, M.A. Comparative X-ray structures of the major binding protein for the immunosuppressant FK506 (tacrolimus) in unliganded form and in complex with FK506 and rapamycin. *Acta Crystallogr D Biol Crystallogr* **1995**, *51*, 511-521, doi:10.1107/S09074444994014514.
36. Bracher, A.; Kozany, C.; Thost, A.K.; Hausch, F. Structural characterization of the PPlase domain of FKBP51, a cochaperone of human Hsp90. *Acta Crystallogr D Biol Crystallogr* **2011**, *67*, 549-559, doi:10.1107/S0907444911013862.
37. Quinta, H.R.; Maschi, D.; Gomez-Sanchez, C.; Piwien-Pilipuk, G.; Galigniana, M.D. Subcellular rearrangement of hsp90-binding immunophilins accompanies neuronal differentiation and neurite outgrowth. *J Neurochem* **2010**, *115*, 716-734, doi:10.1111/j.1471-4159.2010.06970.x.
38. Cheung-Flynn, J.; Prapapanich, V.; Cox, M.B.; Riggs, D.L.; Suarez-Quian, C.; Smith, D.F. Physiological role for the cochaperone FKBP52 in androgen receptor signaling. *Mol Endocrinol* **2005**, *19*, 1654-1666, doi:10.1210/me.2005-0071.
39. LeMaster, D.M.; Mustafi, S.M.; Brecher, M.; Zhang, J.; Heroux, A.; Li, H.; Hernandez, G. Coupling of Conformational Transitions in the N-terminal Domain of the 51-kDa FK506-binding Protein (FKBP51) Near Its Site of Interaction with the Steroid Receptor Proteins. *J Biol Chem* **2015**, *290*, 15746-15757, doi:10.1074/jbc.M115.650655.
40. Pomplun, S.; Sippel, C.; Hahle, A.; Tay, D.; Shima, K.; Klages, A.; Unal, C.M.; Riess, B.; Toh, H.T.; Hansen, G., et al. Chemogenomic Profiling of Human and Microbial FK506-Binding Proteins. *J Med Chem* **2018**, *61*, 3660-3673, doi:10.1021/acs.jmedchem.8b00137.
41. Pomplun, S.; Wang, Y.; Kirschner, A.; Kozany, C.; Bracher, A.; Hausch, F. Rational design and asymmetric synthesis of potent and neurotrophic ligands for FK506-binding proteins (FKBPs). *Angew Chem Int Ed Engl* **2015**, *54*, 345-348, doi:10.1002/anie.201408776.
42. Kolos, J.M.; Voll, A.M.; Bauder, M.; Hausch, F. FKBP Ligands-Where We Are and Where to Go? *Front Pharmacol* **2018**, *9*, 1425, doi:10.3389/fphar.2018.01425.
43. An, S.; Fu, L. Small-molecule PROTACs: An emerging and promising approach for the development of targeted therapy drugs. *EBioMedicine* **2018**, *36*, 553-562, doi:10.1016/j.ebiom.2018.09.005.
44. Sakamoto, K.M.; Kim, K.B.; Kumagai, A.; Mercurio, F.; Crews, C.M.; Deshaies, R.J. Protacs: chimeric molecules that target proteins to the Skp1-Cullin-F box complex for ubiquitination and degradation. *Proc Natl Acad Sci U S A* **2001**, *98*, 8554-8559, doi:10.1073/pnas.141230798.
45. Schneekloth, A.R.; Pucheault, M.; Tae, H.S.; Crews, C.M. Targeted intracellular protein degradation induced by a small molecule: En route to chemical proteomics. *Bioorg Med Chem Lett* **2008**, *18*, 5904-5908, doi:10.1016/j.bmcl.2008.07.114.
46. Gadd, M.S.; Testa, A.; Lucas, X.; Chan, K.H.; Chen, W.; Lamont, D.J.; Zengerle, M.; Ciulli, A. Structural basis of PROTAC cooperative recognition for selective protein degradation. *Nat Chem Biol* **2017**, *13*, 514-521, doi:10.1038/nchembio.2329.

47. Lu, J.; Qian, Y.; Altieri, M.; Dong, H.; Wang, J.; Raina, K.; Hines, J.; Winkler, J.D.; Crew, A.P.; Coleman, K., et al. Hijacking the E3 Ubiquitin Ligase Cereblon to Efficiently Target BRD4. *Chem Biol* **2015**, *22*, 755-763, doi:10.1016/j.chembiol.2015.05.009.
48. Olson, C.M.; Jiang, B.; Erb, M.A.; Liang, Y.; Doctor, Z.M.; Zhang, Z.; Zhang, T.; Kwiatkowski, N.; Boukhali, M.; Green, J.L., et al. Pharmacological perturbation of CDK9 using selective CDK9 inhibition or degradation. *Nat Chem Biol* **2018**, *14*, 163-170, doi:10.1038/nchembio.2538.
49. Ohoka, N.; Okuhira, K.; Ito, M.; Nagai, K.; Shibata, N.; Hattori, T.; Ujikawa, O.; Shimokawa, K.; Sano, O.; Koyama, R., et al. In Vivo Knockdown of Pathogenic Proteins via Specific and Nongenetic Inhibitor of Apoptosis Protein (IAP)-dependent Protein Erasers (SNIPERs). *J Biol Chem* **2017**, *292*, 4556-4570, doi:10.1074/jbc.M116.768853.
50. Buhimschi, A.D.; Armstrong, H.A.; Toure, M.; Jaime-Figueroa, S.; Chen, T.L.; Lehman, A.M.; Woyach, J.A.; Johnson, A.J.; Byrd, J.C.; Crews, C.M. Targeting the C481S Ibrutinib-Resistance Mutation in Bruton's Tyrosine Kinase Using PROTAC-Mediated Degradation. *Biochemistry* **2018**, *57*, 3564-3575, doi:10.1021/acs.biochem.8b00391.
51. Sun, B.; Fiskus, W.; Qian, Y.; Rajapakshe, K.; Raina, K.; Coleman, K.G.; Crew, A.P.; Shen, A.; Saenz, D.T.; Mill, C.P., et al. BET protein proteolysis targeting chimera (PROTAC) exerts potent lethal activity against mantle cell lymphoma cells. *Leukemia* **2018**, *32*, 343-352, doi:10.1038/leu.2017.207.
52. Zhou, B.; Hu, J.; Xu, F.; Chen, Z.; Bai, L.; Fernandez-Salas, E.; Lin, M.; Liu, L.; Yang, C.Y.; Zhao, Y., et al. Discovery of a Small-Molecule Degradator of Bromodomain and Extra-Terminal (BET) Proteins with Picomolar Cellular Potencies and Capable of Achieving Tumor Regression. *J Med Chem* **2018**, *61*, 462-481, doi:10.1021/acs.jmedchem.6b01816.
53. Burslem, G.M.; Smith, B.E.; Lai, A.C.; Jaime-Figueroa, S.; McQuaid, D.C.; Bondeson, D.P.; Toure, M.; Dong, H.; Qian, Y.; Wang, J., et al. The Advantages of Targeted Protein Degradation Over Inhibition: An RTK Case Study. *Cell Chem Biol* **2018**, *25*, 67-77 e63, doi:10.1016/j.chembiol.2017.09.009.
54. Bondeson, D.P.; Mares, A.; Smith, I.E.; Ko, E.; Campos, S.; Miah, A.H.; Mulholland, K.E.; Routly, N.; Buckley, D.L.; Gustafson, J.L., et al. Catalytic in vivo protein knockdown by small-molecule PROTACs. *Nat Chem Biol* **2015**, *11*, 611-617, doi:10.1038/nchembio.1858.
55. Bondeson, D.P.; Smith, B.E.; Burslem, G.M.; Buhimschi, A.D.; Hines, J.; Jaime-Figueroa, S.; Wang, J.; Hamman, B.D.; Ishchenko, A.; Crews, C.M. Lessons in PROTAC Design from Selective Degradation with a Promiscuous Warhead. *Cell Chem Biol* **2018**, *25*, 78-87 e75, doi:10.1016/j.chembiol.2017.09.010.
56. Itoh, Y.; Ishikawa, M.; Naito, M.; Hashimoto, Y. Protein knockdown using methyl bestatin-ligand hybrid molecules: design and synthesis of inducers of ubiquitination-mediated degradation of cellular retinoic acid-binding proteins. *J Am Chem Soc* **2010**, *132*, 5820-5826, doi:10.1021/ja100691p.
57. Okuhira, K.; Demizu, Y.; Hattori, T.; Ohoka, N.; Shibata, N.; Nishimaki-Mogami, T.; Okuda, H.; Kurihara, M.; Naito, M. Development of hybrid small molecules that induce degradation of estrogen receptor-alpha and necrotic cell death in breast cancer cells. *Cancer Sci* **2013**, *104*, 1492-1498, doi:10.1111/cas.12272.
58. Ricking, K.M.; Mahan, S.; Corona, C.R.; McDougall, M.; Vasta, J.D.; Robers, M.B.; Urh, M.; Daniels, D.L. Quantitative Live-Cell Kinetic Degradation and Mechanistic Profiling of PROTAC Mode of Action. *ACS Chem Biol* **2018**, *13*, 2758-2770, doi:10.1021/acscchembio.8b00692.
59. Mullard, A. First targeted protein degrader hits the clinic. *Nat Rev Drug Discov* **2019**, *10.1038/d41573-019-00043-6*, doi:10.1038/d41573-019-00043-6.
60. Taipale, M.; Tucker, G.; Peng, J.; Krykbaeva, I.; Lin, Z.Y.; Larsen, B.; Choi, H.; Berger, B.; Gingras, A.C.; Lindquist, S. A quantitative chaperone interaction network reveals the architecture of cellular protein homeostasis pathways. *Cell* **2014**, *158*, 434-448, doi:10.1016/j.cell.2014.05.039.
61. Schopf, F.H.; Biebl, M.M.; Buchner, J. The HSP90 chaperone machinery. *Nat Rev Mol Cell Biol* **2017**, *18*, 345-360, doi:10.1038/nrm.2017.20.
62. Smith, D.F.; Faber, L.E.; Toft, D.O. Purification of unactivated progesterone receptor and identification of novel receptor-associated proteins. *J Biol Chem* **1990**, *265*, 3996-4003.

63. Smith, D.F.; Albers, M.W.; Schreiber, S.L.; Leach, K.L.; Deibel, M.R., Jr. FKBP54, a novel FK506-binding protein in avian progesterone receptor complexes and HeLa extracts. *J Biol Chem* **1993**, *268*, 24270-24273.
64. Smith, D.F.; Whitesell, L.; Nair, S.C.; Chen, S.; Prapapanich, V.; Rimerman, R.A. Progesterone receptor structure and function altered by geldanamycin, an hsp90-binding agent. *Mol Cell Biol* **1995**, *15*, 6804-6812.
65. Mayer, M.P.; Le Breton, L. Hsp90: breaking the symmetry. *Mol Cell* **2015**, *58*, 8-20, doi:10.1016/j.molcel.2015.02.022.
66. Rohl, A.; Rohrberg, J.; Buchner, J. The chaperone Hsp90: changing partners for demanding clients. *Trends Biochem Sci* **2013**, *38*, 253-262, doi:10.1016/j.tibs.2013.02.003.
67. Cheung-Flynn, J.; Roberts, P.J.; Riggs, D.L.; Smith, D.F. C-terminal sequences outside the tetratricopeptide repeat domain of FKBP51 and FKBP52 cause differential binding to Hsp90. *J Biol Chem* **2003**, *278*, 17388-17394, doi:10.1074/jbc.M300955200.
68. Scheufler, C.; Brinker, A.; Bourenkov, G.; Pegoraro, S.; Moroder, L.; Bartunik, H.; Hartl, F.U.; Moarefi, I. Structure of TPR domain-peptide complexes: critical elements in the assembly of the Hsp70-Hsp90 multichaperone machine. *Cell* **2000**, *101*, 199-210, doi:10.1016/S0092-8674(00)80830-2.
69. Schulke, J.P.; Wochnik, G.M.; Lang-Rollin, I.; Gassen, N.C.; Knapp, R.T.; Berning, B.; Yassouridis, A.; Rein, T. Differential impact of tetratricopeptide repeat proteins on the steroid hormone receptors. *PLoS One* **2010**, *5*, e11717, doi:10.1371/journal.pone.0011717.
70. Li, J.; Richter, K.; Buchner, J. Mixed Hsp90-cochaperone complexes are important for the progression of the reaction cycle. *Nat Struct Mol Biol* **2011**, *18*, 61-66, doi:10.1038/nsmb.1965.
71. Echeverria, P.C.; Picard, D. Molecular chaperones, essential partners of steroid hormone receptors for activity and mobility. *Biochim Biophys Acta* **2010**, *1803*, 641-649, doi:10.1016/j.bbamcr.2009.11.012.
72. Barent, R.L.; Nair, S.C.; Carr, D.C.; Ruan, Y.; Rimerman, R.A.; Fulton, J.; Zhang, Y.; Smith, D.F. Analysis of FKBP51/FKBP52 chimeras and mutants for Hsp90 binding and association with progesterone receptor complexes. *Mol Endocrinol* **1998**, *12*, 342-354, doi:10.1210/mend.12.3.0075.
73. Baughman, G.; Wiederrecht, G.J.; Chang, F.; Martin, M.M.; Bourgeois, S. Tissue distribution and abundance of human FKBP51, and FK506-binding protein that can mediate calcineurin inhibition. *Biochem Biophys Res Commun* **1997**, *232*, 437-443.
74. Reynolds, P.D.; Roveda, K.P.; Tucker, J.A.; Moore, C.M.; Valentine, D.L.; Scammell, J.G. Glucocorticoid-resistant B-lymphoblast cell line derived from the Bolivian squirrel monkey (*Saimiri boliviensis boliviensis*). *Lab Anim Sci* **1998**, *48*, 364-370.
75. Wan, Y.; Nordeen, S.K. Identification of genes differentially regulated by glucocorticoids and progestins using a Cre/loxP-mediated retroviral promoter-trapping strategy. *J Mol Endocrinol* **2002**, *28*, 177-192.
76. Vermeer, H.; Hendriks-Stegeman, B.I.; van der Burg, B.; van Buul-Offers, S.C.; Jansen, M. Glucocorticoid-induced increase in lymphocytic FKBP51 messenger ribonucleic acid expression: a potential marker for glucocorticoid sensitivity, potency, and bioavailability. *J Clin Endocrinol Metab* **2003**, *88*, 277-284, doi:10.1210/jc.2002-020354.
77. Kester, H.A.; van der Leede, B.M.; van der Saag, P.T.; van der Burg, B. Novel progesterone target genes identified by an improved differential display technique suggest that progestin-induced growth inhibition of breast cancer cells coincides with enhancement of differentiation. *J Biol Chem* **1997**, *272*, 16637-16643.
78. Hubler, T.R.; Denny, W.B.; Valentine, D.L.; Cheung-Flynn, J.; Smith, D.F.; Scammell, J.G. The FK506-binding immunophilin FKBP51 is transcriptionally regulated by progestin and attenuates progestin responsiveness. *Endocrinology* **2003**, *144*, 2380-2387, doi:10.1210/en.2003-0092.
79. Hubler, T.R.; Scammell, J.G. Intronic hormone response elements mediate regulation of FKBP5 by progestins and glucocorticoids. *Cell Stress Chaperones* **2004**, *9*, 243-252.
80. Amler, L.C.; Agus, D.B.; LeDuc, C.; Sapinoso, M.L.; Fox, W.D.; Kern, S.; Lee, D.; Wang, V.; Leysens, M.; Higgins, B., et al. Dysregulated expression of androgen-responsive and nonresponsive genes in the androgen-independent prostate cancer xenograft model CWR22-R1. *Cancer Res* **2000**, *60*, 6134-6141.

81. Mousses, S.; Wagner, U.; Chen, Y.; Kim, J.W.; Bubendorf, L.; Bittner, M.; Pretlow, T.; Elkahoul, A.G.; Trepel, J.B.; Kallioniemi, O.P. Failure of hormone therapy in prostate cancer involves systematic restoration of androgen responsive genes and activation of rapamycin sensitive signaling. *Oncogene* **2001**, *20*, 6718-6723, doi:10.1038/sj.onc.1204889.
82. Zhu, W.; Zhang, J.S.; Young, C.Y. Silymarin inhibits function of the androgen receptor by reducing nuclear localization of the receptor in the human prostate cancer cell line LNCaP. *Carcinogenesis* **2001**, *22*, 1399-1403.
83. Paakinaho, V.; Makkonen, H.; Jaaskelainen, T.; Palvimo, J.J. Glucocorticoid receptor activates paired FKBP51 locus through long-distance interactions. *Mol Endocrinol* **2010**, *24*, 511-525, doi:10.1210/me.2009-0443.
84. Riggs, D.L.; Roberts, P.J.; Chirillo, S.C.; Cheung-Flynn, J.; Prapapanich, V.; Ratajczak, T.; Gaber, R.; Picard, D.; Smith, D.F. The Hsp90-binding peptidylprolyl isomerase FKBP52 potentiates glucocorticoid signaling in vivo. *EMBO J* **2003**, *22*, 1158-1167, doi:10.1093/emboj/cdg108.
85. Riggs, D.L.; Cox, M.B.; Tardif, H.L.; Hessling, M.; Buchner, J.; Smith, D.F. Noncatalytic role of the FKBP52 peptidyl-prolyl isomerase domain in the regulation of steroid hormone signaling. *Mol Cell Biol* **2007**, *27*, 8658-8669, doi:10.1128/MCB.00985-07.
86. Ebong, I.O.; Beilsten-Edmands, V.; Patel, N.A.; Morgner, N.; Robinson, C.V. The interchange of immunophilins leads to parallel pathways and different intermediates in the assembly of Hsp90 glucocorticoid receptor complexes. *Cell Discov* **2016**, *2*, 16002, doi:10.1038/celldisc.2016.2.
87. Stechschulte, L.A.; Hinds, T.D., Jr.; Khuder, S.S.; Shou, W.; Najjar, S.M.; Sanchez, E.R. FKBP51 controls cellular adipogenesis through p38 kinase-mediated phosphorylation of GRalpha and PPARgamma. *Mol Endocrinol* **2014**, *28*, 1265-1275, doi:10.1210/me.2014-1022.
88. Antunica-Noguerol, M.; Budzinski, M.L.; Druker, J.; Gassen, N.C.; Sokn, M.C.; Senin, S.; Aprile-Garcia, F.; Holsboer, F.; Rein, T.; Liberman, A.C., et al. The activity of the glucocorticoid receptor is regulated by SUMO conjugation to FKBP51. *Cell Death Differ* **2016**, *23*, 1579-1591, doi:10.1038/cdd.2016.44.
89. Sabbagh, J.J.; Cordova, R.A.; Zheng, D.; Criado-Marrero, M.; Lemus, A.; Li, P.; Baker, J.D.; Nordhues, B.A.; Darling, A.L.; Martinez-Licha, C., et al. Targeting the FKBP51/GR/Hsp90 Complex to Identify Functionally Relevant Treatments for Depression and PTSD. *ACS Chem Biol* **2018**, *13*, 2288-2299, doi:10.1021/acscchembio.8b00454.
90. Criado-Marrero, M.; Rein, T.; Binder, E.B.; Porter, J.T.; Koren, J., 3rd; Blair, L.J. Hsp90 and FKBP51: complex regulators of psychiatric diseases. *Philos Trans R Soc Lond B Biol Sci* **2018**, *373*, doi:10.1098/rstb.2016.0532.
91. DeMorrow, S. Role of the Hypothalamic-Pituitary-Adrenal Axis in Health and Disease. *Int J Mol Sci* **2018**, *19*, doi:10.3390/ijms19040986.
92. Garabedian, M.J.; Harris, C.A.; Jeanneteau, F. Glucocorticoid receptor action in metabolic and neuronal function. *F1000Res* **2017**, *6*, 1208, doi:10.12688/f1000research.11375.1.
93. Ni, L.; Yang, C.S.; Gioeli, D.; Frierson, H.; Toft, D.O.; Paschal, B.M. FKBP51 promotes assembly of the Hsp90 chaperone complex and regulates androgen receptor signaling in prostate cancer cells. *Mol Cell Biol* **2010**, *30*, 1243-1253, doi:10.1128/MCB.01891-08.
94. Periyasamy, S.; Hinds, T., Jr.; Shemshedini, L.; Shou, W.; Sanchez, E.R. FKBP51 and Cyp40 are positive regulators of androgen-dependent prostate cancer cell growth and the targets of FK506 and cyclosporin A. *Oncogene* **2010**, *29*, 1691-1701, doi:10.1038/onc.2009.458.
95. Caratti, G.; Matthews, L.; Poolman, T.; Kershaw, S.; Baxter, M.; Ray, D. Glucocorticoid receptor function in health and disease. *Clin Endocrinol (Oxf)* **2015**, *83*, 441-448, doi:10.1111/cen.12728.
96. Pei, H.; Li, L.; Fridley, B.L.; Jenkins, G.D.; Kalari, K.R.; Lingle, W.; Petersen, G.; Lou, Z.; Wang, L. FKBP51 affects cancer cell response to chemotherapy by negatively regulating Akt. *Cancer Cell* **2009**, *16*, 259-266, doi:10.1016/j.ccr.2009.07.016.
97. Luo, K.; Li, Y.; Yin, Y.; Li, L.; Wu, C.; Chen, Y.; Nowsheen, S.; Hu, Q.; Zhang, L.; Lou, Z., et al. USP49 negatively regulates tumorigenesis and chemoresistance through FKBP51-AKT signaling. *EMBO J* **2017**, *36*, 1434-1446, doi:10.15252/embj.201695669.

98. Yu, J.; Qin, B.; Wu, F.; Qin, S.; Nowsheen, S.; Shan, S.; Zayas, J.; Pei, H.; Lou, Z.; Wang, L. Regulation of Serine-Threonine Kinase Akt Activation by NAD(+)-Dependent Deacetylase SIRT7. *Cell Rep* **2017**, *18*, 1229-1240, doi:10.1016/j.celrep.2017.01.009.
99. Fabian, A.K.; Marz, A.; Neimanis, S.; Biondi, R.M.; Kozany, C.; Hausch, F. InterAKTions with FKBP5--mutational and pharmacological exploration. *PLoS One* **2013**, *8*, e57508, doi:10.1371/journal.pone.0057508.
100. Gassen, N.C.; Hartmann, J.; Zannas, A.S.; Kretzschmar, A.; Zschocke, J.; Maccarrone, G.; Hafner, K.; Zellner, A.; Kollmannsberger, L.K.; Wagner, K.V., et al. FKBP51 inhibits GSK3beta and augments the effects of distinct psychotropic medications. *Mol Psychiatry* **2016**, *21*, 277-289, doi:10.1038/mp.2015.38.
101. Jiang, W.; Cazacu, S.; Xiang, C.; Zenklusen, J.C.; Fine, H.A.; Berens, M.; Armstrong, B.; Brodie, C.; Mikkelsen, T. FK506 binding protein mediates glioma cell growth and sensitivity to rapamycin treatment by regulating NF-kappaB signaling pathway. *Neoplasia* **2008**, *10*, 235-243.
102. Kastle, M.; Kistler, B.; Lamla, T.; Bretschneider, T.; Lamb, D.; Nicklin, P.; Wyatt, D. FKBP51 modulates steroid sensitivity and NFkappaB signalling: A novel anti-inflammatory drug target. *Eur J Immunol* **2018**, *48*, 1904-1914, doi:10.1002/eji.201847699.
103. Romano, S.; D'Angelillo, A.; Pacelli, R.; Staibano, S.; De Luna, E.; Bisogni, R.; Eskelinen, E.L.; Mascolo, M.; Cali, G.; Arra, C., et al. Role of FK506-binding protein 51 in the control of apoptosis of irradiated melanoma cells. *Cell Death Differ* **2010**, *17*, 145-157, doi:10.1038/cdd.2009.115.
104. Romano, S.; Xiao, Y.; Nakaya, M.; D'Angelillo, A.; Chang, M.; Jin, J.; Hausch, F.; Masullo, M.; Feng, X.; Romano, M.F., et al. FKBP51 employs both scaffold and isomerase functions to promote NF-kappaB activation in melanoma. *Nucleic Acids Res* **2015**, *43*, 6983-6993, doi:10.1093/nar/gkv615.
105. Srivastava, S.K.; Bhardwaj, A.; Arora, S.; Tyagi, N.; Singh, A.P.; Carter, J.E.; Scammell, J.G.; Fodstad, O.; Singh, S. Interleukin-8 is a key mediator of FKBP51-induced melanoma growth, angiogenesis and metastasis. *Br J Cancer* **2015**, *112*, 1772-1781, doi:10.1038/bjc.2015.154.
106. Romano, M.F.; Avellino, R.; Petrella, A.; Bisogni, R.; Romano, S.; Venuta, S. Rapamycin inhibits doxorubicin-induced NF-kappaB/Rel nuclear activity and enhances the apoptosis of melanoma cells. *Eur J Cancer* **2004**, *40*, 2829-2836, doi:10.1016/j.ejca.2004.08.017.
107. Zhang, Q.; Lenardo, M.J.; Baltimore, D. 30 Years of NF-kappaB: A Blossoming of Relevance to Human Pathobiology. *Cell* **2017**, *168*, 37-57, doi:10.1016/j.cell.2016.12.012.
108. Cildir, G.; Low, K.C.; Tergaonkar, V. Noncanonical NF-kappaB Signaling in Health and Disease. *Trends Mol Med* **2016**, *22*, 414-429, doi:10.1016/j.molmed.2016.03.002.
109. Mitchell, S.; Vargas, J.; Hoffmann, A. Signaling via the NFkappaB system. *Wiley Interdiscip Rev Syst Biol Med* **2016**, *8*, 227-241, doi:10.1002/wsbm.1331.
110. Akiyama, T.; Shiraishi, T.; Qin, J.; Konno, H.; Akiyama, N.; Shinzawa, M.; Miyauchi, M.; Takizawa, N.; Yanai, H.; Ohashi, H., et al. Mitochondria-nucleus shuttling FK506-binding protein 51 interacts with TRAF proteins and facilitates the RIG-I-like receptor-mediated expression of type I IFN. *PLoS One* **2014**, *9*, e95992, doi:10.1371/journal.pone.0095992.
111. Bouwmeester, T.; Bauch, A.; Ruffner, H.; Angrand, P.O.; Bergamini, G.; Croughton, K.; Cruciat, C.; Eberhard, D.; Gagneur, J.; Ghidelli, S., et al. A physical and functional map of the human TNF-alpha/NF-kappa B signal transduction pathway. *Nat Cell Biol* **2004**, *6*, 97-105, doi:10.1038/ncb1086.
112. Erlejman, A.G.; De Leo, S.A.; Mazaira, G.I.; Molinari, A.M.; Camisay, M.F.; Fontana, V.; Cox, M.B.; Piwien-Pilipuk, G.; Galigniana, M.D. NF-kappaB transcriptional activity is modulated by FK506-binding proteins FKBP51 and FKBP52: a role for peptidyl-prolyl isomerase activity. *J Biol Chem* **2014**, *289*, 26263-26276, doi:10.1074/jbc.M114.582882.
113. Hinz, M.; Broemer, M.; Arslan, S.C.; Otto, A.; Mueller, E.C.; Dettmer, R.; Scheidereit, C. Signal responsiveness of IkappaB kinases is determined by Cdc37-assisted transient interaction with Hsp90. *J Biol Chem* **2007**, *282*, 32311-32319, doi:10.1074/jbc.M705785200.
114. Chambraud, B.; Radanyi, C.; Camonis, J.H.; Shazand, K.; Rajkowski, K.; Baulieu, E.E. FAP48, a new protein that forms specific complexes with both immunophilins FKBP59 and FKBP12. Prevention by the immunosuppressant drugs FK506 and rapamycin. *J Biol Chem* **1996**, *271*, 32923-32929.

115. Neye, H. Mutation of FKBP associated protein 48 (FAP48) at proline 219 disrupts the interaction with FKBP12 and FKBP52. *Regul Pept* **2001**, *97*, 147-152.
116. Brouillard, P.; Boon, L.M.; Mulliken, J.B.; Enjolras, O.; Ghassibe, M.; Warman, M.L.; Tan, O.T.; Olsen, B.R.; Vikkula, M. Mutations in a novel factor, glomulin, are responsible for glomuvenous malformations ("glomangiomas"). *Am J Hum Genet* **2002**, *70*, 866-874, doi:10.1086/339492.
117. Pashkova, N.; Gakhar, L.; Winistorfer, S.C.; Yu, L.; Ramaswamy, S.; Piper, R.C. WD40 repeat propellers define a ubiquitin-binding domain that regulates turnover of F box proteins. *Mol Cell* **2010**, *40*, 433-443, doi:10.1016/j.molcel.2010.10.018.
118. Bashir, T.; Dorrello, N.V.; Amador, V.; Guardavaccaro, D.; Pagano, M. Control of the SCF(Skp2-Cks1) ubiquitin ligase by the APC/C(Cdh1) ubiquitin ligase. *Nature* **2004**, *428*, 190-193, doi:10.1038/nature02330.
119. Tron, A.E.; Arai, T.; Duda, D.M.; Kuwabara, H.; Olszewski, J.L.; Fujiwara, Y.; Bahamon, B.N.; Signoretti, S.; Schulman, B.A.; DeCaprio, J.A. The glomuvenous malformation protein Glomulin binds Rbx1 and regulates cullin RING ligase-mediated turnover of Fbw7. *Mol Cell* **2012**, *46*, 67-78, doi:10.1016/j.molcel.2012.02.005.
120. Duda, D.M.; Olszewski, J.L.; Tron, A.E.; Hammel, M.; Lambert, L.J.; Waddell, M.B.; Mittag, T.; DeCaprio, J.A.; Schulman, B.A. Structure of a glomulin-RBX1-CUL1 complex: inhibition of a RING E3 ligase through masking of its E2-binding surface. *Mol Cell* **2012**, *47*, 371-382, doi:10.1016/j.molcel.2012.05.044.
121. Suzuki, S.; Suzuki, T.; Mimuro, H.; Mizushima, T.; Sasakawa, C. Shigella hijacks the glomulin-clAPs-inflammasome axis to promote inflammation. *EMBO Rep* **2018**, *19*, 89-101, doi:10.15252/embr.201643841.
122. Suzuki, S.; Mimuro, H.; Kim, M.; Ogawa, M.; Ashida, H.; Toyotome, T.; Franchi, L.; Suzuki, M.; Sanada, T.; Suzuki, T., et al. Shigella IpaH7.8 E3 ubiquitin ligase targets glomulin and activates inflammasomes to demolish macrophages. *Proc Natl Acad Sci U S A* **2014**, *111*, E4254-4263, doi:10.1073/pnas.1324021111.
123. Brouillard, P.; Boon, L.M.; Revencu, N.; Berg, J.; Domp Martin, A.; Dubois, J.; Garzon, M.; Holden, S.; Kangesu, L.; Labreze, C., et al. Genotypes and phenotypes of 162 families with a glomulin mutation. *Mol Syndromol* **2013**, *4*, 157-164, doi:10.1159/000348675.
124. Brouillard, P.; Ghassibe, M.; Penington, A.; Boon, L.M.; Domp Martin, A.; Temple, I.K.; Cordisco, M.; Adams, D.; Piette, F.; Harper, J.I., et al. Four common glomulin mutations cause two thirds of glomuvenous malformations ("familial glomangiomas"): evidence for a founder effect. *J Med Genet* **2005**, *42*, e13, doi:10.1136/jmg.2004.024174.
125. Gassen, N.C.; Fries, G.R.; Zannas, A.S.; Hartmann, J.; Zschocke, J.; Hafner, K.; Carrillo-Roa, T.; Steinbacher, J.; Preissinger, S.N.; Hoesjmakers, L., et al. Chaperoning epigenetics: FKBP51 decreases the activity of DNMT1 and mediates epigenetic effects of the antidepressant paroxetine. *Sci Signal* **2015**, *8*, ra119, doi:10.1126/scisignal.aac7695.
126. Jirawatnotai, S.; Sharma, S.; Michowski, W.; Suktitipat, B.; Geng, Y.; Quackenbush, J.; Elias, J.E.; Gygi, S.P.; Wang, Y.E.; Sicinski, P. The cyclin D1-CDK4 oncogenic interactome enables identification of potential novel oncogenes and clinical prognosis. *Cell Cycle* **2014**, *13*, 2889-2900, doi:10.4161/15384101.2014.946850.
127. Jinwal, U.K.; Koren, J., 3rd; Borysov, S.I.; Schmid, A.B.; Abisambra, J.F.; Blair, L.J.; Johnson, A.G.; Jones, J.R.; Shults, C.L.; O'Leary, J.C., 3rd, et al. The Hsp90 cochaperone, FKBP51, increases Tau stability and polymerizes microtubules. *J Neurosci* **2010**, *30*, 591-599, doi:10.1523/JNEUROSCI.4815-09.2010.
128. Gaali, S.; Feng, X.; Hahle, A.; Sippel, C.; Bracher, A.; Hausch, F. Rapid, Structure-Based Exploration of Pipecolic Acid Amides as Novel Selective Antagonists of the FK506-Binding Protein 51. *J Med Chem* **2016**, *59*, 2410-2422, doi:10.1021/acs.jmedchem.5b01355.
129. Hamilton, C.L.; Abney, K.A.; Vasauskas, A.A.; Alexeyev, M.; Li, N.; Honkanen, R.E.; Scammell, J.G.; Cioffi, D.L. Serine/threonine phosphatase 5 (PP5C/PPP5C) regulates the ISOC channel through a PP5C-FKBP51 axis. *Pulm Circ* **2018**, *8*, 2045893217753156, doi:10.1177/2045893217753156.
130. Kadeba, P.I.; Vasauskas, A.A.; Chen, H.; Wu, S.; Scammell, J.G.; Cioffi, D.L. Regulation of store-operated calcium entry by FK506-binding immunophilins. *Cell Calcium* **2013**, *53*, 275-285, doi:10.1016/j.ceca.2012.12.008.

131. Lopez, E.; Berna-Erro, A.; Hernandez-Cruz, J.M.; Salido, G.M.; Redondo, P.C.; Rosado, J.A. Immunophilins are involved in the altered platelet aggregation observed in patients with type 2 diabetes mellitus. *Curr Med Chem* **2013**, *20*, 1912-1921.
132. Lopez, E.; Berna-Erro, A.; Salido, G.M.; Rosado, J.A.; Redondo, P.C. FKBP52 is involved in the regulation of SOCE channels in the human platelets and MEG 01 cells. *Biochim Biophys Acta* **2013**, *1833*, 652-662, doi:10.1016/j.bbamcr.2012.11.029.
133. Lopez, E.; Berna-Erro, A.; Salido, G.M.; Rosado, J.A.; Redondo, P.C. FKBP25 and FKBP38 regulate non-capacitative calcium entry through TRPC6. *Biochim Biophys Acta* **2015**, *1853*, 2684-2696, doi:10.1016/j.bbamcr.2015.07.023.
134. Martinez, N.J.; Chang, H.M.; Borrajo Jde, R.; Gregory, R.I. The co-chaperones Fkbp4/5 control Argonaute2 expression and facilitate RISC assembly. *RNA* **2013**, *19*, 1583-1593, doi:10.1261/rna.040790.113.
135. Novotna, A.; Pavsek, P.; Dvorak, Z. Construction and characterization of a reporter gene cell line for assessment of human glucocorticoid receptor activation. *Eur J Pharm Sci* **2012**, *47*, 842-847, doi:10.1016/j.ejps.2012.10.003.
136. Oswald, F.; Liptay, S.; Adler, G.; Schmid, R.M. NF-kappaB2 is a putative target gene of activated Notch-1 via RBP-Jkappa. *Mol Cell Biol* **1998**, *18*, 2077-2088, doi:10.1128/mcb.18.4.2077.
137. Hampf, M.; Gossen, M. A protocol for combined Photinus and Renilla luciferase quantification compatible with protein assays. *Anal Biochem* **2006**, *356*, 94-99, doi:10.1016/j.ab.2006.04.046.
138. Holden, N.S.; Squires, P.E.; Kaur, M.; Bland, R.; Jones, C.E.; Newton, R. Phorbol ester-stimulated NF-kappaB-dependent transcription: roles for isoforms of novel protein kinase C. *Cell Signal* **2008**, *20*, 1338-1348, doi:10.1016/j.cellsig.2008.03.001.
139. Hellweg, C.E.; Arenz, A.; Bogner, S.; Schmitz, C.; Baumstark-Khan, C. Activation of nuclear factor kappa B by different agents: influence of culture conditions in a cell-based assay. *Ann N Y Acad Sci* **2006**, *1091*, 191-204, doi:10.1196/annals.1378.066.
140. Liptay, S.; Schmid, R.M.; Nabel, E.G.; Nabel, G.J. Transcriptional regulation of NF-kappa B2: evidence for kappa B-mediated positive and negative autoregulation. *Mol Cell Biol* **1994**, *14*, 7695-7703, doi:10.1128/mcb.14.12.7695.
141. Avila, G.; Lee, E.H.; Perez, C.F.; Allen, P.D.; Dirksen, R.T. FKBP12 binding to RyR1 modulates excitation-contraction coupling in mouse skeletal myotubes. *J Biol Chem* **2003**, *278*, 22600-22608, doi:10.1074/jbc.M205866200.
142. Leuner, K.; Li, W.; Amaral, M.D.; Rudolph, S.; Calfa, G.; Schuwald, A.M.; Harteneck, C.; Inoue, T.; Pozzo-Miller, L. Hyperforin modulates dendritic spine morphology in hippocampal pyramidal neurons by activating Ca(2+) -permeable TRPC6 channels. *Hippocampus* **2013**, *23*, 40-52, doi:10.1002/hipo.22052.
143. Leuner, K.; Kazanski, V.; Muller, M.; Essin, K.; Henke, B.; Gollasch, M.; Harteneck, C.; Muller, W.E. Hyperforin--a key constituent of St. John's wort specifically activates TRPC6 channels. *FASEB J* **2007**, *21*, 4101-4111, doi:10.1096/fj.07-8110com.
144. Heiser, J.H.; Schuwald, A.M.; Sillani, G.; Ye, L.; Muller, W.E.; Leuner, K. TRPC6 channel-mediated neurite outgrowth in PC12 cells and hippocampal neurons involves activation of RAS/MEK/ERK, PI3K, and CAMKIV signaling. *J Neurochem* **2013**, *127*, 303-313, doi:10.1111/jnc.12376.
145. Schiedel, M.; Herp, D.; Hammelmann, S.; Swyter, S.; Lehotzky, A.; Robaa, D.; Olah, J.; Ovadi, J.; Sippl, W.; Jung, M. Chemically Induced Degradation of Sirtuin 2 (Sirt2) by a Proteolysis Targeting Chimera (PROTAC) Based on Sirtuin Rearranging Ligands (SirReals). *J Med Chem* **2018**, *61*, 482-491, doi:10.1021/acs.jmedchem.6b01872.
146. Cohen, S.; Janicki-Deverts, D.; Doyle, W.J.; Miller, G.E.; Frank, E.; Rabin, B.S.; Turner, R.B. Chronic stress, glucocorticoid receptor resistance, inflammation, and disease risk. *Proc Natl Acad Sci U S A* **2012**, *109*, 5995-5999, doi:10.1073/pnas.1118355109.
147. Romano, S.; Mallardo, M.; Romano, M.F. FKBP51 and the NF-kappaB regulatory pathway in cancer. *Curr Opin Pharmacol* **2011**, *11*, 288-293, doi:10.1016/j.coph.2011.04.011.
148. Zannas, A.S.; Jia, M.; Hafner, K.; Baumert, J.; Wiechmann, T.; Pape, J.C.; Arloth, J.; Kodel, M.; Martinelli, S.; Roitman, M., et al. Epigenetic upregulation of FKBP5 by aging and stress contributes to NF-kappaB-driven inflammation and cardiovascular risk. *Proc Natl Acad Sci U S A* **2019**, *116*, 11370-11379, doi:10.1073/pnas.1816847116.

149. Xin, H.B.; Rogers, K.; Qi, Y.; Kanematsu, T.; Fleischer, S. Three amino acid residues determine selective binding of FK506-binding protein 12.6 to the cardiac ryanodine receptor. *J Biol Chem* **1999**, *274*, 15315-15319.
150. Swanson, K.D.; Reigh, C.; Landreth, G.E. ATP-stimulated activation of the mitogen-activated protein kinases through ionotropic P2X2 purinoreceptors in PC12 cells. Difference in purinoreceptor sensitivity in two PC12 cell lines. *J Biol Chem* **1998**, *273*, 19965-19971, doi:10.1074/jbc.273.32.19965.
151. Dong, X.; Smoll, E.J.; Ko, K.H.; Lee, J.; Chow, J.Y.; Kim, H.D.; Insel, P.A.; Dong, H. P2Y receptors mediate Ca²⁺ signaling in duodenocytes and contribute to duodenal mucosal bicarbonate secretion. *Am J Physiol Gastrointest Liver Physiol* **2009**, *296*, G424-432, doi:10.1152/ajpgi.90314.2008.
152. Muller, M.; Essin, K.; Hill, K.; Beschmann, H.; Rubant, S.; Schempp, C.M.; Gollasch, M.; Boehncke, W.H.; Harteneck, C.; Muller, W.E., et al. Specific TRPC6 channel activation, a novel approach to stimulate keratinocyte differentiation. *J Biol Chem* **2008**, *283*, 33942-33954, doi:10.1074/jbc.M801844200.
153. Estacion, M.; Li, S.; Sinkins, W.G.; Gosling, M.; Bahra, P.; Poll, C.; Westwick, J.; Schilling, W.P. Activation of human TRPC6 channels by receptor stimulation. *J Biol Chem* **2004**, *279*, 22047-22056, doi:10.1074/jbc.M402320200.
154. Estacion, M.; Sinkins, W.G.; Jones, S.W.; Applegate, M.A.; Schilling, W.P. Human TRPC6 expressed in HEK 293 cells forms non-selective cation channels with limited Ca²⁺ permeability. *J Physiol* **2006**, *572*, 359-377, doi:10.1113/jphysiol.2005.103143.
155. Riazanski, V.; Gabdoulkhakova, A.G.; Boynton, L.S.; Eguchi, R.R.; Deriy, L.V.; Hogarth, D.K.; Loaec, N.; Oumata, N.; Galons, H.; Brown, M.E., et al. TRPC6 channel translocation into phagosomal membrane augments phagosomal function. *Proc Natl Acad Sci U S A* **2015**, *112*, E6486-6495, doi:10.1073/pnas.1518966112.
156. Schmidt, M.; Bienek, C.; van Koppen, C.J.; Michel, M.C.; Jakobs, K.H. Differential calcium signalling by m2 and m3 muscarinic acetylcholine receptors in a single cell type. *Naunyn Schmiedebergs Arch Pharmacol* **1995**, *352*, 469-476.
157. Carroll, R.C.; Peralta, E.G. The m3 muscarinic acetylcholine receptor differentially regulates calcium influx and release through modulation of monovalent cation channels. *EMBO J* **1998**, *17*, 3036-3044, doi:10.1093/emboj/17.11.3036.
158. Yan, Z.; Bai, X.; Yan, C.; Wu, J.; Li, Z.; Xie, T.; Peng, W.; Yin, C.; Li, X.; Scheres, S.H.W., et al. Structure of the rabbit ryanodine receptor RyR1 at near-atomic resolution. *Nature* **2015**, *517*, 50-55, doi:10.1038/nature14063.
159. Huse, M.; Chen, Y.G.; Massague, J.; Kuriyan, J. Crystal structure of the cytoplasmic domain of the type I TGF beta receptor in complex with FKBP12. *Cell* **1999**, *96*, 425-436.
160. Chaikuad, A.; Alfano, I.; Kerr, G.; Sanvitale, C.E.; Boergermann, J.H.; Triffitt, J.T.; von Delft, F.; Knapp, S.; Knaus, P.; Bullock, A.N. Structure of the bone morphogenetic protein receptor ALK2 and implications for fibrodysplasia ossificans progressiva. *J Biol Chem* **2012**, *287*, 36990-36998, doi:10.1074/jbc.M112.365932.
161. Sun, X.; Wang, J.; Yao, X.; Zheng, W.; Mao, Y.; Lan, T.; Wang, L.; Sun, Y.; Zhang, X.; Zhao, Q., et al. A chemical approach for global protein knockdown from mice to non-human primates. *Cell Discov* **2019**, *5*, 10, doi:10.1038/s41421-018-0079-1.
162. Guo, J.; Liu, J.; Wei, W. Degrading proteins in animals: "PROTAC"tion goes in vivo. *Cell Res* **2019**, *29*, 179-180, doi:10.1038/s41422-019-0144-9.